THE UNIVERSITY OF CHICAGO

# SUPRAMOLECULAR FUNCTIONALIZATION OF PLANAR SURFACES USING GALLIUM-PORPHYRIN MONOLAYERS

A DISSERTATION SUBMITTED TO

THE FACULTY OF THE DIVISION OF THE PHYSICAL SCIENCES

IN CANDIDACY FOR THE DEGREE OF

DOCTOR OF PHILOSOPHY

DEPARTMENT OF CHEMISTRY

BY

JUDITH MARIE KAMM

CHICAGO, ILLINOIS

DECEMBER 2017

## TABLE OF CONTENTS

**Page**

## LIST OF FIGURES

## LIST OF TABLES

## LIST OF SCHEMES

**Scheme** **Page**

## ACKNOWLEDGEMENTS

I would first like to thank my advisor, Professor Mike Hopkins for taking such an interest in me as a scientist and an individual. I've learned so much about how to be a good researcher, a good writer, a good mentor, and a good person. I'd also like to thank my undergraduate advisor, Professor Tom Smith and my chemistry teacher Walter "Karl with a K" Erhardt for encouraging my continuing interest in chemistry; I really wouldn't be here without all of you. I also wouldn't be here without my dissertation committee, Professors Rich Jordan and Dmitri Talapin, who really helped me out throughout my time here and in the last hectic push at the end. I'd also like to thank Melinda Moore for always knowing the next step to take and reassuring me that everything would work out and Dr. Vera Dragisich for her steadfast advice and hard work on my behalf.

I'd next like to give a special thanks to my family, who sent me lots of love and cookies during my time getting my Ph.D. Bruizer, Jess & Stevie, and Chuckles & Diana always know how to cheer me up, and Henry David Kamm Broomell won't know it for a while, but he really helped me out when I needed him most. My parents are as supportive of me twenty-two grades of school later as they always have been, and I'm especially grateful to them.

The Hopkins Group was a really amazing place to work and I wouldn't have traded it for anything. Wayne Lau was my partner in crime both in lab and in dim sum. Dan O'Hanlon was distracting in the best way possible, and I learned so much from him about science, board games and trivia I will probably never need. Mark Westwood was always willing to get coffee with me and discuss fantasy football tactics. This project never would have gotten started without the hard work of Cam Iverson, and I'm really grateful to his dedication to a tough cause. I'm sure that Andrew Grorud will be an incredibly worthy successor and I wish him the very best. Mollye

Levin made me laugh every single day and Noah Lewis was an awesome undergrad to work with. I'm also grateful to have overlapped with all of the other wonderfully talented people in this lab: Chris Hansen, Nathan La Porte, Davis Moravec, Ayush Gupta, Dylan Lynch, and Hannah Friedman.

I'd very much like to thank all of my friends that helped me get through the good and bad times of grad school. My former roommates Mary Andorfer, Joe Gair, and Laura Toth are all delightfully joyful people that were always willing to share bowls of mac and cheese and episodes of Buffy the Vampire Slayer with me. I'm really honored to say that Chad Heaps became one of my very best friends, and we're both unbelievably lucky that Clare Heaps came into our lives. And while Group Theory might not ever record our hit single, we can still be proud to be one of the best puzzling teams in Chicago. I had a genuine blast getting to know a lot of the hilariously intelligent people at UChicago: Jon Raybin, Alex Schneider, Erica Sturm, Ken Ellis-Guardiola, Donglin Zhao, Landon Durak, Matt Kurley, Dmitriy Dolzhnikov, Becca Black, Johnny Zimmerman, and EW Malchosky, just to name a few.

Finally, a very special thank you to Hunter Vibbert. He's the person I always have the most fun with and want to share every experience with. I'll never be able to say exactly how important he is to me and how much his love and support has helped me, but I hope he knows.

*To my friends, my family, and my pandas*

## ABSTRACT

There are few general methods for the nanoscale organization of functional modules in three dimensions, an issue that needs to be addressed as device fabrication reaches its lower length-scale limits. The bottom-up self-assembly approach aims to organize such functional subunits into repeating patterns at nanometer length scales in ways that their collective assembly at an interface makes them addressable. The central hypothesis investigated here is that five-coordinate gallium-porphyrin monolayers with covalently bound axial ligands are good candidates for supports in such a bottom-up approach. The two-dimensional assembly of porphyrins on planar surfaces is a richly developed field, and the incorporation of a metal that can axially coordinate to a ligand of interest offers a modular method of extending the assembly into the third dimension.

This work describes a dual approach to the functionalization of self-assembled five-coordinate gallium(III)octaethylporphyrin (Ga(OEP)X) monolayers. The first is a covalent functionalization of the axial ligand to incorporate functional modules. To initially investigate the effects of covalently adding a fifth ligand to self-assembled arrays of metalloporphyrins, a series of Ga(OEP)X complexes (X = Cl, Br, I, $O_3SCF_3$, CCPh) was studied via density functional theory (DFT) and scanning tunneling microscopy (STM) at the solid-liquid interface. Additional functionality was then incorporated using ethynylferrocene and zinc ethynyltetraphenylporphyrin ligands. The assembly of select complexes was also investigated on a variety of substrates including highly oriented pyrolytic graphite (HOPG), single layer graphene on copper foil, and monolayer $MoS_2$.

The second approach for surface functionalization described in this work is the supramolecular incorporation of fullerenes into the inter-ligand cavities formed by the unit cell

of the self-assembled monolayer. This approach both takes advantage of the favorable size match between the unit cell in Ga(OEP)X monolayers with that of fullerene guest molecules and further axially incorporates a ligand predicted to have affinity for fullerenes. Various templating ligands were investigated (1-ethynylpyrene, 2-ethynylpyrene, 3-ethynylthiophene, 9-ethynylanthracene, 9-ethynyltriptycene, and 1-pyrenecarboxylate) by molecular modeling and STM. The various factors that affect fullerene templating, such as ligand height, deposition method, and concentration are discussed.

# CHAPTER 1

## Introduction

There exist few general methods for the nanoscale organization of function-rich molecules and nanoparticles that allow for precise control over their three-dimensional (3D) positioning, as is necessary to explore and develop the full range of collective functions that might emerge from such assemblies.[1] In order to continue to push the lower length-scale limits of device fabrication and to harness the unique properties of the materials within these devices, there is a growing need for new design strategies. Driven by the needs for scalability and micron-scale connectivity of such devices, bottom-up noncovalent self-assembly on surfaces is often invoked as a desirable approach because it enables, in principle, the precise, repetitive positioning of functional subunits on nanometer length scales at an interface that can make them addressable.[2-4] In the design of these assemblies, it will be of great importance to engineer methods of accurately patterning the functional constituents in order to gain cooperative function necessary for practical device integration and scalability.

The ordered self-assembly of molecules into two-dimensional (2D) monolayers on atomically flat substrates has been extensively studied.[2, 5-8] In monolayers of this type, the molecules are typically oriented such that a substantial portion of their surface is in contact (physisorbed) with the substrate, and the 2D patterns they form are governed by intermolecular interactions among substituents along their backbones, periphery, and/or termini. Thus, they are distinct from the extensively studied class of self-assembled end-bound molecular monolayers whose archetypes are alkane-thiols on gold surfaces, in which a thiol-gold bond anchors the molecule to the substrate and the alkyl group extends above the surface.[9-14] There have been relatively few efforts to use 2D monolayers as platforms for organizing molecules or nanostructures in 3D. Examples include the use of triazatriangulenium ions as a platform for a

"click type" attachment of functional molecules,[15-20] and the "nanocrane" approach of Janus tectons that aim to lift functional unit off of the surface at defined spacings.[21] This speaks to the possibility of developing a general method for using 2D monolayers as a basis for organization that is controllable in all three dimensions; we aim to find a system that is highly modular and therefore structurally and functionally tunable (Figure 1.1).

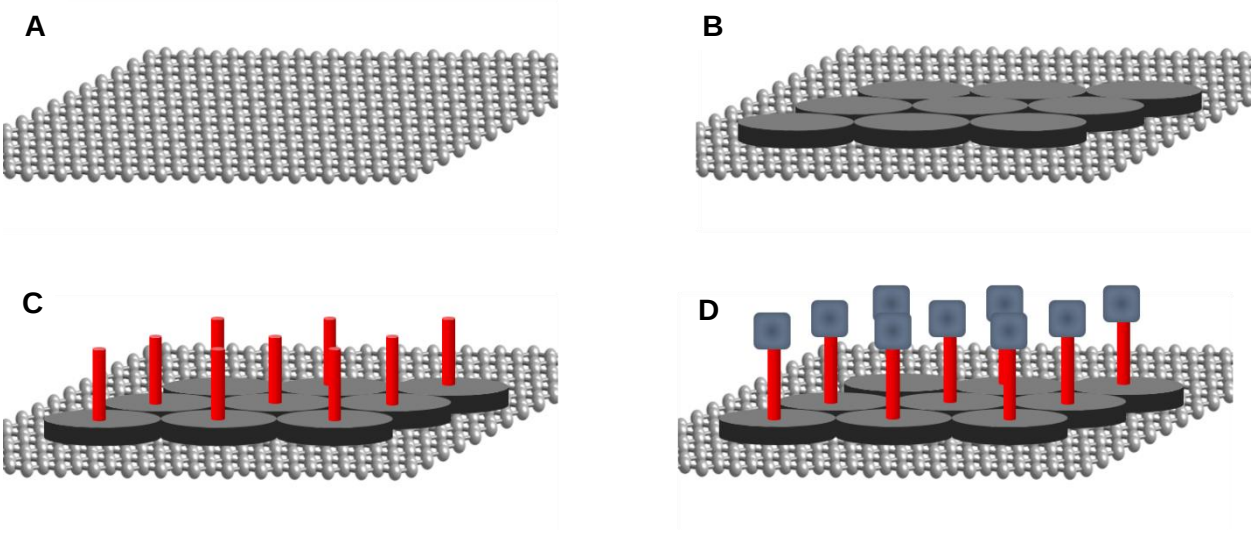


**Figure 1.1.** Schematic of the bottom-up approach to the functionalization of surfaces into the third dimension. (A) An atomically smooth surface that allows micron-scale electrical contact. (**B**) 2D self-assembled molecular monolayer in which the (*x*,*y*) coordinates of each molecule are controlled by its shape and peripheral substituents. (C) 2D self-assembled monolayer of an analogue of the molecules in (B), in which an orthogonal substituent or ligand of defined length establishes a specific (*x*,*y*,*z*) coordinate at its terminus. (D) Attachment of a functional subunit to the terminus in (C), showing the encoding of their positions in the design criteria outlined in (B) and (C). Deposition of this molecule results in location of the functional unit at pre-determined sites in the monolayer, patterned by self-assembly methods.

Porphyrins are particularly intriguing candidates as building blocks in bottom-up self-assembled systems for several reasons. First, they have a wealth of optical, catalytic, biomimetic, and photophysical properties that could be used to enrich the functionality of the assemblies.[22-29] Secondly, they possess a modular structure that allows for great diversity in both the structure and function that can be tuned into the assemblies (Figure 1.2). Both the peripheral substituents and metal centers can be varied via well-studied synthetic methods.[30-32] Further, if a five- or six-

coordinate metal is incorporated, axial ligation gives yet another point of modular functionalization. Perhaps most importantly, planar porphyrins (and some 5- and 6-coordinate porphyrins) have been shown to self-assemble on two-dimensional substrates into robust, well-ordered arrays under myriad conditions, making them excellent candidates for studies incorporating them for developing scalable, functionalized materials.

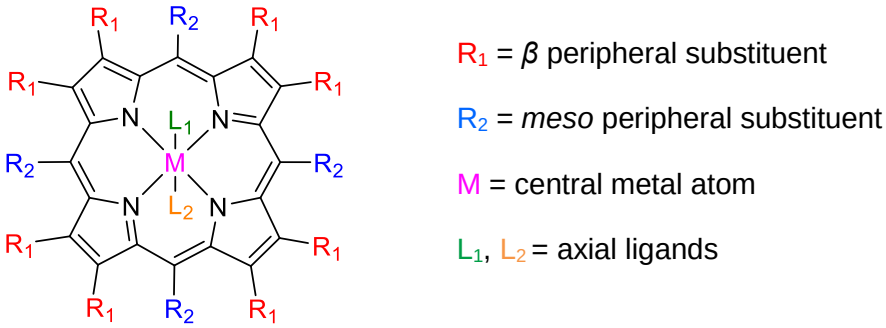


**Figure 1.2** Generic porphyrin structure highlighting its modular nature.

The two-dimensional assembly behavior of both free-base and metalloporphyrins has been well-characterized by scanning tunneling microscopy (STM) under a wide variety of conditions.[22-26, 33] STM has become the standard method of choice for such studies due to its ability to gain insight into submolecular level structure, its sensitivity to changes in electronic structure, and the wide variety of conditions under which it can perform.[2, 25, 26, 33, 34] Many hundreds of porphyrin studies on atomically flat substrates have been done under ultra-high vacuum (UHV) conditions[33] which offer the benefit of resolution of great atomic and electronic details, but are more arduous to prepare and carry out, and less emulate the conditions needed for practical, scalable devices. Assembly has been observed on a wide range of substrates, including a variety of metals (Au, Ag, Cu, among others), and highly oriented pyrolytic graphite (HOPG).[25, 26] HOPG offers several benefits as a substrate: atomically flat surfaces can be easily

prepared via the adhesive tape method, the favorable π-π interactions create robust porphyrin-HOPG assemblies, and the substrate is compatible with preparation and imaging under ambient conditions (e.g., at the solid-air and solid-liquid interfaces).[25]

While many factors play a role in governing the assembly of molecules into 2D monolayers on a surface, porphyrin-porphyrin intermolecular interactions are important in determining the 2D lattice structures that form, particularly under ambient conditions.[24-26] Varying the peripheral substituents on the porphyrin will have a large influence on the type of assembly observed. These are generally determined by the types of interactions that the peripheral groups are able to form with each other (i.e. van der Waals, hydrogen bonding, metal-coordination interactions). The type of interaction can influence the shape of the lattice, ranging from a close packed, pseudo-hexagonal unit cell in octaethylporphyrin with compact peripheral side chains to a more open, lamellar lattice in *meso*-tetralkyl-substituted porphyrins. The spacing between the porphyrin cores also varies with the change in substituents, with distance ranging from ~1.3 nm for octaethylporphyrins[35] to ~3.3 nm for the longest-chain alkyl-substituted porphyrins.[36]

While the surface chemistry of four-coordinate porphyrins has been thoroughly studied, reports of monolayers of metalloporphyrins that possess axial ligands are comparative rare, particularly those studied under ambient conditions. However, monolayers of axially ligated metalloporphyrins are of potential interest in several contexts. The reversibility of the metal-ligand bond in systems with small equilibrium binding constants has made these attractive candidates for applications in catalysis, energy transfer, and small-molecule sensing, with the surface itself often influencing these phenomena in interesting ways.[33, 34, 37] Many of these examples involve small molecule-binding (i.e. NO, CO, $NH_3$) or ligand transfer (i.e. Cl) reactions under UHV conditions.[33, 38, 39] A few examples have sought to elucidate the

thermodynamics of these systems at the solid-liquid interface, such as studies of the binding of $O_2$ to porphyrins on the surface.[37, 40]

Another primary interest in axially ligated metalloporphyrins lies in their ability to act as scaffolds for the bottom-up construction of architectures perpendicular to the surface, with the metal atom acting as an attachment point for further functionalization. This approach looks to utilize the controllable pattern of the underlying 2D monolayer as a template for regular sites to extend into the 3rd dimension. Examples using this motif that extend beyond halide[41-43] and oxo[35, 37, 44] ligands include Zn(OEP) coordination polymers,[45, 46] imidazole,[34] and various pyridyl derivatives.[47-49] However, these latter examples are based off of dative interactions between the central metal atom and axial ligand that have been shown to be labile during STM scanning.[47] A covalent metal–ligand bond would both be more robust and would allow the deposited material to be fully characterized prior to deposition.

In this work, we test the central hypothesis that monolayers of five-coordinate metalloporphyrins can act as a scaffold for the 3D organization of materials. We aim to use two complementary approaches: covalent axial ligation of pre-determined sites with desirable functional modules, and supramolecular interactions of axial affinity groups for target guest molecules. This hypothesis is built on the understanding that we can use the wealth of reported knowledge about the 2D assembly of porphyrins on surfaces to position the central metal atoms precisely within the monolayer. The metal atom then acts as an anchor point for the covalent ligation of a subunit that extends perpendicular to the surface at a defined distance based on the choice in ligand (Figure 1.1D). This subunit then either acts on its own to bring further functionality into the assembly or interacts supramolecularly with other functional modules.

As discussed above, there are relatively few reports of five-coordinate metalloporphyrin assemblies on surfaces, and therefore, a systematic study of the effects that axial ligands have on assembly behavior under ambient conditions is required. The complexes of Ga(III)octaethylporphyrin (OEP) are good candidates for such an investigation. Gallium(III) is the metal of choice for initial investigations for several reasons. First, it is capable of forming five-coordinate, square-pyramidal complexes with a covalently bound axial ligand.[50-52] Secondly, the synthesis of several Ga(OEP)X compounds are reported in the literature,[53-62] and given that harsh reaction conditions are employed, such as in the cases of Ga(OEP)Cl,[55] synthesized in refluxing glacial acetic acid, and Ga(OEP)I,[55] synthesized under a continuous flow of HI gas, Ga(OEP)X compounds are predicted to be a robust and air-stable class of molecules suitable for surface studies. Finally, prior work in both the literature[57] and our lab[63, 64] has demonstrated that gallium(III) porphyrins with various acetylide ligands can be made straightforwardly from the reaction of the Ga(Por)Cl with LiCCR ligand of choice, making functionalization synthetically modular.

Likewise, OEP is a good candidate for initial investigations into the effects of covalent axial ligation on porphyrin surface assembly. Four-coordinate M(OEP) complexes are known to form well-ordered and well-studied monolayers on HOPG at the solid–air and solid–liquid interfaces (M = Ni,[34, 35, 65-67] Co,[37, 44, 67, 68] Pt,[69, 70] Cu,[71, 72] Zn[71, 73]). While the crystal structures of four-coordinate M(OEP) complexes show that the porphyrin core is planar or very slightly ruffled,[74-79] those reported for Ga(OEP)X[50, 53, 56, 59, 60] exhibit a slight dome in the porphyrin structure, with the gallium atom above the $N_4$ plane, which is in turn above the plane of the porphyrin macrocycle (Figure 1.3). Such distortions may affect any of several interactions that have been shown to contribute to adsorption of M(OEP) complexes onto HOPG, including metal-graphite

interactions and π-π stacking.[80, 81] We predict we are more likely to observe any effects of these distortions on surface assembly in monolayers of OEP complexes, compared to porphyrins with bulkier peripheral substituents, because the compact ethyl side chains are predicted to have minimal impact on the assembly of the monolayers.[82]

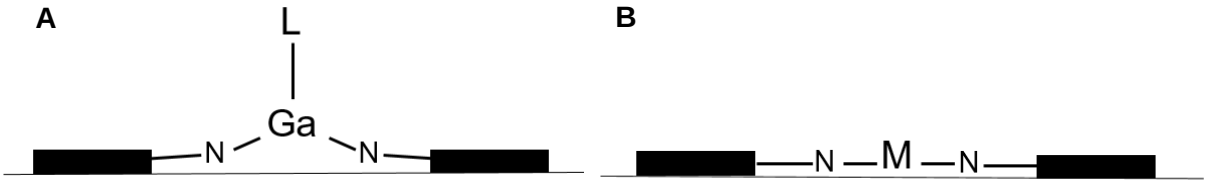


**Figure 1.3.** Illustration of doming effect predicted in Ga(OEP)X molecules assembled on HOPG (A) as compared to planar four-coordinate analogs (B) showing the distortion of the gallium atom above the plane of the porphyrin macrocycle.

Once a systematic study of the effects of incorporating a covalently-coordinated axial ligand is completed, we aim to axially incorporate functional units that are capable of exhibiting collective function in an assembly. This type of functionality may include, but is not limited to, redox chemistry, magnetism, photoactivity, or mechanical action. Previous examples of such incorporation extending into the third dimension include derivatives of the photoactive azobenzene molecule that is capable of acting as a molecular switch,[18, 47] porphyrin chromophores,[15] fullerenes,[21] and derivatives of the electroactive ferrocene molecule,[14] among others. Prior work in our lab[64] has demonstrated that axial oligo-phenylene-ethynylene ligands, of interest due to their applicability as molecular wire components,[83] can be covalently ligated to *meso*-substituted tetradecyl porphyrins ($TC_{10}P$) and their assembly behavior on HOPG at the solid-liquid interface observed. However, these Ga($TC_{10}P$)X monolayers tended to give multiple lattices; we now aim to both further expand the range of functional ligands incorporated to both photo- and electroactive components while maintaining a predictable 2D assembly structure.

With the first goal of covalent functionalization of porphyrin monolayers in mind, we further hypothesize that we can combine our knowledge of the 2D assembly of porphyrins on surfaces to axially ligate an affinity group that can template the supramolecular assembly of a nanoparticle (Figure 1.4). This is a complementary approach to the covalent attachment of functional modules previously discussed that will (a) build up complex and unique surface architectures and (b) place functional units in atomically defined proximity.[2, 26] Developing new, spatially controllable approaches for the self-assembly of nanoparticle arrays directly at the interface is important to advancing their potential applications.[84, 85] By employing a five-coordinate porphyrin monolayer template, we propose to construct a surface corral whose unit cell is commensurate with a target nanoparticle and whose axial ligand has affinity for said nanoparticle. A range of lattice constants is available by employing longer *meso*-tetra(alkyl)porphyrins (TC$_n$P, $n$ = 10–19); the free-base porphyrins form monolayers on HOPG at the solid–liquid interface with lattice constants that range up to 3.3 nm.[36, 49, 86-90] The resulting unit cell is in the range of very small gold nanoparticles.[91]

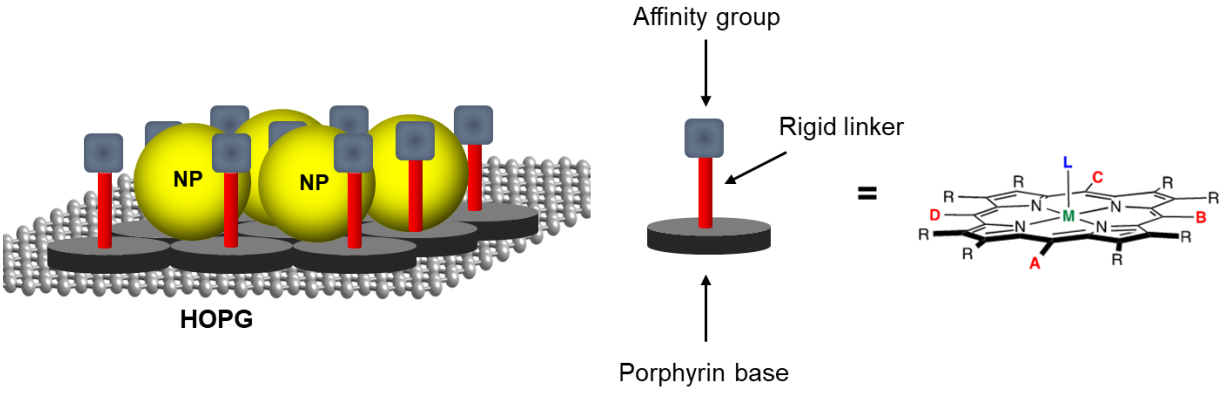


**Figure 1.4.** Proposed method of supramolecular assembly of nanoparticles into arrays of five-coordinate metalloporphyrin monolayers with a unit cell of appropriate size and an axial ligand of appropriate affinity.

As a starting point, however, we first turn our attention to the unit cell formed by M(OEP) monolayers. From literature reports[35, 37] and preliminary work done in our lab,[63] we expect these to have a pseudo-hexagonal cell commensurate with templating a small nanoparticle such as $C_{60}$ (Figure 1.5). We therefore aim to synthesize a Ga(OEP)X molecule with an axial ligand that has affinity for fullerenes. The numerous potential applications of fullerenes in solar cells, sensors, electronics, optical devices, light harvesters, and molecular machines make them promising candidates for the incorporation into functional devices.[92, 93] Because they can be straightforwardly functionalized,[94] this is also a highly versatile class of molecules for investigation. Their applications often require that they be part of a larger assembly, interfacing with additional materials (i.e. in bulk-heterojunction solar cells)[95, 96] or in contact with a solid support[97] to take full advantage of their unique properties. In our proposed motif, we spatially organize the fullerenes via electron donor-acceptor interactions with the axial ligand while interfacing them to the surface where they are in close contact with the porphyrin.

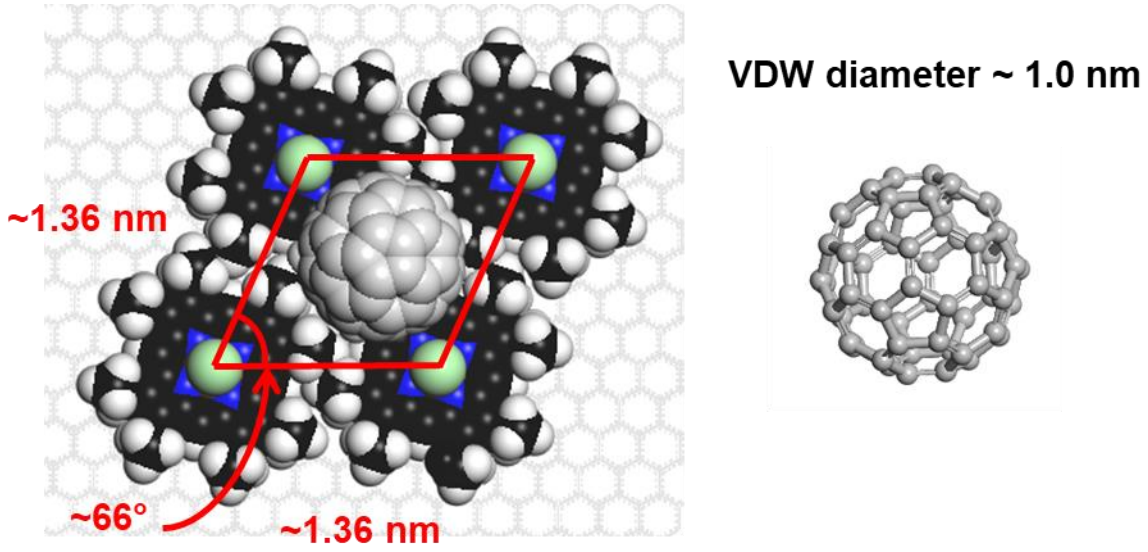


**Figure 1.5.** Molecular model of the predicted approximate pseudo-hexagonal unit cell of M(OEP) complexes on HOPG commensurate with the van der Waals diameter of one fullerene molecule.

Supramolecular assemblies involving fullerenes are preferable to those prepared by covalent functionalization for a number of reasons.[97-100] First, equivalent bonding sites in the fullerenes make forming extended regular polymeric 2D and 3D structures difficult. Second, covalent synthesis of assemblies will necessarily require multiple steps, which can be cumbersome, whereas thermodynamically driving the self-assembly of nanostructures offers an "ease" of construction. Third, supramolecular assemblies offer a large scope in the types of molecules and interactions that can be explored under a variety of conditions. Finally, covalent functionalization often causes the fullerene to lose some of the attendant properties that make it an attractive molecule for incorporation into devices, and therefore the supramolecular organization of pristine $C_{60}$ is a common target.

Carbon nanostructures are prone to forming aggregates,[98] and the basic spherical shape of the fullerene molecules themselves offer a limited range of self-assembled structures that can form on a surface;[101] this has led to the development of several motifs of rationally designed surface-assisted templates to aid in the assembly of the fullerene onto the surface.[97, 102] These templates

can be effective by creating a "nanowell" of the appropriate size to host one or more guest molecule.[103-106] However, these wells must be precisely engineered to the correct size and often rely on surface-assisted interactions for successful templating. Other approaches have further incorporated functional groups that have affinity for the fullerene, such as thiophene units, in an effort to increase the fullerene-template interactions.[107-110] We aim to combine the two approaches by utilizing a unit cell with an appropriate size and an axial affinity group with donor-acceptor interactions as a unique templating method.

In the following work, we describe the efforts towards answering two fundamental questions: (1) Can monolayers of five-coordinate metalloporphyrins be used as frameworks for the 3D organization of functional units that are covalently templated to the pattern of the underlying 2D monolayer; and (2) Can monolayers of five-coordinate metalloporphyrins be used to supramolecularly template the assembly of a small nanoparticle under ambient conditions?

Chapters 2 and 3 describe efforts toward answering the first question. In Chapter 2, we provide a systematic study of varying the axial ligand across a series of Ga(OEP)X complexes (OEP = octaethylporphyrin; X = Cl, Br, I, $O_3SCF_3$, CCPh). We describe density functional theory predictions of how the structure varies with axial ligand and STM studies detailing any effects these changes have on their assembly behavior at the solid-liquid interface (HOPG, 1-phenyloctane). Chapter 3 describes efforts to covalently add functionality into our self-assembled arrays by axial ligation of electroactive (ferrocene) and photoactive (porphyrin) ligands of great height and steric bulk such that models of the forecasted on-surface geometry predict hindered rotation of some axial ligands. Attempts at varying the linker motif between acetylide and carboxylate are also discussed.

Building off of the results in Chapters 2 and 3 in which a highly reproducible unit cell in Ga(OEP)X-type complexes is observed, despite variations in axial ligand, we then turned towards the second question of the supramolecular assembly of the small nanoparticle $C_{60}$ and its derivative [6,6]-phenyl-$C_{61}$-butyric acid methyl ester (PCBM) in Chapters 4 and 5. In Chapter 4, we describe our initial templating efforts using 1-ethynylpyrene and 2-ethynylpyrene axial ligands as an affinity group to guide the assembly of fullerenes into the intra-ligand cavity formed by the porphyrin monolayer. In Chapter 5, we describe the exploration of the factors that potentially comprise an effective fullerene template, through the incorporation of several different affinity group ligands (3-ethynylthiophene, 9-ethynylanthracene, 9-ethynyltriptycene, and pyrenecarboxylate).

### 1.1. References


1. Parviz, B. A.; Ryan, D.; Whitesides, G. M. Using Self-assembly for the Fabrication of Nano-Scale Electronic and Photonic Devices. *IEEE Trans. Adv. Packag.* **2003**, *26*, 233-241.

2. Barth, J. V.; Costantini, G.; Kern, K. Engineering Atomic and Molecular Nanostructures at Surfaces. *Nature* **2005**, *437*, 671-679.

3. Liddle, J. A.; Gallatin, G. M. Nanomanufacturing: A Perspective. *ACS Nano* **2016**, *10*, 2995-3014.

4. Lu, W.; Lieber, C. M. Nanoelectronics From the Bottom Up. *Nat. Mater.* **2007**, *6*, 841-850.

5. Barth, J. V. Molecular Architectonic on Metal Surfaces. *Annu. Rev. Phys. Chem.* **2007**, *58*, 375-407.

6. Kudernac, T.; Lei, S. B.; Elemans, J. A. A. W.; De Feyter, S. Two-Dimensional Supramolecular Self-Assembly: Nanoporous Networks on Surfaces. *Chem. Soc. Rev.* **2009**, *38*, 402-421.

7. Otero, R.; Gallego, J. M.; de Parga, A. L. V.; Martín, N.; Miranda, R. Molecular Self-Assembly at Solid Surfaces. *Adv. Mater.* **2011**, *23*, 5148-5176.

8. Ariga, K.; Lee, M. V.; Mori, T.; Yu, X. Y.; Hill, J. P. Two-Dimensional Nanoarchitectonics Based on Self-Assembly. *Adv. Colloid Interface Sci.* **2010**, *154*, 20-29.

9. Chan, Y. H.; Schuckman, A. E.; Perez, L. M.; Vinodu, M.; Drain, C. M.; Batteas, J. D. Synthesis and Characterization of a Thiol-Tethered Tripyridyl Porphyrin on Au(111). *J. Phys. Chem. C* **2008**, *112*, 6110-6118.

10. Imahori, H.; Kashiwagi, Y.; Endo, Y.; Hanada, T.; Nishimura, Y.; Yamazaki, I.; Araki, Y.; Ito, O.; Fukuzumi, S. Structure and Photophysical Properties of Porphyrin-Modified Metal Nanoclusters with Different Chain Lengths. *Langmuir* **2004**, *20*, 73-81.

11. Rivas, M. V.; De Leo, L. P. M.; Hamer, M.; Carballo, R.; Williams, F. J. Self-Assembled Monolayers of Disulfide Cu Porphyrins on Au Surfaces: Adsorption Induced Reduction and Demetalation. *Langmuir* **2011**, *27*, 10714-10721.

12. Jeong, H.; Kim, D.; Wang, G.; Park, S.; Lee, H.; Cho, K.; Hwang, W. T.; Yoon, M. H.; Jang, Y. H.; Song, H.; Xiang, D.; Lee, T. Redox-Induced Asymmetric Electrical Characteristics of Ferrocene-Alkanethiolate Molecular Devices on Rigid and Flexible Substrates. *Adv. Funct. Mater.* **2014**, *24*, 2472-2480.

13. Sun, Y. Y.; Peng, Z. L.; Hou, R.; Liang, J. H.; Zheng, J. F.; Zhou, X. Y.; Zhou, X. S.; Jin, S.; Niu, Z. J.; Mao, B. W. Enhancing Electron Transport in Molecular Wires by Insertion of a Ferrocene Center. *Phys. Chem. Chem. Phys.* **2014**, *16*, 2260-2267.

14. Kitagawa, T.; Matsubara, H.; Komatsu, K.; Hirai, K.; Okazaki, T.; Hase, T. Ideal Redox Behavior of the High-Density Self-Assembled Monolayer of a Molecular Tripod on a Au(111) Surface with a Terminal Ferrocene Group. *Langmuir* **2013**, *29*, 4275-4282.

15. Otte, F. L.; Lemke, S.; Schutt, C.; Krekiehn, N. R.; Jung, U.; Magnussen, O. M.; Herges, R. Ordered Monolayers of Free-Standing Porphyrins on Gold. *J. Am. Chem. Soc.* **2014**, *136*, 11248-11251.

16. Baisch, B.; Raffa, D.; Jung, U.; Magnussen, O. M.; Nicolas, C.; Lacour, J.; Kubitschke, J.; Herges, R. Mounting Freestanding Molecular Functions onto Surfaces: The Platform Approach. *J. Am. Chem. Soc.* **2009**, *131*, 442-443.

17. Kuhn, S.; Baisch, B.; Jung, U.; Johannsen, T.; Kubitschke, J.; Herges, R.; Magnussen, O. Self-Assembly of Triazatriangulenium-Based Functional Adlayers on Au(111) Surfaces. *Phys. Chem. Chem. Phys.* **2010**, *12*, 4481-4487.

18. Jung, U.; Kuhn, S.; Cornelissen, U.; Tuczek, F.; Strunskus, T.; Zaporojtchenko, V.; Kubitschke, J.; Herges, R.; Magnussen, O. Azobenzene-Containing Triazatriangulenium Adlayers on Au(111): Structural and Spectroscopic Characterization. *Langmuir* **2011**, *27*, 5899-5908.

19. Lemke, S.; Chang, C. H.; Jung, U.; Magnussen, O. M. Reversible Potential-Induced Switching of Alkyl Chain Aggregation in Octyl-Triazatriangulenium Adlayers on Au(111). *Langmuir* **2015**, *31*, 3115-3124.

20. Lemke, S.; Ulrich, S.; Claussen, F.; Bloedorn, A.; Jung, U.; Herges, R.; Magnussen, O. M. Triazatriangulenium Adlayers on Au(111): Superstructure as a Function of Alkyl Side Chain Length. *Surf. Sci.* **2015**, *632*, 71-76.

21. Du, P.; Kreher, D.; Mathevet, F.; Maldivi, P.; Charra, F.; Attias, A. J. Surface-Confined Supramolecular Self-Assembly of Molecular Nanocranes for Chemically Lifting and Positioning $C_{60}$ above a Conducting Substrate. *ChemPhysChem* **2015**, *16*, 3774-3778.

22. Jurow, M.; Schuckman, A. E.; Batteas, J. D.; Drain, C. M. Porphyrins as Molecular Electronic Components of Functional Devices. *Coord. Chem. Rev.* **2010**, *254*, 2297-2310.

23. Drain, C. M.; Varotto, A.; Radivojevic, I. Self-Organized Porphyrinic Materials. *Chem. Rev.* **2009**, *109*, 1630-1658.

24. Mohnani, S.; Bonifazi, D. Supramolecular Architectures of Porphyrins on Surfaces: The Structural Evolution from 1D to 2D to 3D to Devices. *Coord. Chem. Rev.* **2010**, *254*, 2342-2362.

25. Otsuki, J. STM Studies on Porphyrins. *Coord. Chem. Rev.* **2010**, *254*, 2311-2341.

26. Auwärter, W.; Écija, D.; Klappenberger, F.; Barth, J. V. Porphyrins at Interfaces. *Nat. Chem.* **2015**, *7*, 105-120.

27. Mazur, U.; Hipps, K. W. Kinetic and Thermodynamic Processes of Organic Species at the Solution-Solid Interface: The View Through an STM. *Chem. Comm.* **2015**, *51*, 4737-4749.

28. Panda, M. K.; Ladomenou, K.; Coutsolelos, A. G. Porphyrins in Bio-Inspired Transformations: Light-Harvesting to Solar Cell. *Coord. Chem. Rev.* **2012**, *256*, 2601-2627.

29. Son, H. J.; Jin, S. Y.; Patwardhan, S.; Wezenberg, S. J.; Jeong, N. C.; So, M.; Wilmer, C. E.; Sarjeant, A. A.; Schatz, G. C.; Snurr, R. Q.; Farha, O. K.; Wiederrecht, G. P.; Hupp, J. T. Light-Harvesting and Ultrafast Energy Migration in Porphyrin-Based Metal-Organic Frameworks. *J. Am. Chem. Soc.* **2013**, *135*, 862-869.

30. Littler, B. J.; Ciringh, Y.; Lindsey, J. S. Investigation of Conditions Giving Minimal Scrambling in the synthesis of Trans-Porphyrins from Dipyrromethanes and Aldehydes. *J. Org. Chem.* **1999**, *64*, 2864-2872.

31. Senge, M. O. Stirring the Porphyrin Alphabet Soup-Functionalization Reactions for Porphyrins. *Chem. Commun.* **2011**, *47*, 1943-1960.

32. Hiroto, S.; Miyake, Y.; Shinokubo, H. Synthesis and Functionalization of Porphyrins through Organometallic Methodologies. *Chem. Rev.* **2017**, *117*, 2910-3043.

33. Gottfried, J. M. Surface Chemistry of Porphyrins and Phthalocyanines. *Surf. Sci. Rep.* **2015**, *70*, 259–379.

34. Nandi, G.; Chilukuri, B.; Hipps, K. W.; Mazur, U. Surface Directed Reversible Imidazole Ligation to Nickel(II) Octaethylporphyrin at the Solution/Solid Interface: A Single Molecule Level Study. *Phys. Chem. Chem. Phys.* **2016**, *18*, 20819-20829.

35. Oncel, N.; Bernasek, S. L. Ni(II)- and Vanadyloctaethylporphyrin Self-Assembled Layers Formed on Bare and 5-(Octadecyloxy)isophthalic Acid Covered Graphite. *Langmuir* **2009**, *25*, 9290-9295.

36. Chin, Y.; Panduwinata, D.; Sintic, M.; Sum, T. J.; Hush, N. S.; Crossley, M. J.; Reimers, J. R. Atomic-Resolution Kinked Structure of an Alkylporphyrin on Highly Ordered Pyrolytic Graphite. *J. Phys. Chem. Lett.* **2011**, *2*, 62–66.

37. Friesen, B. A.; Bhattarai, A.; Mazur, U.; Hipps, K. W. Single Molecule Imaging of Oxygenation of Cobalt Octaethylporphyrin at the Solution/Solid Interface: Thermodynamics from Microscopy. *J. Am. Chem. Soc.* **2012**, *134*, 14897-14904.

38. Gopakumar, T. G.; Tang, H.; Morillo, J.; Berndt, R. Transfer of Cl Ligands Between Adsorbed Iron Tetraphenylporphyrin Molecules. *J. Am. Chem. Soc.* **2012**, *134*, 11844-11847.

39. Hieringer, W.; Flechtner, K.; Kretschmann, A.; Seufert, K.; Auwarter, W.; Barth, J. V.; Gorling, A.; Steinruck, H. P.; Gottfried, J. M. The Surface Trans Effect: Influence of Axial Ligands on the Surface Chemical Bonds of Adsorbed Metalloporphyrins. *J. Am. Chem. Soc.* **2011**, *133*, 6206-6222.

40. den Boer, D.; Li, M.; Habets, T.; Iavicoli, P.; Rowan, A. E.; Nolte, R. J. M.; Speller, S.; Amabilino, D. B.; De Feyter, S.; Elemans, J. A. A. W. Detection of Different Oxidation States of Individual Manganese Porphyrins During Their Reaction with Oxygen at a Solid/Liquid Interface. *Nat. Chem.* **2013**, *5*, 621-627.

41. Nicholls, D.; Ware, B.; Zhang, Z.; Oncel, N. A Scanning Tunneling Microscopy Study on Self-Assembled Fe(III) Meso-tetra(4-carboxyphenyl) Porphyrin Chloride Chains. *Thin Solid Films* **2013**, *534*, 308-311.

42. Hulsken, B.; Van Hameren, R.; Gerritsen, J. W.; Khoury, T.; Thordarson, P.; Crossley, M. J.; Rowan, A. E.; Nolte, R. J. M.; Elemans, J. A. A. W.; Speller, S. Real-Time Single-Molecule Imaging of Oxidation Catalysis at a Liquid-Solid Interface. *Nat. Nanotechnol.* **2007**, *2*, 285-289.

43. Li, M.; den Boer, D.; Iavicoli, P.; Adisoejoso, J.; Uji-i, H.; Van der Auweraer, M.; Amabilino, D. B.; Elemans, J. A. A. W.; De Feyter, S. Tip-Induced Chemical Manipulation of Metal Porphyrins at a Liquid/Solid Interface. *J. Am. Chem. Soc.* **2014**, *136*, 17418-17421.

44. Miyake, Y.; Tanaka, H.; Ogawa, T. Scanning Tunneling Microscopy Investigation of Vanadyl and Cobalt(II) Octaethylporphyrin Self-Assembled Monolayer Arrays on Graphite. *Colloids Surf., A* **2008**, *313*, 230-233.

45. Ferreira, Q.; Alcacer, L.; Morgado, J. Stepwise Preparation and Characterization of Molecular Wires Made of Zinc Octaethylporphyrin Complexes Bridged by 4,4 '-Bipyridine on HOPG. *Nanotechnology* **2011**, *22*, 435604.

46. Ferreira, Q.; Braganca, A. M.; Alcacer, L.; Morgado, J. Conductance of Well-Defined Porphyrin Self-Assembled Molecular Wires up to 14 nm in Length. *J. Phys. Chem. C* **2014**, *118*, 7229-7234.

47. Otsuki, J.; Seki, E.; Taguchi, T.; Asakawa, M.; Miyake, K. STM Observation of Labile Axial Ligands to Zinc Porphyrin at Liquid/Solid Interface. *Chem. Lett.* **2007**, *36*, 740-741.

48. Ikeda, T.; Asakawa, M.; Goto, M.; Miyake, K.; Ishida, T.; Shimizu, T. STM Observation of Alkyl-Chain-Assisted Self-Assembled Monolayers of Pyridine-Coordinated Porphyrin Rhodium Chlorides. *Langmuir* **2004**, *20*, 5454-5459.

49. Visser, J.; Katsonis, N.; Vicario, J.; Feringa, B. L. Two-Dimensional Molecular Patterning by Surface-Enhanced Zn-Porphyrin Coordination. *Langmuir* **2009**, *25*, 5980–5985.

50. Brancato-Buentello, K. E.; Coutsolelos, A. G.; Scheidt, W. R. Chloro(2,3,7,8,12,13,17,18-octaethylporphinato)gallium(III). *Acta Crystallogr., Sect. C: Cryst. Struct. Commun.* **1996**, *52*, 2707-2710.

51. Balch, A. L.; Latosgrazynski, L.; Noll, B. C.; Phillips, S. L. Acetylide Complexes of Diamagnetic Gallium(III) and Paramagnetic Iron(III) Porphyrins. *Inorg. Chem.* **1993**, *32*, 1124-1129.

52. Carmalt, C. J.; King, S. J. Gallium(III) and Indium(III) Alkoxides and Aryloxides. *Coord. Chem. Rev.* **2006**, *250*, 682-709.

53. Boukhris, A.; Lecomte, C.; Coutsolelos, A.; Guilard, R. Alkylsulfonato(Porphyrinato)Gallium(III): Crystal-Structure Determination of Methylsulfonato(Octaethyl-2,3,7,8,12,13,17,18-Porphyrinato)-Gallium(III). *J. Organomet. Chem.* **1986**, *303*, 151-165.

54. Ohno, O.; Kaizu, Y.; Kobayashi, H. Luminescence of Some Metalloporphins Including the Complexes of the IIIb Metal Group. *J. Chem. Phys.* **1985**, *82*, 1779-1787.

55. Coutsolelos, A.; Guilard, R.; Bayeul, D.; Lecomte, C. Gallium(III) Porphyrins - Synthesis and Physicochemical Characteristics of Halogeno Gallium(III) Porphyrins X-Ray Crystal-Structure of Chloro-(5,10,15,20-Tetraphenylporphyrinato) Gallium(III). *Polyhedron* **1986**, *5*, 1157-1164.

56. Coutsolelos, A.; Guilard, R.; Boukhris, A.; Lecomte, C. Synthesis and Characterization of Azido-Gallium(III) and Thiocyanato-Gallium(III) Porphyrins - Crystal-Structure of Azido(2,3,7,8,12,13,17,18-octaethyl-porphyrinato)Gallium(III). *J. Chem. Soc., Dalton Trans.* **1986**, 1779-1783.

57. Kadish, K. M.; Boisselier-Cocolios, B.; Coutsolelos, A.; Mitaine, P.; Guilard, R. Electrochemistry and Spectroelectrochemistry of Gallium(III) Porphyrins - Redox Properties of 5-Coordinate Ionic and σ-Bonded Complexes. *Inorg. Chem.* **1985**, *24*, 4521-4528.

58. Kadish, K. M.; Xu, Q. Y.; Barbe, J. M.; Guilard, R. Synthesis and Reactivity of σ-Bonded Silicon Metalloporphyrins - Spectroscopic Characterization and Electrochemistry of $(P)Si(R)_2$, (P)Si(R)X, and $(P)SiX_2$, Where R = $C_6H_5$ or $CH_3$ and X = $OH^-$ or $ClO_4^-$. *Inorg. Chem.* **1988**, *27*, 1191-1198.

59. Okamura, T.; Iwamura, T.; Yamamoto, H.; Ueyama, N. Synthesis and Molecular Structures of S-2-$FcNHCOC_6H_4SH$ and [$M^{III}$(OEP)(S-2-$FcNHCOC_6H_4$)] (Fc = ferrocenyl, M = Fe, Ga): Electrochemical Contributions of Intramolecular SH···O=C and NH···S Hydrogen Bonds. *J. Organomet. Chem.* **2007**, *692*, 248-256.

60. Okamura, T.; Nishikawa, N.; Ueyama, N.; Nakamura, A. Synthesis and Structures of (Porphinato)(Thiolato)Gallium(III) Complexes. *Chem. Lett.* **1998**, 199-200.

61. Guilard, R.; Zrineh, A.; Tabard, A.; Courthaudon, L.; Han, B. C.; Ferhat, M.; Kadish, K. M. Metalloporphyrins with Metal Metal σ-Bonds - Synthesis, Spectroscopic Characterization, and Electrochemistry of $(P)MRe(Co)_5$ Where P Is the Dianion of Octaethylporphyrin (OEP) or Tetraphenylporphyrin (TPP) and M = Al, Ga, In or Tl. *J. Organomet. Chem.* **1991**, *401*, 227-243.

62. Kadish, K. M.; Cornillon, J. L.; Coutsolelos, A.; Guilard, R. Synthesis, Electrochemistry, and Ligand-Addition Reactions of Gallium(III) Porphyrins. *Inorg. Chem.* **1987**, *26*, 4167-4173.

63. Iverson, C. P. Ph. D. Thesis. The University of Chicao, Chicago, IL, 2012.

64. Lau, W.-Y. Ph. D. Thesis. The University of Chicago, Chicago, IL, 2016.

65. Scudiero, L.; Hipps, K. W. Controlled Manipulation of Self-Organized Ni(II)-Octaethylporphyrin Molecules Deposited from Solution on HOPG with a Scanning Tunneling Microscope. *J. Phys. Chem. C* **2007**, *111*, 17516-17520.

66. Ogunrinde, A.; Hipps, K. W.; Scudiero, L. A Scanning Tunneling Microscopy Study of Self-Assembled Nickel(II) Octaethylporphyrin Deposited from Solutions on HOPG. *Langmuir* **2006**, *22*, 5697-5701.

67. Bhattarai, A.; Mazur, U.; Hipps, K. W. Desorption Kinetics and Activation Energy for Cobalt Octaethylporphyrin from Graphite at the Phenyloctane Solution-Graphite Interface: An STM Study. *J. Phys. Chem. C* **2015**, *119*, 9386-9394.

68. Bhattarai, A.; Marchbanks-Owens, K.; Mazur, U.; Hipps, K. W. Influence of the Central Metal Ion on the Desorption Kinetics of a Porphyrin from the Solution/HOPG Interface. *J. Phys. Chem. C* **2016**, *120*, 18140-18150.

69. Oncel, N.; Bernasek, S. L. The Effect of Molecule-Molecule and Molecule-Substrate Interaction in the Formation of Pt-Octaethyl Porphyrin Self-Assembled Monolayers. *Appl. Phys. Lett.* **2008**, *92*, 133305-133305-3.

70. Bussetti, G.; Trabattoni, S.; Uttiya, S.; Sassella, A.; Riva, M.; Picone, A.; Brambilla, A.; Duò, L.; Ciccacci, F.; Finazzi, M. Controlling Drop-Casting Deposition of 2D Pt-Octaethyl Porphyrin Layers on Graphite. *Synth. Met.* **2014**, *195*, 201-207.

71. Zou, Z. Q.; Wei, L. Y.; Chen, F.; Liu, Z. M.; Thamyongkit, P.; Loewe, R. S.; Lindsey, J. S.; Mohideen, U.; Bocian, D. F. Solution STM Images of Porphyrins on HOPG Reveal That Subtle Differences in Molecular Structure Dramatically Alter Packing Geometry. *J. Porphyrins Phthalocyanines* **2005**, *9*, 387-392.

72. Hao, Y. B.; Weatherup, R. S.; Eren, B.; Somorjai, G. A.; Salmeron, M. Influence of Dissolved $O_2$ in Organic Solvents on CuOEP Supramolecular Self-Assembly on Graphite. *Langmuir* **2016**, *32*, 5526-5531.

73. Zou, Z. Q.; Chen, F. In Situ Scanning Tunneling Microscopy Studies of Zinc(II) Octaethylporphyrin Arrays Self-Assembled on Graphite and Au(111) Surfaces in Organic Solution. *J. Appl. Phys.* **2008**, *103*, 094304-094304-4.

74. Cullen, D. L.; Meyer, E. F. Crystal and Molecular-Structure of Triclinic Form of 1,2,3,4,5,6,7,8-Octaethylporphinatonickel(II) - Comparison with Tetragonal Form. *J. Am. Chem. Soc.* **1974**, *96*, 2095-2102.

75. Brennan, T. D.; Scheidt, W. R.; Shelnutt, J. A. New Crystalline Phase of (Octaethylporphinato)Nickel(II) - Effects of π-π-Interactions on Molecular-Structure and Resonance Raman-Spectra. *J. Am. Chem. Soc.* **1988**, *110*, 3919-3924.

76. Strauss, S. H.; Silver, M. E.; Long, K. M.; Thompson, R. G.; Hudgens, R. A.; Spartalian, K.; Ibers, J. A. Comparison of the Molecular and Electronic-Structures of (2,3,7,8,12,13,17,18-Octaethylporphyrinato)Iron(II) and (Trans-7,8-Dihydro-2,3,7,8,12,13,17,18-Octaethyl-Porphyrinato)Iron(II). *J. Am. Chem. Soc.* **1985**, *107*, 4207-4215.

77. Scheidt, W. R.; Turowskatyrk, I. Crystal and Molecular-Structure of (Octaethylporphinato)Cobalt(II) - Comparison of the Structures of 4-Coordinate M(TPP) and M(OEP) Derivatives (M=Fe-Cu) - Use of Area Detector Data. *Inorg. Chem.* **1994**, *33*, 1314-1318.

78. Pak, R.; Scheidt, W. R. Structure of (2,3,7,8,12,13,17,18-Octaethylporphinato)Copper(II). *Acta Crystallogr., Sect. C: Cryst. Struct. Commun.* **1991**, *47*, 431-433.

79. Meyer, E. F. Crystal and Molecular Structure of Nickel(II)Octaethylporphyrin. *Acta Crystallogr., Sect. B: Struct. Crystallogr. Cryst. Chem.* **1972**, *B 28*, 2162-&.

80. Gruden-Pavlovic, M.; Grubisic, S.; Zlatar, M.; Niketic, S. R. Molecular Mechanics Study of Nickel(II) Octaethylporphyrin Adsorbed on Graphite(0001). *Int. J. Mol. Sci.* **2007**, *8*, 810-829.

81. Chilukuri, B.; Mazur, U.; Hipps, K. W. Effect of Dispersion on Surface Interactions of Cobalt(II) Octaethylporphyrin Monolayer on Au(111) and HOPG(0001) Substrates: A Comparative First Principles Study. *Phys. Chem. Chem. Phys.* **2014**, *16*, 14096-14107.

82. Yin, S. X.; Wang, C.; Qiu, X. H.; Xu, B.; Bai, C. L. Theoretical Study of the Effects of Intermolecular Interactions in Self-Assembled Long-Chain Alkanes Adsorbed on Graphite Surface. *Surf. Interface Anal.* **2001**, *32*, 248-252.

83. Bunz, U. H. F. Poly(aryleneethynylene)s: Syntheses, Properties, Structures, and Applications. *Chem. Rev.* **2000**, *100*, 1605-1644.

84. Shipway, A. N.; Katz, E.; Willner, I. Nanoparticle Arrays on Surfaces for Electronic, Optical, and Sensor Applications. *ChemPhysChem* **2000**, *1*, 18-52.

85. Zhang, J. P.; Liu, Y.; Ke, Y. G.; Yan, H. Periodic Square-Like Gold Nanoparticle Arrays Templated by Self-Assembled 2D DNA Nanogrids on a Surface. *Nano. Lett.* **2006**, *6*, 248-251.

86. Katsonis, N.; Vicario, J.; Kudernac, T.; Visser, J.; Pollard, M. M.; Feringa, B. L. Self-Organized Monolayer of *meso*-Tetradodecylporphyrin Coordinated to Au(111). *J. Am. Chem. Soc.* **2006**, *128*, 15537–15541.

87. Hulsken, B.; van Hameren, R.; Thordarson, P.; Gerritsen, J. W.; Nolte, R. J. M.; Rowan, A. E.; Crossley, M. J.; Elemans, J. A. A. W.; Speller, S. Scanning Tunneling Microscopy and Spectroscopy Studies of Porphyrins at Solid–Liquid Interfaces. *Jpn. J. Appl. Phys.* **2006**, *45*, 1953–1955.

88. Plamont, R.; Kikkawa, Y.; Takahashi, M.; Kanesato, M.; Giorgi, M.; Chan Kam Shun, A.; Roussel, C.; Balaban, T. S. Nanoscopic Imaging of *meso*-Tetraalkylporphyrins Prepared in High Yields Enabled by Montmorrilonite K10 and 3 Å Molecular Sieves. *Chem. - Eur. J.* **2013**, *19*, 11293–11300.

89. Coenen, M. J. J.; den Boer, D.; van den Bruele, F. J.; Habets, T.; Timmers, K. A. A. M.; van der Maas, M.; Khoury, T.; Panduwinata, D.; Crossley, M. J.; Reimers, J. R.; van Enckevort, W. J. P.; Hendriksen, B. L. M.; Elemans, J. A. A. W.; Speller, S. Polymorphism in Porphyrin Monolayers: The Relation Between Adsorption Configuration and Molecular Conformation. *Phys. Chem. Chem. Phys.* **2013**, *15*, 12451–12458.

90. Coenen, M. J. J.; Cremers, M.; den Boer, D.; van den Bruele, F. J.; Khoury, T.; Sintic, M.; Crossley, M. J.; van Enckevort, W. J. P.; Hendriksen, B. L. M.; Elemans, J. A. A. W.; Speller, S. Little Exchange at the Liquid/Solid Interface: Defect-Mediated Equilibration of Physisorbed Porphyrin Monolayers. *Chem. Commun.* **2011**, *47*, 9666–9668.

91. Geng, J.; Kong, B.-S.; Yang, S. B.; Jung, H.-T. Preparation of Graphene Relying on Porphyrin Exfoliation of Graphite. *Chem. Commun.* **2010**, *46*, 5091–5093.

92. Langa, F.; Nierengarten, J. F., *Fullerenes: Principles and Applications*. 2nd ed.; Royal Society of Chemistry: Cambridge, 2011.

93. Verner, R. F.; Benvegnu, C., *Handbook on Fullerene: Synthesis, Properties and Applications*. Nova Science Publishers: New York, 2012.

94. Prato, M. [60]Fullerene Chemistry for Materials Science Applications. *J. Mat. Chem.* **1997**, *7*, 1097–1109.

95. Lu, L. Y.; Zheng, T. Y.; Wu, Q. H.; Schneider, A. M.; Zhao, D. L.; Yu, L. P. Recent Advances in Bulk Heterojunction Polymer Solar Cells. *Chem. Rev.* **2015**, *115*, 12666-12731.

96. Pivrikas, A.; Sariciftci, N. S.; Juška, G.; Österbacka, R. A Review of Charge Transport and Recombination in Polymer/Fullerene Organic Solar Cells. *Prog. Photovoltaics* **2007**, *15*, 677-696.

97. Otero, R.; Gallego, J. M.; Martín, N.; Miranda, R., Supramolecular Chemistry of Fullerenes on Solid Surfaces. In *Supramolecular Chemistry of Fullerenes and Carbon Nanotubes*, 1st ed.; Martín, N.; Nierengarten, J. F., Eds. Wiley-VCH: Verlag, 2012; pp 237-261.

98. Bonifazi, D.; Enger, O.; Diederich, F. Supramolecular [60]Fullerene Chemistry on Surfaces. *Chem. Soc. Rev.* **2007**, *36*, 390-414.

99. Haino, T.; Ikeda, T., Fullerene-Containing Supramolecular Polymers and Dendrimers. In *Supramolecular Chemistry of Fullerenes and Carbon Nanotubes*, 1st ed.; Martín, N.; Nierengarten, J. F., Eds. Wiley-VCH: Verlag, 2012; pp 173-202.

100. Sanchez, L.; Otero, R.; Gallego, J. M.; Miranda, R.; Martin, N. Ordering Fullerenes at the Nanometer Scale on Solid Surfaces. *Chem. Rev.* **2009**, *109*, 2081-2091.

101. Uemura, S.; Samori, P.; Kunitake, M.; Hirayama, C.; Rabe, J. P. Crystalline $C_{60}$ Monolayers at the Solid-Organic Solution Interface. *J. Mater. Chem.* **2002**, *12*, 3366-3367.

102. Teyssandier, J.; De Feyter, S.; Mali, K. S. Host-Guest Chemistry in Two-Dimensional Supramolecular Networks. *Chem. Commun.* **2016**, *52*, 11465-11487.

103. Theobald, J. A.; Oxtoby, N. S.; Phillips, M. A.; Champness, N. R.; Beton, P. H. Controlling Molecular Deposition and Layer Structure with Supramolecular Surface Assemblies. *Nature* **2003**, *424*, 1029-1031.

104. Blunt, M. O.; Russell, J. C.; Gimenez-Lopez, M. D.; Taleb, N.; Lin, X. L.; Schroder, M.; Champness, N. R.; Beton, P. H. Guest-Induced Growth of a Surface-Based Supramolecular Bilayer. *Nat. Chem.* **2011**, *3*, 74-78.

105. Li, M.; Deng, K.; Lei, S. B.; Yang, Y. L.; Wang, T. S.; Shen, Y. T.; Wang, C. R.; Zeng, Q. D.; Wang, C. Site-Selective Fabrication of Two-Dimensional Fullerene Arrays by Using a Supramolecular Template at the Liquid-Solid Interface. *Angew. Chem., Int. Ed.* **2008**, *47*, 6717-6721.

106. Griessl, S. J. H.; Lackinger, M.; Jamitzky, F.; Markert, T.; Hietschold, M.; Heckl, W. M. Room-Temperature Scanning Tunneling Microscopy Manipulation of Single $C_{60}$ Molecules at the Liquid-Solid interface: Playing Nanosoccer. *J. Phys. Chem. B* **2004**, *108*, 11556-11560.

107. Mena-Osteritz, E.; Bäuerle, P. Complexation of $C_{60}$ on a Cyclothiophene Monolayer Template. *Adv. Mater.* **2006**, *18*, 447-451.

108. MacLeod, J. M.; Ivasenko, O.; Fu, C. Y.; Taerum, T.; Rosei, F.; Perepichka, D. F. Supramolecular Ordering in Oligothiophene-Fullerene Monolayers. *J. Am. Chem. Soc.* **2009**, *131*, 16844-16850.

109. Pan, G. B.; Cheng, X. H.; Hoger, S.; Freyland, W. 2D Supramolecular Structures of a Shape-Persistent Macrocycle and Co-Deposition with Fullerene on HOPG. *J. Am. Chem. Soc.* **2006**, *128*, 4218-4219.

110. Piot, L.; Silly, F.; Tortech, L.; Nicolas, Y.; Blanchard, P.; Roncali, J.; Fichou, D. Long-Range Alignments of Single Fullerenes by Site-Selective Inclusion into a Double-Cavity 2D Open Network. *J. Am. Chem. Soc.* **2009**, *131*, 12864-12865.

# CHAPTER 2

## Axial Ligand Effects on the Structures of Self-Assembled Gallium–Porphyrin Monolayers on HOPG

**NOTE:** This work has previously been published in an alternative format in Kamm, J. M.; Iverson, C. P; Lau, W.-Y.; Hopkins, M. D. *Langmuir* **2016**, *32*, 487–495.

### 2.1. Introduction

The self-assembly of molecules into ordered 2D monolayers on planar surfaces has been extensively studied. Interest in these molecular arrays has been motivated, in part, by the prospect that they may have useful applications derived from the collective properties of their subunits and the nanometer length scales of their repeating patterns.[1-5] Among building blocks for these arrays, porphyrin complexes have been of particular interest because of the possibility that the diverse optical, photophysical, redox, and catalytic properties of these molecules could be used to enrich the functionality of the assemblies.[6-11] Structural studies of porphyrin monolayers using scanning tunneling microscopy (STM) have shown that robust, well-ordered arrays self-assemble on a variety of atomically flat substrates, including metals (e.g. Au(111), Cu(111)) and highly oriented pyrolytic graphite (HOPG), using deposition conditions that range from evaporation in ultra-high vacuum to benchtop, room-temperature immersion of substrates into porphyrin solutions.[8-11] The wide range of conditions under which ordered porphyrin arrays form makes them excellent systems both for fundamental physical studies and for developing scalable functionalized-surface materials.

Within the area of porphyrin surface chemistry, monolayers of metalloporphyrins that possess axial ligands have been much less studied than those composed of planar free-base and 4-coordinate metalloporphyrins. Monolayers of axially ligated metalloporphyrins are of potential

interest in several contexts. For metalloporphyrins whose axial ligation is characterized by comparatively small equilibrium binding constants, the reversibility of metal–ligand bond formation opens possibilities for catalysis, small-molecule sensing, or switchable modulation of the electronic properties of the assembly. Examples of these phenomena include the surface-enhanced reversible binding of $O_2$ to Co octaethylporphyrin (OEP) on HOPG,[12] axial-ligand-induced redox chemistry of metalloporphyrins on surfaces,[13, 14] and the surface *trans* effect observed with axial-ligand binding to Fe, Co, and Zn porphyrin complexes on Ag(111).[15] Axially ligated metalloporphyrins are also of interest because they could provide bottom-up scaffolds for construction of supramolecular structures perpendicular to the surface, as has been illustrated by HOPG-supported Zn(OEP) coordination polymers[16, 17] and by frameworks for the 3D organization of functional units that are templated to the pattern of the underlying 2D monolayer.[18]

One fundamental difference between the structures of 4-coordinate and 5-coordinate metalloporphyrins is that, whereas 4-coordinate porphyrins are usually planar, 5-coordinate porphyrins generally possess domed structures in which the metal center is positioned above the plane of the porphyrin macrocycle.[19] Crystal structures show that five-coordinate gallium OEPs[20-24] afford domed structures with the gallium atom displaced above the $N_4$ plane which is in turn slightly above the least-squares $C_{20}$ plane. The extent of the core doming effect in Ga(OEP)X compounds noticeably varies depending on the identity of axial ligand, with Ga-$N_4$ displacements ranging between 0.34 Å for Ga(OEP)($SO_3$Me)[21] and 0.457 Å for Ga(OEP)(SPh).[23] In contrast, their four-coordinate analogs have planar (Ni(II) triclinic forms,[25, 26] Fe(II),[27] Co(II),[28] Cu(II)[29]) or slightly ruffled (Ni(II) tetragonal form[30]) cores. The crystal structure of

Sn(II)OEP[25] shows that the tin atom lies 1.018 Å from the $N_4$ plane, though this distortion is expected for heavy elements.

Such structural distortions are likely to affect the nature and strength of surface–molecule interactions and, therefore, the stability and/or structures of their monolayers. Computational studies have shown that the adsorption of 4-coordinate M(OEP) complexes onto HOPG is characterized by a complex balance of forces that include electrostatic adsorption energies, charge redistribution, and changes to the porphyrin core due to π-π stacking and metal–graphite interactions,[31, 32] all of which, in principle, could be perturbed by distortions to the porphyrin core planarity. However, there have not been systematic experimental studies of how the stability and structures of metalloporphyrin monolayers depend on the nature of the axial ligand.

In order to probe the extent to which the properties of 5-coordinate porphyrin monolayers are sensitive to the nature of the axial ligand, the structures of Ga(OEP)X monolayers on HOPG have been studied by STM. OEP was chosen as the porphyrin ligand for this study because its compact side chains minimize the contributions of the peripheral substituents to the porphyrin–surface interaction,[33] thus enhancing the consequences of structural changes brought about by the axial ligand. Further, its 4-coordinate M(OEP) complexes form well-ordered and well-studied monolayers on HOPG at the solid–air and solid–liquid interfaces (M = Ni,[34-38] Co,[12, 37, 39, 40] Pt,[41, 42] Cu,[43, 44] Zn[43, 45]). Gallium(III) was selected as the metal for probing axial-ligand effects because Ga(OEP)X compounds possess domed structures in which the displacement of the Ga center above the OEP $N_4$ plane varies as a function of axial ligand.[20-24] In this chapter, the molecular and monolayer structures of Ga(OEP)X derivatives with axial ligands that span a range of electron withdrawing and donating character (Ga(OEP)X, X = $O_3SCF_3$, Cl, Br, I, CCPh) are described. Density functional theory calculations of these complexes show that the nonplanar

distortion is a sensitive function of the axial ligand. STM studies of their monolayers on HOPG show that while all derivatives exhibit the same 2D structure, the extent of surface coverage depends on the X ligand. Further, Ga(OEP)I is capable of forming a bilayer structure whose periodicity is distinct from that of other derivatives.

**2.2. Experimental**

Detailed experimental procedures and characterization for all complexes can be found in Chapter 6.1. Ga(OEP)Cl was prepared by reacting $GaCl_3$ with $H_2OEP$ under refluxing acidic conditions and was used as the starting material for all other compounds. Ga(OEP)Br, Ga(OEP)I, and Ga(OEP)($O_3SCF_3$) were prepared by reacting Ga(OEP)Cl with the corresponding trimethysilyl halide/pseudohalide at room temperature. Ga(OEP)(CCPh) was prepared by first reacting HCCPh with $^n$BuLi to generate LiCCPh, which was then reacted with Ga(OEP)Cl at room temperature to yield the final product. All compounds were characterized by $^1$H NMR, UV-vis, and LDI-MS. While all compounds have been reported in the literature, not all have been fully characterized, and additional characterization details were recorded and reported in Section 6.1.5 as necessary.

Further, the gas-phase optimized structures of all compounds were calculated by density functional theory (DFT) as described in Section 6.1.2. Both the minimum-energy structures and the structure predicted to be adopted by the molecules on the surface (with all eight ethyl chains oriented away from the surface) were calculated and the structures and energies compared. The self-assembly of the compounds at the solid-liquid (1-phenyloctane) interface was studied via scanning tunneling microscopy (STM). Detailed deposition and structural analysis methods can be found in Sections 6.1.3 and 6.1.4.

## 2.3. Results and Discussion

**2.3.1. Synthesis and Characterization of Ga(OEP)X Compounds.** The compounds Ga(OEP)Br,[46] Ga(OEP)I,[47] and Ga(OEP)(OTf)[21] have been synthesized previously by reactions between Ga(OEP)Cl and HX in methanol or toluene, with the conditions for the iodo compound requiring an extended reaction time under a continuous flow of HI gas. We wondered if these compounds could be synthesized more efficiently and under milder conditions by reactions between Ga(OEP)Cl and $SiMe_3X$ in toluene at room temperature, following the example of the synthesis of $Zr(OEP)(OTf)_2$ from the reaction between $Zr(OEP)Cl_2$ and $SiMe_3(OTf)$.[48] The progress of these reactions is conveniently monitored by $^1$H NMR spectroscopy, in which the chemical shift of the *meso* C–H resonance is diagnostic (X = Cl, δ 10.36; Br, 10.41; I, 10.43; OTf, 10.44). In general, after a single treatment of Ga(OEP)Cl with $SiMe_3X$ a trace amount of unreacted Ga(OEP)Cl could be detected by $^1$H NMR in the reaction mixture; thus, the procedure was repeated, after which unreacted Ga(OEP)Cl was no longer detected. The synthesis of Ga(OEP)(CCPh) proceeds readily when Ga(OEP)Cl is reacted with LiCCPh. All compounds were characterized by $^1$H NMR spectroscopy, electronic-absorption spectroscopy, and LDI-TOF mass spectrometry.

The $^1$H NMR spectra of the compounds (Figures 6.2–6.3, 6.5–6.8) are consistent with literature reports of metallated octaethylporphyrin complexes.[21, 47, 49-51] A notable feature of this type of compound is a complex multiplet at ca. 4.0 ppm attributable to the methylene protons of the ethyl chain. It has been hypothesized in related thallium[49] and mercury[50] octaethylporphyrin complexes that such inequivalence is due to diasteriotopicity brought on by the metal atom being out of the plane of the porphyrin macrocycle. Further, significant upfield shifts of ligated phenyl acetylide resonances in Ga(OEP)(CCPh), as compared to those of the free phenylacetylene

ligand, are noted. These shifts are due to the strong ring current influence of the porphyrin, and has the largest effect on the protons closest to the porphyrin ring (7.40 → 5.32 ppm for *o*-$C_6H_5$ resonance compared to 6.89 → 6.00 ppm for *p*-$C_6H_5$ resonance in $C_6D_6$).

Likewise, the UV-vis spectra of all compounds taken in toluene (Figure 6.9, Table 6.2) are in good agreement with reports of metallated octaethylporphyrin complexes in solution.[21, 22, 51-55] Upon metalation, the four Q-bands ($S_0 \rightarrow S_1$) observed for the free-base are reduced to two, as the symmetry of the molecule is increased. In all Ga(OEP)X cases reported here, Q(0,0) is higher in intensity than Q(1,0). The position of these bands is somewhat sensitive to ligand substitution, with a 12 nm variation in Q(1,0) observed between Ga(OEP)($O_3SCF_3$) and Ga(OEP)(CCPh) (531 nm and 543 nm, respectively), but very little variation observed across the halide series (see Table 6.2). Red-shifting in metalloporphyrins can result from distortions from planarity;[56] the shifts observed correlate with predicted out-of-plane gallium atom displacements calculated by density functional theory (discussed in next section). The prominent Soret bands ($S_0 \rightarrow S_2$) range from 399 nm (Ga(OEP)($O_3SCF_3$)) to 416 nm (Ga(OEP)I) with an associated vibronic feature to the blue of this. Additional bands in the UV can be observed, a combination of weak porphyrin and ligand-derived absorption features.

Ga(OEP)Br was additionally characterized by $^{13}C\{^1H\}$ NMR spectroscopy and elemental analysis, as characterization data were not provided in the original report of this compound.[46] The formulation of Ga(OEP)(CCPh) was confirmed by LDI-TOF mass spectrometric data, because the $^1H$ NMR chemical shifts for the samples prepared in this study differ from those reported previously by up to 0.5 ppm and the electronic-absorption band maxima differ in wavelength by up to 10 nm (Table S2).[51] $^{19}F$-NMR of Ga(OEP)($O_3SCF_3$) in $C_6D_6$ shows one singlet at –80.36 ppm, confirming only one fluorine containing material is present. All

compounds are stable in $C_6D_6$ solution in air for at least 3 days, as monitored by $^1$H NMR spectroscopy; thus, they are stable well beyond the time scale of the STM measurements, which are on the order of hours. Solutions of Ga(OEP)I and Ga(OEP)(CCPh) decompose into unknown porphyrinic products on extended exposure to air over several weeks.

**2.3.2. DFT Calculations of Ga(OEP)X Compounds.** The gas-phase molecular structures of Ga(OEP)X compounds were calculated using density functional theory (DFT) in order to probe the influence of the axial ligand on the structure about the Ga center and the planarity of the porphyrin ring. The calculated structures of the complexes are shown in Figure 2.1. The core porphyrin structures of all compounds except Ga(OEP)($O_3SCF_3$) exhibit approximate $C_{4v}$ symmetry, as indicated by equivalences among Ga–N bond distances and N–Ga–X bond angles. For Ga(OEP)($O_3SCF_3$), the axial asymmetry of the triflate ligand produces small distortions from $C_{4v}$ symmetry ($\angle$(N–Ga–O) = 96.5–102.4˚, $d$(Ga–N) = 2.029–2.032 Å, Table 2.1). For all compounds, the minimum-energy geometry is that in which the OEP methyl groups lie on the opposite side of the OEP plane from axial ligand. The rotamer in which they lie on the same side of the OEP plane as the axial ligand, as expected when the complex is adsorbed to HOPG (vide infra),[36, 57] is very close in energy.

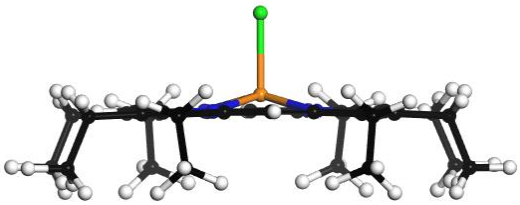

Ga(OEP)Cl

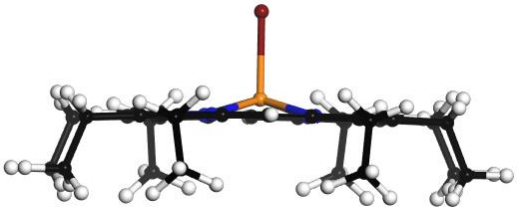

Ga(OEP)Br

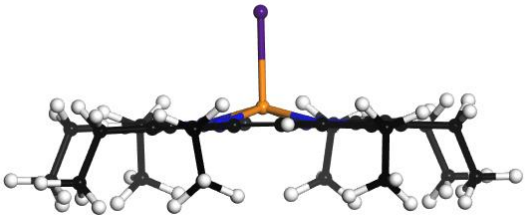

Ga(OEP)I

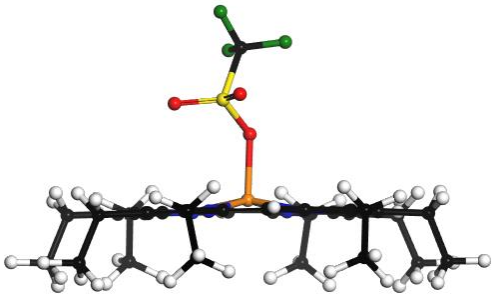

Ga(OEP)($O_3SCF_3$)

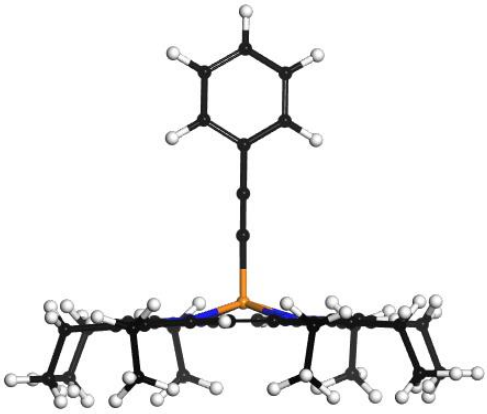

Ga(OEP)(CCPh)

**Figure 2.1.** Calculated molecular structures of Ga(OEP)X complexes. Atoms are color coded: Ga, orange; N, blue; C, black; H, white; Cl, lime green; Br, brown; I, purple; O, red; S, yellow; F, green.

All Ga(OEP)X compounds are calculated to possess a domed structure in which the Ga atom is positioned above the plane of the porphyrin ring (Figures 2.1 and 2.2); such distortions have

been observed experimentally in the crystal structures of similar Ga(OEP)X compounds.[20-24] The Ga atom is situated 0.34–0.50 Å above the $N_4$ plane, which in turn lies ~0.02–0.05 Å above the least-squares plane defined by the $C_{20}$ ring (Table 6.3). The out-of-plane distortions for the rotamer in which the OEP methyl groups are oriented toward the X ligand are of similar magnitude (Table 6.3). The lower and upper limits of the range of Ga displacement are defined, respectively, by Ga(OEP)($O_3SCF_3$) (Ga–$N_4$, 0.336 Å; $N_4$–$C_{20}$, 0.017 Å) and Ga(OEP)(CCPh) (Ga–$N_4$, 0.495 Å; $N_4$–$C_{20}$, 0.048 Å), with the three halide derivatives having roughly equal intermediate domed distortions (Ga–$N_4$, 0.445–0.452 Å; $N_4$–$C_{20}$, 0.026–0.034 Å). Thus, the nature of the axial ligand has the potential to affect the contact distance between the Ga atom and HOPG surface in monolayers of Ga(OEP)X compounds.

**Table 2.1.** Selected Bond Distances (Å) and Angles (°) for Ga(OEP)X Complexes Calculated by Density Functional Theory.

| | | X | | | | |
|---|---|---|---|---|---|---|
| Nuclei | Cl (exptl)[20] | Cl | Br | I | $O_3SCF_3$ | CCPh |
| Ga–X | 2.2397(13) | 2.2201 | 2.3799 | 2.6011 | 1.9348 | 1.9559 |
| Ga–N(1) | 2.033(4) | 2.054 | 2.054 | 2.054 | 2.030 | 2.068 |
| Ga–N(2) | 2.030(4) | 2.054 | 2.054 | 2.054 | 2.029 | 2.068 |
| Ga–N(3) | 2.038(4) | 2.054 | 2.054 | 2.055 | 2.032 | 2.068 |
| Ga–N(4) | 2.037(4) | 2.054 | 2.054 | 2.055 | 2.030 | 2.068 |
| N(1)–Ga–X | 102.2(1) | 102.5 | 102.6 | 103.0 | 100.3 | 103.9 |
| N(2)–Ga–X | 100.9(1) | 102.5 | 102.7 | 103.0 | 102.4 | 103.9 |
| N(3)–Ga–X | 101.3(1) | 102.5 | 102.4 | 102.4 | 98.8 | 103.9 |
| N(4)–Ga–X | 100.8(1) | 102.5 | 102.5 | 102.5 | 96.5 | 103.8 |

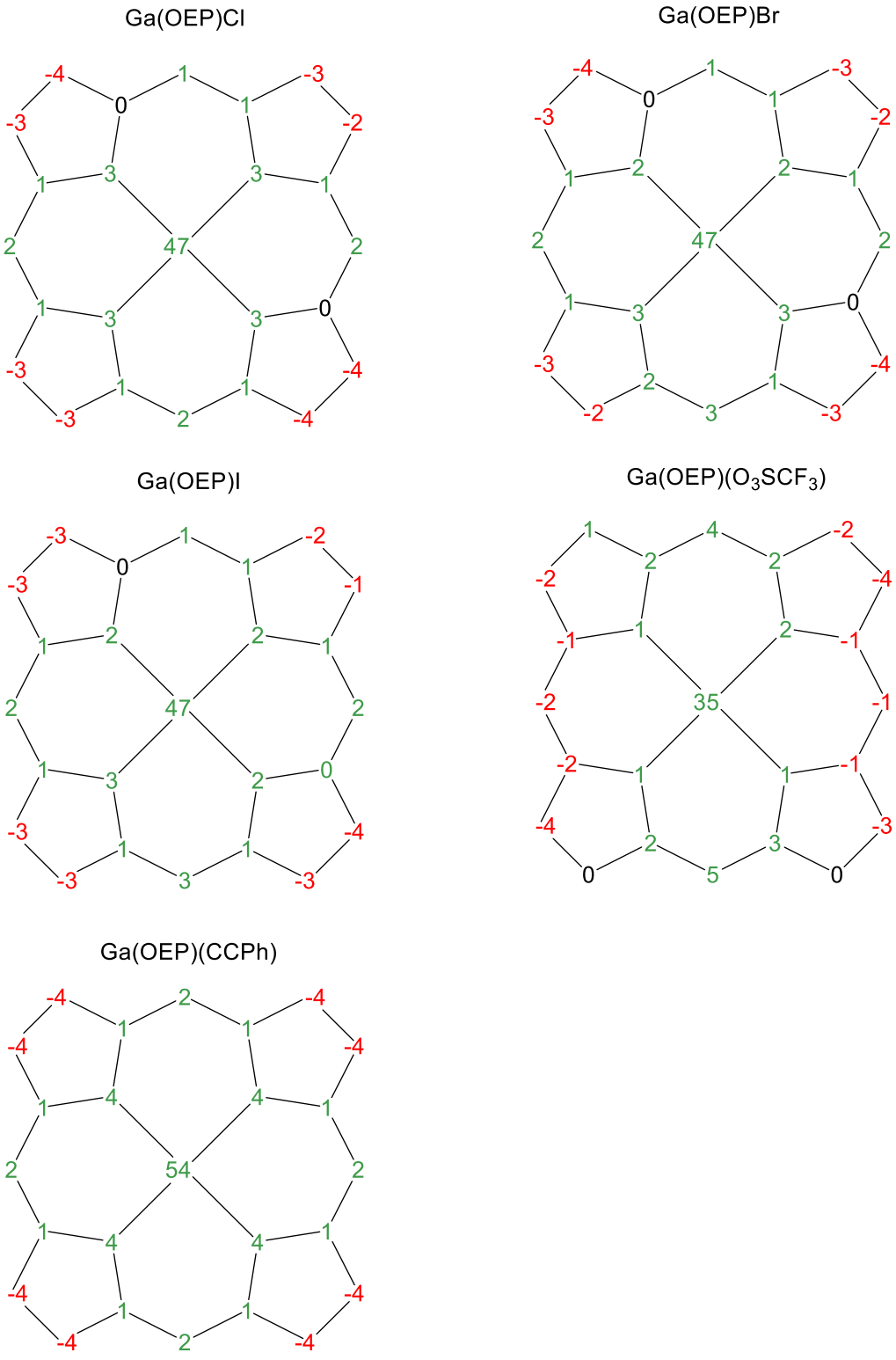


**Figure 2.2.** Calculated (DFT) displacements of Ga(OEP)X nuclei from the mean plane of the $C_{20}N_4$ OEP macrocycle. Ethyl groups and X ligands are not shown. Displacements are given in 0.01 Å.

**2.3.3. STM Imaging of Ga(OEP)X on HOPG.** Deposition of a 1-phenyloctane solution of Ga(OEP)X compounds on HOPG results in their self-assembly into well-ordered monolayers, as determined by STM imaging of these samples at the solid–liquid interface. The monolayers were studied at two concentrations: 0.25 mM (all compounds) and 0.5 mM (all compounds except Ga(OEP)($O_3SCF_3$), whose saturation solubility in 1-phenyloctane is < 0.5 mM). For each compound, the lattice parameters (vide infra) at the two concentrations are statistically indistinguishable. Ordered arrays whose widths span hundreds of nanometers are observed. Representative large-scale images for Ga(OEP)Cl and Ga(OEP)Br are shown in Figure 2.3. For samples at the higher concentration (0.5 mM), large-scale images (100 nm × 100 nm) typically do not exhibit regions of exposed graphite by the time the first image is acquired following deposition (i.e., within 5–10 minutes). At the lower concentration (0.25 mM), regions of exposed graphite are observed in the earliest images of the monolayers; these regions gradually fill in for Ga(OEP)Cl, Ga(OEP)Br and Ga(OEP)I (see Figure 2.4 for example), but persist for Ga(OEP)(CCPh) and Ga(OEP)($O_3SCF_3$) (Figure 2.8a). Except as noted below for Ga(OEP)I, the possibility that multilayer porphyrin structures were being observed was excluded by examining the height of the porphyrin layer relative to that of the adjacent bare graphite surface at the edges of the arrays.

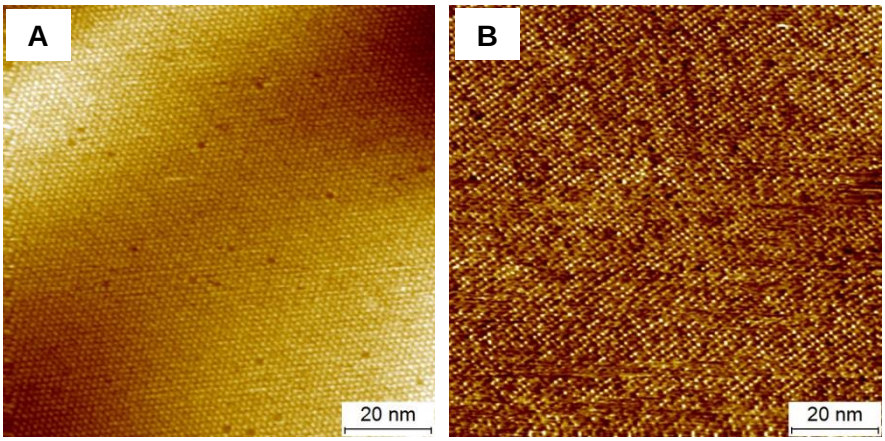


**Figure 2.3.** STM images of (A) Ga(OEP)Cl and (B) Ga(OEP)Br on HOPG at the solid–liquid interface (1-phenyloctane, 0.5 mM) showing long-range ordering of the monolayers. The images were acquired at: (A) $I$ = 10 pA, $V$ = –600 mV; (B) $I$ = 15 pA, $V$ = –500 mV.

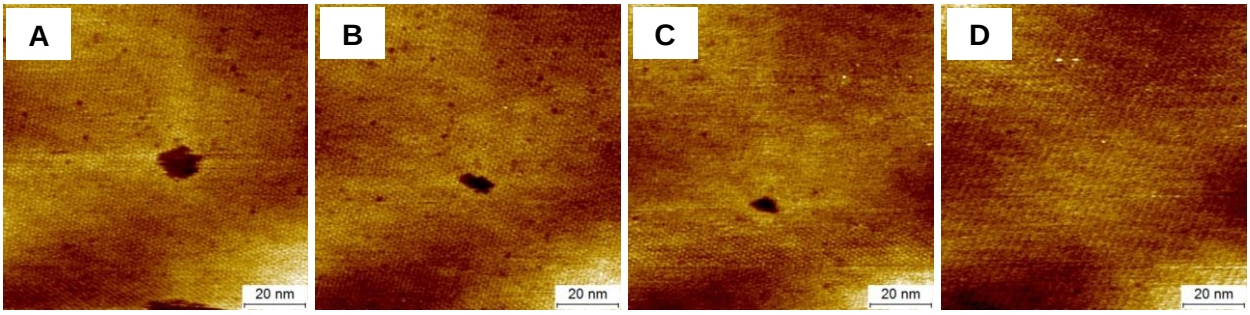


**Figure 2.4.** STM images of Ga(OEP)Cl on HOPG at the solid–liquid interface (1-phenyloctane, 0.25 mM) at various times following deposition, showing the filling in of a region of exposed graphite: (A) $t$ = 14 min; (B) $t$ = 16 min; (C) $t$ = 20 min; (D) $t$ = 22 min. All images were acquired at $I$ = 8 pA, $V$ = –500 mV.

STM images at higher spatial resolution of Ga(OEP)Cl and Ga(OEP)Br monolayers on HOPG show that individual porphyrin molecules appear either as bright dots against a flat background or as ring-shaped features, depending on the bias voltage. The images and cross-sectional profiles for Ga(OEP)Cl displaying the dot and ring features are shown in Figures 2.5a and 2.5b, respectively. The corresponding data for Ga(OEP)Br (Figure 2.5c and 2.5d) are very similar to those for Ga(OEP)Cl. The spacing of features is observed to be periodic; where defects in the lattice are observed, they appear to have no effect on the periodicity of adjacent molecules. The chemical nature of these defects is not yet understood. Possibilities include that the site is occupied by a Ga(OEP)X compound whose appearance is affected by an underlying HOPG

defect; a vacancy in the monolayer (which may be filled by one or more solvent molecules); or a site occupied by a four-coordinate M(OEP) compound. This latter possibility either requires the presence of an impurity that is undetectable by NMR spectroscopy (i.e., < 0.5%) or from the loss of the X ligand. Attempts to induce these defects by changing the bias and current settings proved unsuccessful, suggesting that they are not a result of the STM imaging process.

In a previous STM study of Ni(OEP) monolayers on HOPG by Ogunrinde, et al., it was observed that the Ni(OEP) molecules appear either as a large bright region or a bright ring with a dark center, depending on the bias voltage.[36] These images were assigned as representing tunneling through the central region of the porphyrin ring and through the porphyrin periphery, respectively. By analogy, the dot features (Figure 2.5a and 2.5c) are attributed to tunneling through the Ga–X units and the ring features (Figures 2.5b and Figure 2.5d) are attributed to the porphyrin periphery. These observations indicate that the porphyrins are assembled on the surface with the porphyrin macrocycle parallel to the HOPG plane and the Ga–X bond perpendicular to the surface.

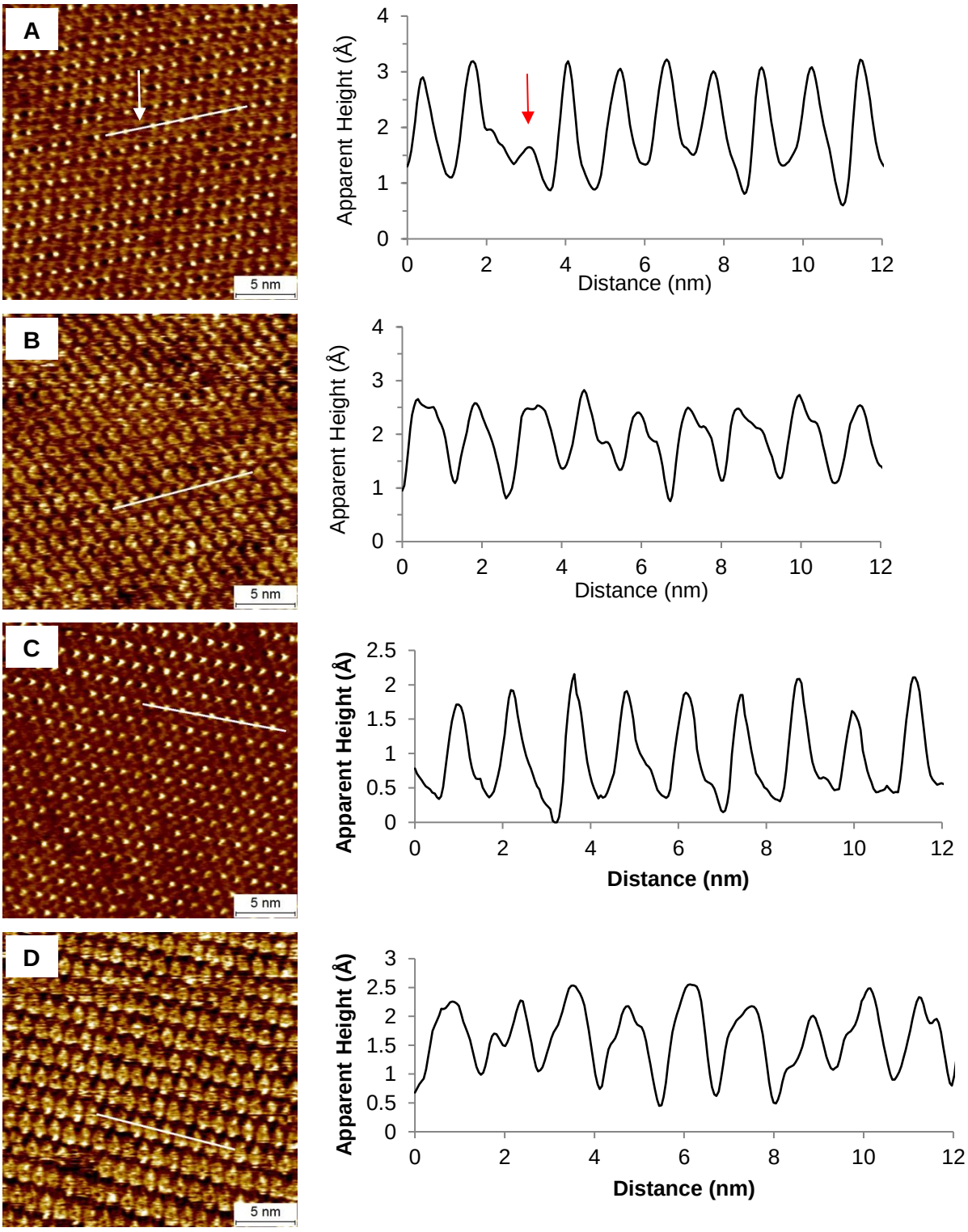


**Figure 2.5.** STM images and cross-sectional profiles of Ga(OEP)Cl (a and b) and Ga(OEP)Br (c and d) monolayers on HOPG at the solid–liquid interface (1-phenyloctane, 0.5 mM): (a) $I$ = 22 pA, $V$ = –600 mV; (b) $I$ = 20 pA, $V$ = –850 mV; (c) $I$ = 22 pA, $V$ = –300 mV; (d) $I$ = 20 pA, $V$ = –700 mV. The cross-sectional profiles are taken along the white lines shown on the STM images. The location of a defect in (a) is indicated by arrows.

STM images of Ga(OEP)I, Ga(OEP)($O_3SCF_3$), and Ga(OEP)(CCPh) monolayers on HOPG under 1-phenyloctane and corresponding cross-sectional profiles are shown in Figure 2.6. The images are qualitatively similar to those for Ga(OEP)Cl and Ga(OEP)Br, with the noteworthy exception that Ga(OEP)I exhibits a partial bilayer structure (vide infra). For Ga(OEP)I, the cross-sectional profiles in regions where the bilayer is absent resemble those for the Ga(OEP)Cl and Ga(OEP)Br that exhibit the dot features, in that they exhibit peaks of consistent height. In contrast, the images for Ga(OEP)($O_3SCF_3$) and Ga(OEP)(CCPh), which have multi-atom axial ligands, are more diffuse than those for the halide derivatives and exhibit less consistent apparent heights. Broad distributions in apparent height have also been observed in other studies of five-coordinate porphyrins that have datively bound multi-atom axial ligands.[58, 59] Across the data for all Ga(OEP)X compounds, there is no correlation between the apparent height and that calculated for the free compound in the gas phase by DFT calculations (e.g., the calculated height for Ga(OEP)(CCPh) is ~9 Å; the apparent height is ~2 Å).

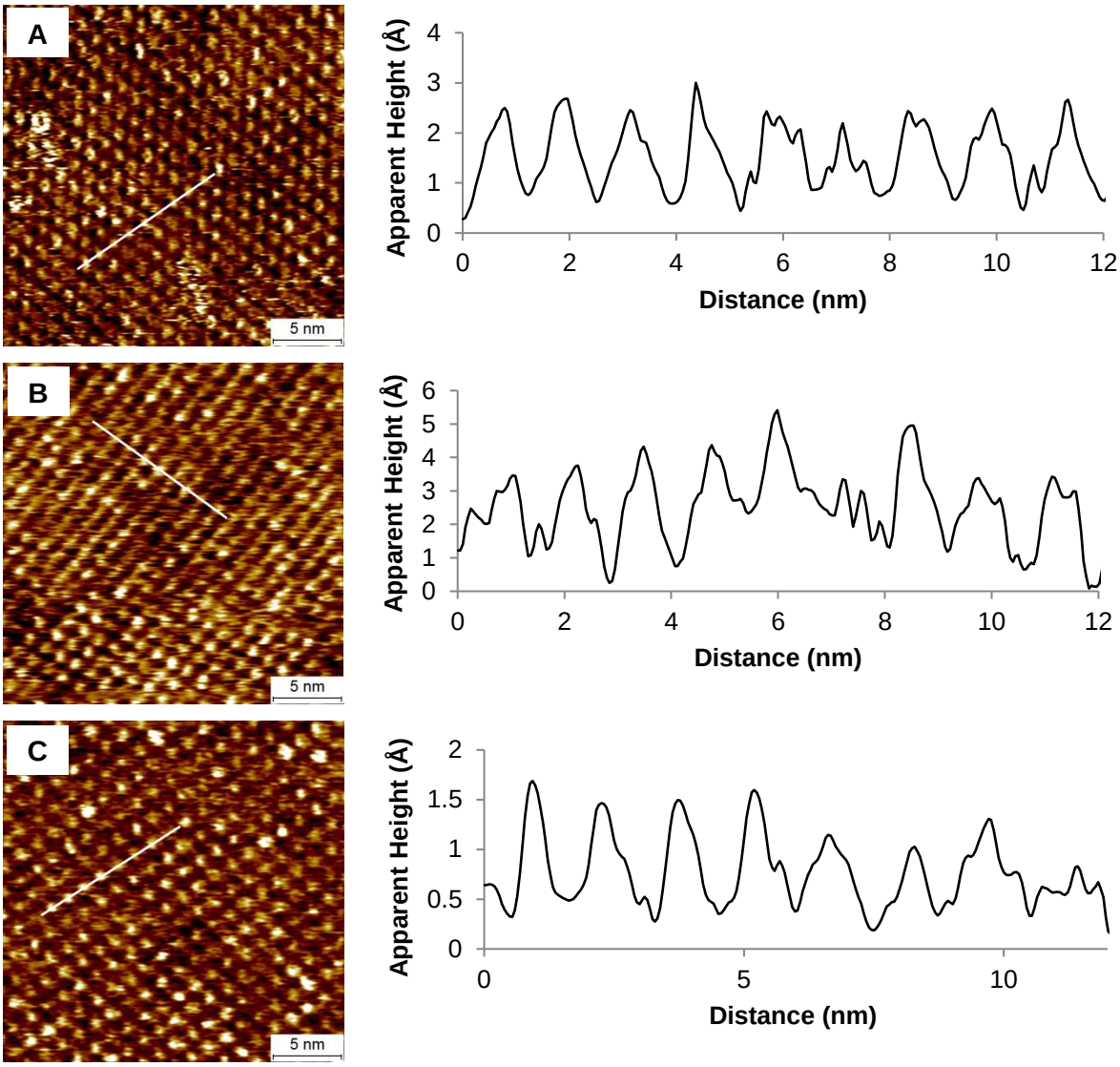


**Figure 2.6.** STM images and cross-sectional profiles of Ga(OEP)X (X = I, $O_3SCF_3$, CCPh) monolayers on HOPG at the solid–liquid interface (1-phenyloctane): (a) Ga(OEP)I, obtained in a region with no second layer (0.5 mM, $I$ = 15 pA, $V$ = –350 mV); (b) Ga(OEP)($O_3SCF_3$) (0.25 mM, $I$ = 15 pA, $V$ = –500 mV); (c) Ga(OEP)(CCPh) (0.5 mM, $I$ = 12.5 pA, $V$ = –600 mV). The cross-sectional profiles were taken along the white lines shown on the STM images.

The lattice parameters for the Ga(OEP)X monolayers (Table 2.2) are consistent with pseudo-hexagonal 2D packing of the molecules, with the $a$ and $b$ vectors being approximately equal in length and forming an angle to each other of ~66˚. The unit-cell dimensions are essentially independent of the nature of the axial ligand, lying in the ranges $a$ = 1.35–1.39 nm, $b$ = 1.34–1.37 nm, Γ = 66–68˚; the endpoints of these ranges differ by amounts comparable to the

experimental uncertainties. The packing densities also span a narrow range (~0.58–0.61 molecules/nm$^2$). Although the images are not of sufficient resolution to show the orientation of the OEP ethyl groups, it is reasonable to conclude from these results that the axial-ligand-dependent doming observed for the free compounds does not affect their intermolecular orientation. The assignment of a pseudo-hexagonal cell assumes that there is only one molecule per unit cell since the orientation of the ethyl groups cannot be resolved. However, in a study of CoOEP on HOPG under 1-phenyloctane it was suggested on the basis of molecular modeling that a body-centered unit cell minimizes the overlap of the ethyl groups better than the typically invoked pseudo-hexagonal cell.[12] This possibility cannot be excluded for the Ga(OEP)X compounds.

The pseudo-hexagonal packing for five-coordinate Ga(OEP)X is qualitatively similar to that observed in prior studies of four-coordinate M(OEP) compounds (M = Ni,[34-37] Co,[12, 37, 39, 40] Pt,[41, 42] Cu,[43, 44] and Zn[43, 45]) on HOPG under similar experimental conditions, and of that of the single five-coordinate OEP compound that has been studied (V(OEP)(O)).[34, 39] Of these compounds Ni(OEP) has been the most studied and, thus, provides the logical reference point for the lattice parameters for Ga(OEP)X compounds. The unit-cell parameters for Ni(OEP) on HOPG in 1-phenyloctane under our conditions (Table 2.2) are approximately equal to those for the Ga(OEP)X arrays, indicating that the addition of the axial ligand does not appreciably alter the packing of the M(OEP) porphyrins. They are also comparable to literature reports under similar deposition conditions (Table 2.3). Further, Ni(OEP) is observed to form arrays whose widths span hundreds of nanometers observed minutes after deposition (Figure 2.7a). Bright porphyrin rings with a dark center can be observed at greater spatial resolution when imaged at negative bias potentials (Figures 2.7b and 2.7c), in good agreement with the literature.[36]

**Table 2.2.** Lattice Parameters of Ga(OEP)X Compounds and Ni(OEP) on HOPG at the Solid–Liquid Interface (1-Phenyloctane).[a]

| | | X | | | | | |
|---|---|---|---|---|---|---|---|
| parameter | Ni(OEP)[b] | Cl | Br | I[c] | I[d] | $O_3SCF_3$ | CCPh |
| *a* (nm) | 1.39 (2) | 1.37 (4) | 1.39 (2) | 1.38 (3) | 1.39 (2) | 1.38 (2) | 1.35 (3) |
| *b* (nm) | 1.35 (3) | 1.35 (2) | 1.37 (3) | 1.37 (2) | 1.39 (4) | 1.35 (3) | 1.34 (3) |
| Γ (°) | 64 (2) | 68 (1) | 66 (2) | 66 (2) | 88 (2) | 66 (1) | 66 (2) |
| density (molecules $nm^{-2}$) | 0.59 | 0.58 | 0.58 | 0.58 | 0.52 | 0.59 | 0.61 |

[a] Parameters were determined for samples of concentration 0.5 mM for all samples except Ga(OEP)($O_3SCF_3$) (0.25 mM); parameters for X = Cl, Br, I, and CCPh at 0.25 mM are statistically indistinguishable from those at the higher concentration. Values in parentheses are standard deviations of the last digit. [b] STM image shown in Figure 2.7. [c] Bottom layer in a region with no second layer. [d] Second layer of a bilayer array.

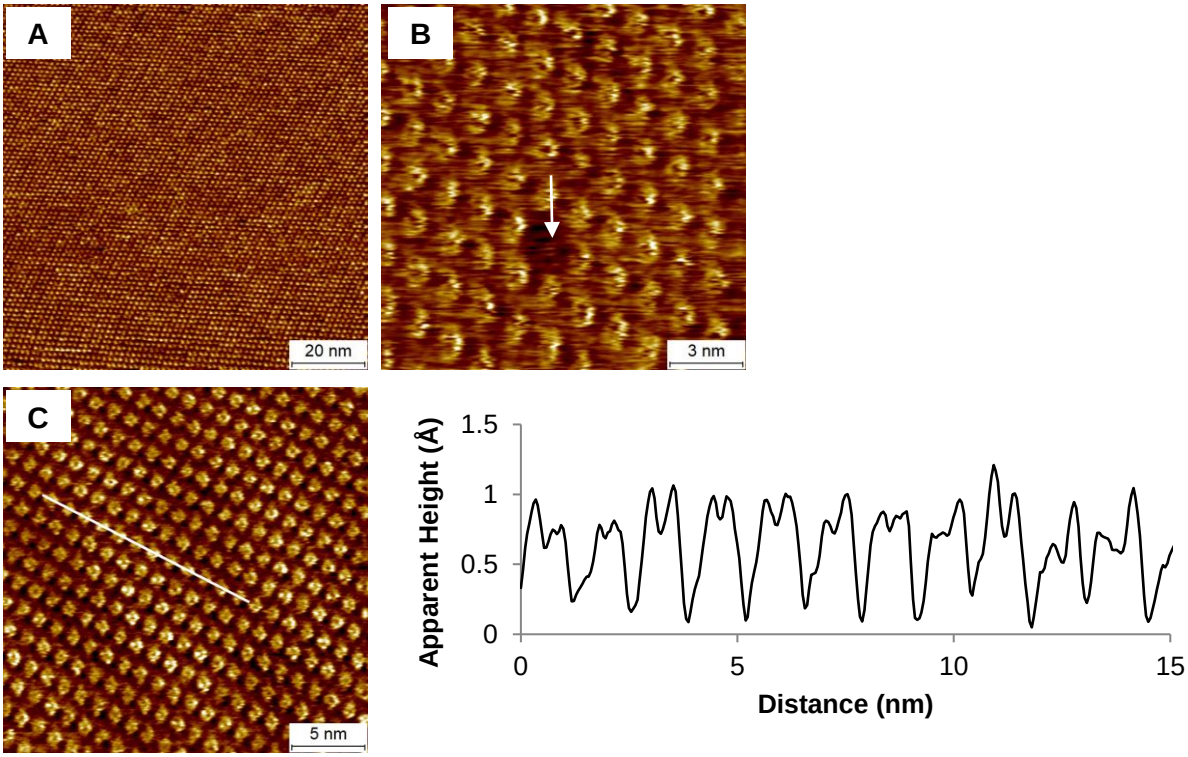


**Figure 2.7.** STM images of Ni(OEP) monolayers on HOPG at the solid–liquid interface (1-phenyloctane, 0.5 mM). (A) Long-range ordering of the monolayer: $I$ = 15 pA, $V$ = –500 mV; (B) Higher spatial resolution showing porphyrin ring structure and transient vacancy marked with arrow: $I$ = 26 pA, $V$ = –600 mV; (C) The cross-sectional profile was taken along the white line shown on the STM image: $I$ = 35 pA, $V$ = –725 mV.

**Table 2.3.** Lattice Parameters for Ni(OEP) on HOPG.[a]

| ref. | imaged interface | dosing condition | *a* (nm) | *b* (nm) | Γ (°) |
|---|---|---|---|---|---|
| *b* | solid-liquid | 1-phenyloctane (<0.11 mM-0.15mM) | 1.28 (0.02) | 1.39 (0.02) | 57 (1) |
| *c* | solid–liquid | 1-phenyloctane (0.5 mM) | 1.48 (0.05) | 1.28 (0.1) | ~70 |
| *c* | solid–liquid | 1-phenyloctane (0.05 mM) | 1.66 (0.1) | 1.73 (0.1) | ~70 |
| *d* | solid–air | immersion ($C_6H_6$, 0.05 mM) | 1.55 (0.03) | 1.47 (0.06) | 70 (5) |
| *d* | solid–air | immersion ($CHCl_3$, 0.05 mM) | 1.60 (0.03) | 1.50 (0.08) | 67 (5) |
| this work | solid–liquid | 1-phenyloctane (0.5 mM) | 1.39 (0.02) | 1.35 (0.03) | 64 (2) |

[a] Pseudo-hexagonal structures only. [b] ref. 37. [c] ref. 34. [d] ref. 36.

Although the nature of the axial ligand of Ga(OEP)X complexes does not affect the lattice parameters of their monolayers on HOPG, it does influence the stability of these monolayers. For Ga(OEP)($O_3SCF_3$) and Ga(OEP)(CCPh), repeated scanning of a fixed region of monolayer under STM conditions typical of this study ($V$ = –400 to –600 mV, $I$ = 8–12 pA) results in progressive removal of the complex from the surface (see Figure 2.8 for an example). In contrast, monolayers of Ga(OEP)Cl, Ga(OEP)Br, and Ga(OEP)I do not exhibit damage as a result of repetitive scanning under similar conditions. The monolayers of these complexes also exhibit different behavior when the sign of the STM bias voltage is toggled. Switching the potential from –500 mV to +500 mV and back to –500 mV does not affect monolayers of Ga(OEP)Cl, Ga(OEP)Br, and Ga(OEP)I. For Ga(OEP)($O_3SCF_3$), however, toggling to the positive potential results in widespread removal of the complex from the HOPG surface (Figure 2.9); switching back to –500 mV allows the monolayer to reform. The lower stability of the monolayers of Ga(OEP)($O_3SCF_3$) and Ga(OEP)(CCPh) as compared to those of the halide derivatives is not straightforwardly related to the magnitude of the domed distortion, because these two complexes represent the lower and upper limits, respectively, of Ga atom displacement from the porphyrin

plane (Table 6.3). These two axial ligands also represent the limits of electron donating (CCPh) and withdrawing ($O_3SCF_3$) ability within the series (calculated fractional charges on Ga: X = $O_3SCF_3$: + 0.23; X = Cl, Br, I: 0.19–0.21; X = CCPh, 0.04), suggesting that the relationship of stability to electronic factors of the complex is also not straightforward. Thus, we speculate that the lower stability of the monolayers of Ga(OEP)($O_3SCF_3$) and Ga(OEP)(CCPh) may be associated with interactions between the multi-atom axial ligands and the STM tip.

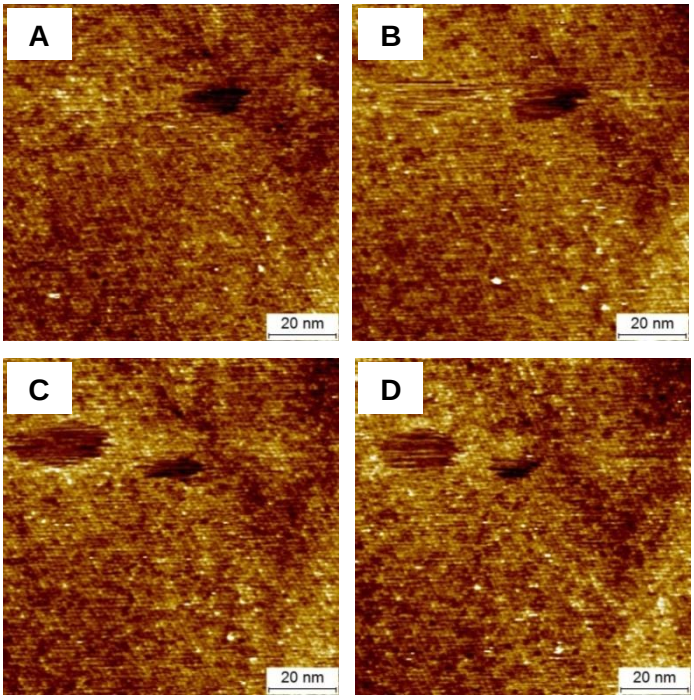


**Figure 2.8.** Sequential STM images of Ga(OEP)($O_3SCF_3$) on HOPG at the solid–liquid interface (1-phenyloctane, 0.25 mM) showing the appearance of exposed HOPG upon repeated scanning ($I$ = 8 pA, $V$ = –400 mV).

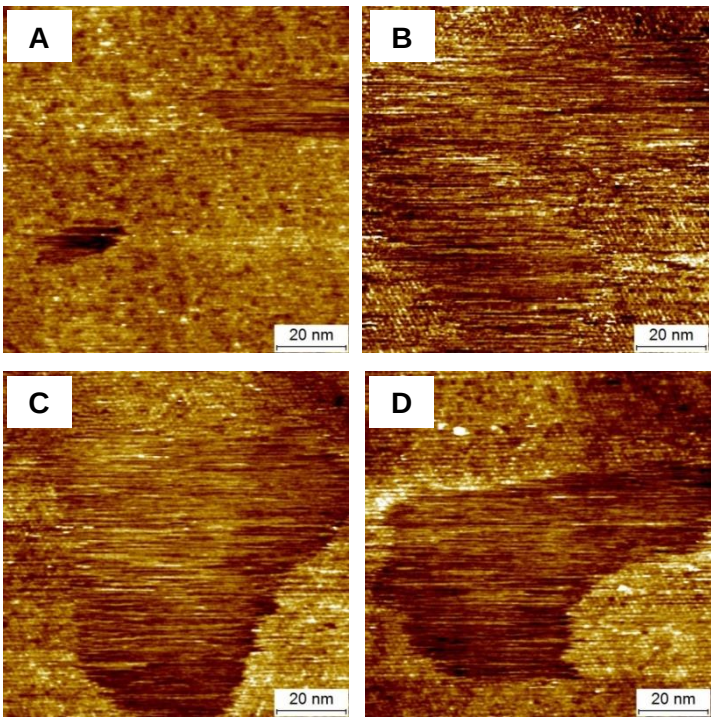


**Figure 2.9.** Sequence of STM images of Ga(OEP)($O_3SCF_3$) on HOPG at the solid–liquid interface (1-phenyloctane, 0.25 mM) showing monolayer removal and reformation as a result of toggling between negative and positive bias voltages, acquired in the order A, B, C, D. Images A, C, and D were acquired at $I$ = 8 pA, $V$ = –500 mV; image B was acquired following 3 scans at $I$ = 8 pA, $V$ = +500 mV.

A second striking influence of the axial ligand on the properties of Ga(OEP)X on HOPG is that Ga(OEP)I reproducibly forms domains in which a bilayer structure is present, under conditions identical to those for which the other Ga(OEP)X compounds exclusively form monolayer structures (i.e., 0.25 mM and 0.5 mM, and standard STM scanning parameters). Representative images are shown in Figure 2.10, in which a second layer appears as islands with widths of 10–50 nm on a continuous bottom layer. The patterns in adjacent islands are not aligned with each other and exhibit a clear interface where they meet (Figures 2.10d and 2.10e). In contrast to the bottom layer, which exhibits the typical Ga(OEP)X pseudo-hexagonal packing (Figure 2.6a), the second layer (Figure 2.10b) is arranged in a square lattice ($a$ = 1.39 (2) nm, $b$ = 1.39 (4) nm, Γ = 88 (2)°) with a lower packing density (Table 2.2). Identical lattice parameters are observed within multiple islands, indicating that these structures are characteristic of the second layer. The

cross-sectional profiles of the second layer resemble in appearance and amplitude those of the dot features seen for Ga(OEP)Cl and Ga(OEP)Br (Figures 2.5a and 2.5c), from which we conclude that the two layers are oriented in a head-to-tail manner with the axial iodo ligand of the top layer extended upward.

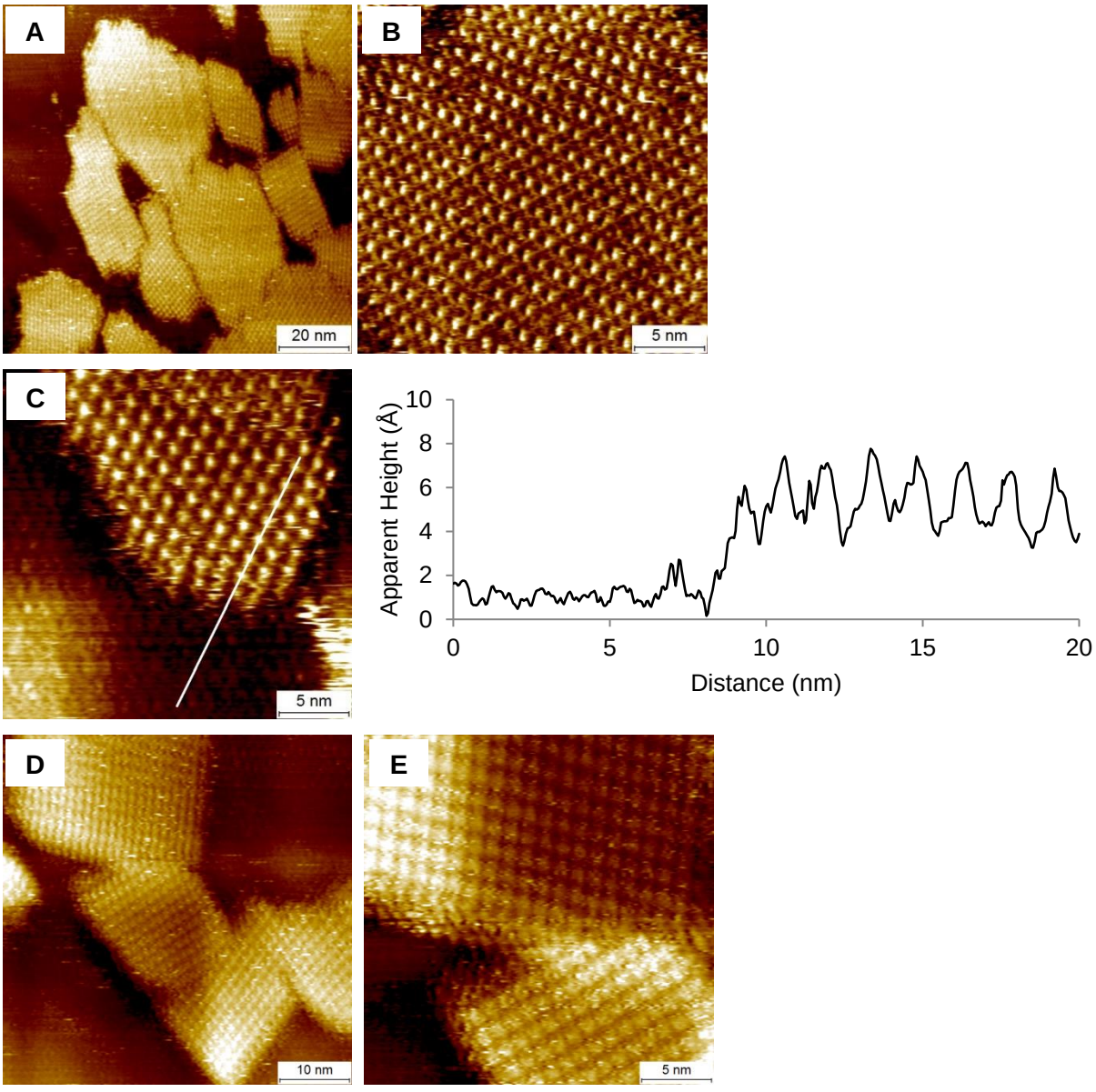


**Figure 2.10.** STM images of bilayer structures of Ga(OEP)I on HOPG (1-phenyloctane, 0.5 mM): (A) large-scale image showing several islands of a second layer ($I$ = 10 pA, $V$ = –500 mV); (B) close-up of an array of the second layer, which exhibits square packing ($I$ = 15 pA, $V$ = –100 mV); (C) a region showing the transition from bottom to second layer, with cross-sectional profile showing the step between the first and second layers ($I$ = 10 pA, $V$ = –500 mV); (D) interface of bilayer islands ($I$ = 12 pA, $V$ = –600 mV); (E) close-up of interface ($I$ = 20 pA, $V$ = –600 mV).

The observation that the structures of the two layers in the Ga(OEP)I bilayer are different from each other contrasts with the only other reported bilayer for M(OEP) complexes on HOPG at the solid–liquid interface, in which it was found that deposition of mixtures containing any two of

Cu(OEP), Zn(OEP), and $H_2$OEP in 1,2-dichlorobenzene produce bilayers in which both layers exhibit pseudo-hexagonal packing.[43] It also contrasts with the structure found for 5-coordinate V(O)(tetraphenoxyphthalocyanine), which forms a bilayer on HOPG at the *n*-alkylbenzene interface (alkyl = heptyl, octyl, decyl) in which the ordered second layer is indexed to the underlying layer, but with a packing density that is one-half that of the on-surface unit cell.[60] It was proposed that the molecules in the two layers are arranged head-to-head, with the structural indexing of the layers resulting from interlayer VO···H(phenoxy) interactions. The observations for Ga(OEP)I that the two layers have different structures and that patterns within adjacent islands of the top layer are not aligned with respect to each other suggests that the structure within the top layer is not principally determined by strong intermolecular interactions between the iodo ligands of the on-surface Ga(OEP)I molecules and specific nuclei of the Ga(OEP)I molecules in the upper layer. Although square-packed lattices of the type observed in the Ga(OEP)I top layer have not been observed for M(OEP) monolayers on HOPG at the interface with 1-phenyloctane, pseudo-square lattices are reported for $H_2$OEP and Cu(OEP) at the interface with 1,2-dichlorobenzene[43, 44] and for Ni(OEP) at the solid–air interface,[35] indicating that this is a favorable packing arrangement for OEP complexes.

Given these considerations, and the fact that the bilayer structure is observed exclusively for Ga(OEP)I even though all Ga(OEP)X complexes possess very similar molecular structures and packing arrangements, we hypothesize that formation of the bilayer structure is a consequence of the greater axial extension and polarizability of the iodo ligand relative to those of the chloro and bromo ligands. In studies of Ni(OEP) monolayers deposited on Au(111) under ultra-high-vacuum conditions, it has been observed that the OEP ethyl groups are oriented such that the methylene hydrogen atoms are directed toward the HOPG surface and the terminal methyl

groups are directed away from the surface.[36, 57] This orientation is thought to be also adopted by M(OEP) compounds on HOPG at the solid–liquid interface.[12] It has also been proposed for Zn(OEP) on HOPG that the ethyl groups adopt a $D_{2d}$-symmetric arrangement with half of the methyl groups directed at the surface, based on imaging at the solid-1,2-dichlorobenzene interface.[45] However, the packing density of these structures is much higher than that found for the Ga(OEP)X, which leads us to conclude that this structure is not relevant for the present systems.

The axial ligands of the Ga(OEP)X monolayers extend above the van der Waals surface defined by these upturned methyl groups; this is evident in space-filling models of Ga(OEP)Cl, Ga(OEP)Br, and Ga(OEP)I (Figure 2.11). Based on structural data from the calculated gas-phase structures, the apex of the van der Waals surface of the iodo ligand lies 1.74 Å above the surface defined by the methyl groups, whereas for Ga(OEP)Cl and Ga(OEP)Br these differences are 1.16 Å and 1.46 Å, respectively. The absence of bilayer formation for the chloro and bromo compounds, and for Ga(OEP)($O_3SCF_3$) and Ga(OEP)(CCPh), indicates that the protrusion of the axial ligand above the methyl surface of the bottom layer is not a sufficient condition to induce adsorption of a second layer. Instead, it suggests that the comparatively large polarizability of the iodo ligand may play a role in providing a surface that is conducive to bilayer formation.

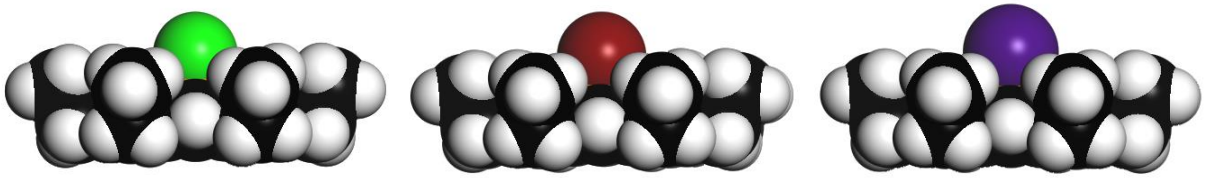

Ga(OEP)Cl Ga(OEP)Br Ga(OEP)I

**Figure 2.11.** Space-filling models (van der Waals) of Ga(OEP)X compounds with methyl groups oriented toward the axial ligand, as expected when adsorbed to HOPG.

## 2.4. Conclusions

Five-coordinate Ga(OEP)X compounds form ordered monolayers on HOPG, hundreds of nanometers in width, at the solid–liquid interface with their 1-phenyloctane solutions. The axial ligand has considerable influence on the magnitude of the dome-shaped structural distortion of free Ga(OEP)X compounds, producing out-of-plane displacements of the Ga atom ranging from 0.35–0.54 Å. However, it does not affect the two-dimensional structures of their monolayers: all compounds exhibit pseudo-hexagonal packing with lattice parameters that are statistically indistinguishable from each other, and are very similar to that of the four-coordinate NiOEP, at both concentrations studied. The reproducibility of this structure across a diverse set of axial ligands is of importance with regard to rationally designing supported multilayer materials based on 5-coordinate Ga(OEP)X platforms. Noteworthy in this latter regard is the monolayer formed by Ga(OEP)(CCPh), for which the height of the perpendicular ligand above the HOPG surface (~0.9 nm) approaches the dimensions of the monolayer unit cell (~1.35 nm).

Varying the axial ligand does change other properties of the Ga(OEP)X assemblies, however. First, it is found that the monolayers of Ga(OEP)($O_3SCF_3$) and Ga(OEP)(CCPh) are susceptible to damage during the STM experiment through repetitive scanning and toggling of the sign of the bias potential, whereas those of the halide complexes are not. The lower stability of the monolayers of Ga(OEP)($O_3SCF_3$) and Ga(OEP)(CCPh) is neither a simple function of the magnitude of the domed distortion or the electron donating/withdrawing ability of the axial ligands, for which these compounds define the lower and upper limits. In addition, Ga(OEP)I is unique among these compounds in that it forms bilayer structures, with the second layer exhibiting a square lattice of lower density than the bottom layer. Because the axial ligands of all Ga(OEP)X compounds protrude above the molecular surface defined by the upward-turned methyl groups of the OEP ligand, it is plausible to conclude that the comparatively large polarizability of the iodo ligand is important in producing a stable bilayer structure. Understanding these ligand effects will be important for future investigations as more complex and functional ligands are supported by these versatile five-coordinate platforms.

## 2.5. References


1. Bonifazi, D.; Mohnani, S.; Llanes-Pallas, A. Supramolecular Chemistry at Interfaces: Molecular Recognition on Nanopatterned Porous Surfaces. *Chem. Eur. J.* **2009**, *15*, 7004-7025.

2. Kudernac, T.; Lei, S. B.; Elemans, J. A. A. W.; De Feyter, S. Two-Dimensional Supramolecular Self-Assembly: Nanoporous Networks on Surfaces. *Chem. Soc. Rev.* **2009**, *38*, 402-421.

3. Barth, J. V. Molecular Architectonic on Metal Surfaces. *Annu. Rev. Phys. Chem.* **2007**, *58*, 375-407.

4. Otero, R.; Gallego, J. M.; de Parga, A. L. V.; Martín, N.; Miranda, R. Molecular Self-Assembly at Solid Surfaces. *Adv. Mater.* **2011**, *23*, 5148-5176.

5. Wang, D.; Wan, L. J.; Bai, C. L. Formation and Structural Transition of Molecular Self-Assembly on Solid Surface Investigated by Scanning Tunneling Microscopy. *Mat. Sci. Eng., R* **2010**, *70*, 169-187.

6. Jurow, M.; Schuckman, A. E.; Batteas, J. D.; Drain, C. M. Porphyrins as Molecular Electronic Components of Functional Devices. *Coord. Chem. Rev.* **2010**, *254*, 2297-2310.

7. Drain, C. M.; Varotto, A.; Radivojevic, I. Self-Organized Porphyrinic Materials. *Chem. Rev.* **2009**, *109*, 1630-1658.

8. Mohnani, S.; Bonifazi, D. Supramolecular Architectures of Porphyrins on Surfaces: The Structural Evolution from 1D to 2D to 3D to Devices. *Coord. Chem. Rev.* **2010**, *254*, 2342-2362.

9. Otsuki, J. STM Studies on Porphyrins. *Coord. Chem. Rev.* **2010**, *254*, 2311-2341.

10. Auwärter, W.; Écija, D.; Klappenberger, F.; Barth, J. V. Porphyrins at Interfaces. *Nat. Chem.* **2015**, *7*, 105-120.

11. Mazur, U.; Hipps, K. W. Kinetic and Thermodynamic Processes of Organic Species at the Solution-Solid Interface: The View Through an STM. *Chem. Comm.* **2015**, *51*, 4737-4749.

12. Friesen, B. A.; Bhattarai, A.; Mazur, U.; Hipps, K. W. Single Molecule Imaging of Oxygenation of Cobalt Octaethylporphyrin at the Solution/Solid Interface: Thermodynamics from Microscopy. *J. Am. Chem. Soc.* **2012**, *134*, 14897-14904.

13. den Boer, D.; Li, M.; Habets, T.; Iavicoli, P.; Rowan, A. E.; Nolte, R. J. M.; Speller, S.; Amabilino, D. B.; De Feyter, S.; Elemans, J. A. A. W. Detection of Different Oxidation States of Individual Manganese Porphyrins During Their Reaction with Oxygen at a Solid/Liquid Interface. *Nat. Chem.* **2013**, *5*, 621-627.

14. Gopakumar, T. G.; Tang, H.; Morillo, J.; Berndt, R. Transfer of Cl Ligands Between Adsorbed Iron Tetraphenylporphyrin Molecules. *J. Am. Chem. Soc.* **2012**, *134*, 11844-11847.

15. Hieringer, W.; Flechtner, K.; Kretschmann, A.; Seufert, K.; Auwarter, W.; Barth, J. V.; Gorling, A.; Steinruck, H. P.; Gottfried, J. M. The Surface Trans Effect: Influence of Axial Ligands on the Surface Chemical Bonds of Adsorbed Metalloporphyrins. *J. Am. Chem. Soc.* **2011**, *133*, 6206-6222.

16. Ferreira, Q.; Alcacer, L.; Morgado, J. Stepwise Preparation and Characterization of Molecular Wires Made of Zinc Octaethylporphyrin Complexes Bridged by 4,4 '-Bipyridine on HOPG. *Nanotechnology* **2011**, *22*, 435604.

17. Ferreira, Q.; Braganca, A. M.; Alcacer, L.; Morgado, J. Conductance of Well-Defined Porphyrin Self-Assembled Molecular Wires up to 14 nm in Length. *J. Phys. Chem. C* **2014**, *118*, 7229-7234.

18. Otsuki, J.; Seki, E.; Taguchi, T.; Asakawa, M.; Miyake, K. STM Observation of Labile Axial Ligands to Zinc Porphyrin at Liquid/Solid Interface. *Chem. Lett.* **2007**, *36*, 740-741.

19. Senge, M. O. Exercises in Molecular Gymnastics - Bending, Stretching and Twisting Porphyrins. *Chem. Commun.* **2006**, 243-256.

20. Brancato-Buentello, K. E.; Coutsolelos, A. G.; Scheidt, W. R. Chloro(2,3,7,8,12,13,17,18-octaethylporphinato)gallium(III). *Acta Crystallogr., Sect. C: Cryst. Struct. Commun.* **1996**, *52*, 2707-2710.

21. Boukhris, A.; Lecomte, C.; Coutsolelos, A.; Guilard, R. Alkylsulfonato(Porphyrinato)Gallium(III): Crystal-Structure Determination of Methylsulfonato(Octaethyl-2,3,7,8,12,13,17,18-Porphyrinato)-Gallium(III). *J. Organomet. Chem.* **1986**, *303*, 151-165.

22. Coutsolelos, A.; Guilard, R.; Boukhris, A.; Lecomte, C. Synthesis and Characterization of Azido-Gallium(III) and Thiocyanato-Gallium(III) Porphyrins - Crystal-Structure of Azido(2,3,7,8,12,13,17,18-octaethyl-porphyrinato)Gallium(III). *J. Chem. Soc., Dalton Trans.* **1986**, 1779-1783.

23. Okamura, T.; Nishikawa, N.; Ueyama, N.; Nakamura, A. Synthesis and Structures of (Porphinato)(Thiolato)Gallium(III) Complexes. *Chem. Lett.* **1998**, 199-200.

24. Okamura, T.; Iwamura, T.; Yamamoto, H.; Ueyama, N. Synthesis and Molecular Structures of S-2-FcNHCOC$_6$H$_4$SH and [M$^{III}$(OEP)(S-2-FcNHCOC$_6$H$_4$)] (Fc = ferrocenyl, M = Fe, Ga): Electrochemical Contributions of Intramolecular SH···O=C and NH···S Hydrogen Bonds. *J. Organomet. Chem.* **2007**, *692*, 248-256.

25. Cullen, D. L.; Meyer, E. F. Crystal and Molecular-Structure of Triclinic Form of 1,2,3,4,5,6,7,8-Octaethylporphinatonickel(II) - Comparison with Tetragonal Form. *J. Am. Chem. Soc.* **1974**, *96*, 2095-2102.

26. Brennan, T. D.; Scheidt, W. R.; Shelnutt, J. A. New Crystalline Phase of (Octaethylporphinato)Nickel(II) - Effects of π-π-Interactions on Molecular-Structure and Resonance Raman-Spectra. *J. Am. Chem. Soc.* **1988**, *110*, 3919-3924.

27. Strauss, S. H.; Silver, M. E.; Long, K. M.; Thompson, R. G.; Hudgens, R. A.; Spartalian, K.; Ibers, J. A. Comparison of the Molecular and Electronic-Structures of (2,3,7,8,12,13,17,18-Octaethylporphyrinato)Iron(II) and (Trans-7,8-Dihydro-2,3,7,8,12,13,17,18-Octaethyl-Porphyrinato)Iron(II). *J. Am. Chem. Soc.* **1985**, *107*, 4207-4215.

28. Scheidt, W. R.; Turowskatyrk, I. Crystal and Molecular-Structure of (Octaethylporphinato)Cobalt(II) - Comparison of the Structures of 4-Coordinate M(TPP) and M(OEP) Derivatives (M=Fe-Cu) - Use of Area Detector Data. *Inorg. Chem.* **1994**, *33*, 1314-1318.

29. Pak, R.; Scheidt, W. R. Structure of (2,3,7,8,12,13,17,18-Octaethylporphinato)Copper(II). *Acta Crystallogr., Sect. C: Cryst. Struct. Commun.* **1991**, *47*, 431-433.

30. Meyer, E. F. Crystal and Molecular Structure of Nickel(II)Octaethylporphyrin. *Acta Crystallogr., Sect. B: Struct. Crystallogr. Cryst. Chem.* **1972**, *B 28*, 2162-&.

31. Gruden-Pavlovic, M.; Grubisic, S.; Zlatar, M.; Niketic, S. R. Molecular Mechanics Study of Nickel(II) Octaethylporphyrin Adsorbed on Graphite(0001). *Int. J. Mol. Sci.* **2007**, *8*, 810-829.

32. Chilukuri, B.; Mazur, U.; Hipps, K. W. Effect of Dispersion on Surface Interactions of Cobalt(II) Octaethylporphyrin Monolayer on Au(111) and HOPG(0001) Substrates: A Comparative First Principles Study. *Phys. Chem. Chem. Phys.* **2014**, *16*, 14096-14107.

33. Yin, S. X.; Wang, C.; Qiu, X. H.; Xu, B.; Bai, C. L. Theoretical Study of the Effects of Intermolecular Interactions in Self-Assembled Long-Chain Alkanes Adsorbed on Graphite Surface. *Surf. Interface Anal.* **2001**, *32*, 248-252.

34. Oncel, N.; Bernasek, S. L. Ni(II)- and Vanadyloctaethylporphyrin Self-Assembled Layers Formed on Bare and 5-(Octadecyloxy)isophthalic Acid Covered Graphite. *Langmuir* **2009**, *25*, 9290-9295.

35. Scudiero, L.; Hipps, K. W. Controlled Manipulation of Self-Organized Ni(II)-Octaethylporphyrin Molecules Deposited from Solution on HOPG with a Scanning Tunneling Microscope. *J. Phys. Chem. C* **2007**, *111*, 17516-17520.

36. Ogunrinde, A.; Hipps, K. W.; Scudiero, L. A Scanning Tunneling Microscopy Study of Self-Assembled Nickel(II) Octaethylporphyrin Deposited from Solutions on HOPG. *Langmuir* **2006**, *22*, 5697-5701.

37. Bhattarai, A.; Mazur, U.; Hipps, K. W. Desorption Kinetics and Activation Energy for Cobalt Octaethylporphyrin from Graphite at the Phenyloctane Solution-Graphite Interface: An STM Study. *J. Phys. Chem. C* **2015**, *119*, 9386-9394.

38. Nandi, G.; Chilukuri, B.; Hipps, K. W.; Mazur, U. Surface Directed Reversible Imidazole Ligation to Nickel(II) Octaethylporphyrin at the Solution/Solid Interface: A Single Molecule Level Study. *Phys. Chem. Chem. Phys.* **2016**, *18*, 20819-20829.

39. Miyake, Y.; Tanaka, H.; Ogawa, T. Scanning Tunneling Microscopy Investigation of Vanadyl and Cobalt(II) Octaethylporphyrin Self-Assembled Monolayer Arrays on Graphite. *Colloids Surf., A* **2008**, *313*, 230-233.

40. Bhattarai, A.; Marchbanks-Owens, K.; Mazur, U.; Hipps, K. W. Influence of the Central Metal Ion on the Desorption Kinetics of a Porphyrin from the Solution/HOPG Interface. *J. Phys. Chem. C* **2016**, *120*, 18140-18150.

41. Oncel, N.; Bernasek, S. L. The Effect of Molecule-Molecule and Molecule-Substrate Interaction in the Formation of Pt-Octaethyl Porphyrin Self-Assembled Monolayers. *Appl. Phys. Lett.* **2008**, *92*, 133305-133305-3.

42. Bussetti, G.; Trabattoni, S.; Uttiya, S.; Sassella, A.; Riva, M.; Picone, A.; Brambilla, A.; Duò, L.; Ciccacci, F.; Finazzi, M. Controlling Drop-Casting Deposition of 2D Pt-Octaethyl Porphyrin Layers on Graphite. *Synth. Met.* **2014**, *195*, 201-207.

43. Zou, Z. Q.; Wei, L. Y.; Chen, F.; Liu, Z. M.; Thamyongkit, P.; Loewe, R. S.; Lindsey, J. S.; Mohideen, U.; Bocian, D. F. Solution STM Images of Porphyrins on HOPG Reveal That Subtle Differences in Molecular Structure Dramatically Alter Packing Geometry. *J. Porphyrins Phthalocyanines* **2005**, *9*, 387-392.

44. Hao, Y. B.; Weatherup, R. S.; Eren, B.; Somorjai, G. A.; Salmeron, M. Influence of Dissolved $O_2$ in Organic Solvents on CuOEP Supramolecular Self-Assembly on Graphite. *Langmuir* **2016**, *32*, 5526-5531.

45. Zou, Z. Q.; Chen, F. In Situ Scanning Tunneling Microscopy Studies of Zinc(II) Octaethylporphyrin Arrays Self-Assembled on Graphite and Au(111) Surfaces in Organic Solution. *J. Appl. Phys.* **2008**, *103*, 094304-094304-4.

46. Ohno, O.; Kaizu, Y.; Kobayashi, H. Luminescence of Some Metalloporphins Including the Complexes of the IIIb Metal Group. *J. Chem. Phys.* **1985**, *82*, 1779-1787.

47. Coutsolelos, A.; Guilard, R.; Bayeul, D.; Lecomte, C. Gallium(III) Porphyrins - Synthesis and Physicochemical Characteristics of Halogeno Gallium(III) Porphyrins X-Ray Crystal-Structure of Chloro-(5,10,15,20-Tetraphenylporphyrinato) Gallium(III). *Polyhedron* **1986**, *5*, 1157-1164.

48. Brand, H.; Arnold, J. Early Transition-Metal Porphyrins - Synthesis, Characterization, and Reactivity of Novel Out-of-Plane Cis-Ligated Zirconium Porphyrin Derivatives. *Organometallics* **1993**, *12*, 3655-3665.

49. Abraham, R. J.; Smith, K. M. Non-Equivalence of Methylene Protons in Octaethylporphinatothallium(III). *Tetrahedron Lett.* **1971**, 3335-3338.

50. Hudson, M. F.; Smith, K. M. Novel Mercury(II) Complexes of Porphyrins. *Tetrahedron* **1975**, *31*, 3077-3083.

51. Kadish, K. M.; Boisselier-Cocolios, B.; Coutsolelos, A.; Mitaine, P.; Guilard, R. Electrochemistry and Spectroelectrochemistry of Gallium(III) Porphyrins - Redox Properties of 5-Coordinate Ionic and σ-Bonded Complexes. *Inorg. Chem.* **1985**, *24*, 4521-4528.

52. Kadish, K. M.; Xu, Q. Y.; Barbe, J. M.; Anderson, J. E.; Wang, E.; Guilard, R. Synthesis, Photochemistry, and Electrochemistry of (P)Ge(R)$_2$ and (P)Ge(R)X (P = TPP or OEP, R = $CH_3$, $CH_2C_6H_5$, or $C_6H_5$, and X = $Cl^-$, $OH^-$, or $ClO_4^-$). *J. Am. Chem. Soc.* **1987**, *109*, 7705-7714.

53. Kadish, K. M.; Xu, Q. Y.; Barbe, J. M.; Guilard, R. Synthesis and Reactivity of σ-Bonded Silicon Metalloporphyrins - Spectroscopic Characterization and Electrochemistry of (P)Si(R)$_2$, (P)Si(R)X, and (P)$SiX_2$, Where R = $C_6H_5$ or $CH_3$ and X = $OH^-$ or $ClO_4^-$. *Inorg. Chem.* **1988**, *27*, 1191-1198.

54. Choi, S. H.; Phillips, J. A.; Ware, W.; Wittschieben, C.; Medforth, C. J.; Smith, K. M. Magnetic Circular-Dichroism Spectroscopic Studies on the Stereochemistry and Coordination Behavior of Nickel Porphyrins. *Inorg. Chem.* **1994**, *33*, 3873-3876.

55. Giovannetti, R., The Use of Spectrophotometry UV-Vis for the Study of Porphyrins. In *Macro to Nano Spectroscopy*, Uddin, J., Ed. InTech: Rijeka, Croatia, 2012; pp 87-108.

56. Evans, J. S.; Musselman, R. L. Red Shifting Due to Nonplanarity in Alkylporphyrins: Solid-State Polarized UV-Vis Spectra and ZINDO Calculations of Two Nickel(II)octaethylporphyrins. *Inorg. Chem.* **2004**, *43*, 5613-5629.

57. Scudiero, L.; Barlow, D. E.; Hipps, K. W. Scanning Tunneling Microscopy, Orbital-Mediated Tunneling Spectroscopy, and Ultraviolet Photoelectron Spectroscopy of Nickel(II) Octaethylporphyrin Deposited from Vapor. *J. Phys. Chem. B* **2002**, *106*, 996-1003.

58. Ikeda, T.; Asakawa, M.; Goto, M.; Miyake, K.; Ishida, T.; Shimizu, T. STM Observation of Alkyl-Chain-Assisted Self-Assembled Monolayers of Pyridine-Coordinated Porphyrin Rhodium Chlorides. *Langmuir* **2004**, *20*, 5454-5459.

59. Sakano, T.; Higashiguchi, K.; Matsuda, K. Comparison of Molecular Conductance Between Planar and Twisted 4-Phenylpyridines by Means of Two-Dimensional Phase Separation of Tetraphenylporphyrin Templates at a Liquid-HOPG Interface. *Chem. Comm.* **2011**, *47*, 8427-8429.

60. Mazur, U.; Hipps, K. W.; Riechers, S. L. Organization of Vanadyl and Metal-Free Tetraphenoxyphthalocyanine Complexes on Highly Oriented Pyrolytic Graphite in the Presence of Paraffinic Solvents: A STM Study. *J. Phys. Chem. C* **2008**, *112*, 20347-20356.

# CHAPTER 3

## Progress Towards Functionalization of HOPG Surfaces with Gallium–Porphyrin Monolayers Presenting Photo- and Electroactive Ligands

### 3.1. Introduction

The central hypothesis of the research described in this thesis is that the axial ligands of ordered 5-coordinate metalloporphyrin monolayers can provide structural supports or corrals for organizing functional subunits. Initial investigations into the deposition of five-coordinate metalloporphyrins under ambient conditions on HOPG described in Chapter 2 show that gallium(III) octaethylporphyrin is a suitable platform for incorporating axial ligands, perpendicular to the surface, into self-assembled arrays. While the multi-atom ligands CCPh and $O_3SCF_3$ resulted in arrays that were slightly less stable than their halide counterparts, large monolayers on the order of hundreds of nanometers in width were observed with only small amounts of monolayer removal at higher current setpoints. Further, the extremely consistent pseudo-hexagonal unit cell observed across all Ga(OEP)X complexes studied, despite minor calculated differences in porphyrin core structure, indicates that predictive methods such as molecular modeling can be employed prior to deposition and STM imaging. This will allow us to forecast how larger axial ligands may interact with each other when assembled in an OEP unit cell on the surface.

In this chapter, we focus on larger axial ligands that are expected to have functional responses. Such larger ligands might take the form of photo- or electro-active components that would move our arrays one step closer to rationally designed functional assemblies with nanometer precision control over the positioning of the components. While we have thus far focused on porphyrins as structural units that possess the ability to self-assemble flat onto a

graphite substrate, we might also take advantage of their unique light harvesting and energy transfer properties as potential candidates for incorporating functionality.[1-4] Because both the surface and other porphyrins can quench these effects, an ideal spatial arrangement would decouple the porphyrins from the substrate and space them apart from each other.[5] Previous attempts at incorporating porphyrins into surface assemblies have generally relied on the alkanethiol-gold interactions to anchor units and extend porphyrins above a Au(111) surface.[6-8] Another method has included the anchoring of ethynylporphyrins in the triaza triangulated triphenylmethane monolayer motif.[5] Our approach would offer a good complement to these due to the modular nature of our design approach; the periphery of the porphyrin can be tuned to adjust the unit cell if needed, the linker ligand can be adjusted to tune the height above the surface as needed, and our synthetic methods can be adapted to incorporate multiple chromophores of interest.

Likewise, ferrocene is a promising target for axial ligation due to its one-electron reversible oxidation and therefore, potential capacity to act as an on-surface redox switch. The unique on-surface properties of assemblies incorporating ferrocenes have been studied for possible applications in spintronics, electrochemical switches, charge storage, and communication devices.[9-11] As with porphyrins, the alkane-thiol on Au(111) motif has been employed to incorporate ferrocenes extending above the surface with controlled spacing.[12-14] Further, they have been incorporated on the periphery of porphyrins and imaged under ultra-high vacuum conditions.[15] Our approach would seek a new, generalized method of attaching redox centers that would allow for imaging under ambient conditions.

In Chapter 2, we introduced the compound Ga(OEP)(CCPh) with the ultimate aim of attaching functional axial substituents through the acetylide linker due to its structural rigidity.

Ethynyl ligands are employed in some of the compounds described in this chapter. However, as larger and more complex axial ligands are incorporated into the arrays, we also sought an alternate linkage motif to potentially eliminate the lithiating agents and air-free synthetic techniques required by ethynyl ligands. Carboxylate linkers were thought to make a good complement to acetylides because they might be synthesized by reacting the carboxylic acid derivative of the ligand of interest with Ga(por)(OH). Drawing from prior studies on aluminum porphyrins with carboxylate and aryloxide ligands as inspiration,[16-20] prior work in our lab demonstrated that gallium (III) *meso*-tetradecylporphyin Ga($TC_{10}P$)(OH) reacts with $HO_2CR$ to provide Ga($TC_{10}P$)($O_2CR$) (R= $C_6H_5$, ferrocene) complexes rapidly at room temperature in toluene.[21] Thus, this method was pursued in the research described in this chapter to synthesize a direct analogue to an acetylide-functionalized Ga(OEP)X complex to compare their predicted structure and on-surface behavior.

The facile synthesis of the carboxylate complexes is also of interest in the context of on-surface synthesis of functionalized arrays. In the practical fabrication of nanodevices, the ease and generality of attaching modules to the surface is of great importance. The general on-surface functionalization of a pre-deposited Ga(por)(OH) monolayer with a carboxylic acid of interest at room temperature would eliminate much of the front-end synthetic work, and allow for various porphyrins and carboxylic acids to be easily investigated. Ferrocene provides a good test subject for initial investigation due to its expected bright STM contrast compared to redox-inactive axial ligands,[21, 22] indicating a successful on-surface reaction.

We report here the synthesis and surface chemistry of several Ga(OEP)X compounds designed to test these points (Figure 3.1). In order to progress towards the bottom-up functionalization of surfaces, these include two ferrocene derivatives of Ga(OEP)X, one with an

acetylide linker (Ga(OEP)(CCFc)) and one with a carboxylate linker (Ga(OEP)($O_2$CFc)), and a Ga(OEP) dyad containing zinc tetraphenylporphyrin attached via an acetylide linker (Ga(OEP)(CCZnTPP)). It has been found that all compounds self-assemble on HOPG at the solid-liquid interface into highly ordered monolayers with pseudo-hexagonal unit cell with dimensions consistent with the Ga(OEP)X series reported in Chapter 2. Ga(OEP)(CCZnTPP) molecular models suggest that the axial porphyrin ligands will not be able to freely rotate in the OEP unit cell, resulting in large-scale on-surface ordering of chromophores. Preliminary STM results suggest that this is indeed the case. Further, the Ga(OEP)($O_2$CFc) complex was investigated for both direct deposition and for possible use for post-deposition modification of a pre-deposited Ga(OEP)(OH) monolayer. While apparent height profiles suggest that Ga(OEP)($O_2$CFc) is present after a $HO_2$CFc solution is added, at this time we cannot conclusively say if this is due to modification of the pre-formed monolayer or deposition of compound formed in solution.

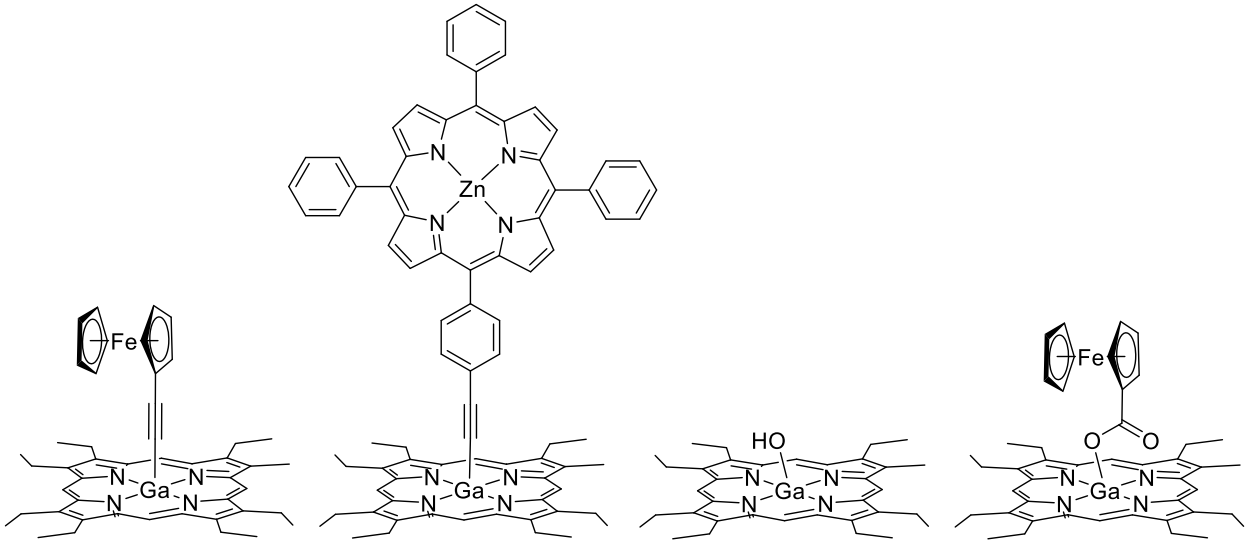


**Figure 3.1.** Ga(OEP)X complexes investigated in this chapter.

### 3.2. Experimental

Detailed information regarding the synthesis and characterization of compounds can be found in Section 6.2.5. In brief, the synthesis of Ga(OEP)(CCFc) followed the same general procedure as that for Ga(OEP)(CCPh), via reaction of lithium ethynylferrocene with Ga(OEP)Cl. Ga(OEP)(OH) was prepared by vigorously mixing an emulsion of Ga(OEP)Cl in dichloromethane and concentrated aqueous sodium hydroxide. This was further reacted with ferrocenecarboxylic acid in THF at room temperature to give Ga(OEP)($O_2$CFc). At the time of this document, it has not yet been possible to develop purification procedures that remove the small amounts of impurities present in both. The synthesis of Ga(OEP)(CCZnTPP) was performed by adding Ga(OEP)Cl to an *in situ* prepared mixture of HCCZnTPP and LiHMDS.

All compounds were geometry-optimized by density functional theory in the gas phase both in the global and in local energy minima with all eight ethyl chains pointing up, the latter being the predicted on-surface geometry. Molecular models of their predicted assembly into a pseudo-hexagonal unit cell were constructed. All compounds were further studied by scanning tunneling microscopy (STM) at the solid-liquid interface and analyzed as described in Sections 6.2.3 and 6.2.4. The post-deposition modification of a Ga(OEP)(OH) monolayer was additionally studied by depositing a 1-phenyloctane solution of ferrocenecarboxylic acid to the pre-formed monolayer and observing any resulting changes by STM.

### 3.3. Results and Discussion

**3.3.1. Synthesis of Functionalized Ga(OEP)X Compounds.** The general methods for synthesis of these compounds are outlined in Scheme 3.1. The synthesis of Ga(OEP)(CCFc) was modeled on that for Ga(OEP)(CCPh), and begin by first lithiating the HCCFc ligand precursor with excess $^n$BuLi to provide LiCCFc, following a literature procedure.[23] An excess of LiCCFc

(3.25 equiv.) was then reacted with Ga(OEP)Cl in THF at −78 °C and slowly warmed to room temperature where it was stirred for several more hours. A reaction attempt carried out only at room temperature resulted in a product that was a mixture of at least four porphyrinic compounds, while shorter reaction times and 1.1 equivalents of LiCCFc resulted in incomplete conversion of the Ga(OEP)Cl to the target compound. Reactions of lithium acetylides with Ga(OEP)Cl at low temperature instead of at room temperature became the standard procedure following this result. Although LiCCFc was prepared using excess $^{n}$BuLi, HCCFc was observed in the crude product. This was removed with pentane washes as HCCFc is soluble while the porphyrin is only sparingly soluble. Ga(OEP)(CCFc) was characterized by $^{1}$H-NMR and $^{13}$C-NMR spectroscopy, LDI-MS, and UV-vis spectroscopy. Significant upfield shifts of the ferrocene resonances are observed in the $^{1}$H NMR spectrum of the compound (4.01 → 3.01 δ for the ferrocene singlet resonance and 4.35/3.83 → 2.82/2.50 δ for the ferrocene triplet resonances in $C_6D_6$), indicating successful ligation. The electronic absorption spectrum (Figure 6.15) is very similar to those observed for Ga(OEP)X complexes in Chapter 2; the ethynylferrocene ligand MLCT band expected near 442 nm (as measured for free ethynylferrocene in toluene) is likely obscured by the onset of the Soret band.

The synthesis of Ga(OEP)(CCZnTPP) was accomplished by the reaction between Ga(OEP)Cl and LiCCZnTPP. To prepare LiCCZnTPP from the HCCZnTPP starting material, a milder lithiating agent than $^{n}$BuLi was sought out because $^{n}$BuLi has been shown to alkylate the *β* position of *meso*-substituted porphyrins,[24, 25] a phenomenon we hoped to avoid. Therefore, test reactions were performed in which HCCZnTPP and lithium bis(trimethylsilyl)amide (LiHMDS) were reacted in a THF solution at -78 °C, as generally described for a related *meso*-phenylethynyl substituted zinc porphyrin,[26] and the solution was slowly warmed to room

temperature. The solution was then quenched with MeI as a method to monitor the extent of lithiation by $^1$H NMR. After 2 hours, the ligand was approximately 80% lithiated, and attempts to optimize these conditions with longer reaction times never resulted in complete lithiation. The dyad was therefore generated *in situ* by first reacting 0.9 equivalents of LiHMDS with HCCZnTPP in THF for four hours starting at –78 °C and warming to room temperature. Addition of a THF solution of Ga(OEP)Cl resulted in a mixture of materials including the target product Ga(OEP)(CCZnTPP) (as confirmed by upfield resonances of the $CCC_6H_4$ moiety in the $^1$H NMR spectrum), Ga(OEP)Cl, HCCZnTPP, and unknown porphyrinic impurities. While multiple pentane washes were effective at reducing the amounts of some of the impurities, the small amount of product prevented further manipulation, and at the time of publication of this document, significant Ga(OEP)Cl and HCCZnTPP impurities remain.

Ga(OEP)OH was synthesized by the literature method of reacting Ga(OEP)Cl with 2M NaOH in a water/dichloromethane suspension.[27] A notable indication of successful formation of the target porphyrin is a singlet at –6.82 ppm from the -OH resonance. Multiple attempts of this synthesis resulted in minor porphyrinic impurities (<2%); one of these had a similar chemical shift to unreacted Ga(OEP)Cl starting material, but did not lessen upon further reaction times with base in dichloromethane or toluene. Other possibilities for impurities include the Ga(OEP)(OH)($H_2O$) complex, which is reported to be the product of passing Ga(OEP)Cl through a basic alumina column,[28] and the {[Ga(OEP)]$_2$OH}X (X = $ClO_4$) dimer, which is formed by slowly reacting Ga(OEP)(OH) with 15 mM $HClO_4$.[27] As the observed impurities are likely a result of the harsh reaction conditions (vigorous stirring with 2M NaOH), an alternate route may be explored in the future. This could include following an analogous synthesis for

$Sn(OEP)(OH)_2$ in which sodium acetate in a THF/water mixture is employed,[29] or a procedure for synthesizing Ga(OEP)(OH) performed in methanol with an acidic workup.[30]

The Ga(OEP)($O_2CFc$) complex was prepared following methods previously used in our lab for analogous tetraalkylporphryin compounds.[21] Ga(OEP)(OH) was dissolved in THF and a slight excess of ferrocene carboxylic acid ($HCO_2Fc$) was added. The reaction is very facile and proceeds rapidly at room temperature. The same porphyrinic impurity that remained in the Ga(OEP)(OH) starting material, noted above, was found in the Ga(OEP)($O_2CFc$) crude product, together with unreacted $HCO_2Fc$. As of this writing, attempts to remove these by washing and recrystallizations have been unsuccessful, due to the commensurate solubilities of both the porphyrins (product and impurity) and $HCO_2Fc$ in a variety of organic solvents. Attempts to wash the crude product with a mild potassium carbonate solution resulted in a mixture of several porphyrins, including Ga(OEP)(OH). Future attempts at synthesizing this material might be made by reacting Ga(OEP)Cl with a deficit of $HCO_2Fc$ ligand and attempting to separate the starting and final porphyrins.

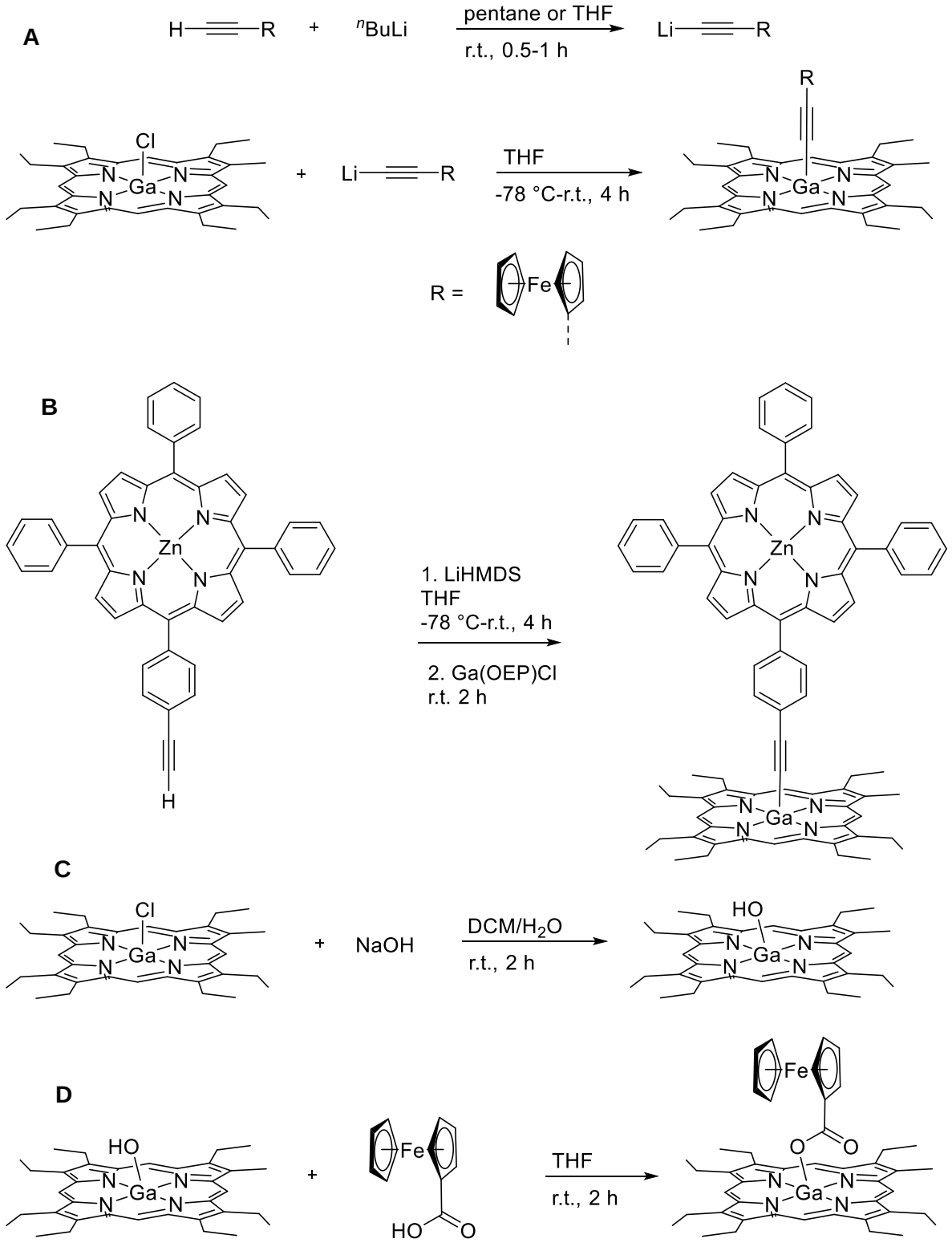


**Scheme 3.1.** General reaction conditions for the synthesis of (A) Ga(OEP)(CCFc), (B) Ga(OEP)(CCZnTPP), (C) Ga(OEP)(OH), and (D) Ga(OEP)($O_2$CFc). The ethynyl precursor for (B) was prepared by a literature method.

**3.3.2. Density Functional Theory Calculations.** DFT calculations were conducted on all compounds to determine their optimized gas-phase structures (Figure 3.2). From selected porphyrin core bond lengths and angles (Table 3.1), we observe that the porphyrins with acetylide linkers (Ga(OEP)(CCFc) and Ga(OEP)(CCZnTPP)) are structurally very similar to the Ga(OEP)(CCPh) studied in Chapter 2, indicating that both electronically and sterically demanding ligands have small effects on the porphyrin core structure. Porphyrins with alternate linkers (Ga(OEP)(OH) and Ga(OEP)($O_2$CFc)) exhibit a less domed and less symmetric structure, which is to be expected given the nature of the gallium-oxygen linkage. For example, the calculated doming for Ga(OEP)($O_2$CFc) has a Ga–$N_4$ plane distance of 0.450 Å and an $N_4$–$C_{20}$ plane distance of 0.035 Å, compared to 0.544 Å and 0.044 Å for the Ga(OEP)(CCFc) analog. Differences in the N−Ga−X angle are also notable (95.8−107.1° for Ga(OEP)($O_2$CFc) and 103.9−104.1° for Ga(OEP)(CCFc)). In Chapter 2, we concluded that the extent of doming of this class of compounds had no effect on surface assembly, and size and nature of the axial ligand played a larger role in any deviations we observed; we expect this trend to continue here.

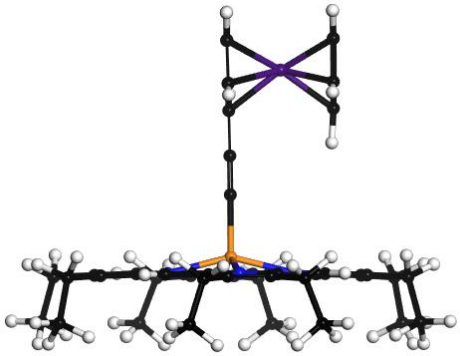

Ga(OEP)(CCFc)

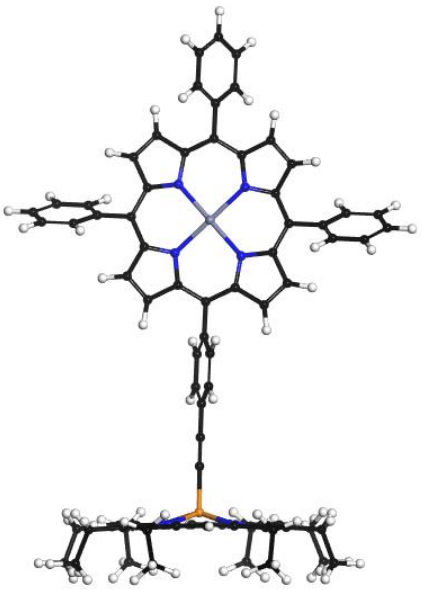

Ga(OEP)(CCZnTPP)

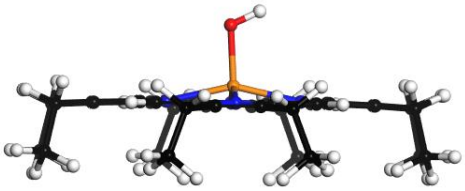

Ga(OEP)(OH)

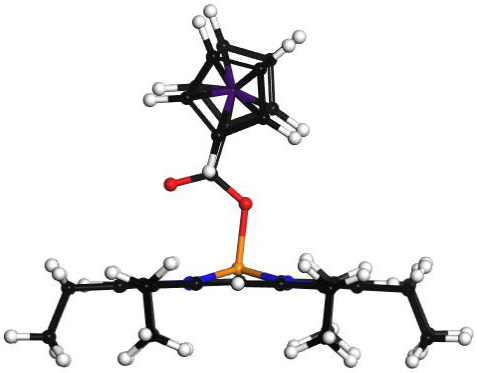

Ga(OEP)($O_2$CFc)

**Figure 3.2.** Gas-phase optimized structures of Ga(OEP)X complexes. Atoms are color coded: Ga, orange; N, blue; C, black; H, white; Fe, purple; Zn, grey; O, red.

**Table 3.1.** Selected Bond Distances (Å) and Angles (°) for Ga(OEP)X Complexes Calculated by Density Functional Theory.

| | X | | | | |
|---|---|---|---|---|---|
| Nuclei | CCPh | CCFc | CCZnTPP | OH | $CO_2Fc$ |
| Ga–X | 1.956 | 1.953 | 1.959 | 1.822 | 1.887 |
| Ga–N(1) | 2.068 | 2.071 | 2.074 | 2.069 | 2.054 |
| Ga–N(2) | 2.068 | 2.069 | 2.073 | 2.052 | 2.038 |
| Ga–N(3) | 2.068 | 2.070 | 2.074 | 2.069 | 2.04 |
| Ga–N(4) | 2.068 | 2.070 | 2.075 | 2.071 | 2.057 |
| N(1)–Ga–X | 103.9 | 104.1 | 104.1 | 104.0 | 97.1 |
| N(2)–Ga–X | 103.9 | 103.9 | 104.5 | 100.0 | 107.3 |
| N(3)–Ga–X | 103.9 | 103.9 | 103.9 | 103.9 | 105.8 |
| N(4)–Ga–X | 103.8 | 104.0 | 103.5 | 105.6 | 96.5 |
| Ga–$C_{20}N_4$ plane | 0.536 | 0.536 | 0.556 | 0.519 | 0.445 |
| Ga–$N_4$ plane | 0.495 | 0.544 | 0.566 | 0.528 | 0.450 |
| Ga–$C_{20}$ plane | 0.544 | 0.500 | 0.502 | 0.478 | 0.416 |
| $N_4$–$C_{20}$ plane | 0.048 | 0.044 | 0.065 | 0.050 | 0.035 |

To predict how these compounds might behave when assembled as monolayers on HOPG, structures were optimized in local minima with all eight ethyl chains rotated up as is the expected orientation when on the surface.[31-33] These calculations were performed with the basis sets 6-31G* for carbon, hydrogen, nitrogen, and oxygen atoms, and the LANL2DZ effective core potential basis set[34, 35] for gallium, zinc, and iron. These are less precise, but less computationally demanding basis sets than the cc-pVTZ basis set[36-38] employed for most optimized structures, and were found to be suitable for on-surface modeling. Space-filling models of these structure were then used to construct molecular models; the molecules were placed in a unit cell typical of an M(OEP) lattice, as exemplified by the compounds in Chapter 2 (example in Figure 3.3).

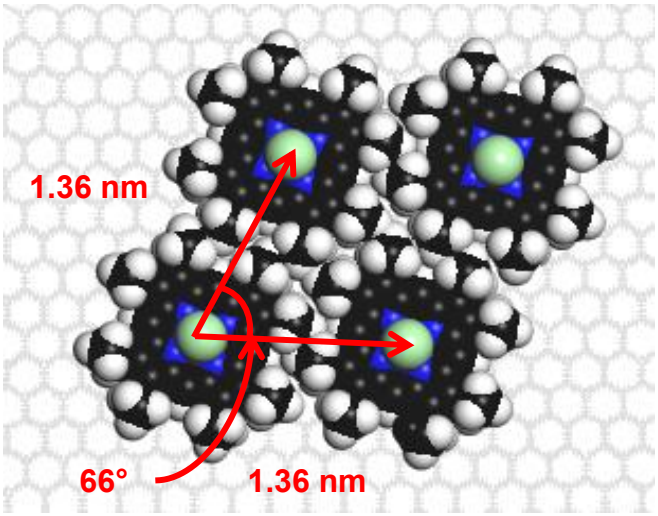


**Figure 3.3.** On-surface space-filling molecular model of Ga(OEP)Cl in the pseudo-hexagonal unit cell representative of the Ga(OEP)X compounds studied in Chapter 2.

These models allowed us to see if sterically bulkier axial ligands are predicted to have free rotation on the surface when organized into a close-packed pseudo-hexagonal lattice. From inspection of these models, the axial ligands of both Ga(OEP)(CCFc) and Ga(OEP)($O_2$CFc) are predicted to have free rotation (Figure 3.4a and b), but Ga(OEP)(CCZnTPP) ligands are predicted to not freely rotate (Figure 3.4c). This agrees with the gas-phase optimized structure that give a *para*-H to *para*-H distance of 1.77 nm on the axial ligand, which is greater than the expected unit cell lattice distance of 1.36 nm. This indicates that the axial CCZnTPP ligand has the potential to present widespread on-surface coplanar alignment (Figure 3.4c). Another possibility is that the steric bulk of the axial ligand could influence the standard underlying pseudohexagonal unit cell to accommodate the ligand. Sterically demanding alkanethiol head groups have been used to alter the packing of SAMs on gold,[39] and substituents are used on the periphery of porphyrins to affect their 2D unit cells,[40, 41] but the use of large, structure-directing axial ligands would offer a different approach. If this disruption of the lattice occurred, it would also provide the first example of a M(OEP) monolayer that does not exhibit the standard pseudo-hexagonal unit cell in our hands.

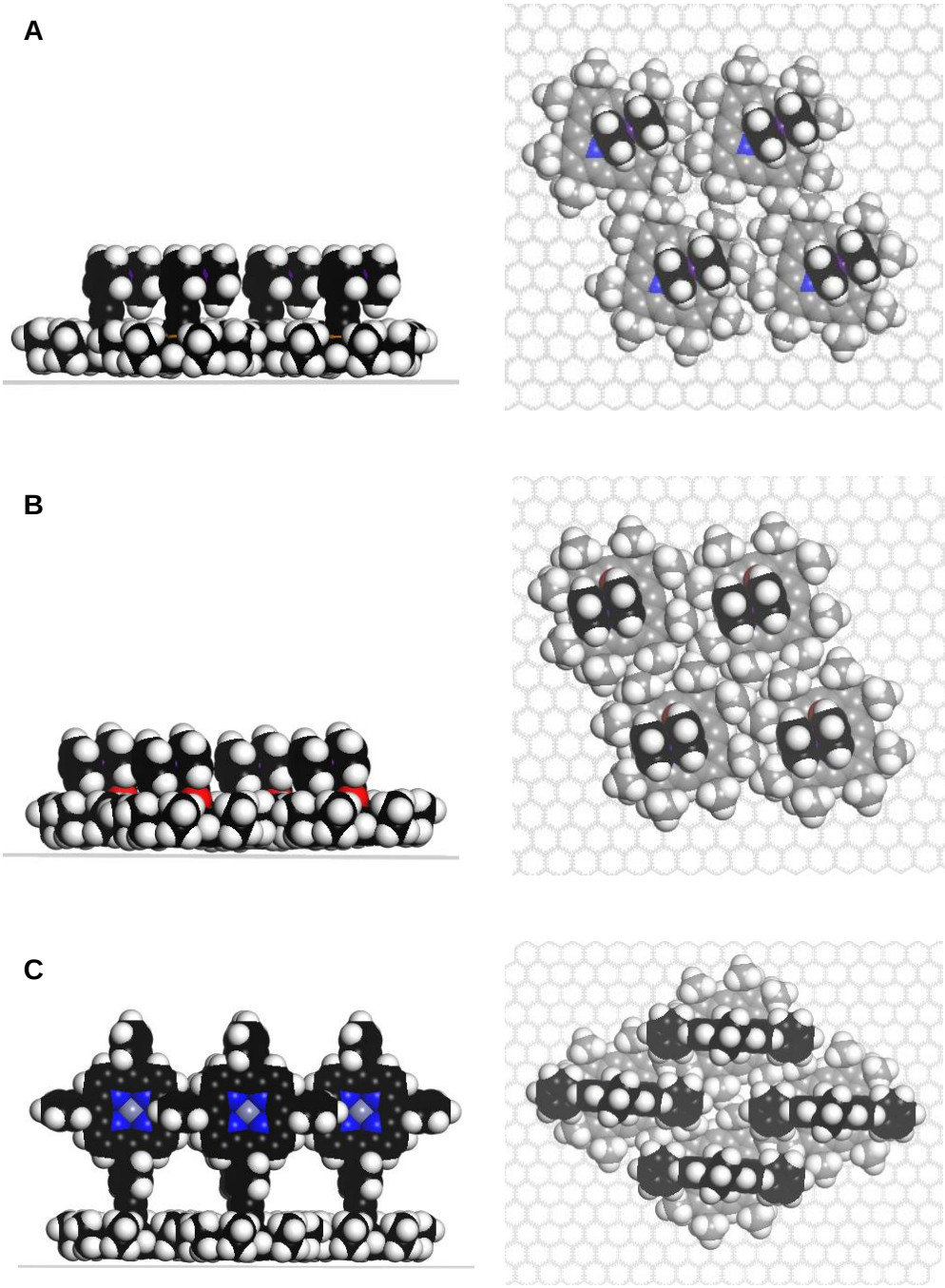


**Figure 3.4.** On-surface space-filling molecular models of Ga(OEP)X complexes in expected pseudo-hexagonal M(OEP) unit cell, side-on and top-down views. (A) Ga(OEP)(CCFc) axial ligands are expected to have free rotation; (B) Ga(OEP)($O_2$CFc) axial ligands are expected to have free rotation; (C) Ga(OEP)(CCZnTPP) axial ligands are expected to align.

### 3.3.3 Scanning Tunneling Microscopy.

**3.3.3.1. Ga(OEP)(CCFc).** When deposited from a 0.5 mM 1-phenyloctane solution, Ga(OEP)(CCFc) is observed to form self-assembled monolayers on HOPG (Figure 3.5). The monolayers are not as extensive as those observed for Ga(OEP)X compounds discussed in Chapter 2, with widths generally spanning approximately 75 nm (Figure 3.5a and b) compared to >100 nm widths observed in Chapter 2. This may indicate monolayer formation is slower than that observed for other Ga(OEP)X compounds due to added steric bulk of the ligand, or that some removal of monolayer may be occurring during the STM experiment; a more systematic time-dependent study of monolayer coverage would shed light on this issue. The lattice parameters are typical of those observed for Ga(OEP)X complexes described in Chapter 2 (a = 1.39 (0.04) nm, b = 1.37 (0.04) nm, Γ= 65 (2)°), indicating the larger axial CCFc ligand has no impact on the porphyrin packing.

An important difference between the STM images for Ga(OEP)(CCFc) and those of the Ga(OEP)X compounds discussed in Chapter 2 is their greater apparent height, averaging ~3.5 Å (Figure 3.5c) compared to ~1.2 Å observed for the Ga(OEP)(CCPh) complex. Like those of other Ga(OEP)X compounds, this height is still noticeably less than the calculated height of the ligand, which is ~8 Å. Electroactive molecules have been observed to give bright features when imaged by STM under bias voltages that allow tunneling through the HOMO-LUMO gap.[22] It has been noted that this bias-dependent effect is not observed in less electroactive molecules, as in a STM study comparing tethered Fe(TPP)Cl to its Zn and free base derivatives,[22] meaning the physical height is less important than the conductivity of the ligand and bias voltage applied when observing apparent height. Ordered arrays of ferrocenes are attractive targets for their

possible applications in molecular switching and charge storage devices.[10, 11] Our results indicate that such ligands could additionally act as "STM contrast agents" in mixed component systems.

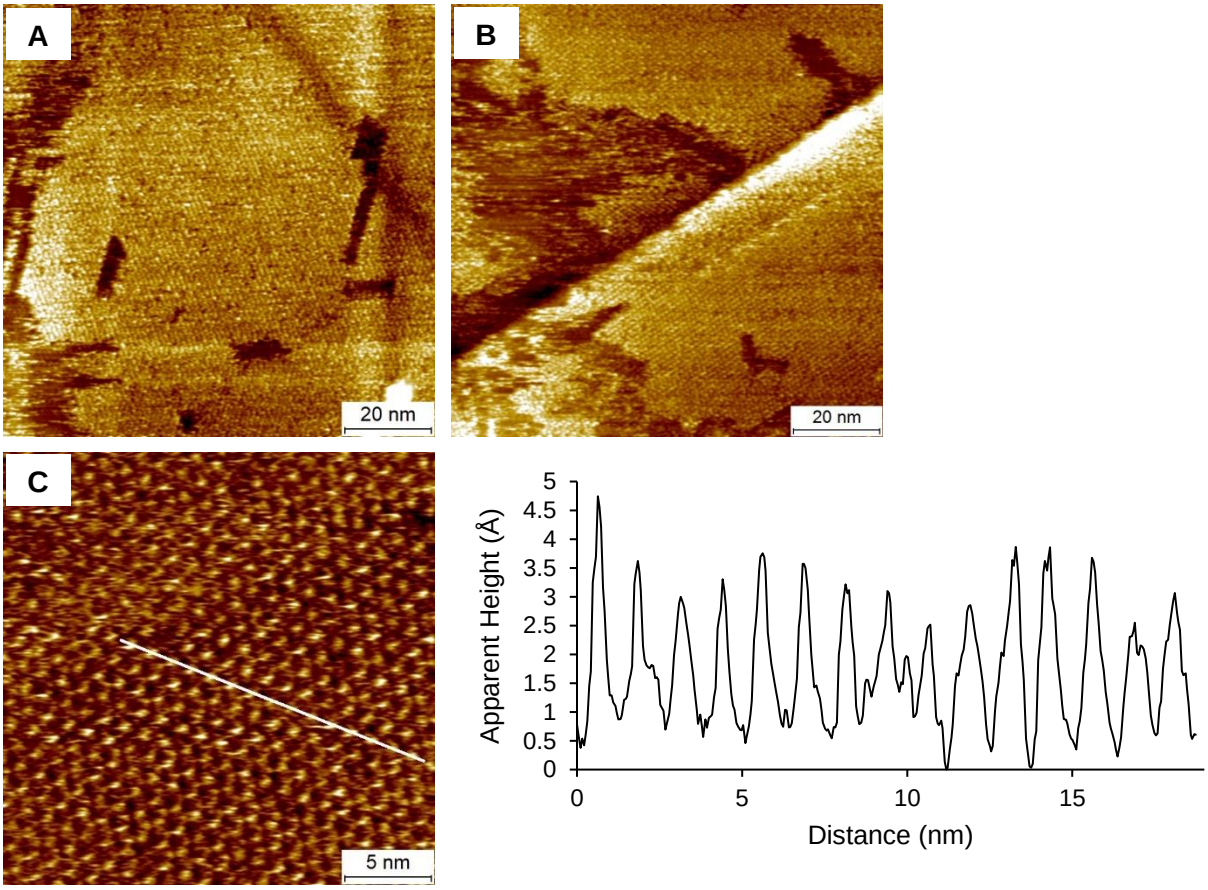


**Figure 3.5.** STM images showing long-range (A and B) and short-range ordering (C) of Ga(OEP)(CCFc) on HOPG at the solid–liquid interface (0.5 mM, 1-phenyloctane). The cross-sectional profile is taken along the white line shown in the STM image (C). The images were acquired at (A): $I$ = 10 pA, $V$ = –500 mV; (B): $I$ = 10 pA, $V$ = –500 mV; (C): $I$ = 8 pA, $V$ = –600 mV.

**3.3.3.2. Ga(OEP)(CCZnTPP).** While the ferrocene ligand of Ga(OEP)(CCFc) does not affect the lattice parameters of the self-assembled monolayer, molecular models based on the DFT optimized structure predicted that the axial ligand would retain free rotation in the pseudo-hexagonal unit cell typical of OEP compounds studied thus far. However, this is not the case for the larger zinc ethynyltetraphenylporphyrin ligand (-CCZnTPP), where a restriction of free rotation is predicted. As discussed in Section 3.3.2, it is predicted that when deposited onto an

HOPG surface, the axial ligands must either align parallel to one another, or the unit cell must be affected to accommodate this larger ligand and allow free rotation.

As discussed in Section 3.3.1, the sample of Ga(OEP)(CCZnTPP) used for STM studies contained a significant HCCZnTPP impurity and a small Ga(OEP)Cl impurity. Compounds of tetraphenylporphyrin are not known to form monolayers on metal or HOPG surfaces under ambient conditions due to the ~60° angle that the meso-phenyl rings form with respect to the plane of the porphyrin; ultra-high vacuum[42] or electrochemical STM[43] conditions are therefore required to study their surface assembly. Monolayer formation from TPP-based molecules requires edge-functionalization (e.g., carboxylic acid phenyl substituents and long-chain phenyl substituents). Even this approach is not always straightforward; in studies of alkoxyphenyl substituted porphyrins with long alkyl (or derivatized alkyl) chains to assist in surface assembly, a mixture of edge-on and face-on porphyrin assemblies can be observed under ambient conditions.[44-46] However, to rule out the possibility of HCCZnTPP assembly contributing to any observed surface structures, surface deposition control studies were performed on this compound. At concentrations and imaging conditions typical of those used in this study, no arrays were observed when HCCZnTPP was deposited on HOPG from a 1-phenyloctane solution.

In preliminary studies, the Ga(OEP)(CCZnTPP) compound was observed to assemble into monolayers on HOPG when deposited from a 1-phenyloctane solution (~0.5 mM). (The concentration of Ga(OEP)(CCZnTPP) accounts for the impurities.) A large-scale image (Figure 3.6a) indicates long-range assembly of the monolayer, though bright streaks (not typically observed for other compounds) appear across the image. We speculate that this may be due to the excess of HCCZnTPP in solution; STM tips have been known to interact with molecules in solution, reducing their effective sharpness.[47] In small-scale images, both ring-shaped features

associated with the OEP macrocycle (Figure 3.6b) and more defined axial features (Figure 3.6c) can be observed by changing the imaging bias, as is observed with compounds in Chapter 2. From these, we observe that the lattice parameters are consistent with a typical pseudo-hexagonal OEP unit cell: a = 1.37 (0.02) nm, b = 1.37 (0.03) nm, Γ = 67 (2)°. This indicates that the large CCZnTPP axial ligand does not affect the self-assembly of the Ga(OEP) base into a close-packed pseudo-hexagonal structure.

Features observed at –800 mV (Figure 3.5c) show the possibility of elongated axial ligand features, specifically, prolate spheroids (indicated by white arrows in the figure) whose long axes are aligned with each other. While further work to repeat these studies on a purified sample is necessary, we tentatively suggest that these elongated features are associated with the planes of the axially ligated ZnTPP molecules, and that their alignment is due to hindered rotation of the ligand. The apparent height of these features is 2–2.5 Å, well below the calculated height of the ligand (~21 Å), and below that of the ethynylferrocene ligand discussed above. However, a previous report of STM of Zn(TPP) tethered to a gold surface showed that the observed STM contrast was not as bright as its conductive Fe(TPP)Cl and Mn(TPP)Br analogs.[22]

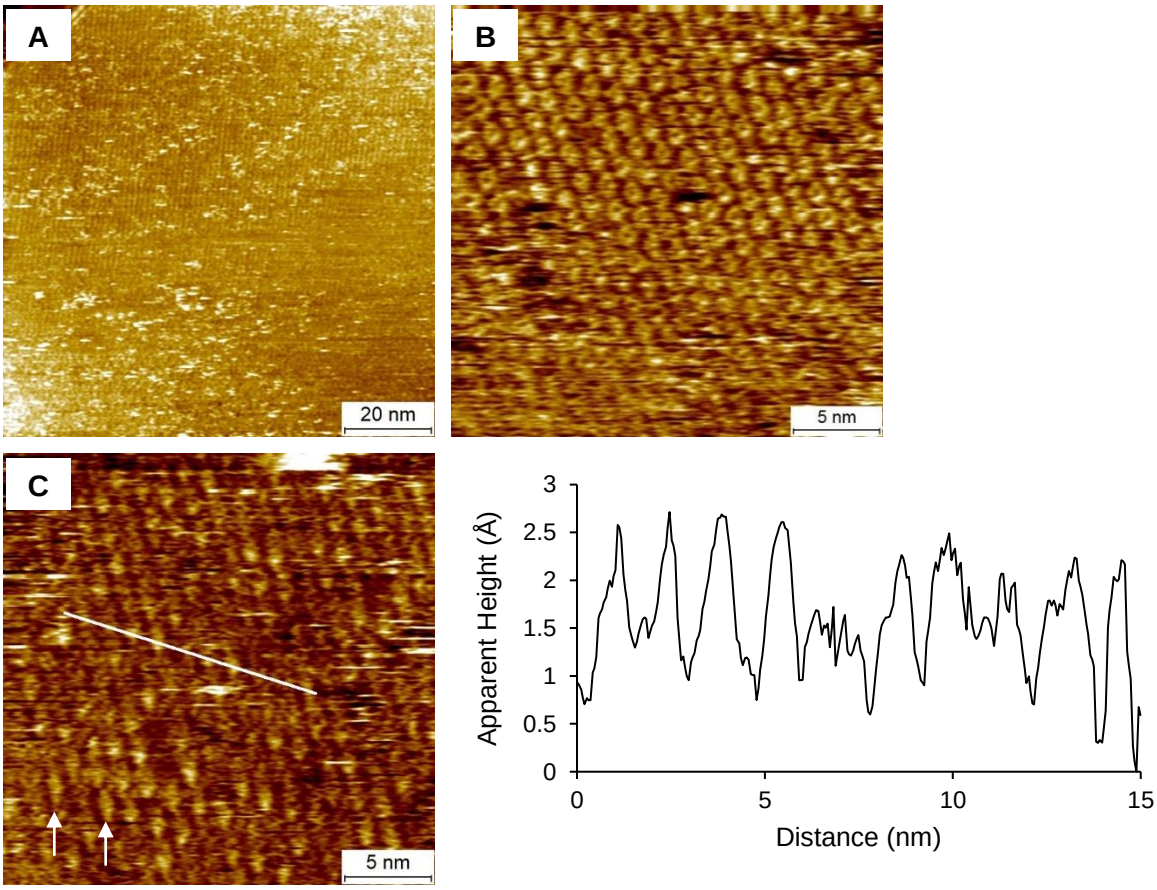


**Figure 3.6.** STM images of a Ga(OEP)(CCZnTPP) monolayer self-assembled on HOPG at the solid–liquid interface (~0.5 mM Ga(OEP)(CCZnTPP)). (A) Shows long-range ordering of porphyrins ($I$ = 8 pA, $V$ = –500 mV); (B) Shows tunneling through porphyrin ring periphery ($I$ = 8 pA, $V$ = –500 mV); (C) Shows tunneling through axial ligand upon changing bias potential with arrows pointing to examples of possibly elongated features. The cross-sectional profile corresponds to the line in image C ($I$ = 8 pA, $V$ = –800 mV).

**3.3.3.3. Ga(OEP)(OH).** The compound Ga(OEP)(OH) was observed to form self-assembled monolayers on HOPG when deposited from a 0.5 M solution in 1-phenyloctane. Monolayer widths spanning greater than 100 nm (Figure 3.7a) were observed to form within 5-10 minutes of deposition. The monolayer appears robust; imaging took place from 8-20 pA with no removal of the monolayer observed after repeated scanning of the same area and experiment times of over 60 minutes. Both the ring-shaped features associated with the heterocycle (Figure 3.7b) and more defined axial ligand features (Figure 3.7c) have been observed for this compound, in agreement with other Ga(OEP)X complexes. Small-scale images and cross-sectional profiles (example in

Figure 3.7c) show ligands with apparent heights with a maximum of ~1.5 Å and an average of ~0.8 Å. This wider range of height variation may be due to a small Ga(OEP)Cl impurity or other porphyrinic impurity, or result from imaging at a bias voltage that does not allow for good resolution of the ligand. Purification of the compound and further STM trials with rigorous bias dependent scans should help clarify this observation. The lattice parameters for this compound were observed to be a = 1.37 (0.02) nm, b = 1.36 (0.02) nm, Γ = 65 (1)°, in accordance with previously reported Ga(OEP)X lattice parameters.

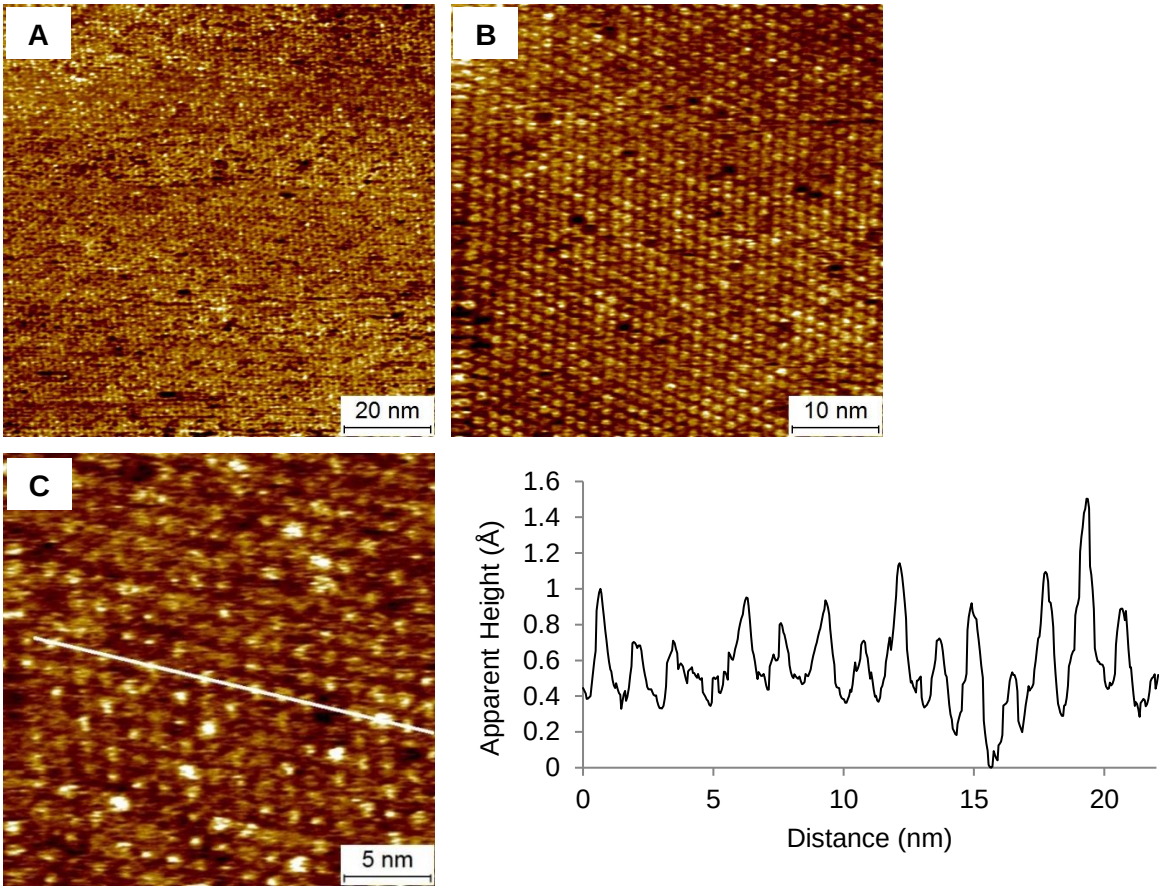


**Figure 3.7.** STM images of a Ga(OEP)(OH) monolayer self-assembled on HOPG at the solid-liquid interface (0.5 mM, 1-phenyloctane). (A) Shows long-range ordering of porphyrins (*I* = 12 pA, *V* = –500 mV); (B) Shows tunneling through porphyrin ring periphery (*I* = 10 pA, *V* = –700 mV); (C) Shows tunneling through axial ligand. The cross-sectional profile corresponds to the line in image C (*I* = 15 pA, *V* = –700 mV).

**3.3.3.4. Ga(OEP)($O_2$CFc).** The surface chemistry of Ga(OEP)($O_2$CFc) on HOPG was investigated in order to examine whether the carboxylate linkage changed the properties of the monolayer relative to the ethynyl linkage used for other compounds and, specifically, the analogue Ga(OEP)(CCFc). The monolayers were prepared in two ways: first, by direct deposition of the compound, and second, under conditions in which a pre-deposited Ga(OEP)(OH) monolayer might react with an added 1-phenyloctane solution of ferrocenecarboxylic acid (FcCOOH). Direct deposition of Ga(OEP)($O_2$CFc) from a 1-phenyloctane solution of ~0.5 mM resulted in the formation of large arrays (Figure 3.8a and b). As in the case of Ga(OEP)(CCFc), these arrays are not as expansive as other Ga(OEP)X type compounds (Figure 3.5 a and b), spanning ~75 nm in width. Also consistent with Ga(OEP)(CCFc) observations are bright features assignable to tunneling through the ferrocene ligand. Cross-sectional profiles give an average apparent height of ~5-6 Å for these bright features (even taller than features observed for the Ga(OEP)(CCFc) which had apparent heights of ~3.5 Å), as indicated in the height profile shown below. Lattice parameters were determined to be a = 1.38 (0.04) nm, b = 1.36 (0.03) nm, Γ = 65 (2)°, in accordance with previously reported Ga(OEP)X lattice parameters.

In contrast to the Ga(OEP)(CCFc) monolayers, dark regions are interspersed with the bright ferrocene features in the Ga(OEP)($O_2$CFc) monolayer. The observation of regions of the pseudo-hexagonal cell that are completely filled with bright features (Figure 3.8c) eliminate the possibility that the axial Fc substituent encroaches into an adjacent cell, causing the incomplete monolayer coverage. This is in agreement with molecular models that indicate the ferrocene ligands will have free rotation within the OEP unit cell (Figure 3.4b). The porphyrin rings were able to be partially imaged (Figure 3.8e) and found to not exhibit vacancies, which suggests that

the dark features in the monolayer are not associated with an absence of an underlying Ga(OEP) unit but are more likely due to Ga(OEP)X base units that do not contain a ferrocene ligand. The compound was observed to be stable in a $C_6D_6$ solution, as monitored by $^1H$ NMR for nine days, so mere degradation of the sample over the time frame of the experiment (several hours) is an unlikely source. Possibilities include small Ga(OEP)Cl or Ga(OEP)(OH) impurities that are highly visible in the STM images due to the difference in apparent height, or removal of the ferrocene ligand during the STM imaging process. Control studies of FcCOOH in 1-phenyloctane deposited on HOPG gave no evidence of monolayer formation, so this is also an unlikely source of the dark spots. Given the difficulty in purification of this compound, and the high proportion of defects of unknown origin in this complex, acetylides were used as the primary linker moving forward in this study.

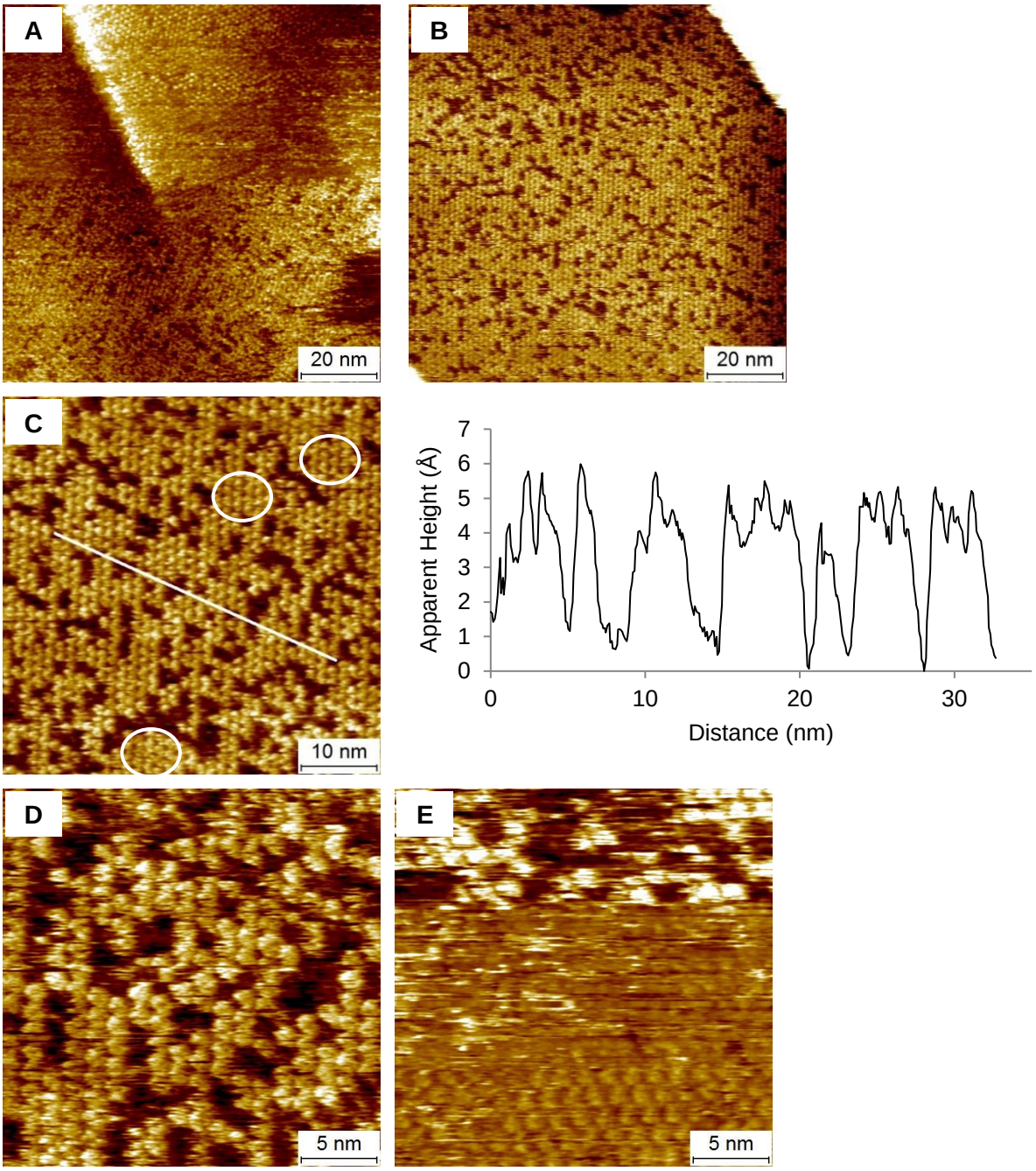


**Figure 3.8.** STM images of a Ga(OEP)($O_2$CFc) monolayer self-assembled on HOPG at the solid-liquid interface (~0.5 mM, 1-phenyloctane). (A) Shows that the monolayer domain extends in width ~75 nm ($I$ = 8 pA, $V$ = –500 mV); (B) Shows large-scale ordering of very bright ferrocene features interspersed with a large number of dark features ($I$ = 8 pA, $V$ = –500 mV); (C) Regions of close-packed ferrocene features are circled. The cross-sectional profile corresponds to the line in image C ($I$ = 8 pA, $V$ = –500 mV); (D) Small-scale image showing noticeably more dark features than for Ga(OEP)X compounds described in Chapter 2 ($I$ = 8 pA, $V$ = –500 mV); (E) Porphyrin ring structure seen in bottom of image ($I$ = 8 pA, $V$ = –400 mV).

To probe whether monolayers of Ga(OEP)($O_2$CFc) could be formed by an on-surface reaction, and eliminate the need for prior synthesis of the fully formed complex, a monolayer of Ga(OEP)(OH) was first prepared on HOPG from a 0.5 mM solution in 1-phenyloctane and imaged at the solid-liquid interface (see Section 3.3.3.3). Notably, the average apparent maximum height of the Ga(OEP)(OH) molecules is ~0.8 Å. A 0.5 mM solution of ferrocenecarboxylic acid in 1-phenyloctane was added in approximately equal volume to the solution on the surface and the STM tip was re-engaged. Within 5-10 minutes of adding the FcCOOH solution, multiple bright features were observed on the underlying monolayer background (Figure 3.9). The apparent height of these bright features is ~5.0 Å when imaged at the same bias potential of –500 mV (Figure 3.9b), which is consistent with the height observed for a monolayer of Ga(OEP)($O_2$CFc) prepared by direct deposition (see above). The initial images are characterized by very bright streaks which may be due to excess material in solution, as described earlier for Ga(OEP)(CCZnTPP).

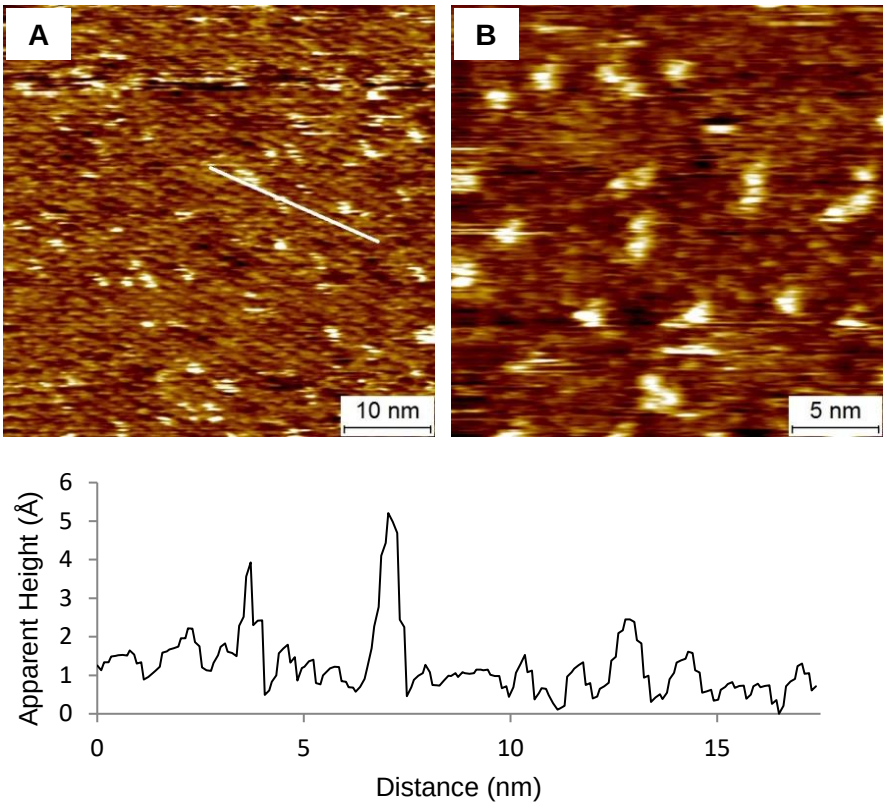


**Figure 3.9.** STM images of a Ga(OEP)(OH) monolayer self-assembled on HOPG (0.5 mM, 1-phenyloctane) at the solid-liquid interface to which a ferrocene carboxylic acid solution has been added (0.5 mM, 1-phenyloctane). (A) t = 5-10 minutes after deposition; shows patterned background with sporadic bright features. The cross-sectional profile corresponds to the line in the image ($I$ = 8 pA, $V$ = –500 mV); (B) Shows small-scale ordering with bright features and streaks ($I$ = 8 pA, $V$ = –500 mV).

At t = ~35 minutes after the FcCOOH solution was deposited, noticeably more bright features were observed (Figure 3.10). However, domain edges on exposed HOPG are also observed where none were previously seen in monolayers of Ga(OEP)(OH). The observation that Ga(OEP)(OH) has been removed from the surface to expose HOPG could be a result of the two-fold reduction in concentration of Ga(OEP)(OH) in the covering solution or a consequence of an on-surface chemical reaction. The bright features appear more concentrated around the edges of the domains, and sequential images show that growth of the domains incorporate more bright features at the edges. This likely indicates that Ga(OEP)(OH) and FcCOOH react in

solution and then deposit at domain edges, while reactions within the monolayer itself occur more slowly.

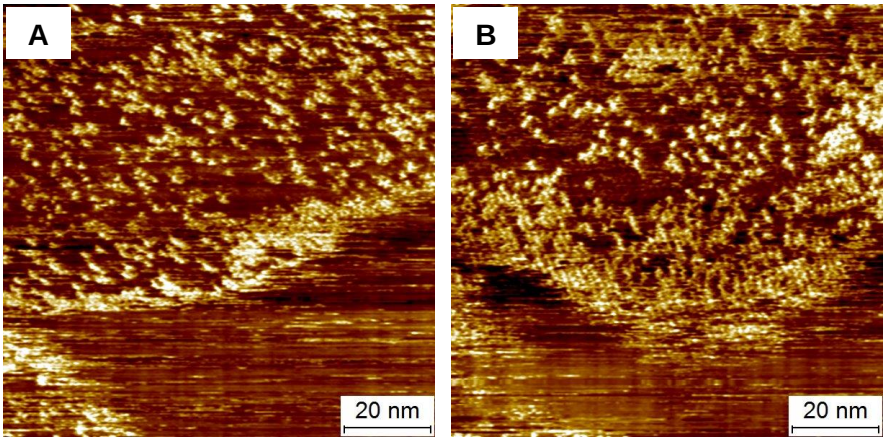


**Figure 3.10.** Sequential STM images of a Ga(OEP)(OH) monolayer self-assembled on HOPG (0.5 mM, 1-phenyloctane) at the solid-liquid interface following addition of FcCOOH solution (0.5 mM, 1-phenyloctane, t = 35–40 minutes). (A) Shows domain boundary with bright features concentrated at the edge of the domain ($I$ = 8 pA, $V$ = –500 mV); (B) Shows domain growth with bright features depositing at edge of domain ($I$ = 8 pA, $V$ = –500 mV).

At t = ~60 minutes after FcCOOH addition coverage of bright spots is extensive, but was not observed to reach 100%; complete monolayer coverage of the HOPG surface was also not observed (Figure 3.11). Lattice parameters for the newly formed monolayer were determined to be a = 1.36 (0.03) nm, b = 1.36 (0.03) nm, Γ = 66 (2)°, in accordance with both the Ga(OEP)(OH) and Ga(OEP)($O_2$CFc) lattices, indicating that self-assembled structure is not affected by the on-surface/solution reaction process. In the analogous experiment in our lab with the gallium *meso*-tetradecylporphyrin analogs, it was observed that the Ga($TC_{10}$P)(OH) and Ga($TC_{10}$P)($O_2$CFc) had different lattices upon direct deposition, and that the hydroxide lattice was retained upon the deposition of FcCOOH, indicating that this was truly an on-surface reaction.[21] Due to the highly reproducible OEP unit cells, we cannot draw the same conclusion by analogy. At this time, we cannot definitely say if this is primarily an on-surface reaction or an in-solution formation of target compound that is then deposited, but preliminary results favor the latter.

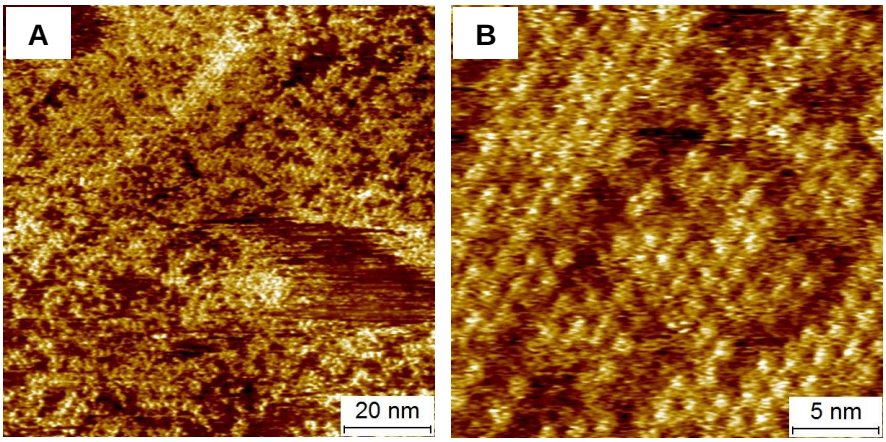


**Figure 3.11.** STM images of a Ga(OEP)(OH) monolayer self-assembled on HOPG at the solid liquid interface (0.5 mM, 1-phenyloctane) with ferrocene carboxylic acid solution added (0.5 mM, 1-phenyloctane, t = ~60 minutes). (A) Shows greater surface coverage of bright features than seen in Figure 3.9 ($I$ = 8 pA, $V$ = –500 mV); (B) Small-scale image of higher degree of ferrocene incorporation ($I$ = 12 pA, $V$ = –700 mV).

### 3.4. Conclusions.

The research described in this chapter has shown that monolayers containing Ga(OEP)X compounds can serve as platforms for the placement of redox- and photoactive functional units incorporated as axial X ligands. Ferrocene axial ligands were successfully incorporated via an ethynyl linker and the resulting complex, Ga(OEP)(CCFc), self-assembles on HOPG into a monolayer with a typical pseudo-hexagonal OEP unit cell. Notably, the ferrocene ligands have a greater apparent height than previous axial ligand studied, indicating that ferrocene could be useful as an "STM contrast agent" in future work. Ferrocene was also incorporated by direct deposition of the slightly impure Ga(OEP)($O_2$CFc) complex in an attempt to explore additional ligand linkages. While monolayers with very bright ferrocene features did form, dark features of indeterminate origin are also present in fairly high proportion as well. Formation of Ga(OEP)($O_2$CFc) was also attempted by an on-surface reaction, although preliminary results indicate that the reaction is taking place in solution and not exclusively, if at all, on the surface, and full coverage of the desired complex was never achieved. Finally, very preliminary STM

results on a Ga(OEP)(CCZnTPP) complex indicate that the dyad self-assembles into monolayers exhibiting the typical pseudo-hexagonal OEP unit cell and may confirm molecular models that the axial porphyrins must align with each other due to hindered rotation.

Overall, we have taken advantage of the propensity of Ga(OEP)X-type molecules to self-assemble into well-formed monolayers with highly reproducible pseudo-hexagonal unit cells in our ultimate goal of bottom-up assemblies of ordered arrays with collective function. The regularity in the unit cell allows us to use predictive methods combining DFT and molecular modeling to predict their assembly properties prior to deposition and STM imaging. Progress has been made towards incorporating electroactive and photoactive units axially into our arrays, in the form of ferrocene and surface-decoupled porphyrins, respectively. Further, we have made strides to expand the scope of ligand linkers beyond acetylides and deposition methods beyond direct deposition of fully synthesized molecules. While synthesis and purification of more complex porphyrin-ligand systems on a small scale needs to be improved, preliminary results indicate that the OEP unit cell is not disrupted by sterically demanding ligands, and that this is a promising system for further investigation.

### 3.5. References

1. Panda, M. K.; Ladomenou, K.; Coutsolelos, A. G. Porphyrins in Bio-Inspired Transformations: Light-Harvesting to Solar Cell. *Coord. Chem. Rev.* **2012**, *256*, 2601-2627.

2. Son, H. J.; Jin, S. Y.; Patwardhan, S.; Wezenberg, S. J.; Jeong, N. C.; So, M.; Wilmer, C. E.; Sarjeant, A. A.; Schatz, G. C.; Snurr, R. Q.; Farha, O. K.; Wiederrecht, G. P.; Hupp, J. T. Light-Harvesting and Ultrafast Energy Migration in Porphyrin-Based Metal-Organic Frameworks. *J. Am. Chem. Soc.* **2013**, *135*, 862-869.

3. Biesaga, M.; Pyrzynska, K.; Trojanowicz, M. Porphyrins in Analytical Chemistry. A Review. *Talanta* **2000**, *51*, 209-224.

4. Chou, J.-H.; Kosal, M. E.; Nalwa, H. S.; Rakow, N. A.; Suslick, K. S., Applications of Porphyrins and Metalloporphyrins to Materials Chemistry. In *The Porphyrin Handbook*, Kadish, K. M.; Smith, K.; Guilard, R., Eds. Academic Press: New York, 2000; Vol. 6, pp 43-131.

5. Otte, F. L.; Lemke, S.; Schutt, C.; Krekiehn, N. R.; Jung, U.; Magnussen, O. M.; Herges, R. Ordered Monolayers of Free-Standing Porphyrins on Gold. *J. Am. Chem. Soc.* **2014**, *136*, 11248-11251.

6. Chan, Y. H.; Schuckman, A. E.; Perez, L. M.; Vinodu, M.; Drain, C. M.; Batteas, J. D. Synthesis and Characterization of a Thiol-Tethered Tripyridyl Porphyrin on Au(111). *J. Phys. Chem. C* **2008**, *112*, 6110-6118.

7. Imahori, H.; Kashiwagi, Y.; Endo, Y.; Hanada, T.; Nishimura, Y.; Yamazaki, I.; Araki, Y.; Ito, O.; Fukuzumi, S. Structure and Photophysical Properties of Porphyrin-Modified Metal Nanoclusters with Different Chain Lengths. *Langmuir* **2004**, *20*, 73-81.

8. Rivas, M. V.; De Leo, L. P. M.; Hamer, M.; Carballo, R.; Williams, F. J. Self-Assembled Monolayers of Disulfide Cu Porphyrins on Au Surfaces: Adsorption Induced Reduction and Demetalation. *Langmuir* **2011**, *27*, 10714-10721.

9. Ormaza, M.; Abufager, P.; Bachellier, N.; Robles, R.; Verot, M.; Le Bahers, T.; Bocquet, M. L.; Lorente, N.; Limot, L. Assembly of Ferrocene Molecules on Metal Surfaces Revisited. *J. Phys. Chem. Lett.* **2015**, *6*, 395-400.

10. Hauquier, F.; Ghilane, J.; Fabre, B.; Hapiot, P. Conducting Ferrocene Monolayers on Nonconducting Surfaces. *J. Am. Chem. Soc.* **2008**, *130*, 2748-2749.

11. Fabre, B. Ferrocene-Terminated Monolayers Covalently Bound to Hydrogen-Terminated Silicon Surfaces. Toward the Development of Charge Storage and Communication Devices. *Accounts Chem. Res.* **2010**, *43*, 1509-1518.

12. Kitagawa, T.; Matsubara, H.; Komatsu, K.; Hirai, K.; Okazaki, T.; Hase, T. Ideal Redox Behavior of the High-Density Self-Assembled Monolayer of a Molecular Tripod on a Au(111) Surface with a Terminal Ferrocene Group. *Langmuir* **2013**, *29*, 4275-4282.

13. Jeong, H.; Kim, D.; Wang, G.; Park, S.; Lee, H.; Cho, K.; Hwang, W. T.; Yoon, M. H.; Jang, Y. H.; Song, H.; Xiang, D.; Lee, T. Redox-Induced Asymmetric Electrical Characteristics of Ferrocene-Alkanethiolate Molecular Devices on Rigid and Flexible Substrates. *Adv. Funct. Mater.* **2014**, *24*, 2472-2480.

14. Sun, Y. Y.; Peng, Z. L.; Hou, R.; Liang, J. H.; Zheng, J. F.; Zhou, X. Y.; Zhou, X. S.; Jin, S.; Niu, Z. J.; Mao, B. W. Enhancing Electron Transport in Molecular Wires by Insertion of a Ferrocene Center. *Phys. Chem. Chem. Phys.* **2014**, *16*, 2260-2267.

15. Shoji, O.; Tanaka, H.; Kawai, T.; Kobuke, Y. Single Molecule Visualization of Coordination-Assembled Porphyrin Macrocycles Reinforced with Covalent Linkings. *J. Am. Chem. Soc.* **2005**, *127*, 8598-8599.

16. Poddutoori, P. K.; Lim, G. N.; Sandanayaka, A. S. D.; Karr, P. A.; Ito, O.; D'Souza, F.; Pilkington, M.; van der Est, A. Axially Assembled Photosynthetic Reaction Center Mimics Composed of Tetrathiafulvalene, Aluminum(III) Porphyrin and Fullerene Entities. *Nanoscale* **2015**, *7*, 12151-12165.

17. Poddutoori, P. K.; Sandanayaka, A. S. D.; Hasobe, T.; Ito, O.; van der Est, A. Photoinduced Charge Separation in a Ferrocene-Aluminum(III) Porphyrin-Fullerene Supramolecular Triad. *J. Phys. Chem. B* **2010**, *114*, 14348-14357.

18. Kumar, P. P.; Maiya, B. G. Aluminium(III) Porphyrin Based Dimers and Trimers: Synthesis, Spectroscopy and Photochemistry. *New J. Chem.* **2003**, *27*, 619-625.

19. Davidson, G. J. E.; Tong, L. H.; Raithby, P. R.; Sanders, J. K. M. Aluminium(III) Porphyrins as Supramolecular Building Blocks. *Chem. Commun.* **2006**, 3087-3089.

20. Ghosh, A.; Maity, D. K.; Ravikanth, M. Aluminium(III) Porphyrin Based Axial-Bonding Type Dyads Containing Thiaporphyrins and Expanded Thiaporphyrins as Axial Ligands. *New J. Chem.* **2012**, *36*, 2630-2641.

21. Lau, W.-Y. Ph. D. Thesis. The University of Chicago, Chicago, IL, 2016.

22. Han, W. H.; Durantini, E. N.; Moore, T. A.; Moore, A. L.; Gust, D.; Rez, P.; Leatherman, G.; Seely, G. R.; Tao, N. J.; Lindsay, S. M. STM Contrast, Electron-Transfer Chemistry, and Conduction in Molecules. *J. Phys. Chem. B* **1997**, *101*, 10719-10725.

23. Yuan, Z.; Taylor, N. J.; Sun, Y.; Marder, T. B.; Williams, I. D.; Cheng, L. T. Synthesis and 2nd-Order Nonlinear-Optical Properties of Three Coordinate Organoboranes with Diphenylphosphino and Ferrocenyl Groups as Electron-Donors: Crystal and Molecular Structures of (E)-D-CH=CH-B(mes)$_2$ and D-C$\equiv$C-B(mes)$_2$ [D=P($C_6H_5$)$_2$, ($\eta$-$C_5H_5$)Fe($\eta$-$C_5H_4$); mes=2,4,6-($CH_3$)$_3$$C_6H_2$]. *J. Organomet. Chem.* **1993**, *449*, 27-37.

24. Senge, M. O. Stirring the Porphyrin Alphabet Soup-Functionalization Reactions for Porphyrins. *Chem. Commun.* **2011**, *47*, 1943-1960.

25. Krattinger, B.; Callot, H. J. Alkylation and Reduction of Porphyrins and N-substituted Porphyrins: New Routes to Chlorins and Phlorins. *Eur. J. Org. Chem.* **1999**, 1857-1867.

26. Darling, S. L.; Stulz, E.; Feeder, N.; Bampos, N.; Sanders, J. K. M. Phosphine-Substituted Porphyrins as Supramolecular Building Blocks. *New J. Chem.* **2000**, *24*, 261-264.

27. Parzuchowski, P. G.; Kampf, J. W.; Rozniecka, E.; Kondratenko, Y.; Malinowska, E.; Meyerhoff, M. E. Gallium(III) and Indium(III) Octaethylporphyrin Dimeric Complexes with a Single μ-Hydroxo Bridge: Synthesis, Structure and Stability in Anion-Containing Organic Media. *Inorg. Chim. Acta* **2003**, *355*, 302-313.

28. Kadish, K. M.; Cornillon, J. L.; Coutsolelos, A.; Guilard, R. Synthesis, Electrochemistry, and Ligand-Addition Reactions of Gallium(III) Porphyrins. *Inorg. Chem.* **1987**, *26*, 4167-4173.

29. Maeda, D.; Shimakoshi, H.; Abe, M.; Fujitsuka, M.; Majima, T.; Hisaeda, Y. Synthesis of a Novel Sn(IV) Porphycene-Ferrocene Triad Linked by Axial Coordination and Solvent Polarity Effect in Photoinduced Charge Separation Process. *Inorg. Chem.* **2010**, *49*, 2872-2880.

30. Bohle, D. S.; Dodd, E. L.; Pinter, T. B. J.; Stillman, M. J. Soluble Diamagnetic Model for Malaria Pigment: Coordination Chemistry of Gallium(III)protoporphyrin-IX. *Inorganic Chemistry* **2012**, *51*, 10747-10761.

31. Ogunrinde, A.; Hipps, K. W.; Scudiero, L. A Scanning Tunneling Microscopy Study of Self-Assembled Nickel(II) Octaethylporphyrin Deposited from Solutions on HOPG. *Langmuir* **2006**, *22*, 5697-5701.

32. Scudiero, L.; Barlow, D. E.; Hipps, K. W. Scanning Tunneling Microscopy, Orbital-Mediated Tunneling Spectroscopy, and Ultraviolet Photoelectron Spectroscopy of Nickel(II) Octaethylporphyrin Deposited from Vapor. *J. Phys. Chem. B* **2002**, *106*, 996-1003.

33. Friesen, B. A.; Bhattarai, A.; Mazur, U.; Hipps, K. W. Single Molecule Imaging of Oxygenation of Cobalt Octaethylporphyrin at the Solution/Solid Interface: Thermodynamics from Microscopy. *J. Am. Chem. Soc.* **2012**, *134*, 14897-14904.

34. Wadt, W. R.; Hay, P. J. Ab Initio Effective Core Potentials for Molecular Calculations - Potentials for Main Group Elements Na to Bi. *J. Chem. Phys.* **1985**, *82*, 284-298.

35. Hay, P. J.; Wadt, W. R. Abinitio Effective Core Potentials for Molecular Calculations - Potentials for the Transition-Metal Atoms Sc to Hg. *J. Chem. Phys.* **1985**, *82*, 270-283.

36. Dunning, T. H. Gaussian Basis Sets for Use in Correlated Molecular Calculations. I. The Atoms Boron through Neon and Hydrogen. *J. Chem. Phys.* **1989**, *90*, 1007-1023.

37. Wilson, A. K.; Woon, D. E.; Peterson, K. A.; Dunning, T. H. Gaussian Basis Sets for Use in Correlated Molecular Calculations. IX. The Atoms Gallium through Krypton. *J. Chem. Phys.* **1999**, *110*, 7667-7676.

38. Balabanov, N. B.; Peterson, K. A. Systematically Convergent Basis Sets for Transition Metals. I. All-Electron Correlation Consistent Basis Sets for the 3d Elements Sc-Zn. *J. Chem. Phys.* **2005**, *123*.

39. Yan, J. W.; Ouyang, R. H.; Jensen, P. S.; Ascic, E.; Tanner, D.; Mao, B. W.; Zhang, J. D.; Tang, C. G.; Hush, N. S.; Ulstrup, J.; Reimers, J. R. Controlling the Stereochemistry and Regularity of Butanethiol Self-Assembled Monolayers on Au(111). *J. Am. Chem. Soc.* **2014**, *136*, 17087-17094.

40. Otsuki, J. STM Studies on Porphyrins. *Coord. Chem. Rev.* **2010**, *254*, 2311-2341.

41. Mohnani, S.; Bonifazi, D. Supramolecular Architectures of Porphyrins on Surfaces: The Structural Evolution from 1D to 2D to 3D to Devices. *Coord. Chem. Rev.* **2010**, *254*, 2342-2362.

42. Gottfried, J. M. Surface Chemistry of Porphyrins and Phthalocyanines. *Surf. Sci. Rep.* **2015**, *70*, 259-379.

43. Hassani, S. S.; Kim, Y. G.; Borguet, E. Self-Assembly of Insoluble Porphyrins on Au(111) Under Aqueous Electrochemical Control. *Langmuir* **2011**, *27*, 14828-14833.

44. Zhou, Y. S.; Wang, B.; Zhu, M. Z.; Hou, J. G. Observation of Co-Existence of 'Face-on' and 'Edge-on' Stacking Styles in a Porphyrin Monolayer. *Chem. Phys. Lett.* **2005**, *403*, 140-145.

45. Otsuki, J.; Namiki, K.; Arai, Y.; Amano, M.; Sawai, H.; Tsukamoto, A.; Hagiwara, T. Face-on and Columnar Porphyrin Assemblies at Solid/Liquid Interface on HOPG. *Chem. Lett.* **2009**, *38*, 570-571.

46. Sakano, T.; Hasegawa, J.; Higashiguchi, K.; Matsuda, K. Chronological Change from Face-On to Edge-On Ordering of Zinc-Tetraphenylporphyrin at the Phenyloctane-Highly Oriented Pyrolytic Graphite Interface. *Chem. - Asian J.* **2012**, *7*, 394-399.

47. den Boer, D.; Han, G. D.; Swager, T. M. Templating Fullerenes by Domain Boundaries of a Nanoporous Network. *Langmuir* **2014**, *30*, 762-767.

# CHAPTER 4

## Fullerene Overlayers on Five-Coordinate Porphyrin Templates Using Axial Ligand Affinity Groups to Facilitate Assembly

### 4.1. Introduction

Supramolecular self-assembly on atomically flat surfaces aims to generate a wide range of complex structures on the nanometer scale and offers new means of tailoring the interface, particularly as we move towards the next generation of devices in nanotechnology. This can be accomplished through a combination of well-studied two-dimensional assembly techniques as well as those designed to build hierarchical assemblies into the third dimension. In the previous chapters, we have focused on determining the relationship between axial functionalization and two-dimensional monolayer assembly. We have also discussed efforts towards covalently functionalizing pre-determined sites in self-assembled monolayers of Ga(OEP)X complexes with electro- and photoactive ligands. We now turn our attention to functionalization of these monolayers through supramolecular host-guest interactions.

The rich properties and potential applications of fullerenes for, among others, solar cells, sensors, and electronics, make them an attractive target for components in functional nanoscale devices.[1, 2] The fact that such applications generally require that the fullerenes be part of a larger ensemble of chemical compounds that are spatially organized around them (e.g., with electron donors in solar cells[3-5]) has motivated extensive study of supramolecular fullerene chemistry, from which has emerged a wealth of design strategies for compounds, macromolecules, and solids in which fullerenes are located in specific or periodic positions.[6-8] Supramolecular materials that self assemble via noncovalent interactions have been a particular focus because of their ability to incorporate pristine fullerenes (with their attendant properties) and their synthetic scalability, as contrasted with covalent assembly approaches. While the fullerenes $C_{60}$ and $C_{70}$

are known to form monolayers on gold surfaces under ambient conditions,[9, 10] attempts to form monolayers of $C_{60}$ on HOPG under the same conditions have been unsuccessful, and it was concluded that their affinity for the surface was not high enough to remove the fullerene from solution.[10] Monolayers are reported under UHV conditions, though even with precisely controlled deposition methods, the buckyballs are prone to forming multilayers and are easily removed during STM scanning.[11]

This has given rise to interest in the template-assisted assembly of fullerenes on HOPG at the solid-liquid interface. Previous attempts have relied on two-dimensional networks to act as the receptor. These networks have been comprised of a variety of components such as carboxylic acids,[12-15] covalent-organic frameworks,[16, 17] components that are known participants in fullerene donor-acceptor pairs such as oligothiophenes,[18-21] or larger macrocycles.[22] While the goal of any template is to exploit the size or recognition groups of the cavity formed to effectively trap the target molecule, such two-dimensional networks often fall short in terms of creating predictable adsorption sites and versatile deposition and imaging conditions. For example, $C_{60}$ templating onto a self-assembled network of cyclothiophene molecules at the HOPG-1,2,4-trichlorobenzene interface showed adsorption both along the rim and in the center of the macrocycle,[18] and a report of templating $C_{60}$ and $C_{84}$ on trimesic acid at the HOPG-1-octanoic acid interface gave templating only along domain boundaries in the trimesic acid network.[12] Further, while porphyrins are known to form solution and solid-state supramolecular assemblies with fullerenes,[23-28] studies of porphyrin-fullerene surface assemblies are carried out under UHV or electrochemical STM conditions.[29] A new type of assembly motif would seek to address these issues.

We hypothesized that employing a square-pyramidal, five-coordinate metalloporphyrin monolayer as a corral to guide the assembly of fullerenes would prove to be an effective templating method at the HOPG-liquid interface. By choosing a porphyrin that self assembles into a lattice with parameters that are amenable to a target nanoparticle and employing an axial ligand that will have affinity for it, patterning could be achieved under ambient conditions, particularly at the solid-liquid (1-phenyloctane) interface. In regards to templating fullerenes, M(OEP) has been demonstrated throughout this work to reliably form well-ordered monolayers that give a pseudo-hexagonal unit cell at the HOPG-1-phenyloctane interface regardless of the axial ligand employed (*a*, *b* = 1.34 (3)–1.39 (2) nm, Γ = 66 (2)–68 (1)˚).[30] This held true even for multi-atom ligands of significant calculated height such as triflate and phenylacetylide. The reliable formation of a cell of these dimensions is predicted to template one $C_{60}$ or functionalized $C_{60}$ molecule per cavity in the monolayer.

In this chapter we describe the synthesis and STM studies of two Ga(OEP)X complexes that contain axial ligands that we predict to have affinity for templating fullerenes due to height and electron donating ability: X = 1-ethynylpyrene and 2-ethynylpyrene (Figure 4.1; Ga(OEP)(CC-1-Pyr), Ga(OEP)(CC-2-Pyr)). It has been shown via NMR[31] and UV-vis[32] spectroscopy that pyrene forms a 1:1 molecular complex with $C_{60}$ in $CCl_4$. Further, in a series of polycyclic aromatic hydrocarbons, it was found that the formation constant of the pyrene-$C_{60}$ complex was approximately ten times that of the smaller donor molecule naphthalene.[32] This affinity towards forming electron donor-acceptor complexes combined with the unit cell parameters of our OEP monolayer makes this an ideal system for demonstrating the templating ability of this system. In this chapter, we describe the results of the sequential deposition of monolayer porphyrin followed by solutions of both $C_{60}$ and its functionalized derivative PCBM. We also discuss the

unique results of depositing pre-mixed solutions of equal volumes of porphyrin and fullerene solutions.

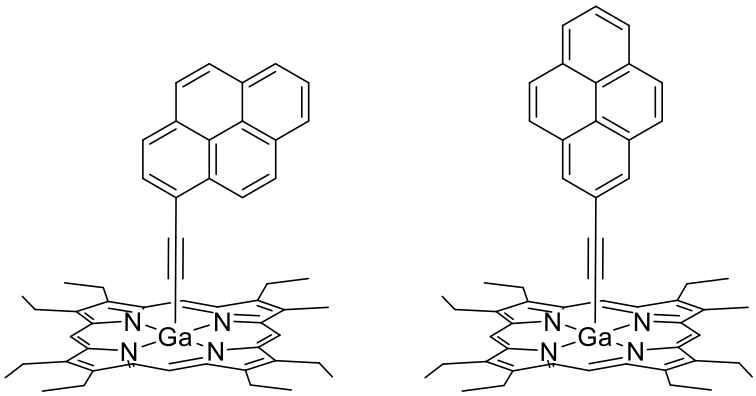


Ga(OEP)(CC-1-Pyr) Ga(OEP)(CC-2-Pyr)

**Figure 4.1.** Ga(OEP)(CCPyr) complexes investigated in this chapter.

### 4.2. Experimental

Detailed experimental procedures and characterization for all complexes can be found in Section 6.3.5. The Ga(OEP)(CCPyr) complexes were synthesized by the general method of reacting Ga(OEP)Cl with the target LiCCPyr ligand in THF at low temperature. The molecular structures of all compounds were optimized by density functional theory in the gas phase both in the global and in local energy minima with all eight ethyl chains pointing up, the latter being the predicted on-surface geometry. Molecular models of their predicted assembly into a pseudo-hexagonal unit cell with a $C_{60}$ molecule within the intraligand cavity were constructed. Further, single point calculations of the optimized structures were carried out, and molecular orbital isosurfaces generated. The compounds were studied by scanning tunneling microscopy at the solid-liquid interface as monolayers, by sequential deposition of monolayer and the fullerenes

$C_{60}$ and PCBM, and by deposition of pre-mixed solutions of porphyrin and $C_{60}$, and analyzed as described in Sections 6.3.3 and 6.3.4.

### 4.3. Results and Discussion

**4.3.1. Synthesis and Characterization of Ga(OEP)(CCPyr) Complexes.** The method of synthesis was analogous to similar gallium porphyrins with acetylide ligands, namely Ga(OEP)(CCPh).[30] The complexes were prepared via the reaction between Ga(OEP)Cl and 1-(LiCC)pyrene or 2-(LiCC)pyrene in THF. These pyrenyl reagents were prepared in several steps beginning with the structurally appropriate bromopyrene; this was used to prepare the trimethylsilylethynyl derivative via Sonogashira coupling, which was then protiodesilylated and lithiated. While the 1-bromopyrene was commercially available as the starting material for the reported Sonogashira coupling with trimethylsilyacetylene,[33] the 2-bromopyrene was first synthesized by a literature method of borylation of pyrene using an $[Ir(\mu\text{-}OMe)cod]_2$ catalyst, followed by reaction with $CuBr_2$ in water.[34] The Sonogashira coupling was done following the method reported for the synthesis of 2,7-bis(trimethylsilylethynyl)pyrene from the di-bromo precursor,[34] which employs a $Pd(dppf)Cl_2$ (dppf = 1,1′-bis(diphenylphosphino)ferrocene) catalyst, citing higher yields than the typically employed $Pd(PPh_3)_2Cl_2$ catalyst. The protected complexes were then deprotected[33, 34] and lithiated with $^n$BuLi.

The complexes were characterized by $^1$H-NMR and $^{13}$C-NMR spectroscopy, mass spectrometry, and electronic absorption spectroscopy (see Section 6.3.5 for full details). The $^1$H NMR spectra of the final products show a significant separation and upfield shift in the resonances of the ethynylpyrene ligands (Figures 6.18 and 6.20). The electronic absorption spectra display Soret and Q bands that are within 1 nm of those for the analogous

Ga(OEP)(CCPh) described in Chapter 2 and features between 350 and 393 nm consistent with absorption bands of 1-ethynylpyrene redshifted by approximately 10 nm (Figure 6.22).

**4.3.2. Density Functional Theory.** Density functional theory (DFT) calculations were conducted on the Ga(OEP)(CCPyr) complexes to determine their optimized gas-phase structures (Figure 4.2). From selected bond distances, bond angles, and the nonplanar distortions of the porphyrin core (Table 4.1), we observed that the ethynylpyrene complexes are essentially identical in structure to one another and to the previously studied acetylide complex, Ga(OEP)(CCPh). Specifically, the calculations indicate similar predicted amounts of doming to the porphyrin core for the Ga(OEP)(CCPh) and both Ga(OEP)(CCPyr) molecules: 0.50 Å and 0.49 Å above the $N_4$ plane, and 0.05 Å and 0.05 Å between the $N_4$ and $C_{20}$ planes respectively. The only significant difference in the calculated structure is the height of the molecules: 9.1 Å above the 24-atom porphyrin plane for the Ga(OEP)(CCPh) molecule vs. 11.4 Å for Ga(OEP)(CC-1-Pyr) and 13.2 Å for Ga(OEP)(CC-2-Pyr). As we have observed with all M(OEP) complexes thus far, the differences among their calculated geometries do not translate to differences in on-surface structure; all compounds form monolayers with the same pseudo-hexagonal lattice parameters on HOPG at the solid-liquid interface. This trend is expected to continue with the Ga(OEP)(CCPyr) complexes reported here.

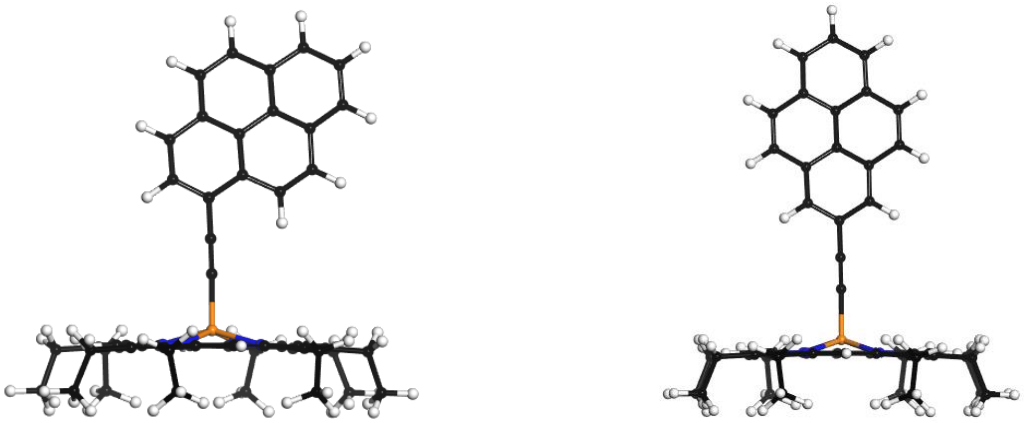

Ga(OEP)(CC-1-Pyr) Ga(OEP)(CC-2-Pyr)

**Figure 4.2.** Gas-phase optimized structures of Ga(OEP)(CCR) complexes. Atoms are color-coded: Ga, orange; N, blue; C, black; H, white.

**Table 4.1.** Selected Bond Distances (Å) and Angles (°) for Ga(OEP)(CCPh), Ga(OEP)(CC-1-Pyr) and Ga(OEP)(CC-2-Pyr) Calculated by Density Functional Theory.

| | | L | |
|---|---|---|---|
| Nuclei | CCPh | CC-1-Pyr | CC-2-Pyr |
| Ga–C | 1.9559 | 1.9587 | 1.9574 |
| Ga–N(1) | 2.068 | 2.068 | 2.068 |
| Ga–N(2) | 2.068 | 2.067 | 2.067 |
| Ga–N(3) | 2.068 | 2.068 | 2.068 |
| Ga–N(4) | 2.068 | 2.068 | 2.069 |
| N(1)–Ga–C | 103.9 | 103.7 | 104.0 |
| N(2)–Ga–C | 103.9 | 104.1 | 104.3 |
| N(3)–Ga–C | 103.9 | 104.0 | 103.9 |
| N(4)–Ga–C | 103.8 | 103.3 | 103.3 |
| Ga–$N_4$ plane (Å) | 0.495 | 0.490 | 0.494 |
| Ga–$C_{20}$ plane (Å) | 0.544 | 0.547 | 0.548 |
| $N_4$–$C_{20}$ planes (Å) | 0.048 | 0.054 | 0.054 |
| 24 atom por plane-“top” of molecule (Å) | 9.1 | 11.4 | 13.2 |

Space-filling models were generated with the Ga(OEP)(CCPyr) complexes arranged in the predicted pseudo-hexagonal OEP unit cell similar to those constructed in Chapter 3 (Figure 4.3), with the addition of a molecule of $C_{60}$ placed in the intra-ligand cavity formed by the four axial pyrenyl units. From these models, it was observed that both intra-ligand cavities form corrals of

the appropriate dimension to accommodate one molecule of $C_{60}$ (Figure 4.3a and c). From side-on views (Figure 4.3b and d), the pyrenyl ligands further appear to have good overlap with the fullerene in the pocket. While the pyrene ligands are expected to have free rotation about the GaCC axis within the cavity prior to fullerene deposition, their orientation post-deposition cannot be predicted with certainty at this time; this may prove to be an important factor in guiding the on-surface assembly of the guest molecule, particularly in the case of the asymmetric Ga(OEP)(CC-1-Pyr), where a different number of "long" and "short" pyrene contacts in each unit cell could be envisioned. However, we are confident, given the invariance of the OEP unit cell dimensions with regards to change in axial ligand, that our system has the potential to accommodate a fullerene molecule.

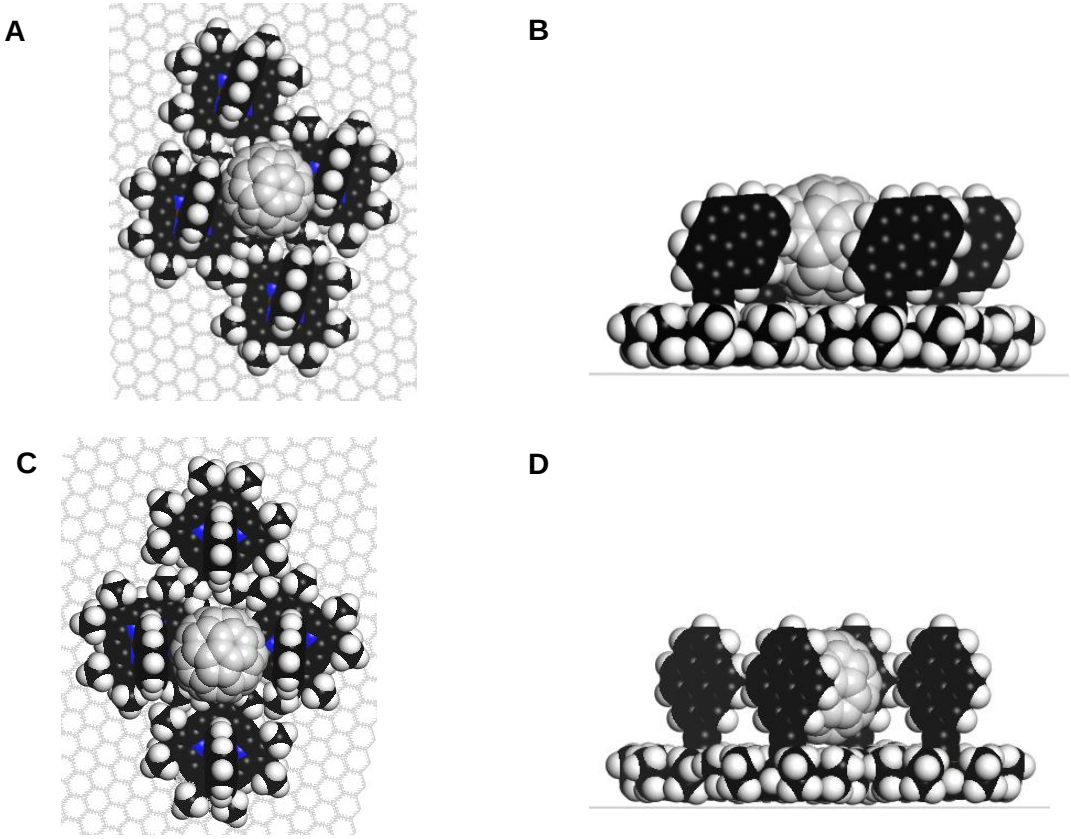


**Figure 4.3.** On-surface molecular model of monolayers of a unit cell of Ga(OEP)(CC-1-Pyr) (A and B) and Ga(OEP)(CC-2-Pyr) (C and D) with one molecule of $C_{60}$ incorporated into the inter-ligand cavities. Top-down (A and C) and side-on (B and D) views are shown.

To gain an understanding of the electronic nature of the Ga(OEP)(CCPyr) complexes, the frontier orbitals of these molecules, as well as their component fragments Ga(OEP)(CCH), 1-ethynylpyrene, and 2-ethynylpyrene were calculated (HOMO–2 through LUMO+2; see Figures 6.16 and 6.17). It was found that the Ga(OEP)(CCPyr) orbitals strongly resemble those of their components, being fully localized on either the porphyrin or pyrenyl fragment and lying at energies similar to those for models of these subunits. This localization is manifested experimentally by their electronic-absorption spectra discussed above (see Figure 6.22), which display features nearly identical to the Ga(OEP)(CCPh) complex and slightly redshifted from those of 1-ethynylpyrene. The structural and electronic modularity of Ga(OEP)(CCPyr) complexes suggest that the affinity of their pyrenyl ligands for fullerenes and assembly of the porphyrin monolayers on HOPG should be similar to those of their free subunits, which is important for isolating the factors that control their ability to incorporate fullerenes into the intra-ligand cavity.

### 4.3.3 Scanning Tunneling Microscopy.

**4.3.3.1. Monolayer Assembly of Ga(OEP)(CCPyr) Complexes.** Deposition of 0.5 mM solutions of Ga(OEP)(CC-1-Pyr) and Ga(OEP)(CC-2-Pyr) on HOPG results in their self assembly into expansive, highly ordered monolayers, as revealed by STM imaging at the solid–liquid interface (Figure 4.4). The monolayers appear in domains that span more than 100 nm in the minimum dimension and, further, are robust, exhibiting no damage after STM scanning for several hours at low current setpoints. This is in contrast with observations in Chapter 2 which saw removal of the monolayer of the multi-atom-axial-ligand complex Ga(OEP)($O_3SCF_3$) upon repeated scanning.

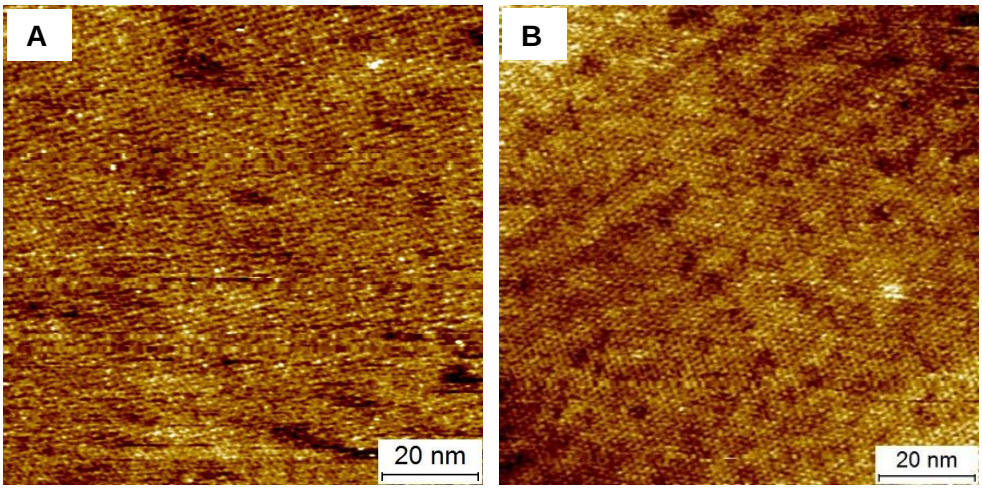


**Figure 4.4.** STM images of (A) Ga(OEP)(CC-1-Pyr) and (B) Ga(OEP)(CC-2-Pyr) on HOPG at the solid–liquid interface showing long-range ordering of the monolayers ([por] = 0.5 mM, 1-phenyloctane). The images were acquired at (A): $I$ = 8 pA, $V$ = –700 mV; (B): $I$ = 8 pA, $V$ = –500 mV).

Variation of the STM bias voltage presents the individual molecules either as ring-shaped features (Figures 4.5a and b) which correspond to the porphyrin macrocycle, or as sharper, bright features that are associated with the axial ligands (Figure 4.5c and d). This phenomenon has been observed in previous STM studies of porphyrin monolayers[30, 35] and interpreted as providing direct evidence that the porphyrin rings are oriented parallel to the surface with the axial ligands perpendicular to it. Structural analyses of these images indicate that, as predicted, the molecules exhibit pseudo-hexagonal packing with lattice parameters for both Ga(OEP)(CCPyr) complexes that are identical, within experimental error, to each other and to those of similar Ga(OEP)X complexes acquired under comparable conditions (Table 4.2). The apparent height of the sharper axial features ranges between ~1.1–1.3 Å. As observed in other STM studies of porphyrin compounds with multi-atom axial ligands,[30, 36] these apparent maximum heights are substantially less than the actual height (Ga(OEP)(CC-1-Pyr), 11.4 Å from base of the porphyrin plane; Ga(OEP)(CC-2-Pyr), 13.2 Å; as calculated by DFT).

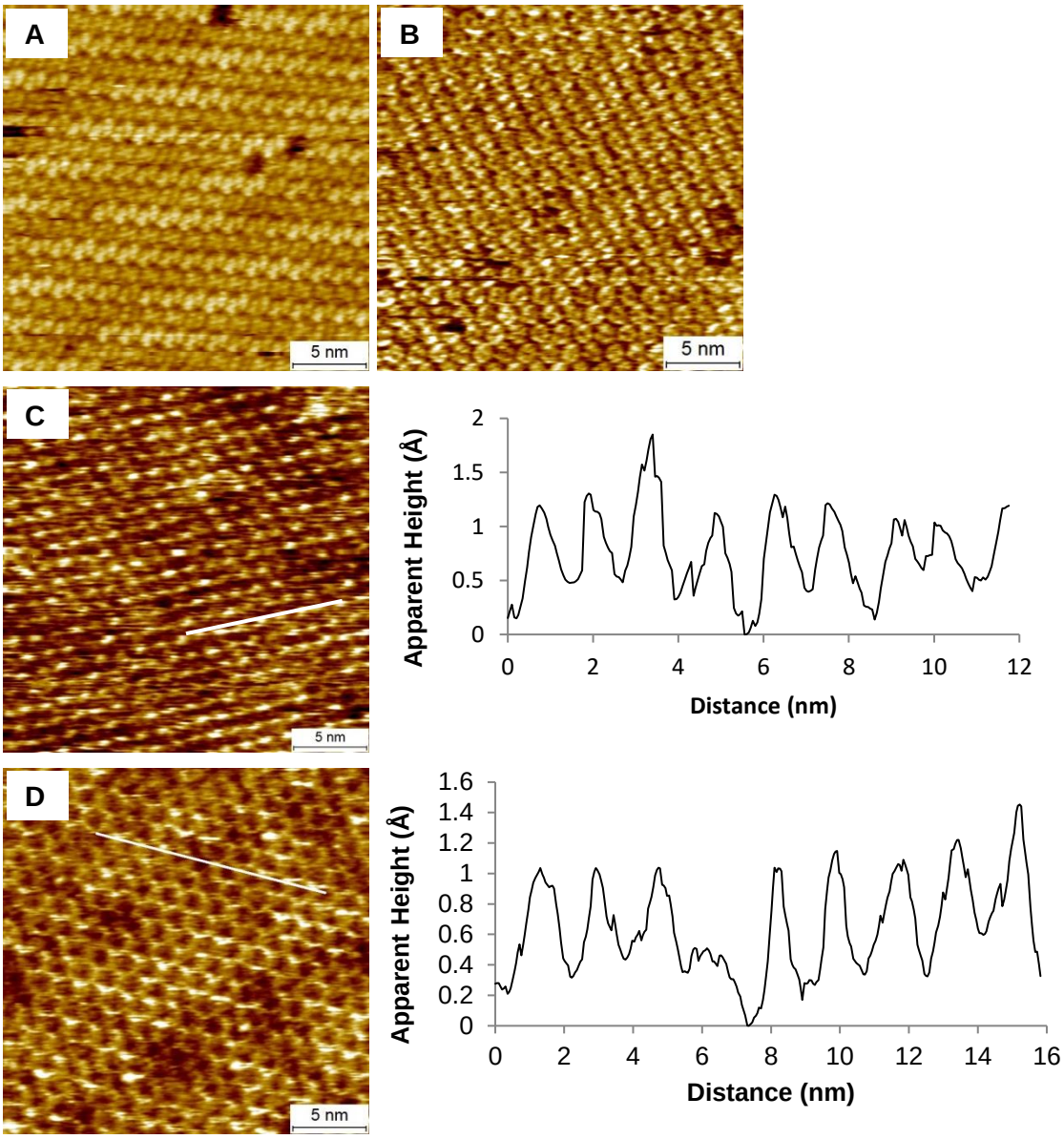


**Figure 4.5.** STM images and cross-sectional profiles of (A and C) Ga(OEP)(CC-1-Pyr) and (B and D) Ga(OEP)(CC-2-Pyr) monolayers on HOPG at the solid–liquid interface showing resolution of the porphyrin macrocyle (A and B) and axial ligand features (C and D) ([por] = 0.5 mM, 1-phenyloctane). The images were acquired at (A): $I$ = 10 pA, $V$ = –900 mV; (B): $I$ = 10 pA, $V$ = –300 mV; (C): $I$ = 10 pA, $V$ = –700 mV; (D): $I$ = 12 pA, $V$ = –800 mV). The height profiles correspond to the white lines shown in the STM images (C) and (D).

**4.3.3.2. Sequential Deposition of Ga(OEP)(CCPyr) and Fullerene Solutions.** Addition of a 3.0 mM solution of $C_{60}$ to monolayers of Ga(OEP)(CC-1-Pyr) on HOPG, prepared as above, produces dramatic changes to the STM images that result from supramolecular incorporation of

the fullerene into the array (denoted Ga(OEP)(CC-1-Pyr)•$C_{60}$). Specifically, the images exhibit extensive, well-defined arrays of mixed bright and dimmer features (Figure 4.6), indicative of a significant variation in apparent height across the surface, and consistent in appearance with literature reports of $C_{60}$ incorporation in 2D surface-assisted templates.[12, 17, 18, 21, 37] Addition of fullerene solutions also results in less coverage of the HOPG surface than that observed by deposition of solely the porphyrin monolayer. Structural analysis of these arrays at higher resolution (Figure 4.6b), reveals that the dimmer features exhibit apparent maximum heights of ~1.1–1.4 Å, similar those found above for the monolayer of Ga(OEP)(CC-1-Pyr), while the bright spots, which are assigned to the fullerene, correspond to maximum heights between 2.0–2.8 Å. Although there are sites and regions where fullerenes are absent, the spacing between all maxima is constant along a given lattice direction and provides cell dimensions identical to those of the monolayers (Table 4.2). This indicates the each $C_{60}$ molecule is associated in the same way with one unit cell of the underlying monolayer.

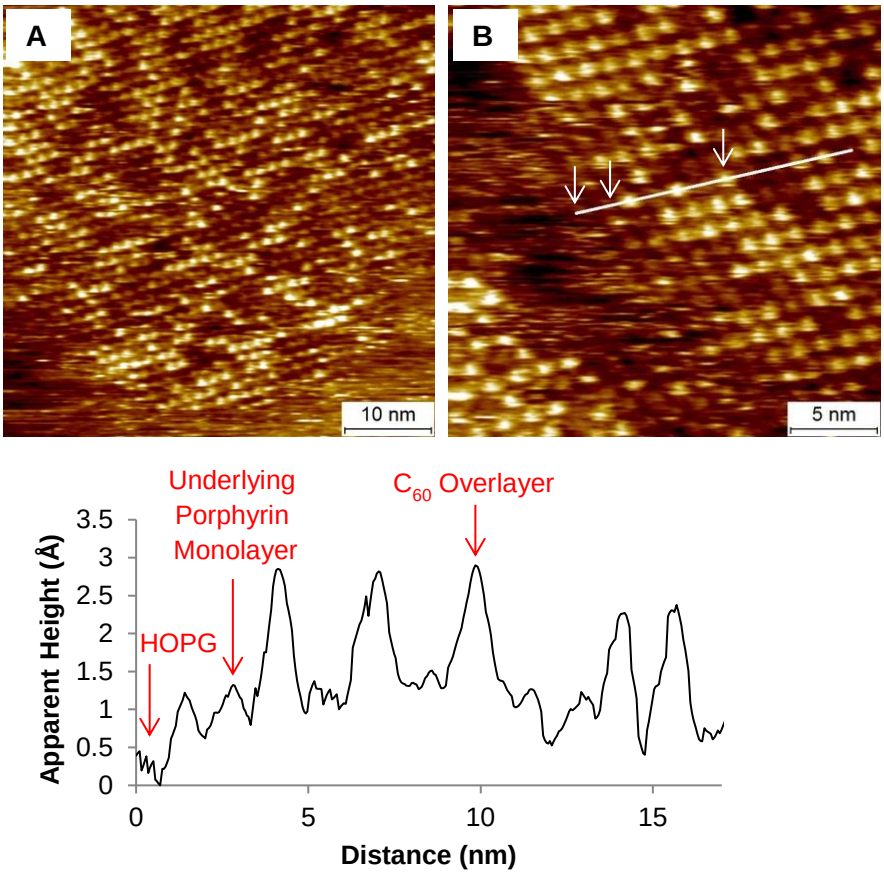


**Figure 4.6.** STM images and cross-sectional profile of Ga(OEP)(CC-1-Pyr) after sequential deposition of porphyrin monolayer followed by a solution of $C_{60}$ on HOPG at the solid–liquid interface, showing random incorporation of the fullerene into the porphyrin array ([por] = 0.5 mM, [$C_{60}$] = 3.0 mM, 1-phenyloctane). The images were acquired at (A): $I$ = 8 pA, $V$ = –700 mV; (B) $I$ = 8 pA, $V$ = –700 mV. The height profile corresponds to the white line shown in the STM image (B) and key structural features in the profile and image are noted with arrows.

Qualitatively similar images are observed for samples in which the concentration of the added fullerene solution is varied across the range 0.05–3.0 mM, where the high end approaches the saturation limit of $C_{60}$[12] (Figures 4.6–4.8). In sequentially depositing solutions of Ga(OEP)(CC-1-Pyr) and $C_{60}$, we observe similar amounts of fullerene incorporation at both the lowest and highest concentrations studied, spanning almost two orders of magnitude. It is also noteworthy that $C_{60}$ occupancy and vacancy within the overlayer show very few changes upon repeated scanning at low current setpoints, as shown in a series of sequential images of

Ga(OEP)(CC-1-Pyr)•$C_{60}$ (Figure 4.7), indicating that incorporation and removal of fullerenes is slow on the STM timescale and resistant to disruption from the STM tip.

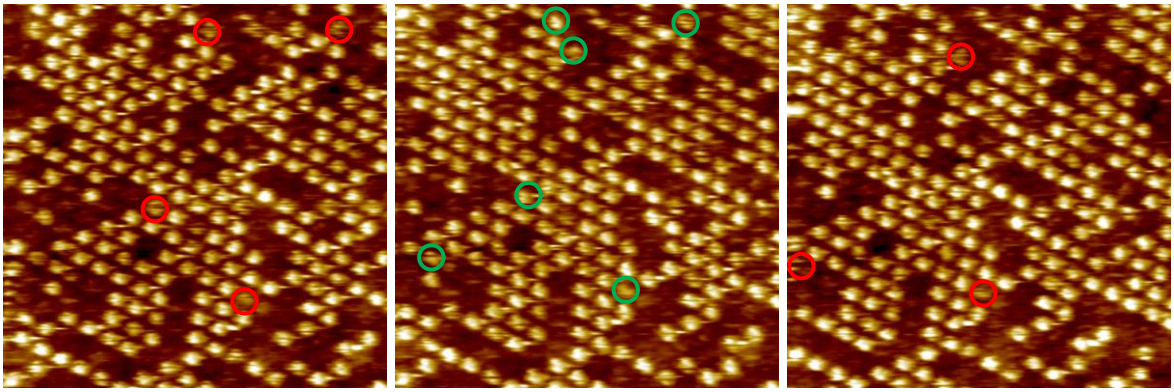

**Figure 4.7.** Sequential STM images of Ga(OEP)(CC-1-Pyr)•$C_{60}$ on HOPG at the solid–liquid interface ([por] = 0.5 mM, [$C_{60}$] = 0.05 mM, 1-phenyloctane; $I$ = 10 pA, $V$ = –700 mV). Red circles are dim spots that are brighter in the previous or following image and green are the brighter spots.

The porphyrin and fullerene layers of these assemblies can be individually imaged under specific conditions, providing insight into finer details of their structures. One important question is whether the vacancies observed in the fullerene overlayers result from vacancies or defects in the underlying porphyrin monolayer. Shown in Figure 4.8 is a sequence of STM images of a fixed region of Ga(OEP)(CC-1-Pyr)•$C_{60}$ where the bias voltage was toggled to allow separate imaging of the $C_{60}$ overlayer (Figure 4.8a) and of the underlying monolayer of the porphyrin (Figure 4.8b). These images indicate that vacancies in the $C_{60}$ overlayer do not coincide with vacancies in the underlying monolayer, which is continuous in this region. Further, structural analysis of the macrocycle structure underlying Ga(OEP)(CC-1-Pyr)•$C_{60}$ provides lattice parameters that are identical, within experimental error, to those of Ga(OEP)(CC-1-Pyr) alone (Table 4.2), indicating that the incorporation of $C_{60}$ does not affect the underlying porphyrin lattice structure.

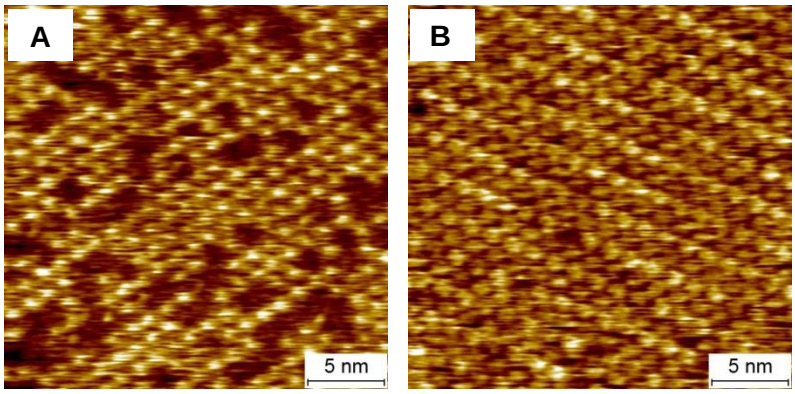


**Figure 4.8.** Sequential STM images of a fixed region of Ga(OEP)(CC-1-Pyr)•$C_{60}$ on HOPG at the solid–liquid interface ([por] = 0.5 mM, [$C_{60}$] = 0.05 mM, 1-phenyloctane) in which the bias voltage is toggled in order to separately image the $C_{60}$ overlayer and underlying monolayer of Ga(OEP)(CC-1-Pyr). The images were acquired at (A): $I$ = 8 pA, $V$ = –900 mV; (B): $I$ = 8 pA, $V$ = –200 mV. The images were collected along the same scan direction; a total of two scans (one up, one down) occurred between the images.

Qualitatively similar observations are observed upon sequential deposition of a 0.5 mM solution of Ga(OEP)(CC-2-Pyr) and 0.05−3.0 mM solutions of $C_{60}$ on HOPG. Random incorporation of the fullerene can be observed across a patterned background (Figure 4.9a−d), and the underlying porphyrin macrocyle can be independently resolved (Figure 4.9e). As observed for the Ga(OEP)(CC-1-Pyr) analog, both the fullerene overlayer, Ga(OEP)(CC-2-Pyr)•$C_{60}$, and the underlying porphyrin monolayer display a retention of the pseudo-hexagonal lattice parameters (Table 4.2). However, the extent of fullerene incorporation into the arrays tends to be both lower and less consistent for Ga(OEP)(CC-2-Pyr) than for Ga(OEP)(CC-1-Pyr); as the concentration of fullerene solution is lowered, the degree of incorporation appears to increase (Figure 4.9). These results indicate that there is most likely a complex set of interactions between the buckyballs and the porphyrins both on the surface and in solution; this is not unexpected as both pyrene[31, 32] and porphyrins themselves[23-28] have well-established affinity for fullerenes. However, the template we have engineered is demonstrated to be successful in its goal and similar in behavior over a wide range of concentrations.

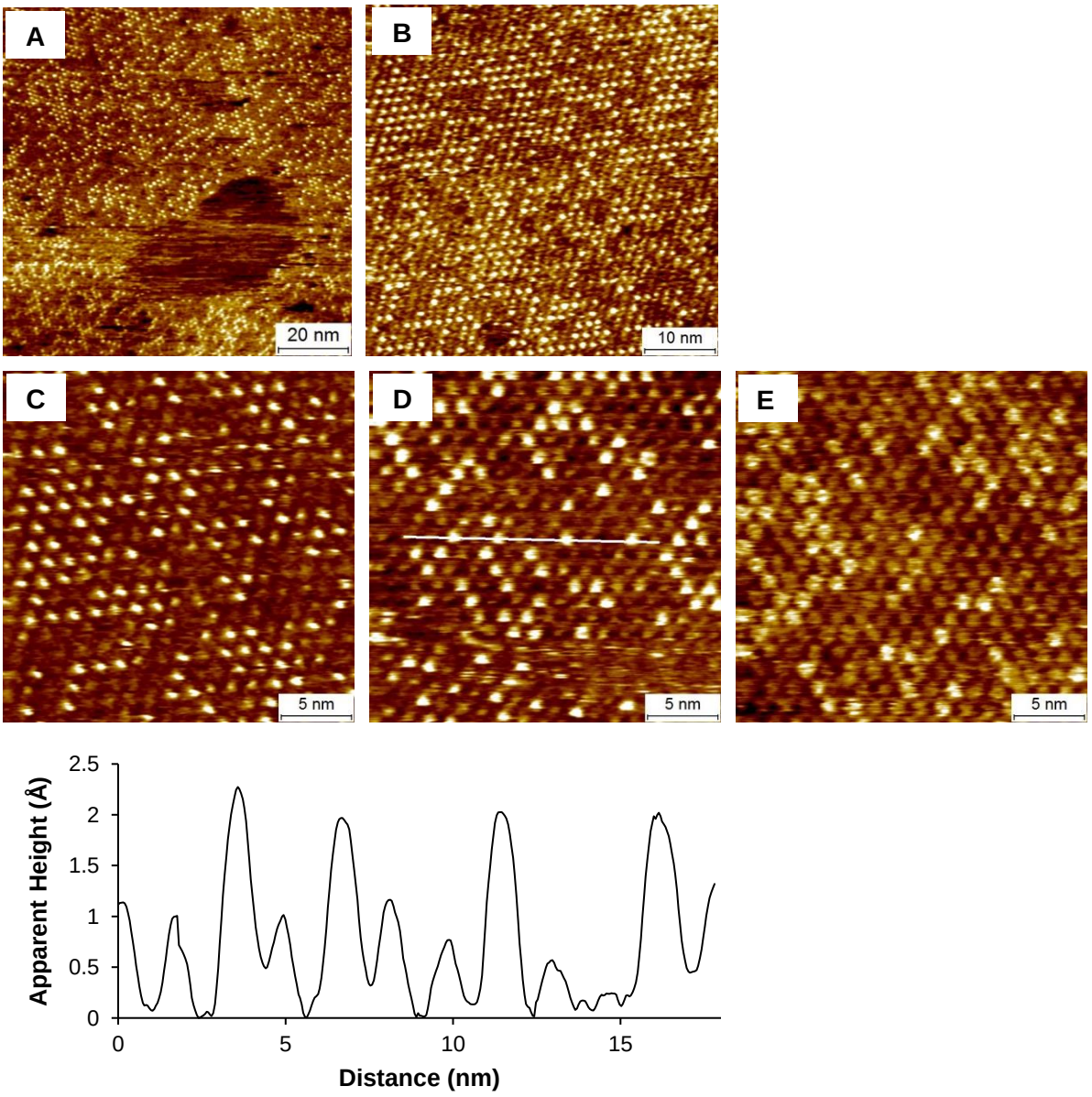


**Figure 4.9.** STM images and height profile of Ga(OEP)(CC-2-Pyr)•$C_{60}$ on HOPG at the solid–liquid interface showing large-scale ordering (A and B), higher-resolution images (C and D), and independent imaging of the underlying porphyrin macrocycle (E) ([por] = 0.5 mM, [$C_{60}$] = 0.05 mM (B and C), 3.0 mM (A, D and E), 1-phenyloctane). The images were acquired at: (A) $I$ = 8 pA, $V$ = –500 mV (B) $I$ = 10 pA, $V$ = –500 mV; (C) $I$ = 10 pA, $V$ = –500 mV; (D) $I$ = 10 pA, $V$= –700 mV; (E) $I$ = 10 pA, $V$= –800 mV. The height profile corresponds to the white line shown in the STM image (D).

We have also successfully applied the same technique to incorporate the functionalized fullerene [6,6]-phenyl-$C_{61}$-butyric acid methyl ester (PCBM) at a concentration of 3.0 mM by sequentially depositing it on both pre-formed Ga(OEP)(CCPyr) monolayers (denoted

Ga(OEP)(CC-1-Pyr)•PCBM and Ga(OEP)(CC-2-Pyr)•PCBM). We observed similar bright features incorporated into a Ga(OEP)(CC-1-Pyr) array within minutes after deposition of the PCBM solution (Figure 4.10) and a similar overall amount of fullerene incorporation when compared to the $C_{60}$ fullerene. Similarly, the porphyrin macrocycle structure can be observed by toggling the bias voltage, revealing nearly complete porphyrin monolayer coverage beneath the fullerene overlayer (Figure 4.10d). Lattice parameters were also consistent with the pseudo-hexagonal OEP cell, as observed with $C_{60}$ incorporation (Table 4.2). This result speaks to the versatility of the corral system we have engineered to template a variety of guest molecules beyond pristine fullerenes.

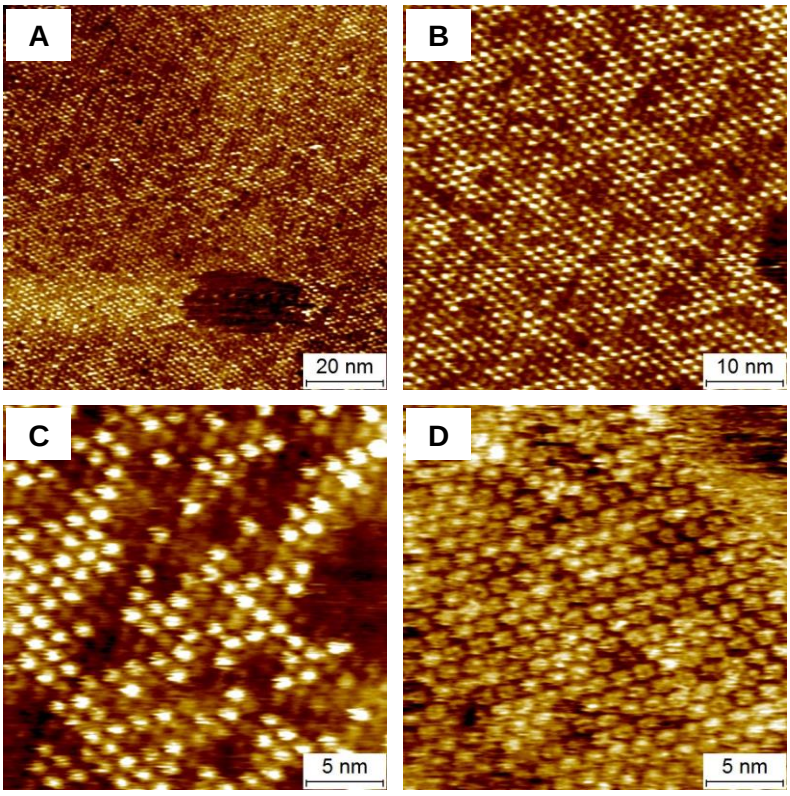


**Figure 4.10.** STM images of Ga(OEP)(CC-1-Pyr)•PCBM on HOPG at the solid-liquid interface (A-C) and the underlying porphyrin macrocycle (D) ([por] = 0.5 mM, [PCBM] = 3.0 mM, 1-phenyloctane). The images were acquired at (A): $I$ = 8 pA, $V$ = –500 mV; (B) $I$ = 8 pA, $V$ = –500 mV; (C) $I$ = 8 pA, $V$ = –900 mV; (D) $I$ = 8 pA, $V$ = –600 mV.

A similar result for Ga(OEP)(CC-2-Pyr)•PCBM overlayers is obtained; this has also led to high-quality images where both the porphyrin macrocycle and fullerene can be simultaneously imaged, allowing for information about the local structure of the fullerene within the pyrene corral to be extracted (Figure 4.11). It is evident from this image that the bright features are offset from the center of the porphyrin ring, supporting the conclusion that the fullerenes are incorporated into the corral. Further, they appear to be principally associated with a single pyrenyl ligand, as the fullerene is offset from the exact center of the unit cell formed by four porphyrin molecules, as shown in the overlaid unit cell in Figure 4.11a. A space-filling molecular model of the proposed structure is shown (Figure 4.11b). Similar observations have been made for Ga(OEP)(CC-1-Pyr)•$C_{60}$ (Figure 4.11c). The asymmetric nature of the 1-ethynylpyrene ligand results in the probable outcome of variable pyrene contacts in each unit cell. However, given the similarities in templating fullerenes and observable local structures, this does not seem to have a strong effect.

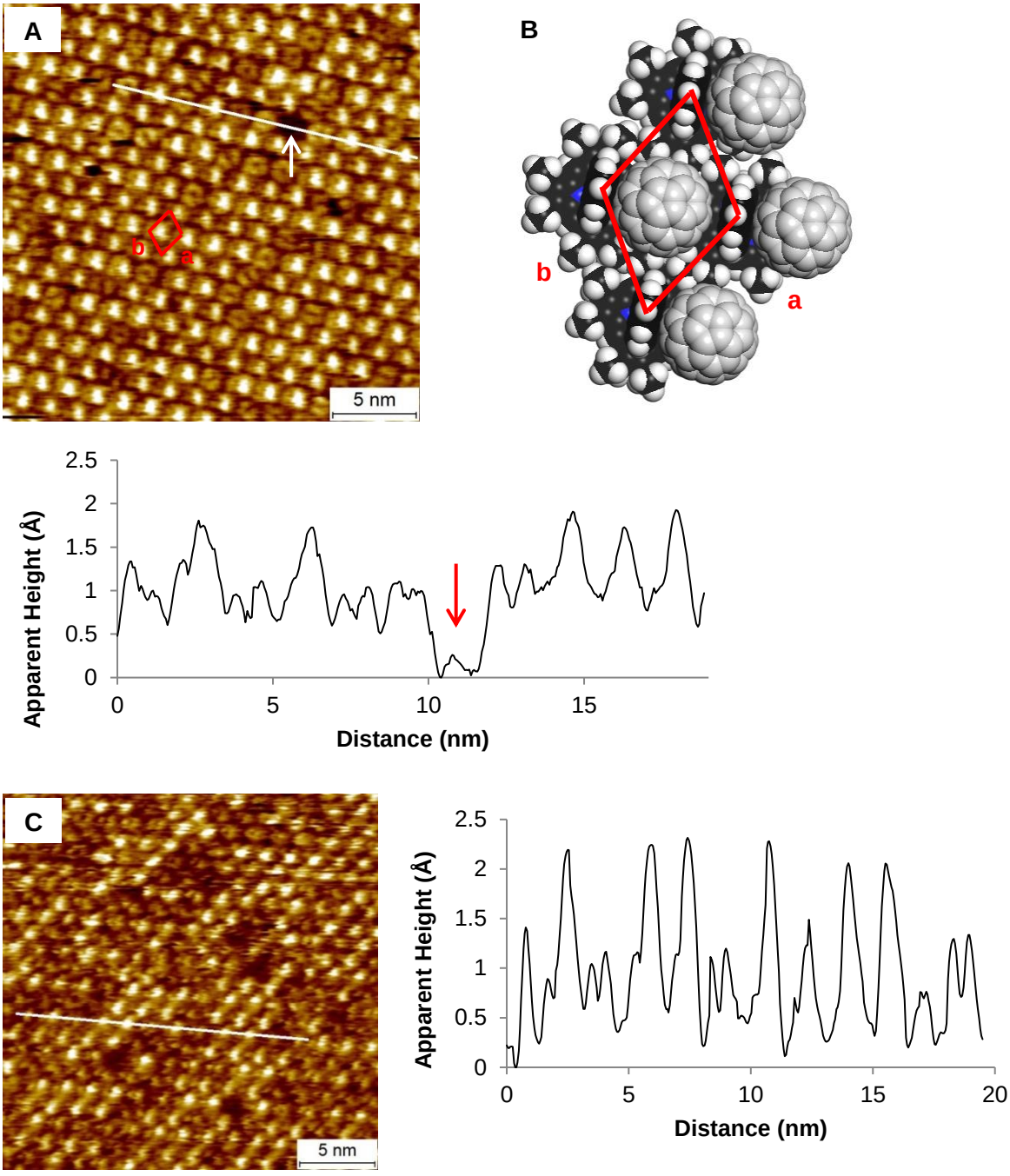


**Figure 4.11.** STM image with cross-sectional profile (A) and proposed molecular model (B) of Ga(OEP)(CC-2-Pyr)•PCBM and STM image with cross-sectional profile (C) of Ga(OEP)(CC-1-Pyr)•$C_{60}$ at the solid-liquid interface on HOPG ([por] = 0.5 mM, [PCBM] = 3.0 mM, [$C_{60}$] = 0.05 mM, 1-phenyloctane). Simultaneous observation of the underlying porphyrin ring structure and offset fullerene in the intra-ligand cavity is seen (A and C). A representative unit cell is noted in the image (A) and model (B) and a vacancy in the porphyrin monolayer is noted in the image and corresponding height profile. The images were acquired at (A): $I$ = 8 pA, $V$ = –700 mV; (B) $I$ = 10 pA, $V$ = –1100 mV. The height profiles correspond to the white lines shown in the STM images (A) and (C).

**4.3.3.3. Deposition of Mixed Ga(OEP)(CCPyr)/$C_{60}$ Solutions.** To investigate the necessity of the sequential deposition process for the formation of supramolecular fullerene overlayers, experiments were performed in which mixed 1-phenyloctane solutions of containing Ga(OEP)(CC-1-Pyr) or Ga(OEP)(CC-2-Pyr) and $C_{60}$ in equal volumes were deposited on HOPG and imaged by STM at the solid–liquid interface (after mixing: [por] = 0.25 mM, [$C_{60}$] = 1.5 mM). The mixed solution of Ga(OEP)(CC-2-Pyr) and $C_{60}$ (denoted Ga(OEP)(CC-2-Pyr)/$C_{60}$) yielded self-assembled structures consisting of a monolayer of porphyrin and an overlayer of $C_{60}$ identical in lattice structure to Ga(OEP)(CC-2-Pyr)•$C_{60}$ provided by sequential deposition, as determined by comparison of lattice constants, the distribution of bright fullerene features, and corresponding apparent height profiles (Figure 4.12; Table 4.2). These arrays span hundreds of nanometers in width within minutes of deposition of the mixed solution. This result indicates that the porphyrin templated organization of fullerenes on surfaces can be accomplished by one-step self assembly, at least in select cases.

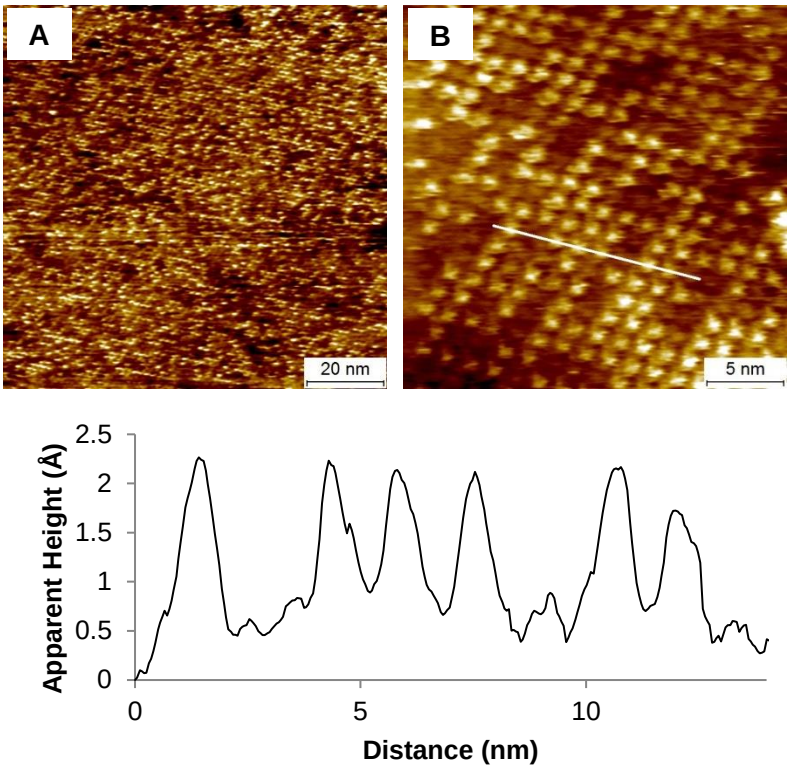


**Figure 4.12.** STM images and cross-sectional profile of a pre-mixed solution of Ga(OEP)(CC-2-Pyr) and $C_{60}$ on HOPG at the solid-liquid interface ([por] = 0.25 mM, [$C_{60}$] = 1.5 mM). The images were acquired at (A): $I$ = 8 pA, $V$ = –700 mV; (B): $I$ = 8 pA, $V$ = –700 mV. The height profile corresponds to the white line shown in the STM image (B).

Unlike the observation for Ga(OEP)(CC-2-Pyr), addition of a mixed solution of Ga(OEP)(CC-1-Pyr)/$C_{60}$ to HOPG resulted in a multi-domain, polymorphic structure immediately upon deposition with myriad domain boundaries (Figures 4.13 and 4.14). These domains consist of three lattice structures that can be identified. One structure is identical in qualitative appearance, lattice constants, and cross-sectional profile to that of the pseudo-hexagonal Ga(OEP)(CC-1-Pyr)•$C_{60}$ prepared by sequential deposition of Ga(OEP)(CC-1-Pyr) and $C_{60}$ (bottom region of Figure 4.13a; Table 4.2). The other two lattices, which have not previously been observed in the deposition of any M(OEP) compound, possess substantially larger cell dimensions and areas than the standard pseudo-hexagonal lattice (a = 2.81 (0.04) nm, b = 2.04 (0.04) nm, Γ = 85 (2)°; a = 2.76 (0.08) nm, b = 1.41 (0.07) nm, Γ = 63 (2)°). These

atypical domains exhibit features with consistent apparent maximum heights of ~2.5–3.0 Å (Figure 4.13b), which is similar to the apparent heights associated with the included $C_{60}$ molecules of Ga(OEP)(CC-1-Pyr)•$C_{60}$. These observations suggest that the lattices are comprised of other supramolecular arrangements and, possibly, stoichiometries, of Ga(OEP)(CC-1-Pyr) and $C_{60}$.

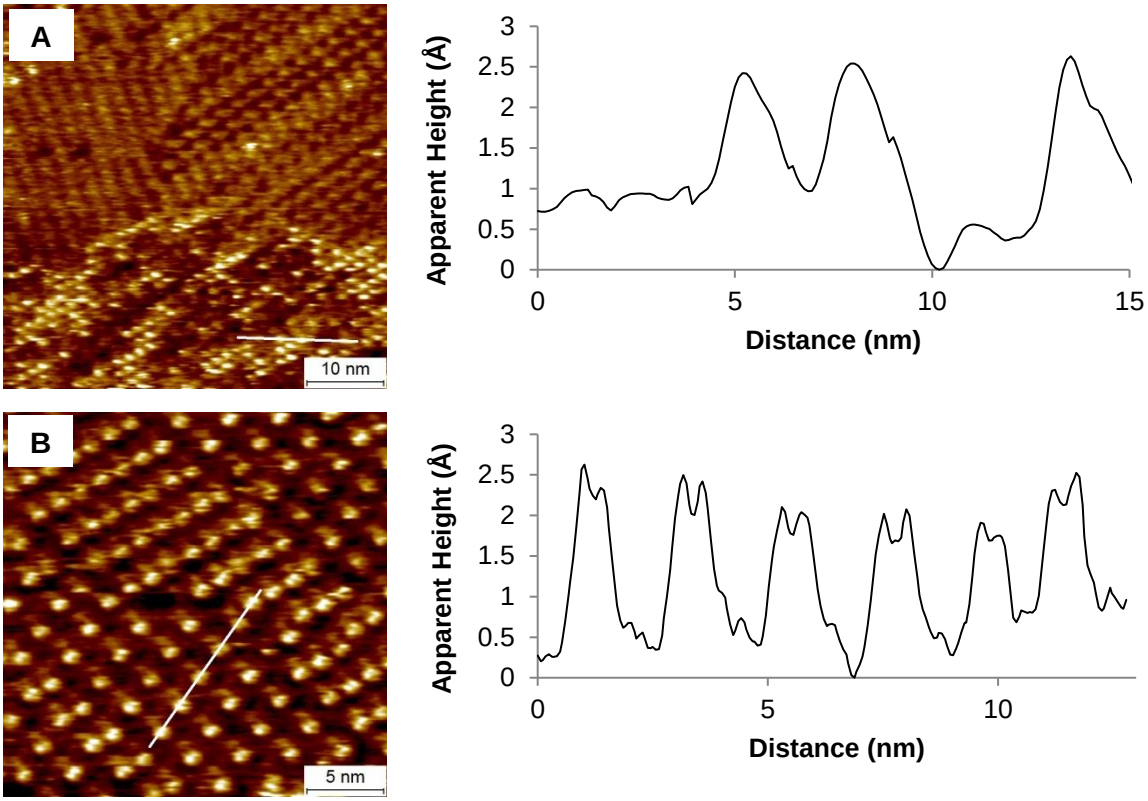


**Figure 4.13**. STM images and cross-sectional profiles of a pre-mixed solution of Ga(OEP)(CC-1-Pyr) and $C_{60}$ on HOPG at the solid-liquid interface ([por] = 0.25 mM, [$C_{60}$] = 1.5 mM): (A) Region showing all three unit cells including pseudo-hexagonal lattice with incorporated fullerene (evident in the bottom 1/3 of the image). (B) Representative example of multi-domain structure with arrays of previously unobserved unit cells. The images were acquired at (A): $I$ = 8 pA, $V$ = –700 mV; (B): $I$ = 8 pA, $V$ = –700 mV. The height profiles correspond to the white lines shown in the STM images.

While the exact nature of these structures has not yet been determined, they appear to be kinetically unstable, interchanging rapidly during imaging (Figure 4.14a and b), and eventually appearing to transition to primarily the pseudo-hexagonal domain (Figure 4.14c and d), which

suggests that the latter is the thermodynamically favorable arrangement; more rigorous studies of the evolution of the domains with time are needed to confirm this observation. While this is the first example of such kinetic instability in our M(OEP) systems, it is not uncommon for multi-domain systems to occur in other self-assembled porphyrin arrays at the solid-liquid interface, most often in long alkyl-chain *meso*-substituted porphyrin arrays.[38-40] The results for simultaneous deposition of Ga(OEP)(CC-2-Pyr) and $C_{60}$ indicates that, with appropriate design, the porphyrin templated organization of fullerenes on surfaces can be accomplished by one-step self assembly. The results for Ga(OEP)(CC-1-Pyr), however, suggest that the solution-phase supramolecular chemistry of the porphyrin and fullerene can play an important role in determining the mechanism and structure of the self assembly processes on the surface. This can result in structural complexities that can be circumvented by sequential deposition methods.

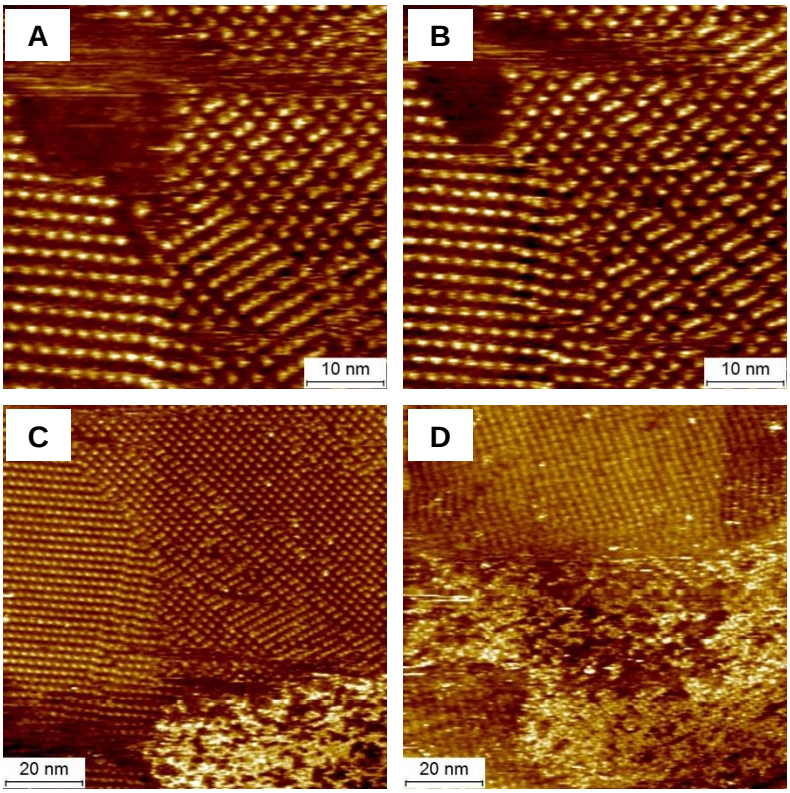


**Figure 4.14.** STM images of a pre-mixed solution of Ga(OEP)(CC-1-Pyr) and $C_{60}$ on HOPG at the solid-liquid interface ([por] = 0.5 mM, [$C_{60}$] = 3.0 mM, equal volumes of 1-phenyloctane solutions mixed): (A) and (B) Sequential STM images showing kinetic instability of the larger unit cells; (C) Long-range ordering of array at t = n; (D) The same array at t = n + 45 minutes showing greater coverage of the pseudo-hexagonal M(OEP) lattice. The images were acquired at (A): $I$ = 8 pA, $V$ = –700 mV; (B): $I$ = 8 pA, $V$ = –700 mV; (C) $I$ = 8 pA, $V$ = –700 mV; (D) $I$ = 8 pA, $V$ = –700 mV.

**Table 4.2.** Lattice Parameters of Ga(OEP)(CCR) Monolayers, Fullerene Overlayers, and Underlying Structures.

| | ***a*** **(nm)** | ***b*** **(nm)** | **Γ (°)** |
|---|---|---|---|
| **Ga(OEP)(CCPh) Monolayer** | 1.35 ± 0.03 | 1.34 ± 0.03 | 66 ± 2 |
| **Ga(OEP)(CC-1-Pyr) Monolayer** | 1.37 ± 0.02 | 1.35 ± 0.02 | 69 ± 2 |
| **Ga(OEP)(CC-2-Pyr) Monolayer** | 1.37 ± 0.02 | 1.36 ± 0.03 | 66 ± 2 |
| **Ga(OEP)(CC-1-Pyr)•$C_{60}$ Overlayer** [a] | 1.36 ± 0.04 | 1.36 ± 0.04 | 66 ± 2 |
| **Ga(OEP)(CC-1-Pyr) Ring Structure Under $C_{60}$** | 1.39 ± 0.02 | 1.36 ± 0.03 | 68 ± 1 |
| **Ga(OEP)(CC-1-Pyr)•PCBM Overlayer** [a] | 1.38 ± 0.05 | 1.35 ± 0.05 | 65 ± 1 |
| **Ga(OEP)(CC-1-Pyr) Ring Structure Under PCBM** | 1.39 ± 0.02 | 1.34 ± 0.03 | 65 ± 1 |
| **Ga(OEP)(CC-2-Pyr)•$C_{60}$ Overlayer** [a] | 1.36 ± 0.07 | 1.35 ± 0.07 | 68 ± 2 |
| **Ga(OEP)(CC-2-Pyr) Ring Structure Under $C_{60}$** | 1.37 ± 0.03 | 1.36 ± 0.03 | 68 ± 2 |
| **Ga(OEP)(CC-2-Pyr) •PCBM Overlayer** [a] | 1.37 ± 0.05 | 1.36 ± 0.05 | 66 ± 2 |
| **Ga(OEP)(CC-2-Pyr) Ring Structure Under PCBM** | 1.37 ± 0.03 | 1.36 ± 0.03 | 66 ± 2 |
| **Ga(OEP)(CC-1-Pyr)/$C_{60}$ Cell 1** [b] | 2.81 ± 0.04 | 2.04 ± 0.04 | 85 ± 2 |
| **Ga(OEP)(CC-1-Pyr)/$C_{60}$ Cell 2** | 2.76 ± 0.08 | 1.41 ± 0.07 | 63 ± 2 |
| **Ga(OEP)(CC-1-Pyr)/$C_{60}$ Cell 3** | 1.39 ± 0.07 | 1.37 ± 0.07 | 63 ± 2 |
| **Ga(OEP)(CC-2-Pyr)/$C_{60}$ Overlayer** [b] | 1.37 ± 0.06 | 1.37 ± 0.06 | 66 ± 2 |
| **Ga(OEP)(CC-2-Pyr)/$C_{60}$ Ring Structure** | 1.37 ± 0.03 | 1.36 ± 0.03 | 65 ± 2 |

[a] Overlayer prepared via sequential deposition of porphyrin and fullerene. [b] Overlayer prepared by deposition of mixed porphyrin/$C_{60}$ solution.

**4.3.3.4. Fullerene Deposition Control Studies.** To ensure that the supramolecular formation of fullerene overlayers on monolayers of Ga(OEP)(CCPyr) complexes is a consequence of the presence of the pyrenyl moieties within these monolayers, a series of control experiments were carried out. First, a control experiment in which $C_{60}$ was deposited directly onto HOPG ([$C_{60}$] =

3.0 mM, 1-phenyloctane) did not yield fullerene monolayers; this finding is consistent with a prior report to this effect at the HOPG-1,2,4-trichlorobenzene interface.[10] This effect is also observed in images of Ga(OEP)(CCPyr)•$C_{60}$ overlayers in which there is also exposed HOPG; no fullerene features are observed on the exposed HOPG itself (e.g., Figure 4.6), indicating that the presence of the porphyrin monolayer is required for fullerene deposition.

Next, monolayers of porphyrins that lack pyrenyl groups were treated with $C_{60}$ under conditions identical to those described that resulted in successful fullerene incorporation for Ga(OEP)(CCPyr) complexes. The porphyrin compounds Ga(OEP)(CCPh) and Ni(OEP) were employed for these control experiments; their monolayers on HOPG exhibit pseudo-hexagonal lattices with dimensions identical to those of the Ga(OEP)(CCPyr) complexes under these deposition conditions.[30, 41] Deposition of solutions of $C_{60}$ ([$C_{60}$] = 0.05 mM and 3.0 mM, 1-phenyloctane) onto preformed monolayers of Ga(OEP)(CCPh) and Ni(OEP) (0.5 mM. 1-phenyloctane) at the solid–liquid interface did not result in formation of a fullerene overlayer, as established by a lack of observable overlayer under any imaging conditions that an array could be imaged. Instead, the original monolayer structure remained intact (Figures 4.15 and 4.16), though noticeable delamination of the Ga(OEP)(CCPh) surface arose upon repeated scanning. We have observed this phenomenon in our previous study of this compound in Chapter 2 though this effect may be amplified by interactions of the porphyrin with the $C_{60}$ in solution or the reduction in concentration of porphyrin solution by the addition of the fullerene.

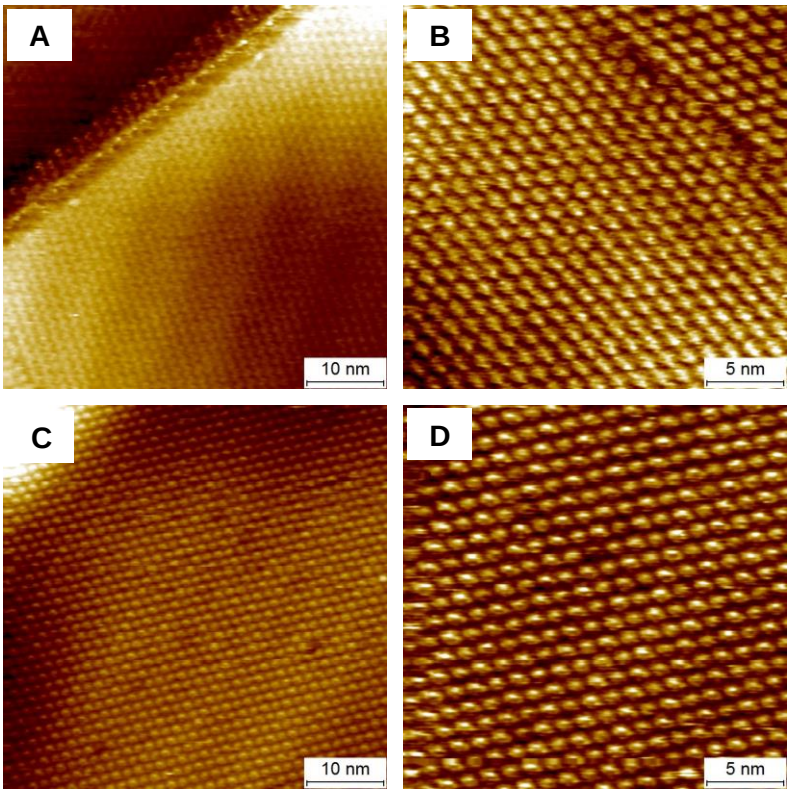


**Figure 4.15.** STM images of a NiOEP monolayer on HOPG at the solid–liquid interface (0.5 mM, 1-phenyloctane) before (A and B) and after (C and D) addition of a $C_{60}$ solution (3.0 mM, 1-phenyloctane). No incorporation of $C_{60}$ into the NiOEP monolayer was observed. The images were acquired at (A): $I$ = 20 pA, $V$ = –700 mV; (B): $I$ = 30 pA, $V$ = –700 mV; (C): $I$ = 20 pA, $V$ = –700 mV; (D): $I$ = 20 pA, $V$ = –700 mV.

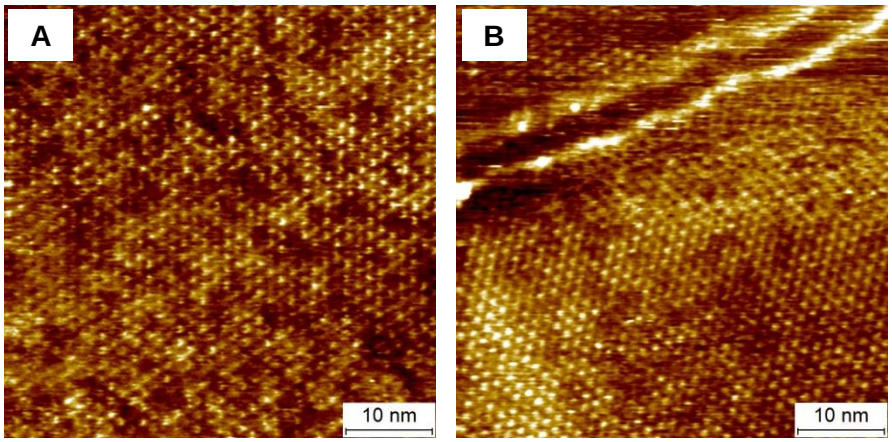


**Figure 4.16.** STM image of a monolayer of Ga(OEP)(CCPh) (0.5 mM, 1-phenyloctane) on HOPG at the solid–liquid interface before (A) and after (B) addition of $C_{60}$ (3.0 mM, 1-phenyloctane). No deposition of $C_{60}$ was observed, though removal of the monolayer was observed after repeated scanning. A similar result was observed after addition of a dilute $C_{60}$ solution (0.05 mM). The images were acquired at: (A): $I$ = 10 pA, $V$ = –500 mV; (B): $I$ = 10 pA, $V$ = –500 mV.

The negative result for the Ni(OEP) monolayer, which lacks axial ligands and therefore presents the exposed porphyrin macrocycle to the solution, demonstrates that the organization of the fullerenes is not principally driven by a fullerene–porphyrin interaction, although Ni(OEP) is known to form close noncovalent contacts with both $C_{60}$ and $C_{70}$ in the solid state.[26, 27] While an example of $C_{60}$ forming an overlayer on NiOEP has previously been observed, the deposition conditions were significantly different; the porphyrin was evaporated from benzene onto a gold substrate and the measurements were carried out under electrochemical conditions.[42] The Ga(OEP)(CCPh) monolayer presents the same corral structure as those of the Ga(OEP)(CCPyr) complexes, but possesses an axial ligand with a weaker affinity for $C_{60}$ than pyrene. It has been reported that pyrene forms a 1:1 molecular complex with $C_{60}$ in a $CCl_4$ solution with a formation constant of 6.8 ± 1.03 L $mol^{-1}$ while that of a smaller polycyclic aromatic hydrocarbon, naphthalene, was determined to be much smaller (0.67 ± 0.01 L $mol^{-1}$).[32] The lack of $C_{60}$ incorporation establishes that the corral structure provided by Ga(OEP)X monolayers is, by itself, insufficient to produce supramolecular organization of fullerenes, and that the equilibrium binding constant of the axial ligand is an important design parameter.

### 4.4. Conclusions

In this chapter, we have designed and synthesized two Ga(OEP)(CCPyr) complexes as a new method of templating the assembly of fullerenes from solution on HOPG. We have taken advantage of the invariance of the M(OEP) unit cell, also observed here in monolayers of both Ga(OEP)(CCPyr) complexes, to rationally design a corral with appropriate dimensions and affinity to attract one fullerene into each intra-ligand cavity. This technique proved successful only when an axial ligand with appropriate size and affinity for the fullerenes was employed; control studies with four-coordinate NiOEP and five-coordinate Ga(OEP)(CCPh) did not result

in fullerene templating. Incorporation was confirmed by imaging the nearly complete underlying porphyrin monolayer macrocycle beneath the bright fullerene features; additionally, simultaneous imaging of the porphyrin ring and bright fullerene features confirms intra-ligand incorporation. We have demonstrated that this templating technique can be applied to $C_{60}$ as well as the functionalized fullerene PCBM with the same effect observed.

Changing the orientation of the axial ligand from the asymmetric 1-ethynylpyrene ligand to the symmetric 2-ethynylpyrene ligand had little effect on the outcome of sequential deposition experiments. Incorporation was observed upon sequential deposition of $C_{60}$ solutions ranging in concentration from 0.05 mM to 3.0 mM. Under certain conditions, as in pre-mixing Ga(OEP)(CC-2-Pyr) and $C_{60}$ solutions, the sequential deposition process proved unnecessary, further simplifying this approach. However, the analogous Ga(OEP)(CC-1-Pyr) experiment proved more complex as a kinetically unstable, multi-domain structure was observed, showing that this approach is not suitable in every case. Overall, we have demonstrated the versatility of this system in templating a variety of fullerenes from solution over a large range of concentrations and a variety of conditions. Due to the modular nature of this design, future experiments could involve tuning the porphyrin periphery and axial ligand to adjust the corral for templating an assortment of guest molecules.

**4.5. References**

1. Langa, F.; Nierengarten, J. F., *Fullerenes: Principles and Applications*. 2nd ed.; Royal Society of Chemistry: Cambridge, 2011.

2. Verner, R. F.; Benvegnu, C., *Handbook on Fullerene: Synthesis, Properties and Applications*. Nova Science Publishers: New York, 2012.

3. Prato, M. [60] Fullerene Chemistry for Materials Science Applications. *J. Mater. Chem.* **1997**, *7*, 1097-1109.

4. Pivrikas, A.; Sariciftci, N. S.; Juška, G.; Österbacka, R. A Review of Charge Transport and Recombination in Polymer/Fullerene Organic Solar Cells. *Prog. Photovoltaics* **2007**, *15*, 677-696.

5. Lu, L. Y.; Zheng, T. Y.; Wu, Q. H.; Schneider, A. M.; Zhao, D. L.; Yu, L. P. Recent Advances in Bulk Heterojunction Polymer Solar Cells. *Chem. Rev.* **2015**, *115*, 12666-12731.

6. Boyd, P. D. W.; Hosseini, A.; van Paauwe, J. D.; Reed, C. A., Porphyrin-Fullerene Supramolecular Chemistry. In *Handbook of Carbon Nano Materials: Fundamentals and Applications*, D'Souza, F.; Kadish, K. M., Eds. World Scientific Publishing Company: Singapore, 2011; Vol. 1, pp 375-390.

7. Bonifazi, D.; Enger, O.; Diederich, F. Supramolecular [60]Fullerene Chemistry on Surfaces. *Chem. Soc. Rev.* **2007**, *36*, 390-414.

8. Giacalone, F.; Herranz, M. Á.; Martin, N., Carbon Nanostructures: Covalent and Macromolecular Chemistry. In *Supramolecular Chemisty of Fullerenes and Carbon Nanotubes*, 1st ed.; Martin, N.; Nierengarten, J. F., Eds. Wiley-VCH: Weinheim, 2012; pp 1-26.

9. Zhang, Y.; Gao, X. P.; Weaver, M. J. Scanning Tunneling Microscopy of $C_{60}$ and $C_{70}$ on Ordered Au(111) and Au(110) : Molecular-Structure and Electron Transmission. *J. Phys. Chem.* **1992**, *96*, 510-513.

10. Uemura, S.; Samori, P.; Kunitake, M.; Hirayama, C.; Rabe, J. P. Crystalline $C_{60}$ Monolayers at the Solid-Organic Solution Interface. *J. Mater. Chem.* **2002**, *12*, 3366-3367.

11. Szuba, S.; Czajka, R.; Kasuya, A.; Wawro, A.; Rafii-Tabar, H. Observation of $C_{60}$ Film Formation on a Highly Oriented Pyrolitic Graphite Substrate via Scanning Tunnelling Microscopy. *Appl. Surf. Sci.* **1999**, *144-45*, 648-652.

12. den Boer, D.; Han, G. D.; Swager, T. M. Templating Fullerenes by Domain Boundaries of a Nanoporous Network. *Langmuir* **2014**, *30*, 762-767.

13. Blunt, M. O.; Russell, J. C.; Gimenez-Lopez, M. D.; Taleb, N.; Lin, X. L.; Schroder, M.; Champness, N. R.; Beton, P. H. Guest-Induced Growth of a Surface-Based Supramolecular Bilayer. *Nat. Chem.* **2011**, *3*, 74-78.

14. Griessl, S. J. H.; Lackinger, M.; Jamitzky, F.; Markert, T.; Hietschold, M.; Heckl, W. M. Room-Temperature Scanning Tunneling Microscopy Manipulation of Single $C_{60}$ Molecules at the Liquid-Solid interface: Playing Nanosoccer. *J. Phys. Chem. B* **2004**, *108*, 11556-11560.

15. Li, M.; Deng, K.; Lei, S. B.; Yang, Y. L.; Wang, T. S.; Shen, Y. T.; Wang, C. R.; Zeng, Q. D.; Wang, C. Site-Selective Fabrication of Two-Dimensional Fullerene Arrays by Using a Supramolecular Template at the Liquid-Solid Interface. *Angew. Chem., Int. Ed.* **2008**, *47*, 6717-6721.

16. Cui, D.; MacLeod, J. M.; Ebrahimi, M.; Perepichka, D. F.; Rosei, F. Solution and Air Stable Host/Guest Architectures From a Single Layer Covalent Organic Framework. *Chem. Commun.* **2015**, *51*, 16510-16513.

17. Plas, J.; Ivasenko, O.; Martsinovich, N.; Lackinger, M.; De Feyter, S. Nanopatterning of a Covalent Organic Framework Host-Guest System. *Chem. Commun.* **2016**, *52*, 68-71.

18. Mena-Osteritz, E.; Bäuerle, P. Complexation of $C_{60}$ on a Cyclothiophene Monolayer Template. *Adv. Mater.* **2006**, *18*, 447-451.

19. MacLeod, J. M.; Ivasenko, O.; Fu, C. Y.; Taerum, T.; Rosei, F.; Perepichka, D. F. Supramolecular Ordering in Oligothiophene-Fullerene Monolayers. *J. Am. Chem. Soc.* **2009**, *131*, 16844-16850.

20. Piot, L.; Silly, F.; Tortech, L.; Nicolas, Y.; Blanchard, P.; Roncali, J.; Fichou, D. Long-Range Alignments of Single Fullerenes by Site-Selective Inclusion into a Double-Cavity 2D Open Network. *J. Am. Chem. Soc.* **2009**, *131*, 12864-12865.

21. Pan, G. B.; Cheng, X. H.; Hoger, S.; Freyland, W. 2D Supramolecular Structures of a Shape-Persistent Macrocycle and Co-Deposition with Fullerene on HOPG. *J. Am. Chem. Soc.* **2006**, *128*, 4218-4219.

22. Mali, K. S.; Zophel, L.; Ivasenko, O.; Mullen, K.; De Feyter, S. Manifestations of Non-Planar Adsorption Geometries of Lead Pyrenocyanine at the Liquid-Solid Interface. *Chem. - Asian J.* **2013**, *8*, 2497-2505.

23. Boyd, P. D. W.; Reed, C. A. Fullerene-Porphyrin Constructs. *Acc. Chem. Res.* **2005**, *38*, 235-242.

24. Boyd, P. D. W.; Hodgson, M. C.; Rickard, C. E. F.; Oliver, A. G.; Chaker, L.; Brothers, P. J.; Bolskar, R. D.; Tham, F. S.; Reed, C. A. Selective Supramolecular Porphyrin/Fullerene Interactions. *J. Am. Chem. Soc.* **1999**, *121*, 10487-10495.

25. Tashiro, K.; Aida, T. Metalloporphyrin Hosts for Supramolecular Chemistry of Fullerenes. *Chem. Soc. Rev.* **2007**, *36*, 189-197.

26. Ishii, T.; Aizawa, N.; Kanehama, R.; Yamashita, M.; Sugiura, K. I.; Miyasaka, H. Cocrystallites Consisting of Metal Macrocycles with Fullerenes. *Coord. Chem. Rev.* **2002**, *226*, 113-124.

27. Olmstead, M. M.; Costa, D. A.; Maitra, K.; Noll, B. C.; Phillips, S. L.; Van Calcar, P. M.; Balch, A. L. Interaction of Curved and Flat Molecular Surfaces. The Structures of Crystalline Compounds Composed of Fullerene ($C_{60}$, $C_{60}O$, $C_{70}$, and $C_{120}O$) and Metal Octaethylporphyrin Units. *J. Am. Chem. Soc.* **1999**, *121*, 7090-7097.

28. Sun, D. Y.; Tham, F. S.; Reed, C. A.; Chaker, L.; Burgess, M.; Boyd, P. D. W. Porphyrin-Fullerene Host-Guest Chemistry. *J. Am. Chem. Soc.* **2000**, *122*, 10704-10705.

29. Yoshimoto, S.; Itaya, K. Advances in Supramolecularly Assembled Nanostructures of Fullerenes and Porphyrins at Surfaces. *J. Porphyrins and Phthalocyanines* **2007**, *11*, 313-333.

30. Kamm, J. M.; Iverson, C. P.; Lau, W.-Y.; Hopkins, M. D. Axial Ligand Effects on the Structures of Self-Assembled Gallium-Porphyrin Monolayers on Highly Oriented Pyrolytic Graphite. *Langmuir* **2016**, *32*, 487-495.

31. Bhattacharya, S.; Nayak, S. K.; Chattopadhyay, S.; Banerjee, M.; Mukherjee, A. K. Study of Molecular Complex Formation Between [60]Fullerene and Two Series of Donors by the NMR Method. *J. Phys. Chem. A* **2001**, *105*, 9865-9868.

32. Datta, K.; Banerjee, M.; Seal, B. K.; Mukherjee, A. K. Ground State EDA Complex Formation Between [60]Fullerene and a Series of Polynuclear Aromatic Hydrocarbons. *J. Chem. Soc., Perkin Trans. 2* **2000**, 531-534.

33. Keller, S.; Yi, C. Y.; Li, C.; Liu, S.-X.; Blum, C.; Frei, G.; Sereda, O.; Neels, A.; Wandlowski, T.; Decurtins, S. Synthesis, Structures, Redox and Photophysical Properties of Benzodifuran-Functionalised Pyrene and Anthracene Fluorophores. *Org. Biomol. Chem.* **2011**, *9*, 6410-6416.

34. Crawford, A. G.; Liu, Z. Q.; Mkhalid, I. A. I.; Thibault, M. H.; Schwarz, N.; Alcaraz, G.; Steffen, A.; Collings, J. C.; Batsanov, A. S.; Howard, J. A. K.; Marder, T. B. Synthesis of 2-and 2,7-Functionalized Pyrene Derivatives: An Application of Selective C-H Borylation. *Chem. - Eur. J.* **2012**, *18*, 5022-5035.

35. Ogunrinde, A.; Hipps, K. W.; Scudiero, L. A Scanning Tunneling Microscopy Study of Self-Assembled Nickel(II) Octaethylporphyrin Deposited from Solutions on HOPG. *Langmuir* **2006**, *22*, 5697-5701.

36. Ikeda, T.; Asakawa, M.; Goto, M.; Miyake, K.; Ishida, T.; Shimizu, T. STM Observation of Alkyl-Chain-Assisted Self-Assembled Monolayers of Pyridine-Coordinated Porphyrin Rhodium Chlorides. *Langmuir* **2004**, *20*, 5454-5459.

37. Teyssandier, J.; De Feyter, S.; Mali, K. S. Host-Guest Chemistry in Two-Dimensional Supramolecular Networks. *Chem. Commun.* **2016**, *52*, 11465-11487.

38. Coenen, M. J. J.; den Boer, D.; van den Bruele, F. J.; Habets, T.; Timmers, K. A. A. M.; van der Maas, M.; Khoury, T.; Panduwinata, D.; Crossley, M. J.; Reimers, J. R.; van Enckevort, W. J. P.; Hendriksen, B. L. M.; Elemans, J. A. A. W.; Speller, S. Polymorphism in Porphyrin Monolayers: The Relation Between Adsorption Configuration and Molecular Conformation. *Phys. Chem. Chem. Phys.* **2013**, *15*, 12451-12458.

39. Lau, W.-Y. Ph. D. Thesis. The University of Chicago, Chicago, IL, 2016.

40. Coenen, M. J. J.; Cremers, M.; den Boer, D.; van den Bruele, F. J.; Khoury, T.; Sintic, M.; Crossley, M. J.; van Enckevort, W. J. P.; Hendriksen, B. L. M.; Elemans, J. A. A. W.; Speller, S. Little exchange at the Liquid/Solid Interface: Defect-Mediated Equilibration of Physisorbed Porphyrin Monolayers. *Chem. Commun.* **2011**, *47*, 9666-9668.

41. Oncel, N.; Bernasek, S. L. Ni(II)- and Vanadyloctaethylporphyrin Self-Assembled Layers Formed on Bare and 5-(Octadecyloxy)isophthalic Acid Covered Graphite. *Langmuir* **2009**, *25*, 9290-9295.

42. Yoshimoto, S.; Sugawara, S.; Itaya, K. Effect of Underlying Ni(II) Porphyrin Adlayer on the Formation of Supramolecular Assembly of Fullerenes on Au(111) in Solution. *Electrochemistry* **2006**, *74*, 175-178.

# CHAPTER 5

## Development of Non-Pyrene Axial Ligands for Fullerene Templating on HOPG

### 5.1. Introduction

Having demonstrated evidence for the hypothesis that ordered arrays of five-coordinate metalloporphyrins could be used as corrals for the organization of small nanoparticles, we now focus on developing a greater understanding of the axial ligand scope that could be employed. From our work in Chapter 4, it is believed that a combination of a unit cell of appropriate dimension (the pseudo-hexagonal OEP unit cell exhibited by the Ga(OEP)X monolayers throughout this study) and an axial ligand with an appropriate affinity for the fullerenes $C_{60}$ and PCBM (1- and 2-ethynylpyrene), resulted in the partial random incorporation of the fullerenes into the assemblies. In order to more rationally design these materials for the purposes of greater fullerene incorporation, fullerene patterning, and future incorporation of a larger range of nanoparticles, we sought a more systematic study of what factors played an important role in the templating process. In this chapter, we discuss variations in ligand height, affinity for fullerene, linker, and shape, and the effects these had on the ambient surface templating of fullerenes.

One of the simplest modifications to test is that of the height of the ligand above the surface. Pyrene, and other polycyclic aromatic hydrocarbons (PAHs), have affinity for fullerenes due to the donor-acceptor interactions between their π-systems.[1] This overlap is assumed to be an important part of our surface-assembled systems as well, as no templating is observed in sequential deposition of Ga(OEP)(CCPh) and $C_{60}$; this is because the phenylacetylide ligand is not expected to have much, if any, affinity for the fullerene in solution. Therefore, by choosing a ligand that is predicted to have similar affinity for $C_{60}$ in solution to pyrene, but whose geometry prevents it from extending as far orthogonally to the HOPG surface, we can test the hypothesis

that a good overlap of π-systems between the ligand and guest molecule is necessary. The axial ligand 9-ethynylanthracene is a good candidate for this. The solution affinity of anthracene for $C_{60}$ is predicted to be similar to that of pyrene.[2, 3] However, its geometry is such that it will extend noticeably less above the surface than both pyrene derivatives previously studied.

Another fairly simple modification is changing the type of linker in our previously developed Ga(OEP)(CCPyr) system from an acetylide to a carboxylate; this is analogous to the change discussed in Chapter 3 for the Ga(OEP)(CCFc) and Ga(OEP)($O_2$CFc) complexes. While the acetylide linker is more rigid, the carboxylate linker provides more conformational freedom, a factor that may work to our advantage. Pyrene derivatives with flexible linkers such as ethylenecarboxylates have been employed for the solubilization and functionalization of single-walled nanotubes, due to pyrene's solution affinity for the carbon nanostructure.[4, 5] In our system, we hope less rigidity could result in better overlap of the affinity group and the fullerene within individual intra-ligand cavities.

We have, until this point, only investigated planar ligands as potential templates. However, we are also interested in ligands with a different shape that might create ordered patterns of fullerenes on the surface. Such a high degree of control over the organization of fullerenes at the nanometer-length scale is desirable. The ideal candidate for this task would selectively block certain sites in the monolayer due to steric constraints, while still maintaining adequate affinity for the fullerenes. The three-fold symmetric axial ligand 9-ethynyltriptycene is a good candidate for this investigation. Triptycene has known solid-state affinity for $C_{60}$, forming single-crystals in a ratio of 3:1 triptycene:$C_{60}$ with one fullerene in each of the three concave faces of the propeller-shaped molecule.[6] Derivatives of triptycene are known to have solution affinity for fullerenes.[7, 8] Further, the 120° angle between aryl planes is a good match for the obtuse angle of

the M(OEP) unit cell (~114°). The third aryl plane is then predicted to extend into a neighboring corral and produce a unique fullerene pattern on the surface.

While PAHs have well-established affinities for fullerenes and have been successful in our OEP-templating motif, we also wanted to expand the scope of ligand types under investigation. In particular, we aimed to introduce a heteroatom into the ligand system and investigate the effects of an ethynylthiophene template. Thiophenes and their derivatives have well-studied affinities for fullerenes in the solid state,[9] and on surfaces.[10-14] They have been also been actively investigated as components in organic photovoltaic devices, particularly in bulk heterojunction solar cells,[15, 16] which make them a promising candidate for widespread nanometer-length scale organization. Although the ethynylthiophene axial ligand is shorter than the ethynylpyrenes previously investigated, a factor predicted to have an impact on fullerene incorporation, the bithiophene[17] and tetrathiafulvalene[18] derivatives would have greater height and could be considered if this proves to be a promising candidate.

To this end, we have synthesized four additional Ga(OEP)X molecules aimed at exploring the parameters that affect the incorporation of fullerenes into the inter-ligand corrals (Figure 5.1). Three of these have axial acetylide linkers, Ga(OEP)(CCR) (R = 3-thiophene (Th), 9-anthrancene (Anthr), 9-triptycene (Trip)), and one is the carboxylate analog of the 1-ethynylpyrene, Ga(OEP)($O_2$CPyr). Molecular modeling was used to predict how fullerenes might interact with each of these compounds when assembled on a surface, and density functional theory was employed to investigate their electronic properties. Of these, only the Ga(OEP)(CCTh) complex was observed to conclusively interact with the fullerenes on the surface, forming a unique multilayer structure upon sequential deposition of the porphyrin and a $C_{60}$ solution. We discuss the steric and electronic factors that may contribute to this.

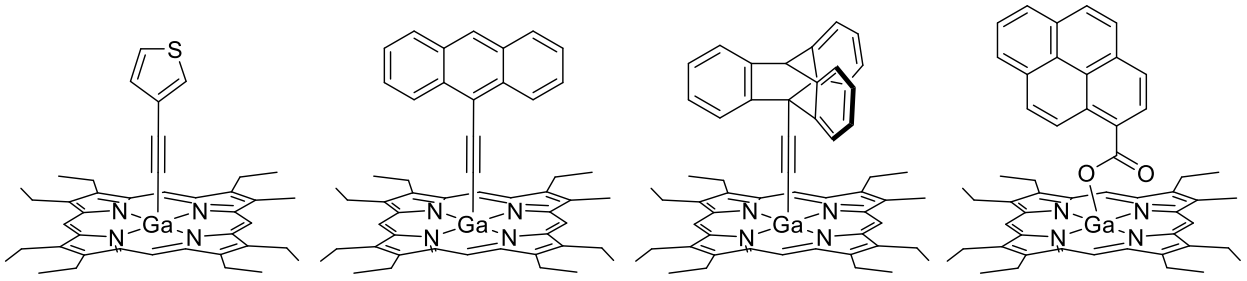


Ga(OEP)(CCTh) Ga(OEP)(CCAnthr) Ga(OEP)(CCTrip) Ga(OEP)($O_2$CPyr)

**Figure 5.1.** Ga(OEP)X complexes investigated in this chapter.

## 5.2. Experimental

Detailed experimental procedures and characterization for all complexes can be found in Section 6.4.5. The Ga(OEP)(CCR) complexes were synthesized by the general method of reacting Ga(OEP)Cl with the target LiCCR ligand in THF at –78 °C. The Ga(OEP)($O_2$CPyr) complex was synthesized by reacting a slight excess of 1-pyrenecarboxylic acid with Ga(OEP)(OH), in an analogous manner to the Ga(OEP)($O_2$CFc) complex described in Chapter 3. Similarly, small impurities remain in this complex at this time.

All compounds were optimized by density functional theory in the gas phase both in the global and in local energy minima with all eight ethyl chains pointing up, the latter being the predicted on-surface geometry. Molecular models of their predicted assembly into a pseudo-hexagonal unit cell were constructed. Further, single point calculations of their optimized structures were carried out, and molecular orbital isosurfaces generated. All compounds were studied by scanning tunneling microscopy at the solid-liquid interface and analyzed as described in Sections 6.4.3 and 6.4.4.

## 5.3. Results and Discussion

**5.3.1 Synthesis and Characterization of Ga(OEP)X Templates**. The general methods for synthesis of these compounds are outlined in Scheme 5.1. All Ga(OEP)(CCR) complexes (R =

Th, Anthr, Trip) were synthesized by the reaction of Ga(OEP)Cl with the corresponding LiCCR salt in THF at –78 °C. The salts were first generated from the HCCR complexes by lithiation with $^{n}$BuLi. While the 3-ethynylthiophene starting material was commercially available, both the Ga(OEP)(CCAnthr) and Ga(OEP)(CCTrip) syntheses first required a coupling of trimethylsilylacetylene and 9-bromoanthracene under standard Sonogoshira conditions.[19] The 9-(trimethylsilyl)anthracene was further reacted with isopentyl nitrite and anthranilic acid in a one-pot diazotization/Diels-Alder reaction to give the 9-(trimethylsilyl)triptycene complex.[19] Both protected complexes were then deprotected with tetrabutylammonium fluoride in THF.[19, 20] The synthesis of the Ga(OEP)($O_2$CPyr) complex followed that of the Ga(OEP)($O_2$CFc) analog described in Chapter 3,[21] by reacting a slight excess of 1-pyrenecarboxylic acid with Ga(OEP)(OH) starting material in THF at room temperature. A small (< 5%) 1-pyrenecarboxylic acid impurity is still present at this time; attempts at recrystallization have so far been unsuccessful due to the similar solubilities of the impurity and the product.

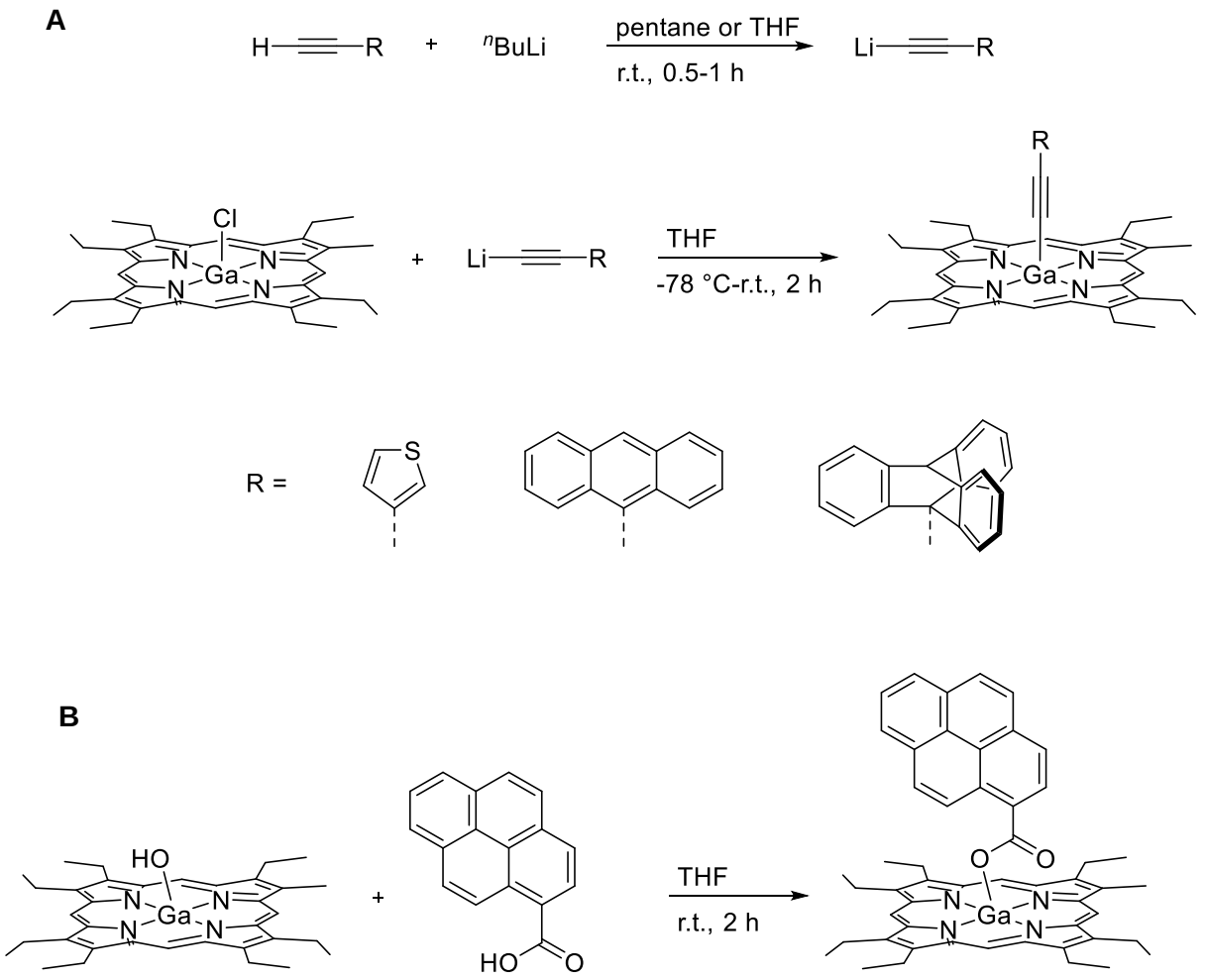


**Scheme 5.1.** General reaction conditions for the synthesis of (A) Ga(OEP)(CCR) complexes and (B) Ga(OEP)($O_2$CPyr) complex studied in this chapter. Ethynyl and Ga(OEP)(OH) precursors are synthesized from literature methods.

All complexes were characterized by $^1$H NMR spectroscopy and show characteristic upfield shifts of ligand resonances compared to the parent ligand, indicating successful attachment to the porphyrin. The Ga(OEP)(CCR) complexes were further characterized by $^{13}$C NMR, electronic absorption, and LDI-TOF spectroscopy; the full details of these can be found in Section 6.4.5. The electronic absorption spectra are qualitatively quite similar to those of other Ga(OEP)(CCR) complexes. Minor differences are observed between 300 nm and 380 nm, as expected based on differences in their ligand-derived absorption features.

**5.3.2 Density Functional Theory.** DFT calculations were conducted on all compounds to determine their optimized gas-phase structures (Figure 5.2). From selected porphyrin core bond lengths and angles (Table 5.1), we observe that all Ga(OEP)(CCR) complexes calculated in this study, including the three new acetylide complexes synthesized and studied here, are structurally very similar (Ga(OEP)(CCPh) is shown as a comparison). Specifically, the Ga–$N_4$ plane distances span a small range from 0.491 Å for Ga(OEP)(CCAnthr) to 0.496 Å for Ga(OEP)(CCTh) and the $N_4$–$C_{20}$ plane distances span a similarly small range from 0.048 Å for Ga(OEP)(CCPh) to 0.054 for Ga(OEP)(CCTrip). The Ga(OEP)($O_2$CPyr) complex is calculated to be structurally very similar to the Ga(OEP)($O_2$CFc) complex discussed in Chapter 3. The calculated doming is less than that of the acetylide complexes, with a Ga–$N_4$ plane distance of 0.408 Å and an $N_4$–$C_{20}$ plane distance of 0.030 Å (compared to 0.450 Å and 0.035 Å for the Ga(OEP)($O_2$CFc), respectively). We also note the unsymmetrical porphyrin core (N−Ga−O angle = 95.8−107.1°) due to the nonlinearity of the gallium-carboxylate linkage. As we have observed with all M(OEP) complexes thus far, the calculated structure does not correlate to a difference in on-surface structure; all compounds form monolayers with the same pseudo-hexagonal lattice parameters on HOPG at the solid-liquid interface. We predict that trend to continue for this new set of complexes.

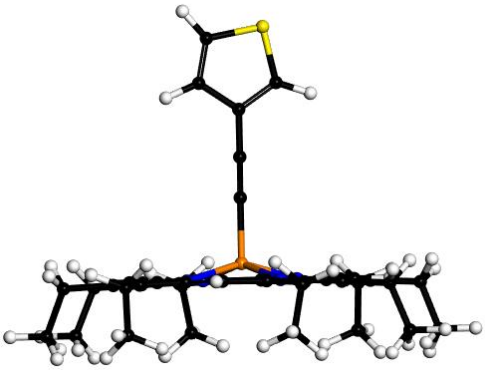

Ga(OEP)(CCTh)

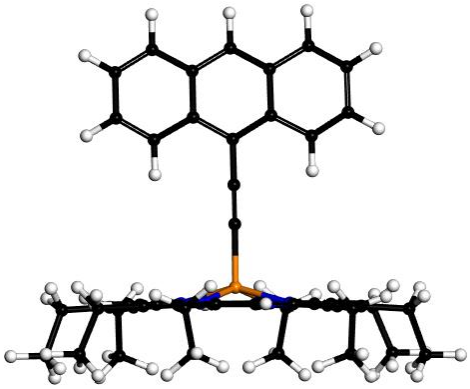

Ga(OEP)(CCAnthr)

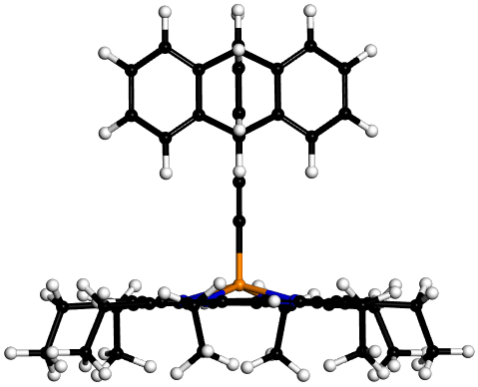

Ga(OEP)(CCTrip)

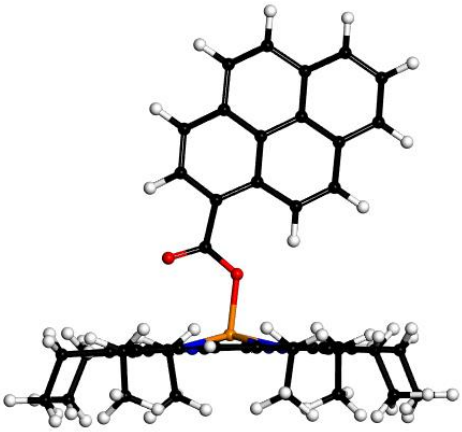

Ga(OEP)($O_2$CPyr)

**Figure 5.2.** Gas-phase optimized structures of Ga(OEP)X complexes. Atoms are color coded: Ga, orange; N, blue; C, black; H, white; S, yellow; O, red.

**Table 5.1.** Selected Bond Distances (Å) and Angles (°) for Ga(OEP)X Complexes Calculated by Density Functional Theory.

| | X | | | | |
|---|---|---|---|---|---|
| Nuclei | CCPh | CCTh | CCAnthr | CCTrip | $O_2$CPyr |
| Ga–X | 1.956 | 1.956 | 1.959 | 1.960 | 1.898 |
| Ga–N(1) | 2.068 | 2.068 | 2.067 | 2.067 | 2.055 |
| Ga–N(2) | 2.068 | 2.069 | 2.067 | 2.067 | 2.036 |
| Ga–N(3) | 2.068 | 2.069 | 2.068 | 2.068 | 2.036 |
| Ga–N(4) | 2.068 | 2.069 | 2.068 | 2.068 | 2.056 |
| N(1)–Ga–X | 103.9 | 103.9 | 104.0 | 103.8 | 96.4 |
| N(2)–Ga–X | 103.9 | 103.9 | 103.9 | 103.7 | 107.1 |
| N(3)–Ga–X | 103.9 | 103.9 | 103.7 | 103.7 | 106.3 |
| N(4)–Ga–X | 103.8 | 103.8 | 103.4 | 103.8 | 95.8 |
| Ga–$C_{20}N_4$ plane | 0.536 | 0.536 | 0.537 | 0.536 | 0.433 |
| Ga–$N_4$ plane | 0.495 | 0.496 | 0.491 | 0.492 | 0.408 |
| Ga–$C_{20}$ plane | 0.544 | 0.545 | 0.544 | 0.545 | 0.438 |
| $N_4$–$C_{20}$ plane | 0.048 | 0.049 | 0.053 | 0.054 | 0.030 |

While the two-dimensional assembly of these complexes is expected to follow the pattern of pseudo-hexagonal unit cells observed for all OEP complexes to this point, these new compounds introduce variations in the space above the porphyrin plane that could have a significant impact on the monolayers' abilities to template fullerenes. First, we note the Ga(OEP)(CCTh) complex contains a sulfur-containing ring, a deviation from the polycyclic aromatic hydrocarbons in Chapter 4 and in this chapter. Further, we note that while the two pyrene ligands studied in Chapter 4 were above 1 nm in expected height (~10.7 Å and ~12.7 Å above the porphyrin plane), the anthracene, triptycene, and thiophene are significantly shorter, (~8.5 Å, ~8.3 Å, ~8.1 Å, respectively). As we consider the suitability of these complexes for templating fullerenes, we consider the total on-surface geometry of the molecules with ethyl chains upturned[22, 23] and VDW radii included. Models based on these considerations were constructed to predict the overlap of the ligand with the fullerene $C_{60}$ when assembled on the surface (Figure 5.3). It is

predicted taking that, taking all geometries into account, the pyrene ligands will have good overlap with the π-system of the fullerene, while the shorter ligands have less overlap. Also included is the predicted "contact point" of the center of the fullerene; this is roughly in the center of the pyrene ligands, as shown in Figure 5.3. However, as seen for thiophene and anthracene (and, by extension, triptycene), the contact point is above the top of the ligand. Given that π-π interactions play an important role in the donor-acceptor supramolecular interactions of fullerenes with other molecules,[1] we predict that this may have an effect on our templates' effectiveness.

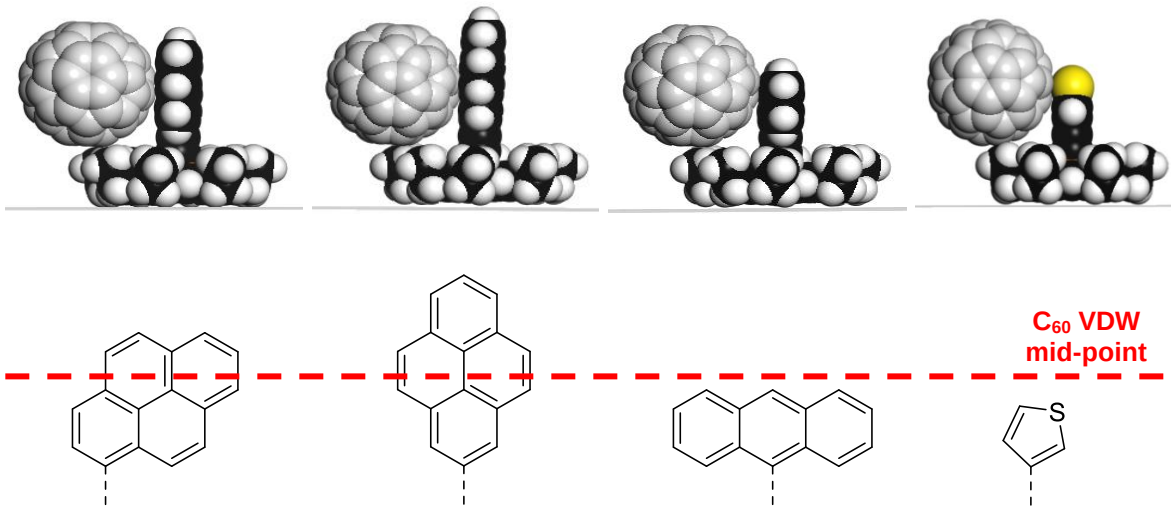


**Figure 5.3** Molecular models of select investigated Ga(OEP)(CCR) templates as assembled on a surface with upturned ethyl chains and their predicted point of contact with the mid-point of an incorporated $C_{60}$ molecule. The Ga(OEP)(CCAnthr) and Ga(OEP)(CCTrip) are predicted to have almost identical points of contact, and the Ga(OEP)($O_2$CPyr) complex contains a flexible linker and the contact point may be variable and are therefore excluded.

Another consideration is the 3-fold symmetric and sterically encumbered ligand present in the Ga(OEP)(CCTrip) complex, a deviation from the planar ligands studied to this point. We have modeled the Ga(OEP)(CCTrip) complex in the expected pseudo-hexagonal OEP unit cell to determine the likely orientation of the propeller-like triptycene ligands on the surface if

fullerenes were to be incorporated into the unit cell. Such modeling (Figure 5.4) suggests two possible orientations of the ligand upon deposition of the fullerene. One of these (Figure 5.4a) results in fullerenes that have the same pseudo-hexagonal OEP unit cell, but offset from the center of the porphyrin. The other (Figure 5.4b), results in the ligands blocking off the adjacent interligand cavities, resulting in a patterned filling of fullerenes in every other row. It is not immediately clear which of these would be thermodynamically favored, but they should be easily distinguishable by STM. The ability to precisely control the placement and spacing of fullerenes in supramolecular assemblies will be invaluable to continue to improve device performances.

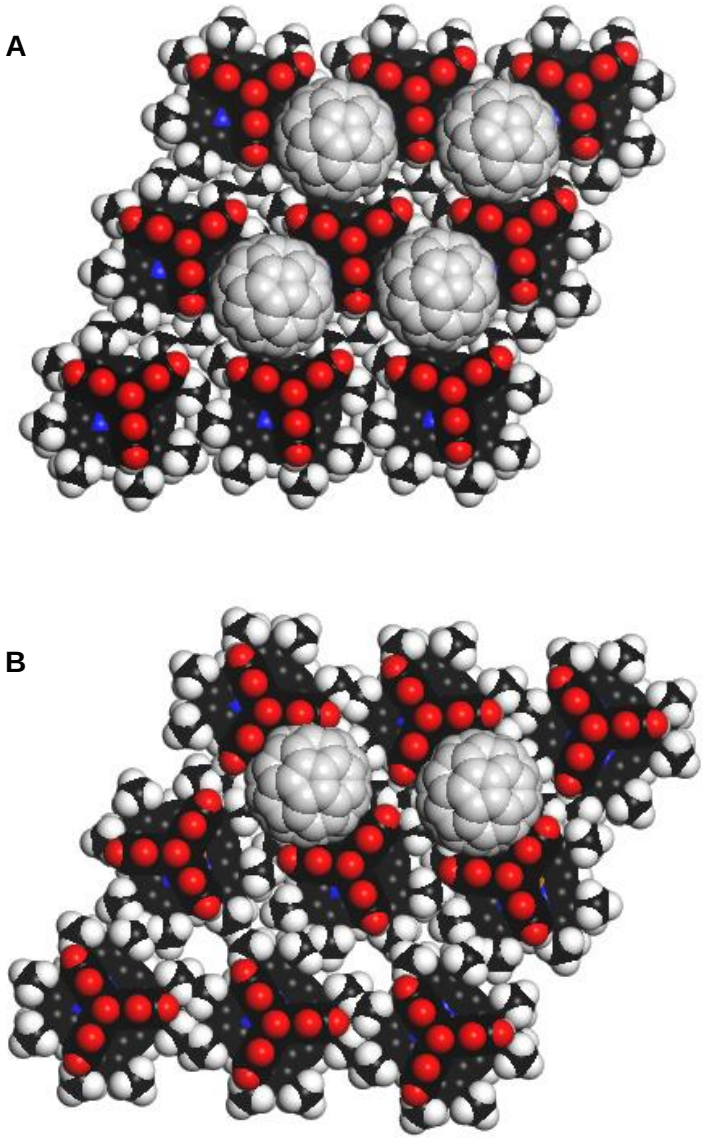


**Figure 5.4.** On-surface molecular model of monolayers of Ga(OEP)(CCTrip) with different orientations of the axial ligand allowing for different packing arrangements of $C_{60}$ into the inter-ligand cavities. The hydrogen atoms on the triptycene ligand are shown in red for clarity.

By changing the axial ligand, we have also changed the electronic structures of the complexes we have designed for templating, an important aspect to consider in donor-acceptor systems. In order to observe any correlations between STM images and electronics as determined by DFT, the frontier orbital energies of the complexes were compared to those calculated for $C_{60}$ and PCBM (HOMO–2 to LUMO+2; Table 5.2). Molecular orbital prediction can be useful to

help design effective candidates in electron-transfer systems;[24] in this case, the ideal template would have a HOMO of ligand parentage that can easily donate to the LUMO of the fullerene (–4.26 eV for $C_{60}$ and –4.11 eV for PCBM). The HOMO energies for the templates investigated span a fairly narrow range (–5.89 eV for Ga(OEP)($O_2$CPyr) to –5.55 eV for Ga(OEP)(CCAnthr)). As discussed in Chapter 4, the complexes are largely electronically modular, with a frontier orbital of primarily axial ligand parentage; however, as shown in Figure 5.5, this orbital can be either the HOMO or HOMO–2, with no clear pattern emerging for which fall into which category. As the complexes known to template fullerenes, Ga(OEP)(CC-1-Pyr) and Ga(OEP)(CC-2-Pyr), vary in their orbital of ligand parentage and fall within the middle of the HOMO energy ranges, we predict that a balance of electronics, sterics, and geometry will play a role in determining what will make an effective template.

**Table. 5.2.** DFT calculated frontier orbital energies of fullerenes and templates investigated in Chapters 4 and 5. All energies are given in eV.

| | Fullerene | | L | | | | | |
|---|---|---|---|---|---|---|---|---|
| Orbital | $C_{60}$ | PCBM | CC-1-Pyr | CC-2-Pyr | CCTh | CCAnthr | CCTrip | $O_2$CPyr |
| LUMO +2 | –4.26 | –3.82 | –2.20 | –2.11 | –1.23 | –2.32 | –1.29 | –2.22 |
| LUMO +1 | –4.26 | –4.06 | –2.93 | –2.92 | –2.89 | –2.94 | –2.96 | –2.97 |
| LUMO | –4.26 | –4.11 | –2.94 | –2.92 | –2.90 | –2.95 | –2.96 | –2.98 |
| HOMO | –7.00 | –6.65 | –5.69 | –5.84 | –5.82 | –5.55 | –5.88 | –5.89 |
| HOMO –1 | –7.00 | –6.79 | –5.86 | –5.97 | –5.94 | –5.86 | –6.01 | –5.91 |
| HOMO –2 | –7.00 | –6.80 | –5.98 | –6.00 | –6.16 | –5.99 | –6.41 | –6.09 |

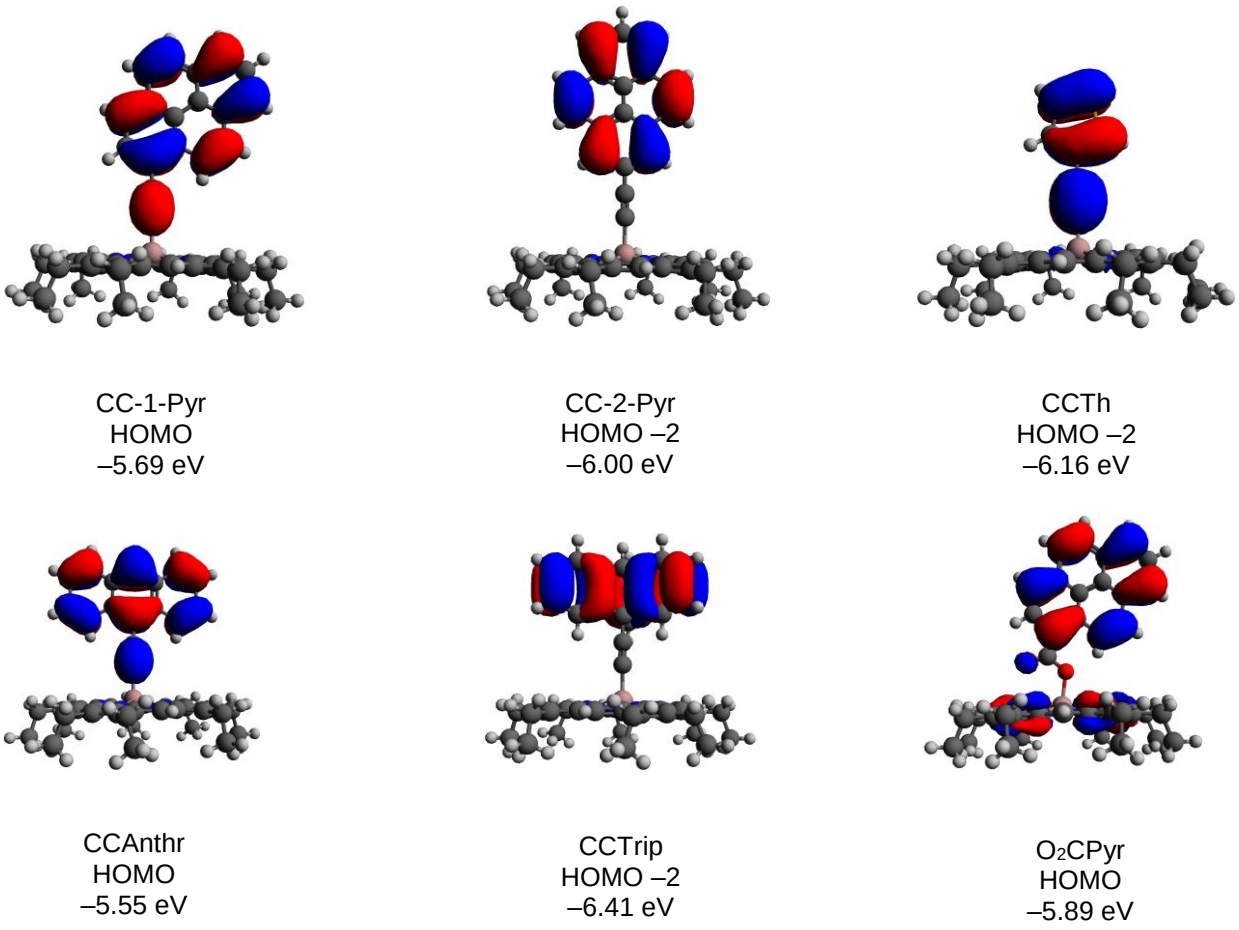


**Figure 5.5.** Highest occupied molecular orbital of primarily ligand parentage for investigated fullerene templates (isosurface value = 0.02).

### 5.3.3. Scanning Tunneling Microscopy.

**5.3.3.1. Ga(OEP)(CCTh).** Initial studies of Ga(OEP)(CCTh) at 0.5 mM, the concentration used throughout this study for most porphyrins, did not result in the formation of observable monolayers. When the concentration of the solution was increased to 0.75 mM, monolayer formation was observed (Figure 5.6), and this concentration is used generally throughout this study. However, later studies indicated that 0.5 mM solutions may indeed be suitable for these studies. The monolayers are variable in size, spanning roughly 30–100 nm in width. It was noted that the edges of arrays are often characterized by straight boundaries (Figure 5.6a and b), an unusual observation for OEP compounds. In studies of the ordering of organic molecules on

HOPG at the solid-liquid interface, it was observed that separately corralled arrays order with rotations of ±60° from one another, due to the symmetry of the underlying substrate;[25] it is possible that these boundaries are due to a similar underlying substrate effect, although the DFT studies reported above give no indication that Ga(OEP)(CCTh) possesses unique structural or electronic characteristics among Ga(OEP)X complexes that could account for this behavior. Smaller-scale images give well-resolved axial ligand features with apparent heights of ~1.2 Å (Figure 5.6c), similar to that seen for Ga(OEP)(CCPh). As predicted, the unit cell of the monolayer was found to be in good agreement with previous pseudo-hexagonal OEP complexes: $a$ = 1.37 (0.03) nm, $b$ = 1.35 (0.04) nm, Γ= 66 (3)°.

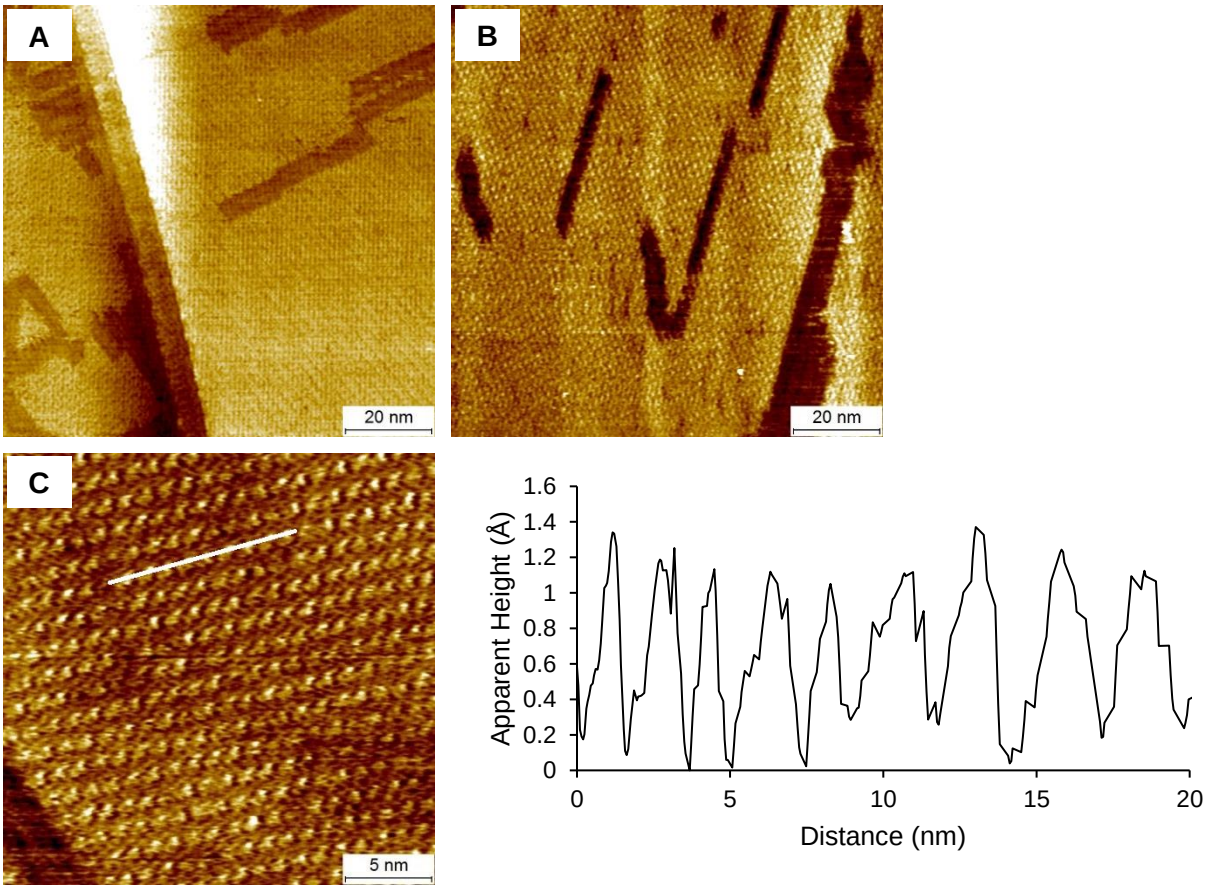


**Figure 5.6.** STM images showing long-range (A and B) and short-range ordering (C) of Ga(OEP)(CCTh) on HOPG at the solid–liquid interface (0.75 mM, 1-phenyloctane). The cross-sectional profile is taken along the white line shown in the STM image (C). The images were acquired at (A): $I$ = 10 pA, $V$ = –500 mV; (B): $I$ = 8 pA, $V$ = –500 mV; (C): $I$ = 12 pA, $V$ = –200 mV.

Upon the sequential deposition of a monolayer of Ga(OEP)(CCTh) followed by a 3.0 mM 1-phenyloctane solution of PCBM, we observed that random incorporation of the fullerene into the array is observed over multiple trials, comparable to what is observed with the Ga(OEP)(CCPyr) (Figure 5.7). The resulting arrays are qualitatively similar in occupancy of fullerene, and delamination of the surface that is observed in large-scale images (Figure 5.7a). Apparent height profiles also reveal a similar increase in apparent height (~2.0 Å for incorporated fullerene compared to ~1.2 Å for monolayer Ga(OEP)(CCTh)). These observations, being consistent with those observed for previous studies of $C_{60}$ overlayers, indicate that the PCBM is not interacting

with the intra-ligand cavity in an unexpected way. Therefore, we hypothesize that the PCBM guest molecule is oriented in the pocket with the functional group toward the solution, as shown in the model in Figure 5.7c.

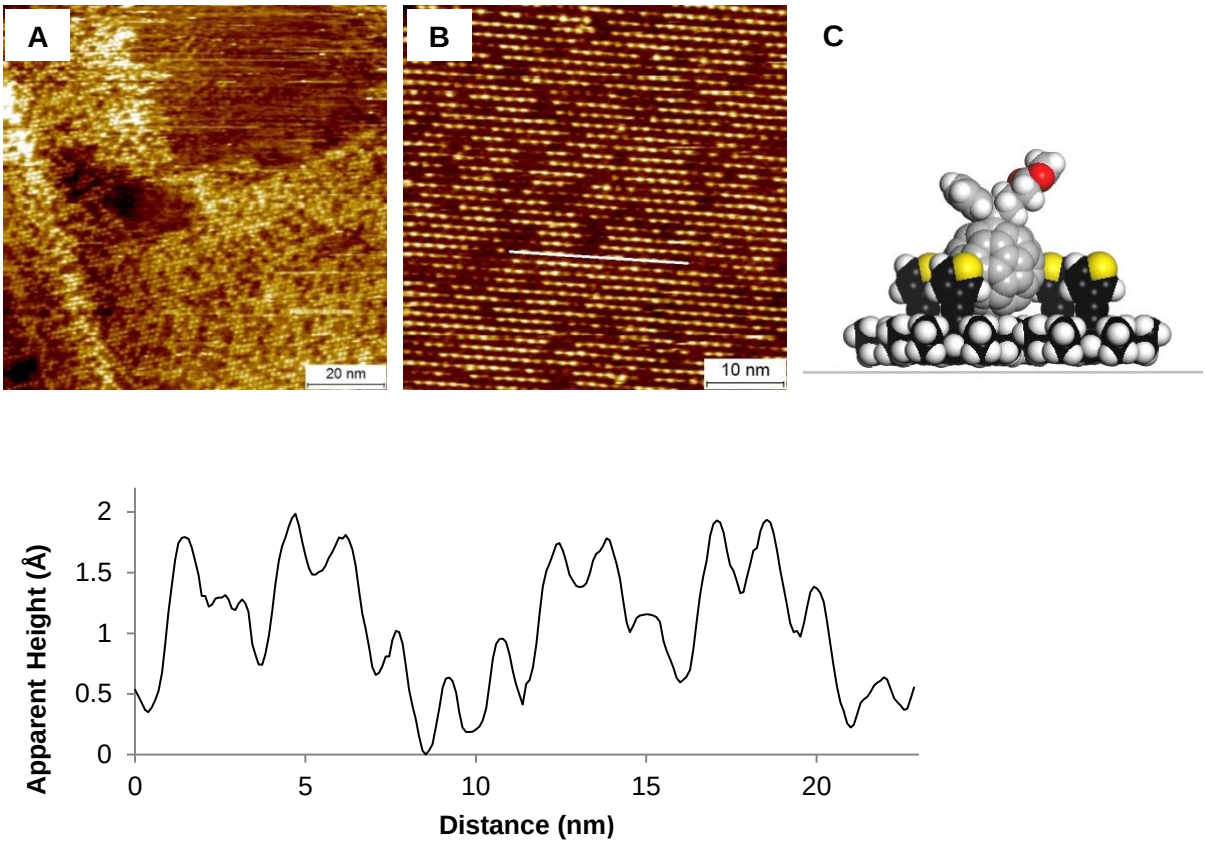


**Figure 5.7.** STM images (A and B) and proposed molecular model (C) showing sequential deposition of Ga(OEP)(CCTh) and PCBM on HOPG at the solid-liquid interface ([por] = 0.75 mM, [PCBM] = 3.0 mM, 1-phenyloctane). No multilayers are observed, while sporadic incorporation of fullerene is observed. The images were acquired at (A): $I$ = 8 pA, $V$ = –500 mV; (B): $I$ = 8 pA, $V$ = –700 mV. The cross-sectional profile is taken along the white line shown in image (B).

The interaction of a Ga(OEP)(CCTh) monolayer with $C_{60}$ is markedly different from that with PCBM. Upon addition of 3.0 mM $C_{60}$ to a preformed monolayer of Ga(OEP)(CCTh), a unique phenomenon is observed immediately after re-engagement of the STM tip; widespread multilayers are formed (Figure 5.8). While these multilayers tend to be accompanied by an

increase in exposed graphite, as observed in sequential deposition experiments of Ga(OEP)(CCPyr) and $C_{60}$ and in the analogous experiment with PCBM discussed above, the now characteristic random incorporation of bright features across a dim patterned background observed in these studies is not seen. A cross-sectional profile of these expansive mulitlayers shows that two distinctive layers can be resolved on top of the exposed HOPG. We note that this unique structure is never observed in STM studies of the Ga(OEP)(CCTh) complex directly deposited onto the surface.

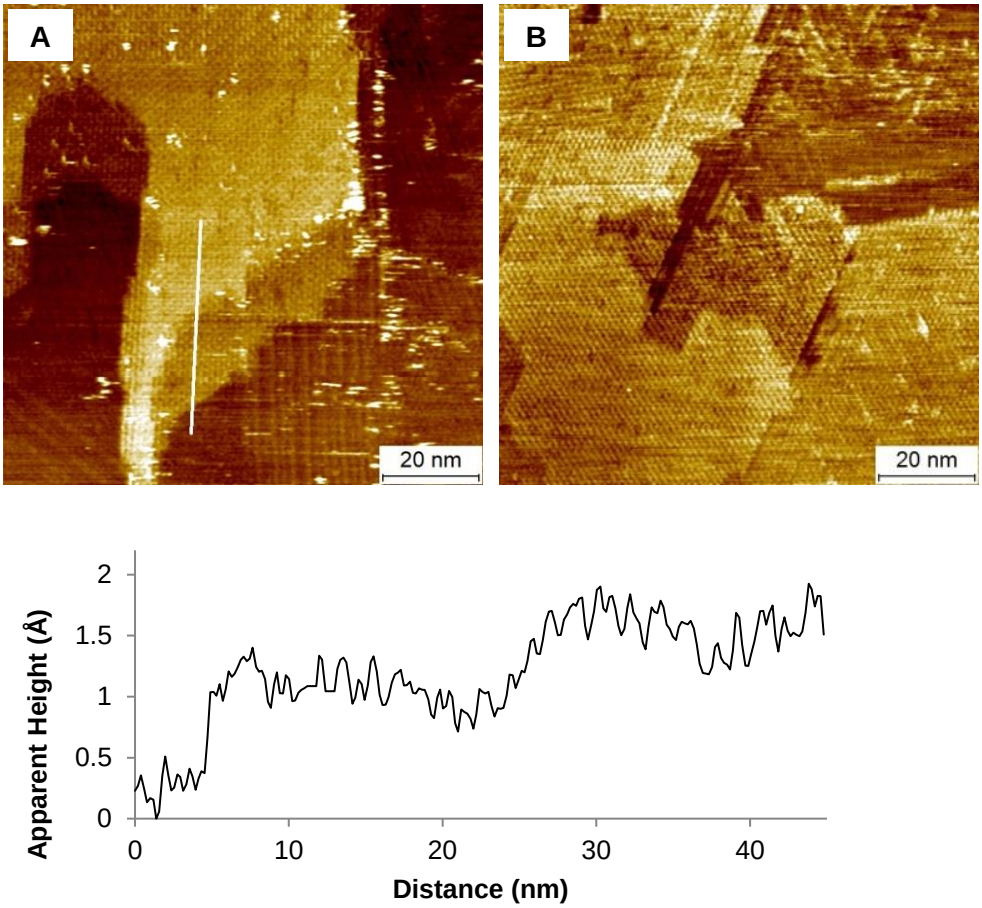


**Figure 5.8.** STM images and cross-sectional profile of Ga(OEP)(CCTh) with $C_{60}$ multilayer arrays formed upon sequential deposition of porphyrin and fullerene on HOPG at the solid-liquid interface showing long-range ordering of the multilayers with an increase in exposed graphite ([por] = 0.75 mM, [$C_{60}$] = 3.0 mM, 1-phenyloctane). The cross-sectional profile is taken along the white line shown in the STM image (A). The images were acquired at (A): $I$ = 8 pA, $V$ = –900 mV; (B): $I$ = 8 pA, $V$ = –600 mV.

Detailed analysis of small-scale images of the multilayers suggests that the top layer is porphyrin in origin (Figure 5.9). While the top layer often appears as well-defined features (Figure 5.9a and c), we have also observed data in which the top layer has a ring-like structure (Figure 5.9b). This is qualitatively similar to our previous observations of the porphyrin macrocycle directly assembled on HOPG, in which a dark center and bright periphery are observed for individual molecules. However, we are not able to distinguish between a top layer of Ga(OEP)(CCTh) that has axial ligand facing up towards the solution and one with axial ligands facing the bottom layer. We also note that images suggest that the bottom and top layers are slightly offset from one another (Figure 5.9a), though the structure of the top layer of the Ga(OEP)(CCTh) array is the same as the bottom (bottom unit cell: $a$ = 1.39 (0.02) nm, $b$ = 1.37 (0.03) nm, Γ= 66 (2)°; top unit cell: $a$ = 1.38 (0.02) nm, $b$ = 1.37 (0.02) nm, Γ= 66 (2)°). Finally, the top layer also exhibits borders with very straight edges (Figure 5.9c), as was observed with the Ga(OEP)(CCTh) monolayer on HOPG, furthering the conclusion that the top layer is porphyrin in nature. While independent bilayer islands were observed for the Ga(OEP)I complex in Chapter 2, these resulted from direct deposition of solutions of the porphyrin alone, formed independent bilayer islands whose lattices were mismatched from one another, and whose top layer had a different structure that that typically observed for monolayer Ga(OEP)X complexes. These differences have led to the conclusion that the Ga(OEP)(CCTh) top layer is not free standing on the bottom layer, but is interacting with the $C_{60}$ to form the observed structure.

The totality of these observations has led us to propose the sandwich-type structure shown in Figure 5.9d in which $C_{60}$ molecules are incorporated between two Ga(OEP)(CCTh) layers. This is consistent with observation of a top porphyrin layer whose lattice is identical to, but offset from, the bottom porphyrin layer. We tentatively suggest that in the top layer of porphyrins the

axial ligands are oriented down, allowing maximum thiophene-fullerene overlap. While we note that we have not been able to resolve $C_{60}$ incorporated into these arrays at any bias voltage, the lack of multilayer formation upon deposition of only Ga(OEP)(CCTh) strongly suggests that its templating effect is the driving force behind their formation. This conclusion is also supported by the observation that bilayers are not observed when PCBM replaces $C_{60}$. Apparent height profiles suggest that the height roughly doubles from the bottom to the top layer; the molecular model we propose predicts the top porphyrin layer to be roughly 1.4 nm from the bottom (~0.8 nm to the top of the Ga(OEP)(CCTh)). However, we have observed several times that apparent and actual height are unrelated. Additional surface analysis methods that would probe the structure of this array would be required to confirm this hypothesis, such as grazing incidence small-angle X-ray scattering (GISAXS).[26, 27] This would ideally be done under solvent-free conditions; however, multiple attempts at removing the solvent and imaging at the solid-air interface resulted in highly unstable arrays.

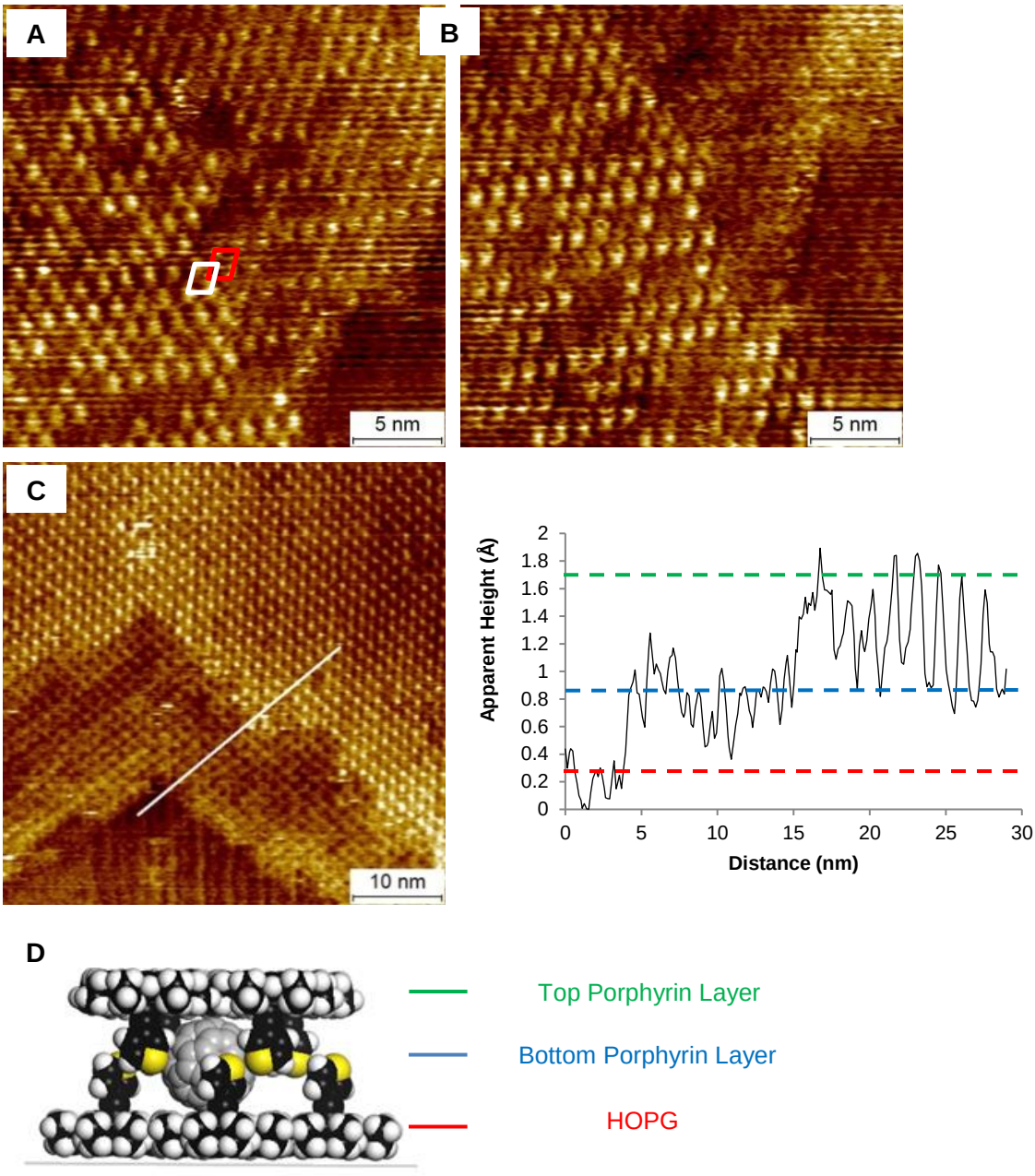


**Figure 5.9.** STM images and proposed molecular model of Ga(OEP)(CCTh) with $C_{60}$ multilayer arrays formed upon sequential deposition of porphyrin and fullerene on HOPG at the solid-liquid interface ([por] = 0.75 mM, [$C_{60}$] = 3.0 mM, 1-phenyloctane). (A) shows small-scale detail of mis-alignment of the bottom and top layers: top layer unit cell shown in white, bottom layer unit cell shown in red; (B) show the porphyrin-ring character of the top layer; (C) shows characteristic straight edges observed in both monolayer and multilayer Ga(OEP)(CCTh); (D) shows the proposed molecular model of the "sandwich" multilayer structure. The cross-sectional profile is taken along the white line shown in the STM image (C). The images were acquired at (A): $I$ = 8 pA, $V$ = –850 mV; (B): $I$ = 8 pA, $V$ = –900 mV; (C): $I$ = 8 pA, $V$ = –700 mV.

Upon sequential deposition of $C_{60}$ at concentrations lower than 3.0 mM, these multilayers are not observed. At a $C_{60}$ concentration of 1.5 mM, we have observed the sporadic random incorporation of bright spots (Figure 5.10a and b), similar to observations in the analogous sequential deposition experiments with the Ga(OEP)(CCPyr) complexes and with Ga(OEP)(CCTh) deposited with PCBM. At even lower concentrations of $C_{60}$ (0.5 mM), we observe little to no incorporation of the fullerene. A few bright features consistent in apparent height to incorporated fullerene (~2.0 Å) are observed within the lattice (Figure 5.10c). However, while multilayer formation has been observed across several trials at the 3.0 mM $C_{60}$ concentration, the observations at lower concentrations have yet to be successfully repeated, instead resulting in absence of $C_{60}$ incorporation, or in removal of the monolayer. Such observations may be consistent with the hypothesis that the $C_{60}$ has a higher affinity for the excess Ga(OEP)(CCTh) in solution than for the surface-assembled porphyrin. This would account for the little incorporation seen at lower concentrations and may account for the unusual behavior seen at high concentrations. Metalloporphyrins are known to have both solid-state and solution affinity for fullerenes,[28-31] and it is likely that there is a complex balance of interactions occurring in our system. Subtle shifts in both $^{1}H$ and $^{13}C$ NMR spectra have been used to confirm complexation in porphyrin-fullerene host-guest systems,[32, 33] and such studies could be considered in the future to gain a greater insight into the nature of the interactions in our Ga(OEP)(CCTh)·$C_{60}$ system.

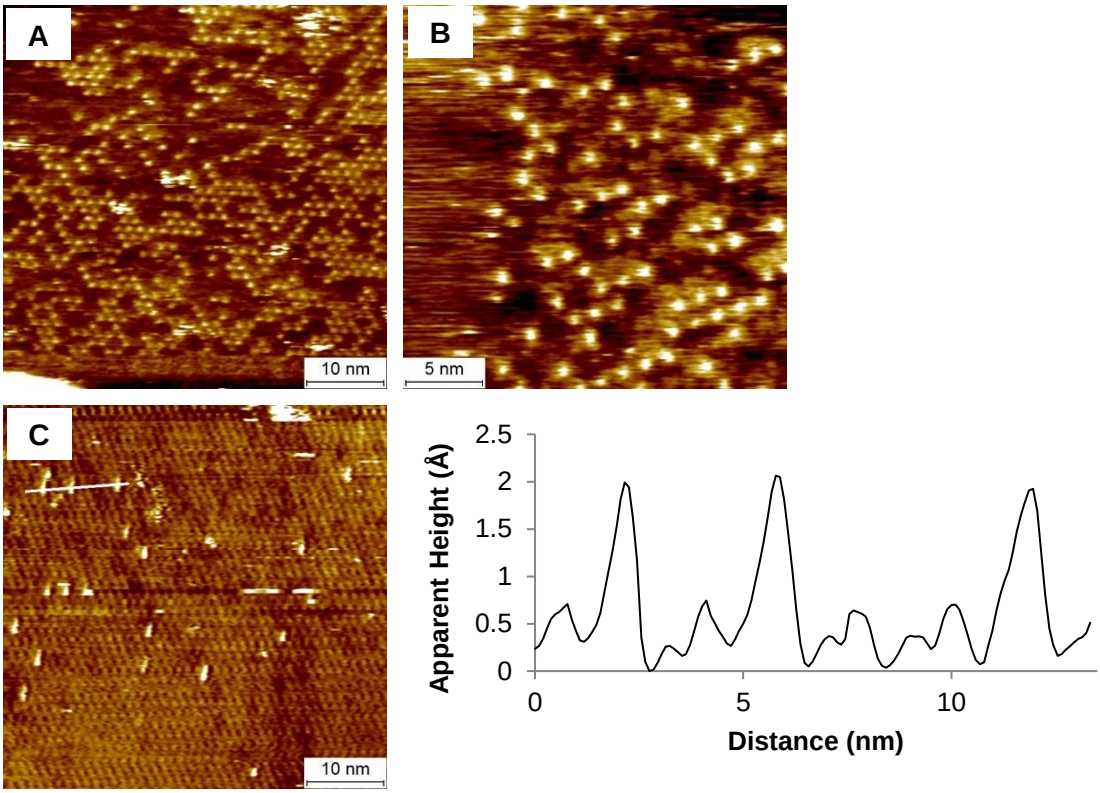


**Figure 5.10.** STM images showing sequential deposition of Ga(OEP)(CCTh) and $C_{60}$ at lower concentrations on HOPG at the solid-liquid interface ([por] = 0.75 mM, 1-phenyloctane). No multilayers are observed, while sporadic incorporation of fullerene may be observed. The cross-sectional profile is taken along the white line shown in the STM image (C). The images were acquired at (A): $I$ = 8 pA, $V$ = –700 mV, [$C_{60}$] = 1.5 mM; (B): $I$ = 8 pA, $V$ = –700 mV, [$C_{60}$] = 1.5 mM; (C): $I$ = 10 pA, $V$ = –900 mV, [$C_{60}$] = 0.5 mM.

As with the Ga(OEP)(CCPyr) complexes discussed in Chapter 4, we wanted to investigate the effects of depositing a pre-mixed solution of porphyrin and fullerene. When a solution of mixed Ga(OEP)(CCTh) and $C_{60}$ in 1-phenyloctane was deposited on HOPG (after mixing: [por] = 0.38 mM, [$C_{60}$] = 1.5 mM), arrays ~50–75 nm in width formed within minutes of deposition (Figure 5.11a). These arrays are qualitatively similar to those that are formed when Ga(OEP)(CCTh) is sequentially deposited with PCBM and those of the Ga(OEP)(CCPyr) complexes sequentially deposited with fullerenes. There is random incorporation of bright features (~1.8−2.0 Å in apparent height) across a patterned background (Figure 5.11b and c). This is a similar effect to that observed in one trial of sequentially deposited Ga(OEP)(CCTh)

with 1.5 mM $C_{60}$, indicating the "all-in-one" deposition method may be successful for templating fullerenes in this system.

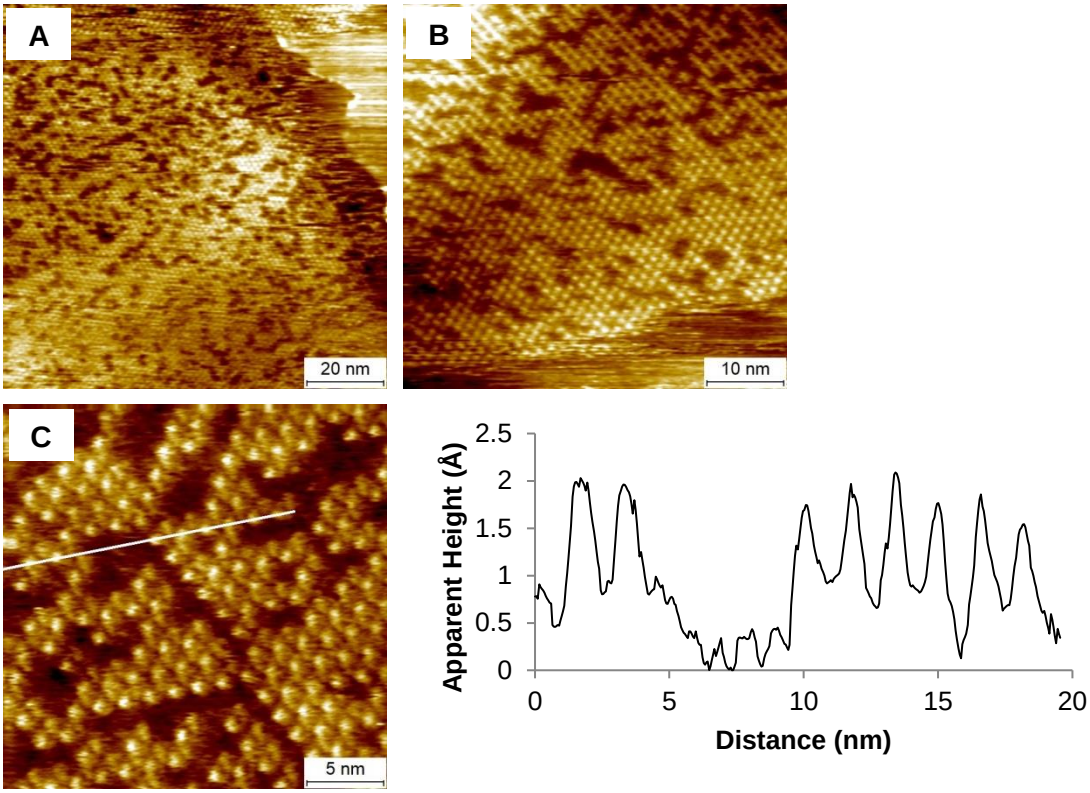


**Figure 5.11.** STM images showing deposition of a pre-mixed solution of Ga(OEP)(CCTh) and $C_{60}$ HOPG at the solid-liquid interface (equal volumes of 1-phenyloctane solutions mixed, [por] = 0.75 mM, [$C_{60}$] = 3.0 mM). No multilayers are observed, while random incorporation of the fullerene is observed throughout the array. The cross-sectional profile is taken along the white line shown in the STM image (C). The images were acquired at (A): $I$ = 8 pA, $V$ = –500 mV; (B): $I$ = 8 pA, $V$ = –900 mV; (C): $I$ = 8 pA, $V$ = –1000 mV.

**5.3.3.2. Ga(OEP)(CCAnthr).** The Ga(OEP)(CCAnthr) complex was deposited on HOPG from a 1-phenyloctane solution at a concentration of 0.25 mM due to the saturation concentration of the compound in 1-phenyloctane being lower than the 0.5 mM typically used for these complexes. Monolayers of the complex spanning greater than 100 nm × 100 nm were observed within minutes of deposition (Figure 5.12a) and the porphyrin macrocycle structure can be clearly imaged (Figure 5.12b). From this, we find that the lattice parameters are the expected pseudo-hexagonal OEP unit cell: $a$ = 1.37 (0.03) nm, $b$ = 1.37 (0.03) nm, Γ = 66 (2)°. However,

these monolayers are also often characterized by a very uneven appearance of the macroscale structure (Figure 5.12c), and poor resolution of the ligand axial features (Figure 5.12d). We tentatively suggest that this is due to a partial bilayer structure; such structures have been observed as both head-to-head and head-to-tail bilayers of five-coordinate phthalocyanines under UHV[34] and the solid-liquid interface.[35] The lower solubility of Ga(OEP)(CCAnthr) in 1-phenyloctane, and the ability of anthracene ligands to π-stack with one-another might make a partial second layer formation favorable. This drastic unevenness is likely to make any resulting changes that might occur to the monolayer after addition of a fullerene solution difficult to resolve.

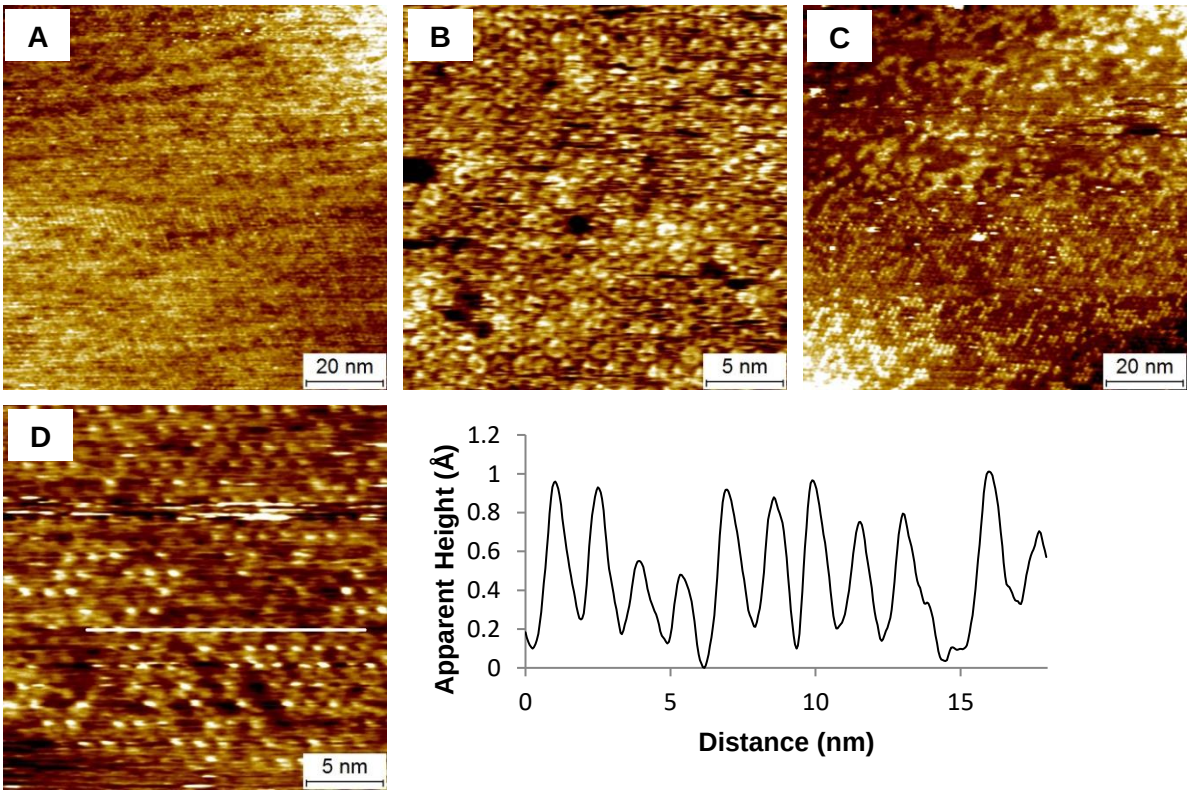


**Figure 5.12.** STM images showing deposition of Ga(OEP)(CCAnthr) on HOPG at the solid-liquid interface (0.25 mM, 1-phenyloctane). (A) and (C) show long-range ordering with (C) showing macroscale unevenness; (B) shows tunneling through the porphyrin macrocycle; (D) shows small-scale unevenness. The cross-sectional profile is taken along the white line shown in the STM image (D). The images were acquired at (A): $I$ = 10 pA, $V$ = –500 mV; (B): $I$ = 8 pA, $V$ = –700 mV; (C): $I$ = 8 pA, $V$ = –700 mV; (D): $I$ = 8 pA, $V$ = –500 mV.

Preliminary results of the sequential deposition of the Ga(OEP)(CCAnthr) complex followed by a 3.0 mM 1-phenyloctane solution of $C_{60}$ were inconclusive. STM images following fullerene deposition were, as predicted, qualitatively similar to the porphyrin monolayer (Figure 5.13); an uneven macroscale structure with a resolved porphyrin macrocycle are observed. The inability to distinguish between the monolayer and a potentially successful fullerene incorporation indicate that this template is not a promising candidate for further study. As molecular models predict the fullerene van der Waals mid-point is well above the top of the ligand (Figure 5.3), any future work investigating this ligand could consider using the taller butadiynyl linker, C≡C−C≡C[36] to test this hydrocarbon's templating abilities at a predicted effective height.

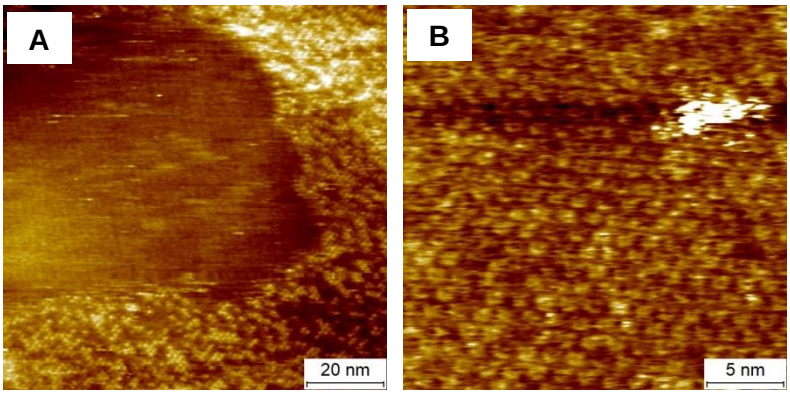


**Figure 5.13.** STM images showing sequential deposition of Ga(OEP)(CCAnthr) and $C_{60}$ on HOPG at the solid-liquid interface ([por] = 0.25 mM, [$C_{60}$] = 3.0 mM, 1-phenyloctane). (A) shows long-range ordering macroscale unevenness and exposed graphite; (B) shows tunneling through the porphyrin macrocycle. The images were acquired at (A): $I$ = 8 pA, $V$ = –700 mV; (B): $I$ = 10 pA, $V$ = –500 mV.

**5.3.3.3. Ga(OEP)(CCTrip).** The Ga(OEP)(CCTrip) complex was deposited from a 0.5 mM 1-phenyloctane solution onto HOPG and the resulting monolayer was imaged at the solid-liquid interface. The arrays are expansive, but show small amounts of exposed graphite and interfaces where arrays have grown together, an unusual observation for Ga(OEP)X monolayers (Figure 5.14a and c). Notably, when imaged at a bias that allows for imaging of the ligand (Figure 5.14c) as opposed to the porphyrin macrocycle (Figure 5.14b), the apparent height is significantly

greater than other acetylide ligands (~2.8 Å compared to ~1.2 Å for the Ga(OEP)(CCPh) discussed in Chapter 2) although the predicted actual height is nearly identical. This measured apparent height is similar to the Ga(OEP)(CCFc) complex discussed in Chapter 3, a compound that contains an electroactive axial ligand. The predicted energy of the highest occupied molecular orbital of ligand parentage for the Ga(OEP)(CCTrip) is the most negative of the compounds studied here, at −6.41 eV, although we might expect a smaller HOMO-LUMO gap to result in greater electron tunneling. As expected, the monolayer exhibits the typical OEP pseudo-hexagonal unit cell: $a$ = 1.37 (0.03) nm, $b$ = 1.36 (0.02) nm, Γ = 65 (3)°.

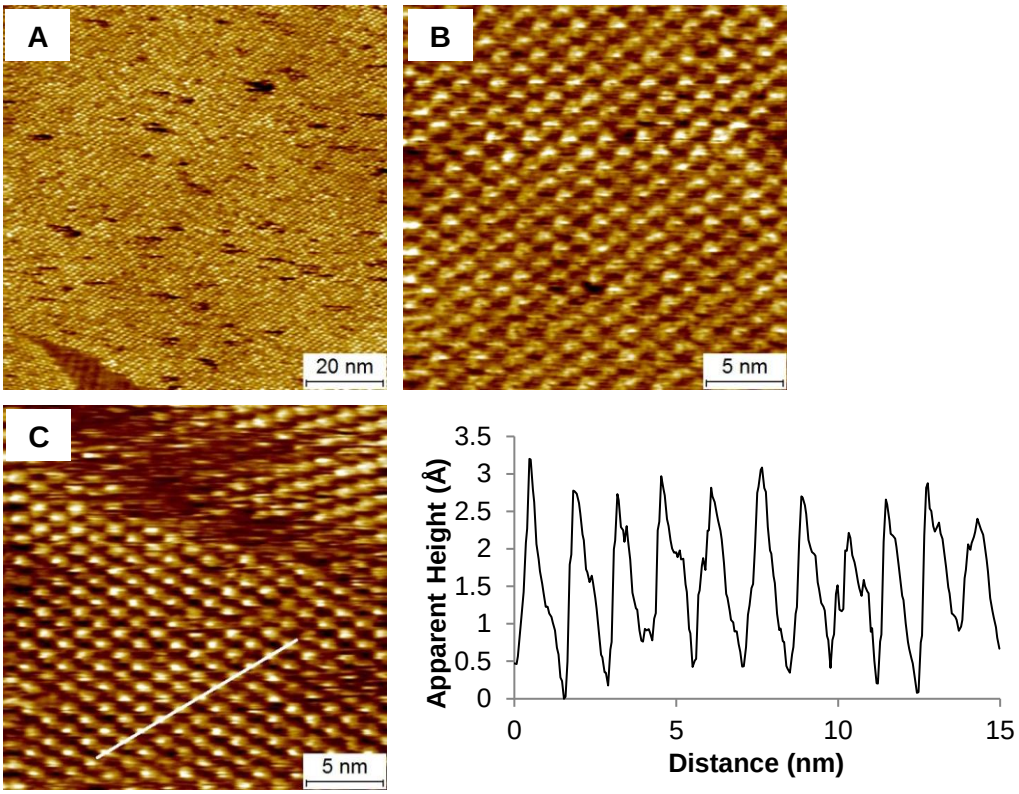


**Figure 5.14.** STM images showing deposition of Ga(OEP)(CCTrip) on HOPG at the solid-liquid interface (0.5 mM, 1-phenyloctane). (A) shows long-range ordering with some exposed graphite where misaligned arrays are present; (B) shows tunneling through the porphyrin macrocycle; (C) tunneling through the axial ligand with some exposed graphite where misaligned arrays are present. The cross-sectional profile is taken along the white line shown in the STM image (C). The images were acquired at (A): $I$ = 8 pA, $V$ = –500 mV; (B): $I$ = 8 pA, $V$ = –600 mV; (C): $I$ = 8 pA, $V$ = –500 mV.

The sequential deposition of Ga(OEP)(CCTrip) followed by a 3.0 mM $C_{60}$ solution in 1-phenyloctane resulted in observations that were inconclusive as to whether fullerene templating had occurred. While sporadic bright features appear across a patterned background (Figure 5.15a and b), the cross-sectional profiles are inconsistent with templated fullerenes observed in Chapter 4, where the fullerene was much taller than the ligand; here, we see that the bright features have consistent apparent heights of ~1.5 Å, significantly shorter than even that of the Ga(OEP)(CCTrip) monolayer itself. To exclude the possibility that the propeller-like ligands were in a kinetically trapped state preventing fullerene incorporation, we also performed experiments where a pre-mixed solution of equal volumes of 1-phenyloctane solutions of the porphyrin and fullerene was deposited (after mixing: [por] = 0.25 mM, [$C_{60}$] = 1.5 mM). This resulted in qualitatively similar images to the pristine monolayer (Figure 5.15c) with no evidence of fullerene incorporation. We conclude that this is not a promising template, likely due to a combination of steric and height factors. This hypothesis could in future be tested by synthesizing the extended butadiynyl-linked[36] Ga(OEP)(C≡C−C≡CTrip) derivative.

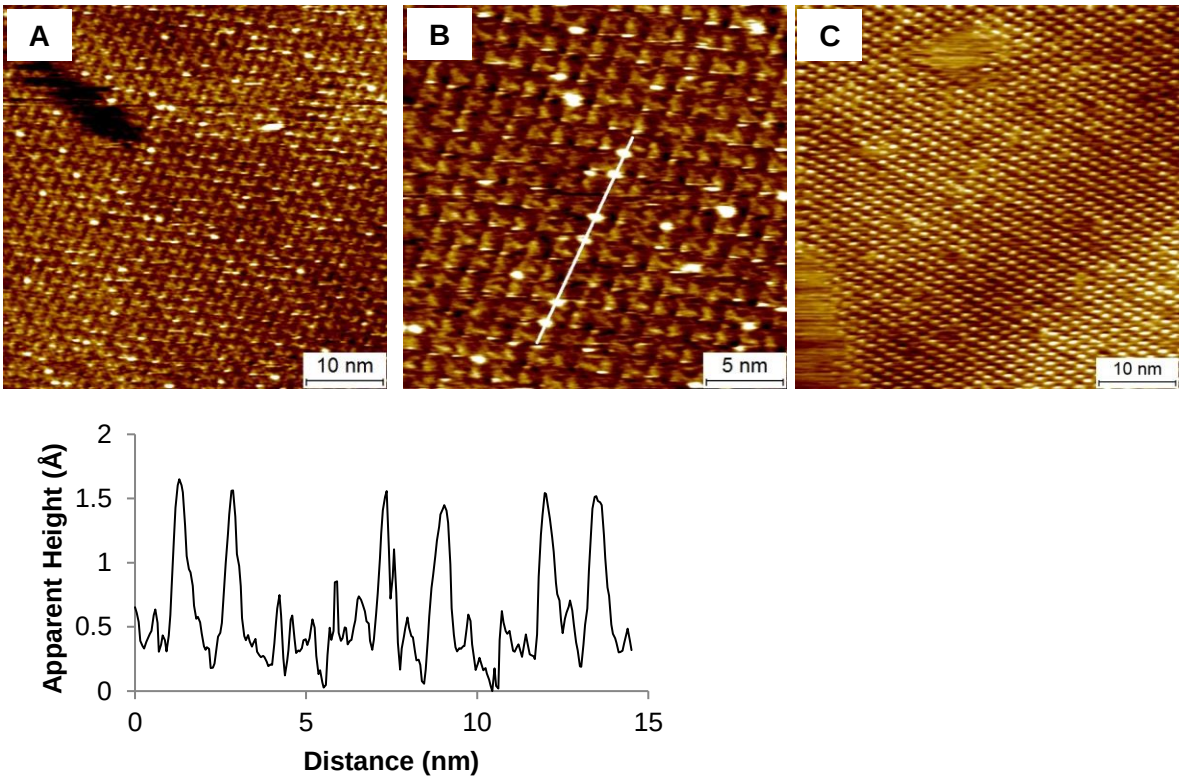


**Figure 5.15.** STM images showing sequential (A and B) and pre-mixed (C) deposition of Ga(OEP)(CCTrip) and $C_{60}$ on HOPG at the solid-liquid interface ([por] = 0.5 mM, [$C_{60}$] = 3.0 mM, 1-phenyloctane). (A) shows sporadic bright features on a patterned background after sequential deposition of porphyrin and $C_{60}$; (B) shows this phenomenon in detail; (C) shows an array formed from the deposition of a 1:1 vol:vol mixture of porphyrin and $C_{60}$. The cross-sectional profile is taken along the white line shown in the STM image (B). The images were acquired at (A): $I$ = 8 pA, $V$ = –700 mV; (B): $I$ = 8 pA, $V$ = –700 mV; (C): $I$ = 8 pA, $V$ = –700 mV.

**5.3.3.4. Ga(OEP)($O_2$CPyr).** The Ga(OEP)($O_2$CPyr) complex was deposited on HOPG from a 0.5 mM 1-phenyloctane solution and was observed to form extensive arrays greater than 100 nm × 100 nm within minutes of deposition (Figure 5.16a). The small 1-pyrenecarboxylic acid impurity noted above did not appear to have any effect on monolayer formation. As with other Ga(OEP)X complexes, the porphyrin macrocycle (Figure 5.16b) and the axial ligand (Figure 5.16c) can be independently imaged. Cross-sectional profiles show that the apparent height is ~1.2 Å, comparable to the Ga(OEP)(CCPyr) complexes studied in Chapter 4. As expected, this

complex assembles with standard pseudo-hexagonal OEP lattice parameters: $a$ = 1.37 (0.02) nm, $b$ = 1.36 (0.03) nm, Γ = 66 (2)°.

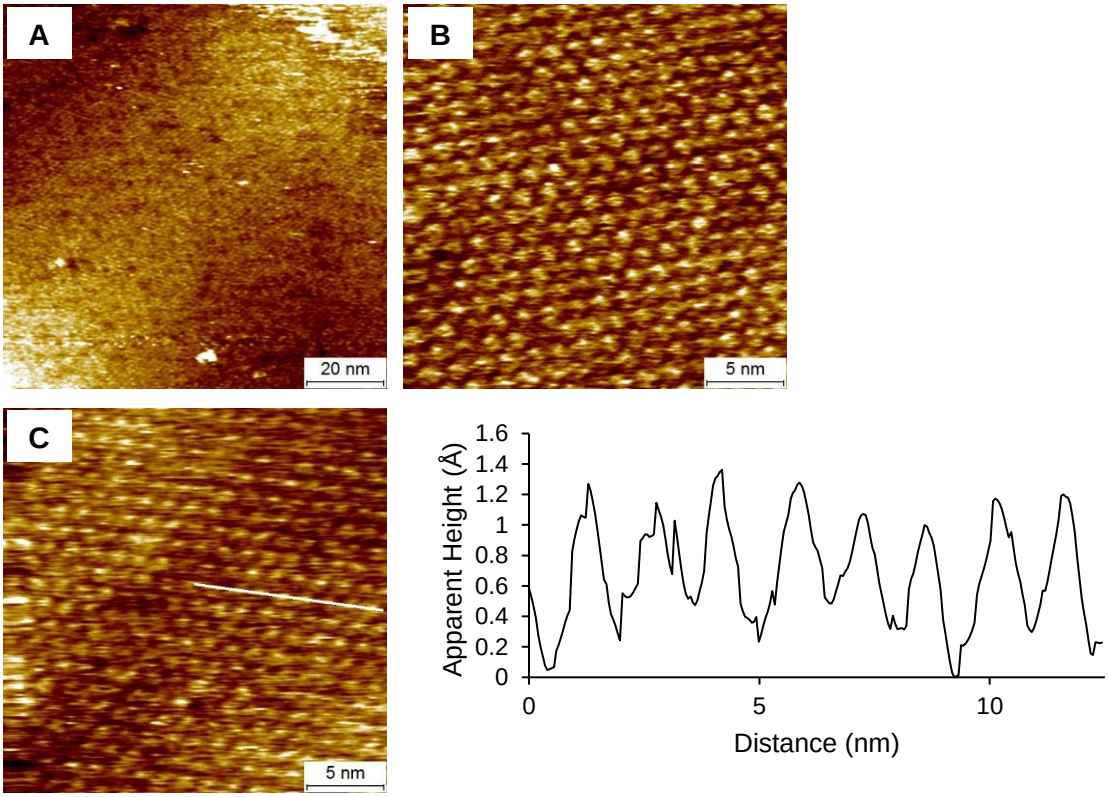


**Figure 5.16.** STM images showing deposition of Ga(OEP)($O_2$CPyr) on HOPG at the solid-liquid interface (0.5 mM, 1-phenyloctane). (A) shows long-range ordering; (B) shows tunneling through the porphyrin macrocycle; (C) tunneling through the axial ligand. The cross-sectional profile is taken along the white line shown in the STM image (C). The images were acquired at (A): $I$ = 8 pA, $V$ = –600 mV; (B): $I$ = 10 pA, $V$ = –700 mV; (C): $I$ = 12 pA, $V$ = –400 mV.

Upon sequential deposition of a 3.0 mM $C_{60}$ solution in 1-phenyloctane, significant removal of the array was observed immediately after re-engaging the STM tip (Figure 5.17a). While small-scale images confirm by imaging through the macrocycle that the porphyrin monolayer remains somewhat intact (Figure 5.17b), these arrays are highly unstable and no fullerene incorporation has been observed. While these are preliminary results, the instability of the arrays after fullerene deposition indicates that the Ga(OEP)($O_2$CPyr) monolayer is also not a promising fullerene template. This removal of the complex may be a result of changing the effective

concentration of porphyrin in solution or may be caused by an interaction with the fullerene; a more systematic study of deposition conditions would be required.

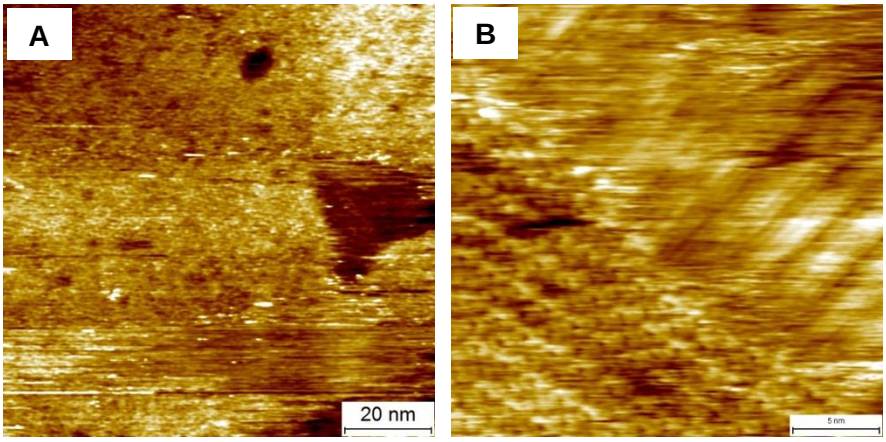


**Figure 5.17.** STM images showing sequential deposition of Ga(OEP)($O_2$CPyr) and $C_{60}$ on HOPG at the solid-liquid interface ([por] = 0.5 mM, [$C_{60}$] = 3.0 mM, 1-phenyloctane). (A) shows wide-spread removal of the array shortly after fullerene deposition (B) shows tunneling through the porphyrin macrocycle. The images were acquired at (A): $I$ = 8 pA, $V$ = –800 mV; (B): $I$ = 8 pA, $V$ = –600 mV.

### 5.4. Conclusions

We have synthesized a variety of new Ga(OEP)X complexes with the intention of exploring the properties that could affect templating fullerenes on the surface under ambient conditions. Of those explored in this chapter, only the Ga(OEP)(CCTh) monolayer resulted in a conclusively different structure before and after fullerene deposition. After sequential deposition of $C_{60}$ at high concentrations, widespread multilayer formation was observed. This was tentatively assigned to $C_{60}$ incorporated between two layers of porphyrins, although more advanced surface characterization techniques are needed to confirm this. When the fullerene PCBM was sequentially deposited on this monolayer, and when pre-mixed solutions of porphyrin and $C_{60}$ were deposited, more sporadic incorporation analogous to previous Ga(OEP)(CCPyr) studies was achieved.

In the case of Ga(OEP)(CCAnthr) complex, difficulties imaging the monolayer itself, due to macroscale unevenness, proved this to be an unsuitable template. Ga(OEP)(CCTrip) imaging studies following $C_{60}$ deposition were inconclusive, but the initial results were not promising; it is believed that a combination of height and sterics may be a barrier. Future work could include extending these ligands farther above the surface using a C≡C–C≡C linker or attempting to use a PAH with predicted higher affinity for $C_{60}$, such as chrysene, to potentially increase incorporation. It was hoped that changing the linker to the Ga(OEP)($O_2$CPyr) complex would provide a conformational degree of freedom that might increase $C_{60}$ affinity in the intraligand cavity. However, widespread removal of the monolayer after fullerene deposition showed this to be an unsuitable template for immediate study. Future work might be done porphyrins beyond OEP that assemble in unit cells of other dimensions in order to potentially increase the ligand interaction with the fullerene and look towards the incorporation of further nanoparticles.

**5.5. References**


1. Peréz, E. M.; Martín, N. π-π Interactions in Carbon Nanostructures. *Chem. Soc. Rev.* **2015**, *44*, 6425-6433.

2. Datta, K.; Banerjee, M.; Seal, B. K.; Mukherjee, A. K. Ground State EDA Complex Formation Between [60]Fullerene and a Series of Polynuclear Aromatic Hydrocarbons. *J. Chem. Soc., Perkin Trans. 2* **2000**, 531-534.

3. Bhattacharya, S.; Nayak, S. K.; Chattopadhyay, S.; Banerjee, M.; Mukherjee, A. K. Study of Molecular Complex Formation Between [60]Fullerene and Two Series of Donors by the NMR Method. *J. Phys. Chem. A* **2001**, *105*, 9865-9868.

4. Guldi, D. M.; Rahman, G. M. A.; Zerbetto, F.; Prato, M. Carbon Nanotubes in Electron Donor-Acceptor Nanocomposites. *Acc. Chem. Res.* **2005**, *38*, 871-878.

5. Tasis, D.; Tagmatarchis, N.; Bianco, A.; Prato, M. Chemistry of Carbon Nanotubes. *Chem. Rev.* **2006**, *106*, 1105-1136.

6. Konarev, D. V.; Drichko, N. V.; Lyubovskaya, R. N.; Shul'ga, Y. M.; Litvinov, A. L.; Semkin, V. N.; Dubitsky, Y. A.; Zaopo, A. Donor-Acceptor Interaction of Fullerene $C_{60}$ with Triptycene in Molecular Complex TPC·$C_{60}$. *J. Mol. Struc.* **2000**, *526*, 25-29.

7. Mondal, S.; Chakraborty, S.; Bhowmick, S.; Das, N. Synthesis of Triptycene-Based Organosoluble, Thermally Stable, and Fluorescent Polymers: Efficient Host Guest Complexation with Fullerene. *Macromolecules* **2013**, *46*, 6824-6831.

8. Hu, S. Z.; Chen, C. F. Triptycene-Derived Oxacalixarene with Expanded Cavity: Synthesis, Structure and Its Complexation with Fullerenes $C_{60}$ and $C_{70}$. *Chem. Commun.* **2010**, *46*, 4199-4201.

9. Shimizu, H.; Gonzalez, J. D. C.; Hasegawa, M.; Nishinaga, T.; Haque, T.; Takase, M.; Otani, H.; Rabe, J. P.; Iyoda, M. Synthesis, Structures, and Photophysical Properties of π-Expanded Oligothiophene 8-mers and Their Saturn-Like $C_{60}$ Complexes. *J. Am. Chem. Soc.* **2015**, *137*, 3877-3885.

10. Mena-Osteritz, E.; Bäuerle, P. Complexation of $C_{60}$ on a Cyclothiophene Monolayer Template. *Adv. Mater.* **2006**, *18*, 447-451.

11. MacLeod, J. M.; Ivasenko, O.; Fu, C. Y.; Taerum, T.; Rosei, F.; Perepichka, D. F. Supramolecular Ordering in Oligothiophene-Fullerene Monolayers. *J. Am. Chem. Soc.* **2009**, *131*, 16844-16850.

12. González, J. D. C.; Iyoda, M.; Rabe, J. P. Templated Bilayer Self-Assembly of Fully Conjugated π-Expanded Macrocyclic Oligothiophenes Complexed with Fullerenes. *Nat. Commun.* **2017**, *8*.

13. Pan, G. B.; Cheng, X. H.; Hoger, S.; Freyland, W. 2D Supramolecular Structures of a Shape-Persistent Macrocycle and Co-Deposition with Fullerene on HOPG. *J. Am. Chem. Soc.* **2006**, *128*, 4218-4219.

14. Piot, L.; Silly, F.; Tortech, L.; Nicolas, Y.; Blanchard, P.; Roncali, J.; Fichou, D. Long-Range Alignments of Single Fullerenes by Site-Selective Inclusion into a Double-Cavity 2D Open Network. *J. Am. Chem. Soc.* **2009**, *131*, 12864-12865.

15. Lu, L. Y.; Zheng, T. Y.; Wu, Q. H.; Schneider, A. M.; Zhao, D. L.; Yu, L. P. Recent Advances in Bulk Heterojunction Polymer Solar Cells. *Chem. Rev.* **2015**, *115*, 12666-12731.

16. Pivrikas, A.; Sariciftci, N. S.; Juška, G.; Österbacka, R. A Review of Charge Transport and Recombination in Polymer/Fullerene Organic Solar Cells. *Prog. Photovoltaics* **2007**, *15*, 677-696.

17. Zhao, X. Y.; Piliego, C.; Kim, B.; Poulsen, D. A.; Ma, B. W.; Unruh, D. A.; Frechet, J. M. J. Solution-Processable Crystalline Platinum-Acetylide Oligomers with Broadband Absorption for Photovoltaic Cells. *Chem. Mater.* **2010**, *22*, 2325-2332.

18. Segura, J. L.; Martin, N. New Concepts in Tetrathiafulvalene Chemistry. *Angew. Chem., Int. Ed.* **2001**, *40*, 1372-1409.

19. Kaleta, J.; Kaletova, E.; Cisarova, I.; Teat, S. J.; Michl, J. Synthesis of Triptycene-Based Molecular Rotors for Langmuir-Blodgett Monolayers. *J. Org. Chem.* **2015**, *80*, 10134-10150.

20. Keller, S.; Yi, C. Y.; Li, C.; Liu, S.-X.; Blum, C.; Frei, G.; Sereda, O.; Neels, A.; Wandlowski, T.; Decurtins, S. Synthesis, Structures, Redox and Photophysical Properties of Benzodifuran-Functionalised Pyrene and Anthracene Fluorophores. *Org. Biomol. Chem.* **2011**, *9*, 6410-6416.

21. Lau, W.-Y. Ph. D. Thesis. The University of Chicago, Chicago, IL, 2016.

22. Ogunrinde, A.; Hipps, K. W.; Scudiero, L. A Scanning Tunneling Microscopy Study of Self-Assembled Nickel(II) Octaethylporphyrin Deposited from Solutions on HOPG. *Langmuir* **2006**, *22*, 5697-5701.

23. Scudiero, L.; Barlow, D. E.; Hipps, K. W. Scanning Tunneling Microscopy, Orbital-Mediated Tunneling Spectroscopy, and Ultraviolet Photoelectron Spectroscopy of Nickel(II) Octaethylporphyrin Deposited from Vapor. *J. Phys. Chem. B* **2002**, *106*, 996-1003.

24. Petsalakis, I. D.; Theodorakopoulos, G. Molecular Orbital Assistance in the Design of Intramolecular and Photoinduced Electron Transfer Systems. *Chem. Phys. Lett.* **2012**, *525-26*, 105-109.

25. Stevens, F.; Buehner, D.; Beebe, T. P. Ordering of Adsorbed Organic Monolayers Confined in Molecule Corrals During Scanning Tunneling Microscopy Observation. *J. Phys. Chem. B* **1997**, *101*, 6491-6496.

26. Cortez, M. L.; Ceolin, M.; Azzaroni, O.; Battaglini, F. Electrochemical Sensing Platform Based on Polyelectrolyte-Surfactant Supramolecular Assemblies Incorporating Carbon Nanotubes. *Anal. Chem.* **2011**, *83*, 8011-8018.

27. Li, Y.; Auras, F.; Lobermann, F.; Doblinger, M.; Schuster, J.; Peter, L.; Trauner, D.; Bein, T. A Photoactive Porphyrin-Based Periodic Mesoporous Organosilica Thin Film. *J. Am. Chem. Soc.* **2013**, *135*, 18513-18519.

28. Boyd, P. D. W.; Reed, C. A. Fullerene-porphyrin constructs. *Accounts of Chemical Research* **2005**, *38*, 235-242.

29. Tashiro, K.; Aida, T. Metalloporphyrin Hosts for Supramolecular Chemistry of Fullerenes. *Chem. Soc. Rev.* **2007**, *36*, 189-197.

30. Olmstead, M. M.; Costa, D. A.; Maitra, K.; Noll, B. C.; Phillips, S. L.; Van Calcar, P. M.; Balch, A. L. Interaction of curved and flat molecular surfaces. The structures of crystalline compounds composed of fullerene (C-60, C60O, C-70, and C120O) and metal octaethylporphyrin units. *Journal of the American Chemical Society* **1999**, *121*, 7090-7097.

31. Ishii, T.; Aizawa, N.; Kanehama, R.; Yamashita, M.; Sugiura, K. I.; Miyasaka, H. Cocrystallites consisting of metal macrocycles with fullerenes. *Coordination Chemistry Reviews* **2002**, *226*, 113-124.

32. Sun, D. Y.; Tham, F. S.; Reed, C. A.; Chaker, L.; Burgess, M.; Boyd, P. D. W. Porphyrin-Fullerene Host-Guest Chemistry. *J. Am. Chem. Soc.* **2000**, *122*, 10704-10705.

33. Boyd, P. D. W.; Hodgson, M. C.; Rickard, C. E. F.; Oliver, A. G.; Chaker, L.; Brothers, P. J.; Bolskar, R. D.; Tham, F. S.; Reed, C. A. Selective Supramolecular Porphyrin/Fullerene Interactions. *J. Am. Chem. Soc.* **1999**, *121*, 10487-10495.

34. Park, J. H.; Ravavar, L.; Kwak, I.; Fullerton-Shirey, S. K.; Choudhury, P.; Kummel, A. C. Growth Mode Transition from Monolayer by Monolayer to Bilayer by Bilayer in Molecularly Flat Titanyl Phthalocyanine Film. *J. Phys. Chem. C* **2017**, *121*, 6721-6728.

35. Mazur, U.; Hipps, K. W.; Riechers, S. L. Organization of Vanadyl and Metal-Free Tetraphenoxyphthalocyanine Complexes on Highly Oriented Pyrolytic Graphite in the Presence of Paraffinic Solvents: A STM Study. *J. Phys. Chem. C* **2008**, *112*, 20347-20356.

36. Semba, K.; Fujihara, T.; Xu, T. H.; Terao, J.; Tsuji, Y. Copper-Catalyzed Highly Selective Semihydrogenation of Non-Polar Carbon-Carbon Multiple Bonds using a Silane and an Alcohol. *Adv. Synth. Catal.* **2012**, *354*, 1542-1550.

# CHAPTER 6

## Supplementary Information

### 6.1. Chapter 2 Supplementary Information

**6.1.1. General Procedures.** Synthetic procedures were performed under a purified nitrogen atmosphere using standard Schlenk and glovebox techniques. Solvents (HPLC-grade, stored under nitrogen) were purified by passing them under nitrogen pressure through an anaerobic, stainless-steel system consisting of either two 4.5 in. × 24 in. (1 gal) columns of activated A2 alumina (THF) or one column of activated A2 alumina and one column of activated BASF R3-11 catalyst (toluene, pentane).[1] THF-$d_8$ was stored over NaK (1:2) alloy, from which it was transferred under vacuum. $C_6D_6$ and $CDCl_3$ were stored over 4Å molecular sieves under nitrogen. The compounds Ga(OEP)Cl[2] and LiCCPh[3] were synthesized according to standard procedures. Other chemicals were obtained from commercial sources and used as received. $^1$H, $^{13}$C, and $^{19}$F NMR spectra were recorded at room temperature using a Bruker DMX 500 or DRX 400 MHz NMR spectrometer. Chemical shifts were measured relative to solvent resonances ($^1$H, $^{13}$C)[4] or $CFCl_3$ ($^{19}$F). Laser-desorption-ionization mass spectra were obtained using a Bruker UltrafleXtreme MALDI-TOF/TOF mass spectrometer on samples deposited without a matrix; the Bruker peptide calibration standard II (750–3150 Da) was used as the calibrant. Electronic-absorption spectra were recorded in quartz cuvettes using a Cary 300 UV-visible spectrophotometer. Elemental analysis was performed by Robertson Microlit Laboratories (Ledgewood, NJ).

**6.1.2. Density Functional Theory (DFT) Calculations.** Calculations were performed using Gaussian09.[5] The minimum-energy structures of Ga(OEP)X complexes were determined in calculations without symmetry constraints (Table 2.1). No imaginary frequencies were obtained in subsequent vibrational calculations, confirming that the optimized structures reside at

potential-surface minima. A benchmarking study of common functionals (B3LYP, BP86, B3PW91, and B3P86) was performed in which calculated bond distances and angles of Ga(OEP)Cl were compared to those from the crystal structure;[6] the hybrid density functional B3P86[7,8] provided the geometry in best agreement with experiment (Table 6.1). All calculations overestimated the Ga–N bond lengths by 0.02–0.03 Å, most likely due to intrinsic differences between calculated gas-phase equilibrium bond lengths and those determined via single-crystal X-ray diffraction methods. This interpretation is supported by the fact that the gas-phase structure of Sn(octamethylporphyrin) determined by electron diffraction[9] exhibits Sn–N bond distances that are ca. 0.02 Å longer than those observed in the X-ray crystal structure of Sn(OEP).[10]

**Table 6.1.** Dependence of Calculated Bond Distances (Å) and Angles (°) for Ga(OEP)Cl on Density Functional.[a]

| | | density functional | | | |
|---|---|---|---|---|---|
| nuclei | exptl.[b] | B3P86[7, 8] | B3LYP[7, 11-13] | BP86[8, 14] | B3PW91[7, 14] |
| Ga–Cl | 2.2397(13) | 2.2356 | 2.2488 | 2.2509 | 2.2397 |
| Ga–N(1) | 2.033(4) | 2.057 | 2.065 | 2.077 | 2.062 |
| Ga–N(2) | 2.030(4) | 2.057 | 2.065 | 2.077 | 2.062 |
| Ga–N(3) | 2.038(4) | 2.057 | 2.065 | 2.077 | 2.062 |
| Ga–N(4) | 2.037(4) | 2.057 | 2.065 | 2.077 | 2.062 |
| N(1)–Ga–X | 102.2(1) | 102.6 | 102.6 | 102.8 | 102.6 |
| N(2)–Ga–X | 100.9(1) | 102.6 | 102.7 | 102.8 | 102.6 |
| N(3)–Ga–X | 101.3(1) | 102.6 | 102.7 | 102.9 | 102.7 |
| N(4)–Ga–X | 100.8(1) | 102.7 | 102.7 | 102.8 | 102.7 |

[a] Calculations were carried out using the LANL2DZ effective core potential basis set for Ga[15] and the 6-31G* basis set for all other atoms. [b] Crystal structure.[6]

For the final calculations on Ga(OEP)X compounds, the cc-pVTZ basis set[16-18] was used for all atoms except iodine, for which the cc-pVTZ-PP basis set with corresponding effective core

potential (ECP) was used.[19] For all complexes, the minimum-energy geometry is that in which the eight peripheral methyl groups lie on the opposite side of the OEP plane from the X ligand. Calculations were also performed on rotamers in which all eight peripheral methyl groups are oriented on the same side of the OEP plane as the X ligand; $C_{4v}$ symmetry was enforced for X = Cl, Br, I, while for X = CCPh, $O_3SCF_3$ the calculations were not symmetry restricted but converged in local minima.

**6.1.3. Scanning Tunneling Microscopy (STM) Sample Preparation.** HOPG wafers (SPI-2 grade, SPI Supplies) measuring 7 mm × 7 mm × 1 mm were mounted to 12 mm diameter metal specimen discs with colloidal silver paste (PELCO, Ted Pella, Inc.). The surface of the HOPG substrate was cleaved with adhesive tape immediately prior to dosing. Stock solutions in toluene at a concentration of 0.25 mM were prepared for each compound. Prior to each STM experiment, an appropriate volume of the toluene solution was reduced to dryness under vacuum and the material re-dissolved in 1-phenyloctane to give solutions of either 0.25 mM or 0.5 mM. One drop of a 1-phenyloctane solution of the porphyrin compound was deposited onto the surface. The complexes Ga(OEP)Cl, Ga(OEP)Br, Ga(OEP)I, and Ga(OEP)(CCPh) were studied at concentrations of both 0.25 mM and 0.5 mM; Ga(OEP)($O_3SCF_3$) was studied only at 0.25 mM because it is not sufficiently soluble in 1-phenyloctane to form the higher-concentration solution. The concentration employed for Ni(OEP) was 0.5 mM. The tip was then directly engaged through the drop and the compound imaged at the solid–liquid interface. All compounds are stable in solution for the duration of the STM measurements; $^1$H-NMR spectra of the compounds in $C_6D_6$ solution under air show no changes over at least 3 days.

**6.1.4. Scanning Tunneling Microscopy (STM) Measurements.** STM images were acquired using a Digital Instruments Nanoscope IIIa standalone STM. Tips were mechanically cut from

$Pt_{0.8}Ir_{0.2}$ wire (Goodfellow). All measurements were taken at room temperature in constant-current mode. For each sample, an image of the underlying graphite surface was acquired. The data for the porphyrin overlayers were corrected post-acquisition for instrument drift in the SPIP software package[20] using the graphite lattice parameters as a reference. Data analysis was performed using WSxM 5.0 software.[21] Images were flattened and low-pass filtered, and sharpened by adjusting the contrast. Reported lattice parameters are averages of those determined from consecutive up- and down-scan images. For each of these images, the unit-cell distances were determined from the average distances of 100 sets of five consecutive porphyrin molecules (see Figure 6.1), and the unit-cell angle was the average of 40 measurements.

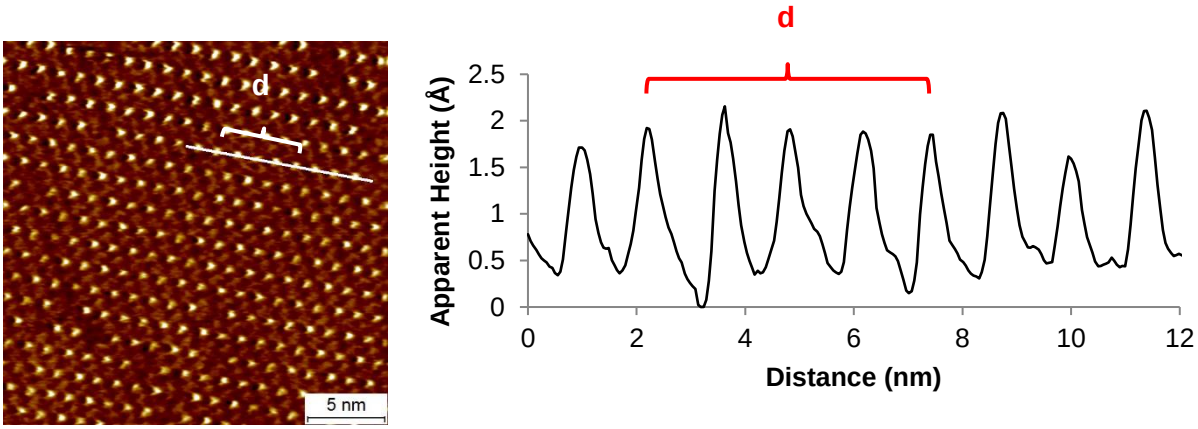


**Figure 6.1**. STM image of Ga(OEP)Br with cross-sectional height profile. One unit cell measurement is given by d/4. 100 such measurements are recorded for an image and its consecutive up- or down-scan counterpart. The average of these is the reported unit cell distance.

### 6.1.5. Synthesis and Characterization of Ga(OEP)X Compounds.

**Preparation of Ga(OEP)($O_3SCF_3$).** The preparation of this compound by a different route has been reported previously.[22] Trimethylsilyl triflate (37.0 μL, 0.204 mmol) was added to a stirred, dark pink solution of Ga(OEP)Cl (0.050 g, 0.079 mmol) in toluene (20 mL) at room temperature. The reaction mixture was stirred for 24 h; the color of the solution was not observed to change. The volatile components were removed under vacuum, yielding a dark pink powder. The $^1H$

NMR spectrum of the crude product indicated the presence of unreacted Ga(OEP)Cl (< 2%), so the solid was dissolved in toluene (20 mL) and allowed to react with additional $SiMe_3(O_3SCF_3)$ (37.0 μL, 0.204 mmol) with stirring at room temperature for 24 h. The solvent was removed under vacuum to yield the product as a dark pink powder that was pure by $^1$H NMR spectroscopy (0.052 g, 88% yield). $^1$H NMR data recorded using $CDCl_3$ as a solvent were in agreement with previously reported results.[22] $^1$H NMR ($C_6D_6$, 400.13 MHz; Figure 6.6): δ 10.44 (s, 4 H, *meso* H), 3.96 (complex m, 16 H, C<u>H</u>$_2$CH$_3$), 1.82 (t, 24 H, CH$_2$C<u>H</u>$_3$). $^{19}$F NMR ($C_6D_6$, 470.59 MHz): δ -80.36 (s). LDI-TOF MS: *m/z* $[M]^+$ = 750.239, predicted = 750.234; $[M–O_3SCF_3]^+$ = 601.291. UV-vis (toluene; Table 6.2 and Figure 6.9): 329, 379, 399, 496, 531, 569 nm.

**Preparation of Ga(OEP)Br.** This compound has been previously reported, but synthetic details and characterization data were not provided.[23] Bromotrimethylsilane (17.0 μL, 0.129 mmol) was added to a stirred, dark pink solution of Ga(OEP)Cl (0.042 g, 0.066 mmol) in toluene (20 mL) at room temperature. The reaction mixture was observed to turn dark purple and cloudy within 2 h; after 24 h the volatile components were removed under vacuum to yield a dark pink powder. The $^1$H NMR spectrum of the crude product indicated the presence of unreacted Ga(OEP)Cl (< 5%), so the solid was dissolved in toluene (20 mL) and allowed to react with additional $SiMe_3Br$ (30.0 μL, 0.228 mmol) with stirring at room temperature for 24 h. The solvent was removed under vacuum to yield the product as a dark pink powder that was pure by $^1$H NMR spectroscopy (0.034 g, 75% yield). $^1$H NMR ($C_6D_6$, 400.13 MHz, Figure 6.3): δ 10.41 (s, 4 H, *meso* H), 3.96 (complex m, 16 H, C<u>H</u>$_2$CH$_3$), 1.82 (t, 24 H, CH$_2$C<u>H</u>$_3$). $^{13}$C{$^1$H} NMR ($C_6D_6$, 125.77 MHz, Figure 6.4): δ 146.62 (*α*), 142.74 (*β*), 97.60 (*meso*), 20.18 (<u>C</u>H$_2$CH$_3$), 18.60 (CH$_2$<u>C</u>H$_3$). LDI-TOF MS: *m/z* $[M]^+$ = 680.224, predicted = 680.201; $[M–Br]^+$ = 601.299. UV-vis

(toluene; Table 6.2 and Figure 6.9): 340, 388, 409, 499, 538, 575 nm. Anal. Calcd. for $C_{36}H_{44}N_4GaBr$: C, 63.36; H, 6.50; N, 8.21. Found: C, 63.38; H, 6.55; N, 8.08.

**Preparation of Ga(OEP)I.** The preparation of this compound by a different synthetic route has been reported previously.[2] Iodotrimethylsilane (50.0 μL, 0.351 mmol) was added to a stirred solution of Ga(OEP)Cl (0.045 g, 0.071 mmol) in toluene (20 mL) at room temperature. After several minutes, the dark pink solution was observed to have turned dark purple and cloudy. The reaction mixture was stirred for 24 h, after which the volatile components were removed under vacuum to yield a dark pink powder. The $^1$H NMR spectrum of the crude product indicated the presence of unreacted Ga(OEP)Cl (< 2%), so the solid was dissolved in toluene (20 mL) and allowed to react with additional $SiMe_3I$ (50.0 μL, 0.351 mmol) with stirring at room temperature for 24 h. The solvent was removed under vacuum to yield the product as a dark pink powder that was pure by $^1$H NMR spectroscopy (0.047 g, 91% yield). $^1$H NMR data recorded using $CDCl_3$ as a solvent were in agreement with previously reported results.[2] $^1$H NMR ($C_6D_6$, 500.13 MHz, Figure 6.5): δ 10.44 (s, 4 H, *meso* H), 3.96 (complex m, 16 H, $C\underline{H}_2CH_3$), 1.82 (t, 24 H, $CH_2C\underline{H}_3$). LDI-TOF MS: *m/z* $[M]^+$ = 728.127, predicted = 728.187; $[M\text{-}I]^+$ = 601.376. UV-vis (toluene; Table 6.2 and Figure 6.9): 351, 396, 416, 501, 540, 577 nm.

**Preparation of Ga(OEP)(CCPh).** NMR, IR, and electronic-absorption spectroscopic data have been reported for this compound,[24, 25] but a detailed synthetic procedure has not been described. To a stirred solution of Ga(OEP)Cl (0.065 g, 0.102 mmol) in THF (25 mL) at room temperature was added a solution of LiCCPh (0.015 g 0.138 mmol) in THF (1 mL). The color of the reaction mixture changed immediately from dark pink to dark purple and a translucent white precipitate formed. After 2 h the volatile components were removed under vacuum, the remaining solid was extracted into toluene, and the solution was filtered through Celite. Removal

of the solvent under vacuum provided the product as a purple powder that was pure by $^{1}$H NMR spectroscopy (0.056 g, 0.079 mmol, 78% yield). $^{1}$H NMR ($C_6D_6$, 500.13 MHz, Figures 6.7): δ 10.39 (s, 4 H, *meso* H), 6.00 (t, 1 H, *p*-$C_6H_5$), 5.81 (t, 2 H, *m*-$C_6H_5$), 5.32 (dd, 2 H, *o*-$C_6H_5$), 3.99 (complex m, 16 H, C<u>H</u>$_2$CH$_3$), 1.84 (t, 24 H, CH$_2$C<u>H</u>$_3$). $^{13}$C{$^{1}$H} NMR (THF-$d_8$, 125.76 MHz, Figure 6.8): δ 146.90 (*α*), 142.97 (*β*), 130.66 (*o*-$C_6H_5$), 126.96 (*m*-$C_6H_5$), 125.70 (*p*-$C_6H_5$), 124.80 (*ipso*-$C_6H_5$), 97.39 (*meso*), 94.72 (Ga<u>CC</u>Ph), 20.31 (<u>C</u>H$_2$CH$_3$), 18.72 (CH$_2$<u>C</u>H$_3$), one Ga<u>CC</u>Ph resonance not observed. LDI-TOF MS: *m/z* [M]$^+$ = 702.296, predicted = 702.321; [M–CCPh]$^+$ = 601.231. UV-vis (toluene; Table 6.2 and Figure 6.9): 340, 392, 413, 504, 543, 580 nm. The $^{1}$H NMR chemical shifts for samples prepared by this method differ from those reported previously by up to 0.5 ppm, and the electronic-absorption band maxima differ in wavelength by up to 10 nm (Table S2).[24] That the present data are attributable to the compound is established by the LDI-TOF-MS data.

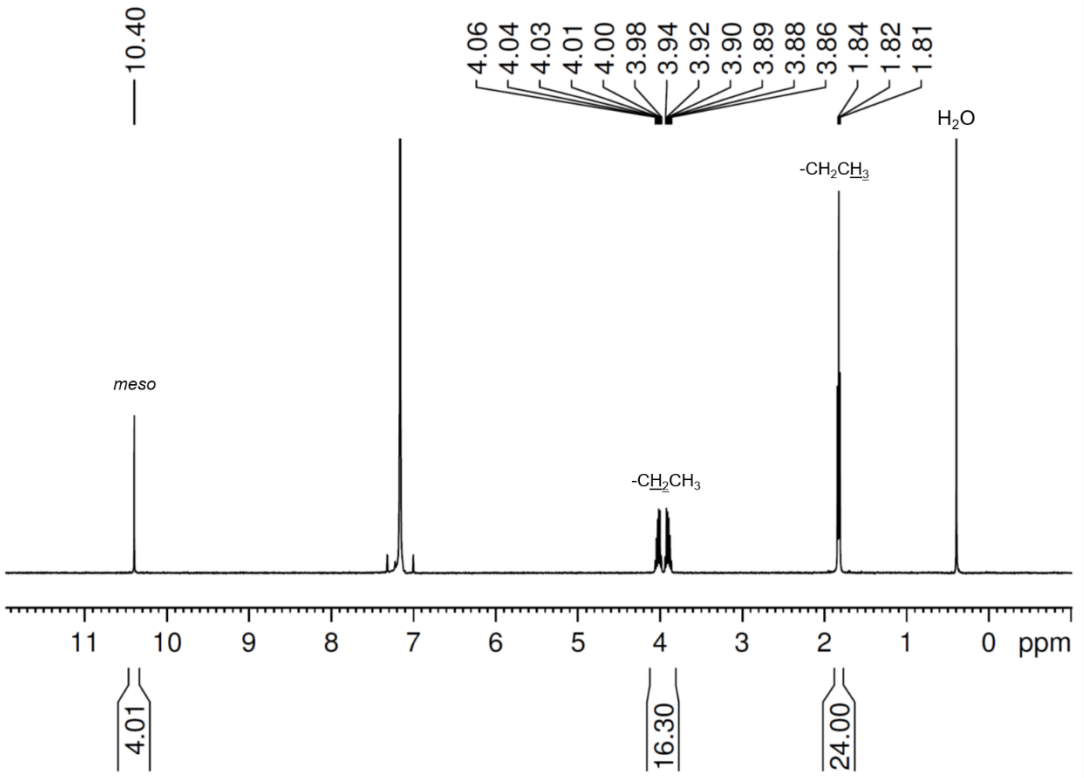


**Figure 6.2.** $^{1}$H NMR spectrum of Ga(OEP)Cl in $C_6D_6$.

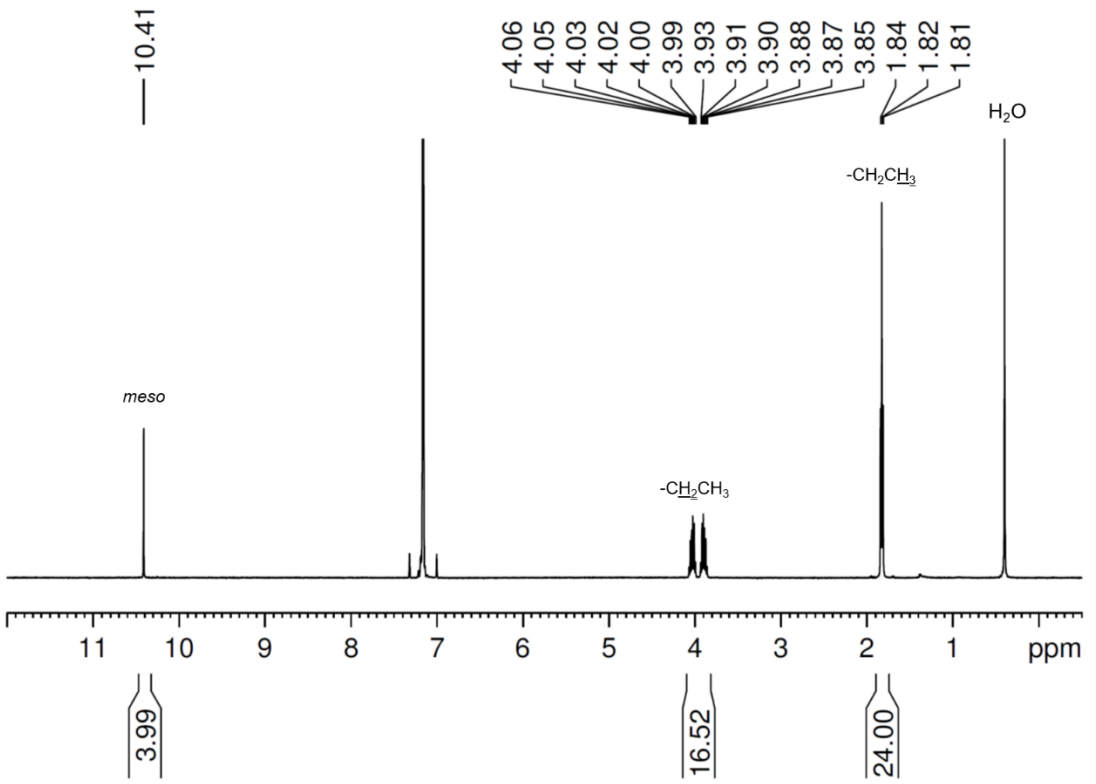


**Figure 6.3.** $^{1}$H NMR spectrum of Ga(OEP)Br in $C_6D_6$.

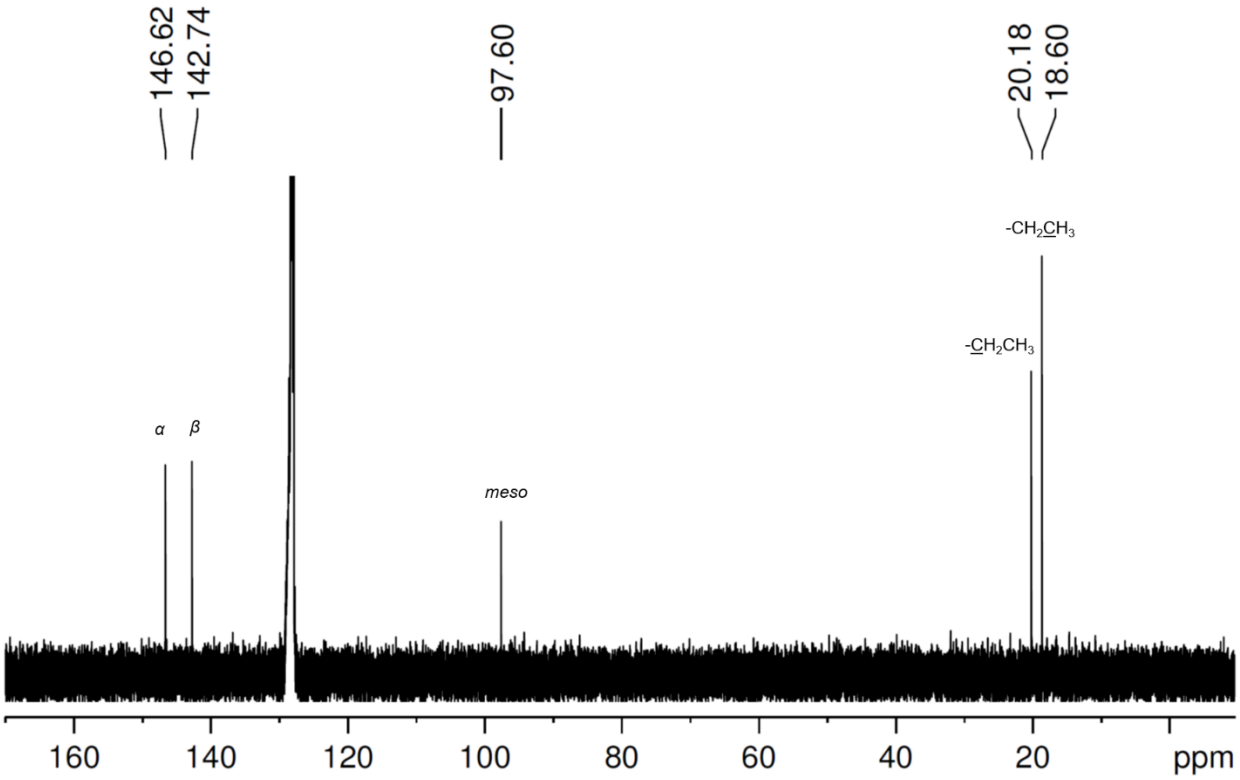


**Figure 6.4.** $^{13}$C{$^{1}$H} NMR spectrum of Ga(OEP)Br in $C_6D_6$.

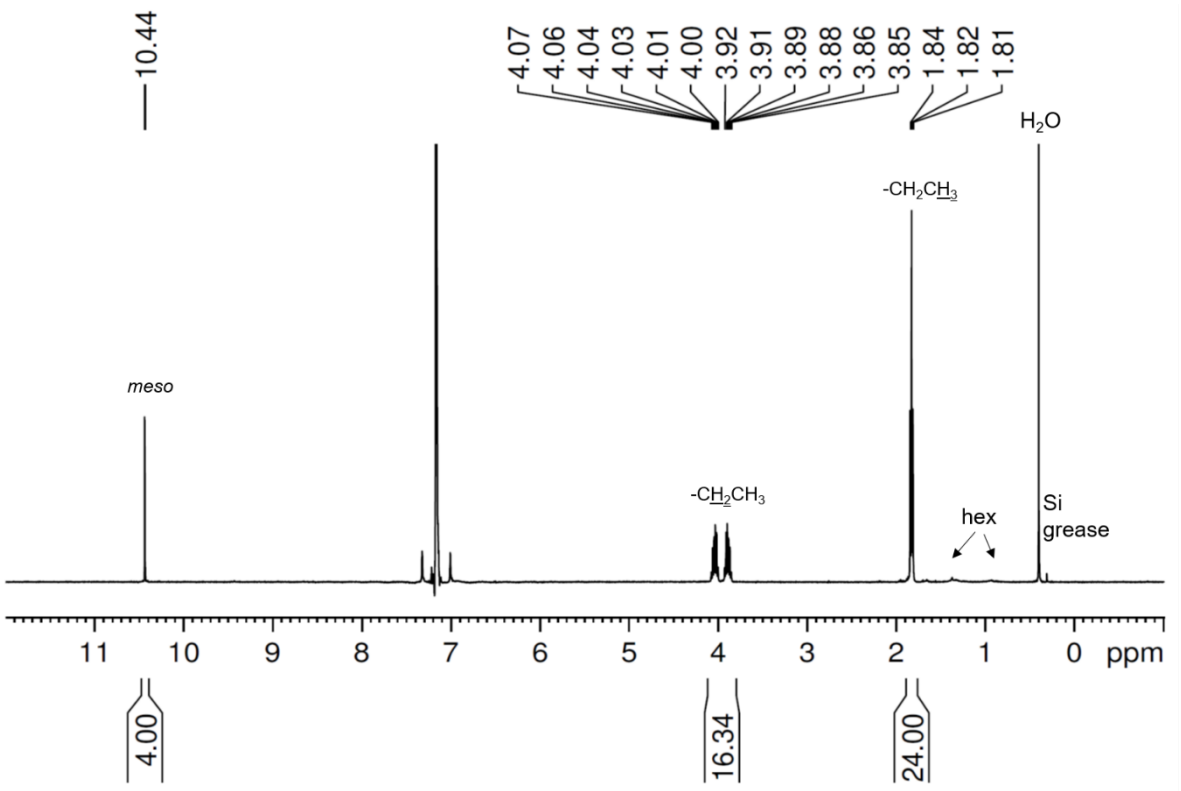


**Figure 6.5.** $^{1}$H NMR spectrum of Ga(OEP)I in $C_6D_6$.

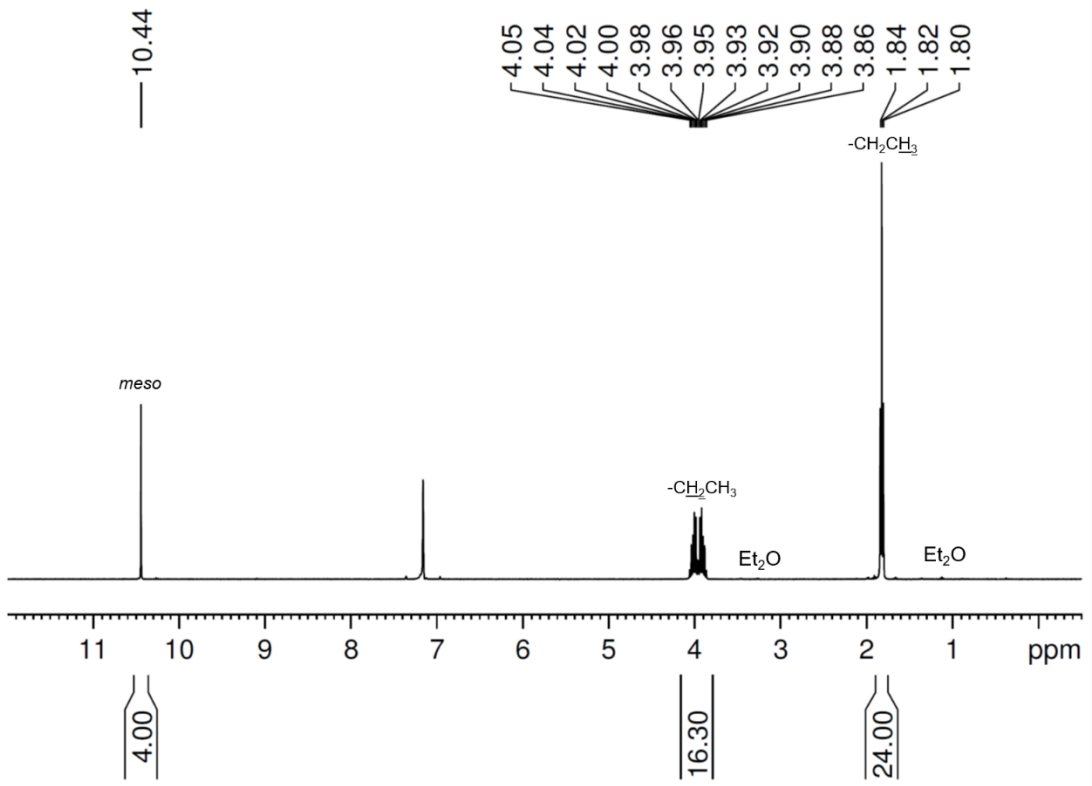


**Figure 6.6.** $^{1}$H NMR spectrum of Ga(OEP)($O_3SCF_3$) in $C_6D_6$.

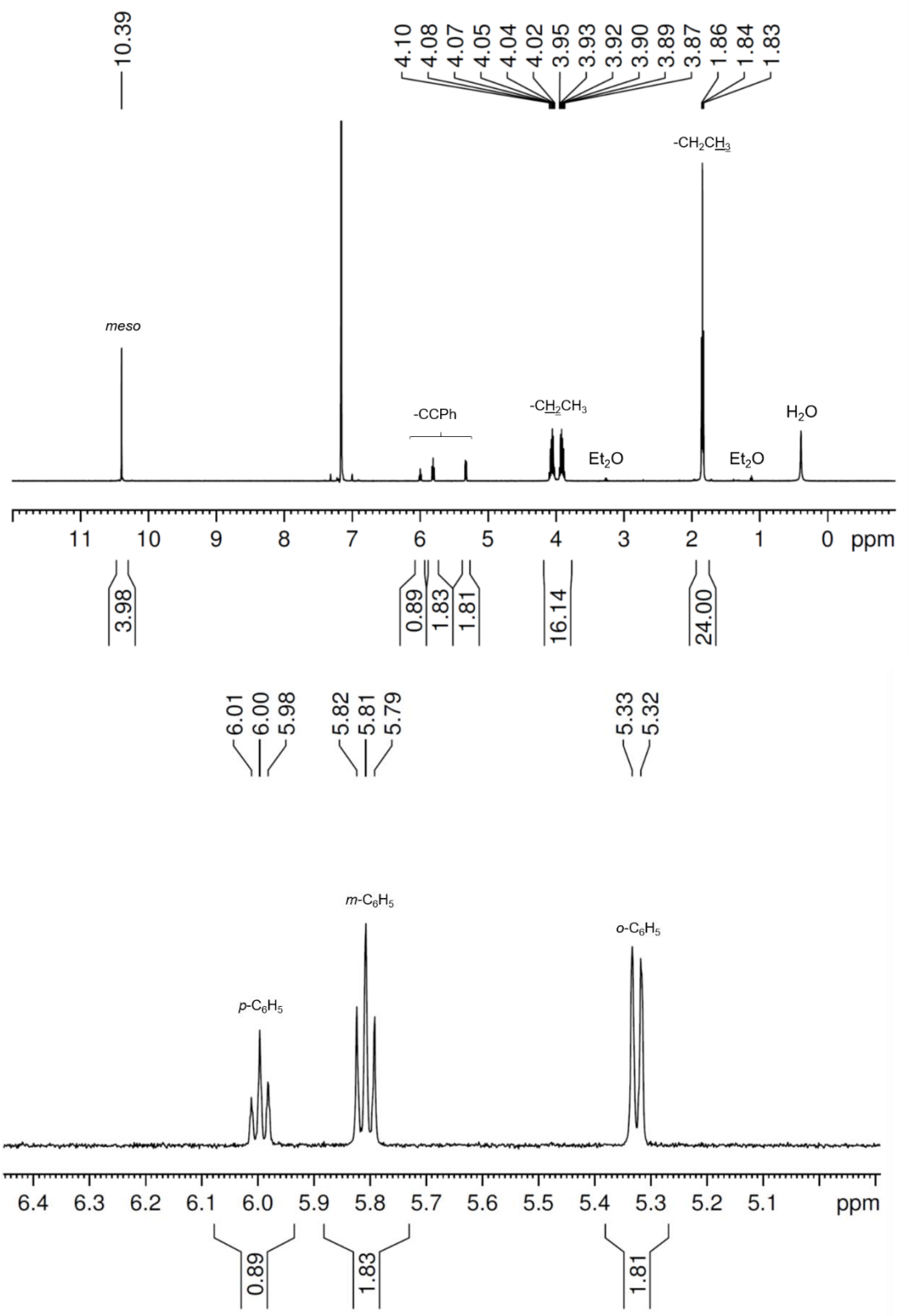


**Figure 6.7.** $^{1}H$ NMR spectrum of Ga(OEP)(CCPh) in $C_6D_6$. The bottom spectrum is an expansion of the top spectrum.

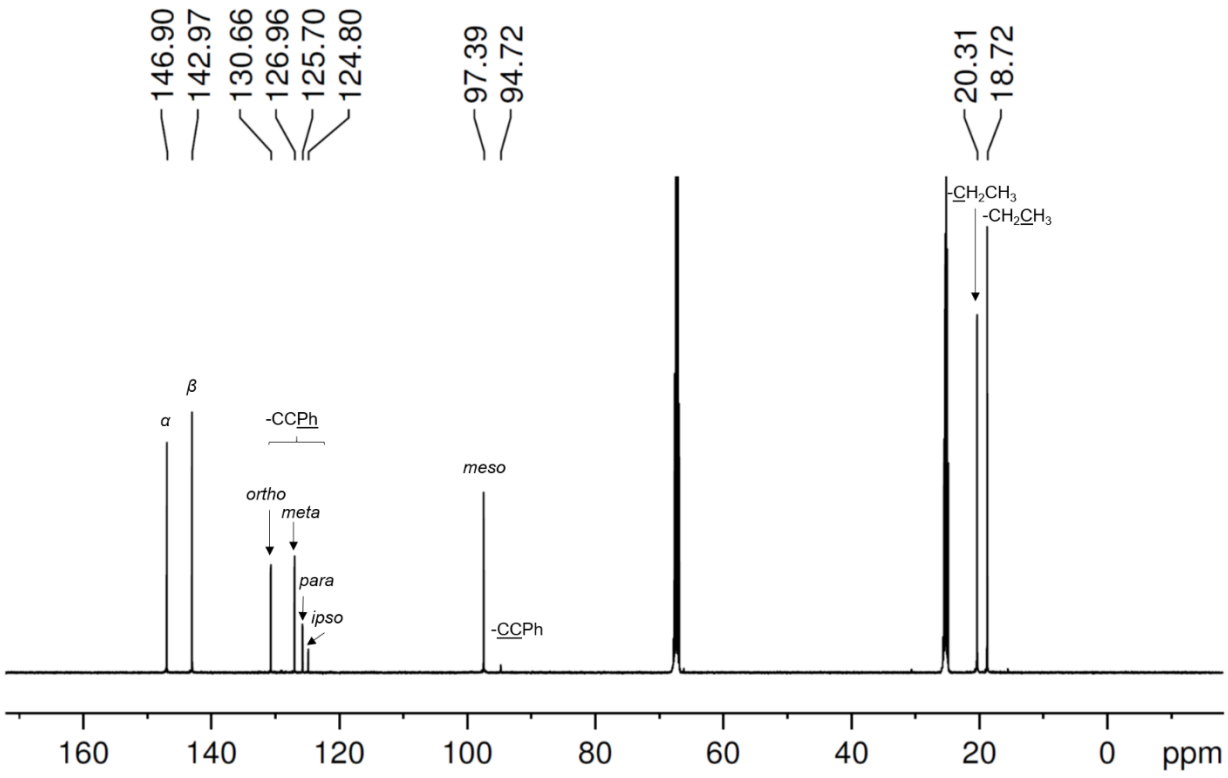


**Figure 6.8.** $^{13}C\{^{1}H\}$ NMR spectrum of Ga(OEP)(CCPh) in THF-$d_8$.

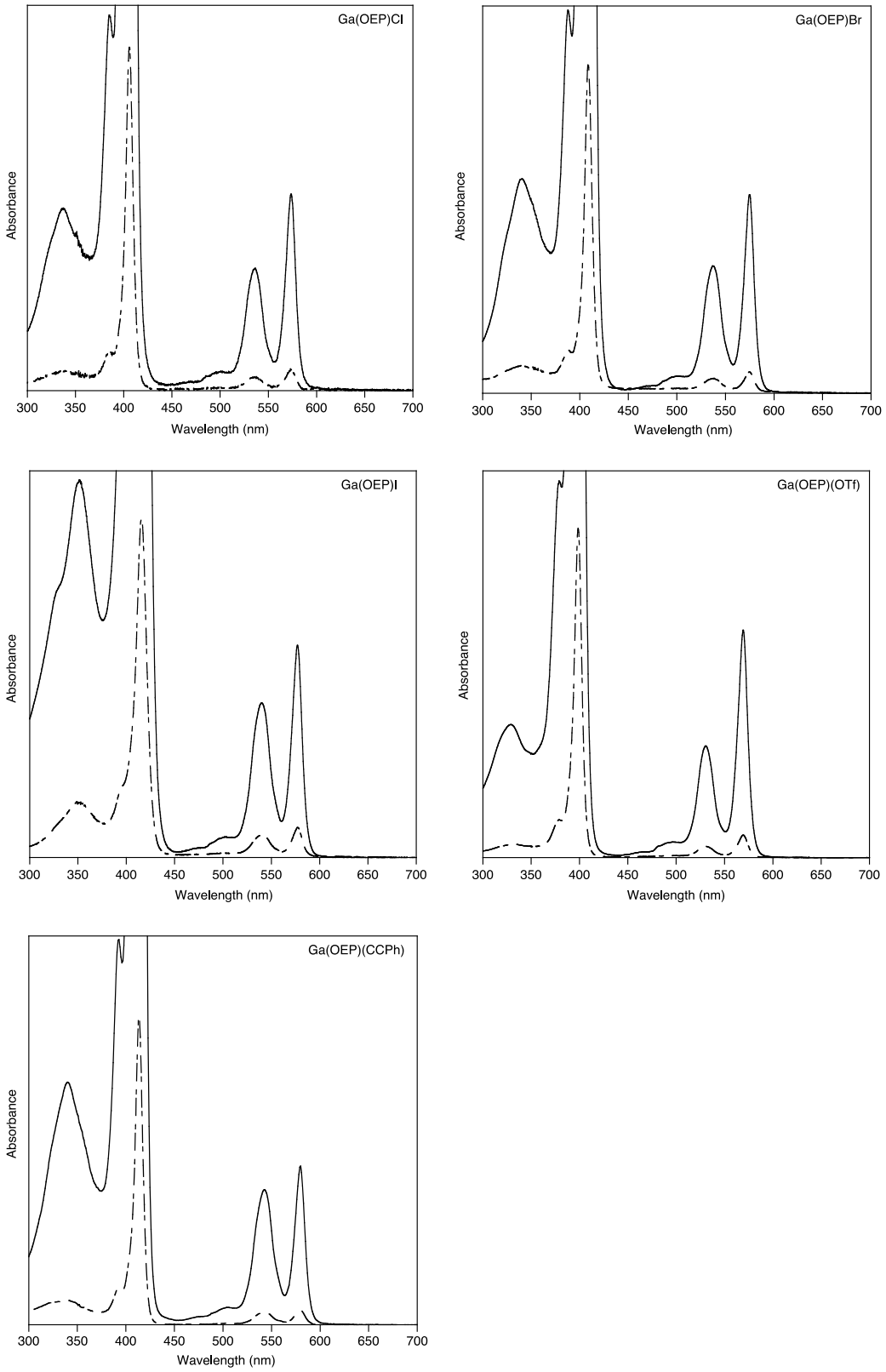


**Figure 6.9.** Electronic-absorption spectra of Ga(OEP)X complexes in toluene solution at room temperature.

**Table 6.2.** Electronic-Absorption Band Maxima (nm) and Relative Intensities of Ga(OEP)X Compounds in Toluene.

| X | λ, nm (rel. int.) |
|---|---|
| Cl | 338 (5.5), 386 (11.3), 406 (100), 500 (0.6), 536 (3.7), 573 (5.9) |
| | lit: 377, 400, 492, 530, 567 (benzene)[24] |
| Br | 340 (6.8), 388 (12.0), 409 (100), 499 (0.6), 538 (4.0), 575 (6.3) |
| | lit: not reported |
| I | 351 (15.7), 396 (20.8), 416 (100), 501 (0.9), 540 (6.4), 577 (8.8) |
| | lit: 377, 397, 489, 529, 567 (methanol)[2] |
| $O_3SCF_3$ | 329 (4.1), 379 (11.5), 399 (100), 496 (0.5), 531 (3.4), 569 (7.0) |
| | lit: 334, 385, 405, 492, 533, 572 (benzene)[22] |
| CCPh | 340 (7.6), 392 (11.9), 413 (100), 504 (0.5), 543 (4.3), 580 (5.0) |
| | lit: 334, 402, 492, 532, 572 (benzene)[24] |

[a] Kadish, K. M.; Boisselier-Cocolios, B.; Coutsolelos, A.; Mitaine, P.; Guilard, R. *Inorg. Chem.* **1985**, *24*, 4521–4528. [b] Coutsolelos, A.; Guilard, R.; Bayeul, D.; Lecomte, C. *Polyhedron* **1986**, *5*, 1157–1164. [c] Boukhris, A.; Lecomte, C.; Coutsolelos, A.; Guilard, R. *J. Organomet. Chem.* **1986**, *303*, 151–165.

**Table 6.3.** Out-of-Plane Displacements (Å) of Selected Ga(OEP)X Nuclei Calculated by Density Functional Theory.

| X;$CH_3$ orientation[a] | Ga–$C_{20}N_4$ plane[b] | Ga–$N_4$ plane[c] | Ga–$C_{20}$ plane[d] | $N_4$–$C_{20}$ plane[e] |
|---|---|---|---|---|
| Cl; $CH_3$ away | 0.473 | 0.445 | 0.479 | 0.034 |
| Cl; $CH_3$ toward | 0.493 | 0.440 | 0.504 | 0.064 |
| Cl, difference | 0.020 | –0.005 | 0.025 | 0.030 |
| Br, $CH_3$ away | 0.472 | 0.446 | 0.477 | 0.030 |
| Br, $CH_3$ toward | 0.491 | 0.442 | 0.501 | 0.059 |
| Br, difference | 0.019 | –0.004 | 0.024 | 0.029 |
| I; $CH_3$ away | 0.474 | 0.452 | 0.478 | 0.026 |
| I; $CH_3$ toward | 0.483 | 0.447 | 0.490 | 0.043 |
| I, difference | 0.009 | –0.005 | 0.012 | 0.017 |
| CCPh; $CH_3$ away | 0.536 | 0.495 | 0.544 | 0.048 |
| CCPh: $CH_3$ toward | 0.564 | 0.494 | 0.578 | 0.083 |
| CCPh, difference | 0.028 | –0.001 | 0.034 | 0.035 |
| OTf; $CH_3$ away | 0.349 | 0.336 | 0.352 | 0.017 |
| OTf; $CH_3$ toward | 0.382 | 0.340 | 0.389 | 0.049 |
| OTf, difference | 0.033 | 0.004 | 0.037 | 0.032 |

[a] $CH_3$ orientation: "away" = opposite side of OEP plane from X; "toward" = same side of OEP plan as X. [b] Distance between Ga and the least-squares plane of the OEP $C_{20}N_4$ macrocycle. [c] Distance between Ga and the least-squares plane defined by the four N atoms. [d] Distance between Ga and the least-squares plane defined by the OEP $C_{20}$ ring. [e] Average distance between the four N atoms and the least-squares plane defined by the OEP $C_{20}$ ring.

## 6.2. Chapter 3 Supplementary Information

**6.2.1. General Procedures.** The general methods can be found in Section 6.1.1 with the following adaptations. All syntheses were performed using standard Schlenk and glovebox techniques with the exception of Ga(OEP)(OH). The axial ligand 5-(4-ethynylphenyl)-10,15,20-triphenylporphyrinatozinc(II) (HCCZnTPP) was prepared by former lab member Nathan La Porte by a one-pot preparation of the 5-[4-(3-methyl-3-hydroxy-1-butyn-1-yl)phenyl]-10,15,20-triphenylporphyrin precursor, followed by metalation and deprotection.[26]

**6.2.2. Density Functional Theory (DFT) Calculations.** Density functional theory calculations were performed as described in Section 6.1.2. The B3P86 functional[7, 8] was used for all calculations. For gas-phase optimized geometries of Ga(OEP)(OH), Ga(OEP)(CCFc), and Ga(OEP)($O_2$CFc), the cc-pVTZ basis set[16, 18, 27] was employed for all atoms. For the Ga(OEP)(CCZnTPP) gas-phase optimized structure, and for structures optimized in local minima with the ethyl chains rotated toward the axial ligand, the 6-31G* (H, C, N, O) and LANL2DZ effective core potential basis sets[15, 28] (Ga, Fe, Zn) were employed. Molecular models were constructed using the Materials Studio software.[29]

**6.2.3. Scanning Tunneling Microscopy (STM) Sample Preparation.** STM samples were prepared as described is Section 6.1.3. Samples of Ga(OEP)(OH), Ga(OEP)(CCFc), and Ga(OEP)($O_2$CFc) in 1-phenyloctane were studied at a concentration of 0.5 mM and Ga(OEP)(CCZnTPP) was prepared to give an effective concentration of ~0.5 mM of the target porphyrin in solution, based on approximation of its purity from $^1$H NMR integration. Post-deposition modification experiments were performed by depositing a drop of 0.5 mM Ga(OEP)(OH) 1-phenyloctane solution and imaging at the solid-liquid interface. The STM tip was disengaged, and one drop of approximately the same volume of a 0.5 mM solution of ferrocenecarboxylic acid in 1-phenyloctane was added. The tip was re-engaged and the resulting assembly imaged.

**6.2.4. Scanning Tunneling Microscopy (STM) Measurements.** STM measurements were carried out as described in Section 6.1.4.

**6.2.5. Synthesis and Characterization of Ga(OEP)L Complexes.**

**Preparation of lithium ethynylferrocene.** This procedure is a modification of one previously reported.[30] To a stirred, bright orange solution of ethynylferrocene (0.151 g, 0.719

mmol) in pentane (10 mL) at room temperature was added a solution of $^{n}$BuLi (600 μL, 1.6 M in hexanes, 0.960 mmol). A yellow-orange precipitate formed immediately. After 2 hr the suspension was filtered and the solid washed several times with pentane to give the product as yellow-orange solid (0.118 g, 0.546 mmol, 76% yield).

**Preparation of Ga(OEP)(CCFc)**. To a stirred solution of Ga(OEP)Cl (0.048 g, 0.075 mmol) in THF (30 mL) at –78 °C was added a solution of lithium ethynylferrocene (0.053 g, 0.245 mmol) in THF (4 mL). The reaction mixture was allowed to warm slowly to room temperature, during which time the color changed from dark pink to very dark purple. After 4 h the volatile components were removed under vacuum, the remaining solid was extracted into toluene, and the solution was filtered through Celite. Removal of the solvent under vacuum provided a dark purple solid that was then washed multiple times with pentane to give a dark pink powder (0.026 g, 0.032 mmol, 43% yield). $^{1}$H NMR ($CD_2Cl_2$, 500.13 MHz; see Figure 6.10): δ 10.39 (s, 4 H, *meso* H), 4.24 (complex m, 16 H, C$\underline{H_2}$CH$_3$), 3.29 (t, 2 H, Fc H), 3.04 (s, 5 H, Fc H), 2.64 (t, 2 H, Fc H), 2.02 (t, 24 H, CH$_2$C$\underline{H_3}$). $^{13}$C{$^{1}$H} NMR ($CD_2Cl_2$, 125.76 MHz; see Figure 6.11): δ 146.53 (α), 143.21 (β), 100.51 (C≡C), 97.34 (*meso*), 93.17 (C≡C), 70.14 (Fc), 69.68 (Fc), 67.14 (Fc), 65.57 (Fc), 20.29 ($\underline{C}H_2CH_3$), 18.89 ($CH_2\underline{C}H_3$). LDI-TOF MS: *m/z* $[M]^+$ = 810.335, predicted = 810.288. UV-vis (toluene; $\lambda_{max}$, nm (rel. int.); see Figure 6.15): 341 (7.8), 392 (12.0), 414 (100), 504 (0.8), 543 (4.4), 580 (5.1).

**Preparation of Ga(OEP)(CCZnTPP).** To a stirred solution of ZnTPPCCH (0.050 g, 0.071 mmol) at –78 °C in THF (20 mL) was added a lithium bis(trimethylsilyl)amide solution (1 M in toluene, 64 μL, 0.064 mmol). Upon addition, the dark purple solution turned a dark blue color. The solution was then slowly warmed to room temperature, changing to a dark green color as it warmed. After 4 h, a solution of Ga(OEP)Cl (0.041 g, 0.064 mmol) in THF (25 mL) was added,

and the reaction mixture stirred at room temperature for an additional 2 h, resulting in a dark purple solution. The solvent was removed *in vacuo*, resulting in a dark purple powder. Multiple pentane washes resulted in a sample that contained the target compound together with significant HCCZnTPP and Ga(OEP)Cl impurities as a dark pink powder (crude yield: 15 mg). $^1$H NMR ($C_6D_6$, 500.13 MHz; see Figure 6.12): δ 10.52 (s, 4 H, *meso* H), 8.93 (m, 4 H, *β* H), 8.68 (d, 2 H, *β* H), 8.18 (d, 2 H, *β* H), 8.16 (m, 2 H, TPP Ph H), 8.07 (m, 4 H, TPP Ph H), 7.44 (complex m, 9 H, TPP Ph H), 6.86 (d, 2 H, Ga CC-*m*-$C_6H_4$), 5.63 (d, 2 H, GaCC-*o*-$C_6H_4$), 4.07 (complex m, 16 H, $CH_2CH_3$), 1.91 (t, 24 H, $CH_2CH_3$).

**Preparation of Ga(OEP)(OH).** This procedure is a modified version of one previously reported.[31] To a stirred solution of Ga(OEP)Cl (0.047 g, 0.074 mmol) in dichloromethane (15 mL) at room temperature was added an aqueous solution of NaOH (2M, 20 mL). The suspension was stirred vigorously at room temperature for 2 h. The dark pink suspension was not observed to change color during this time. The organic phase was collected, washed with water (3 × 30 mL), and dried over $MgSO_4$. The solvent was removed by rotary evaporation to give the product as a dark pink powder (0.044 g, 0.071 mmol, 96% yield). Small amounts (< 2%) of porphyrinic impurities were observed in the $^1$H NMR spectrum and attempts to remove these have been unsuccessful at this time. $^1$H NMR ($C_6D_6$, 500.13 MHz; see Figure 6.13): δ 10.37 (s, 4 H, *meso* H), 3.98 (complex m, 16 H, $CH_2CH_3$), 1.85 (t, 24 H, $CH_2CH_3$), -6.82 (s, 1H, OH).

**Preparation of Ga(OEP)(O$_2$CFc).** This procedure is a modification of similar procedures used previously in our lab for the synthesis of Ga($TC_{10}P$)($O_2CR$) complexes.[32] To a stirred solution of Ga(OEP)(OH) (0.044 g, 0.071 mmol) in THF (20 mL) at room temperature was added a solution of ferrocene carboxylic acid (0.018 mg, 0.078 mmol) in THF (5 mL). The solution was stirred at room temperature for 2 h, during which the color of the dark pink solution

was observed to darken slightly. The solvent was removed under vacuum, yielding the crude product as a dark pink powder (0.044 mg). The $^{1}$H NMR showed unreacted ferrocene carboxylic acid present in the sample (δ 4.86 (t, 2 H), 4.00 (t, 2 H), 3.96 (s, 5 H) in $C_6D_6$), and a small amount (< 2%) of porphyrinic impurity. Attempts to remove these have been unsuccessful at this time. $^{1}$H NMR ($C_6D_6$, 500.13 MHz): δ 10.50 (s, 4 H, *meso* H), 4.02 (complex m, 16 H, $C\underline{H}_2CH_3$), 2.84, (t, 2 H, Fc), 2.73, (s, 5 H, Fc), 2.62, (t, 2 H, Fc), 1.88 (t, 24 H, $CH_2C\underline{H}_3$).

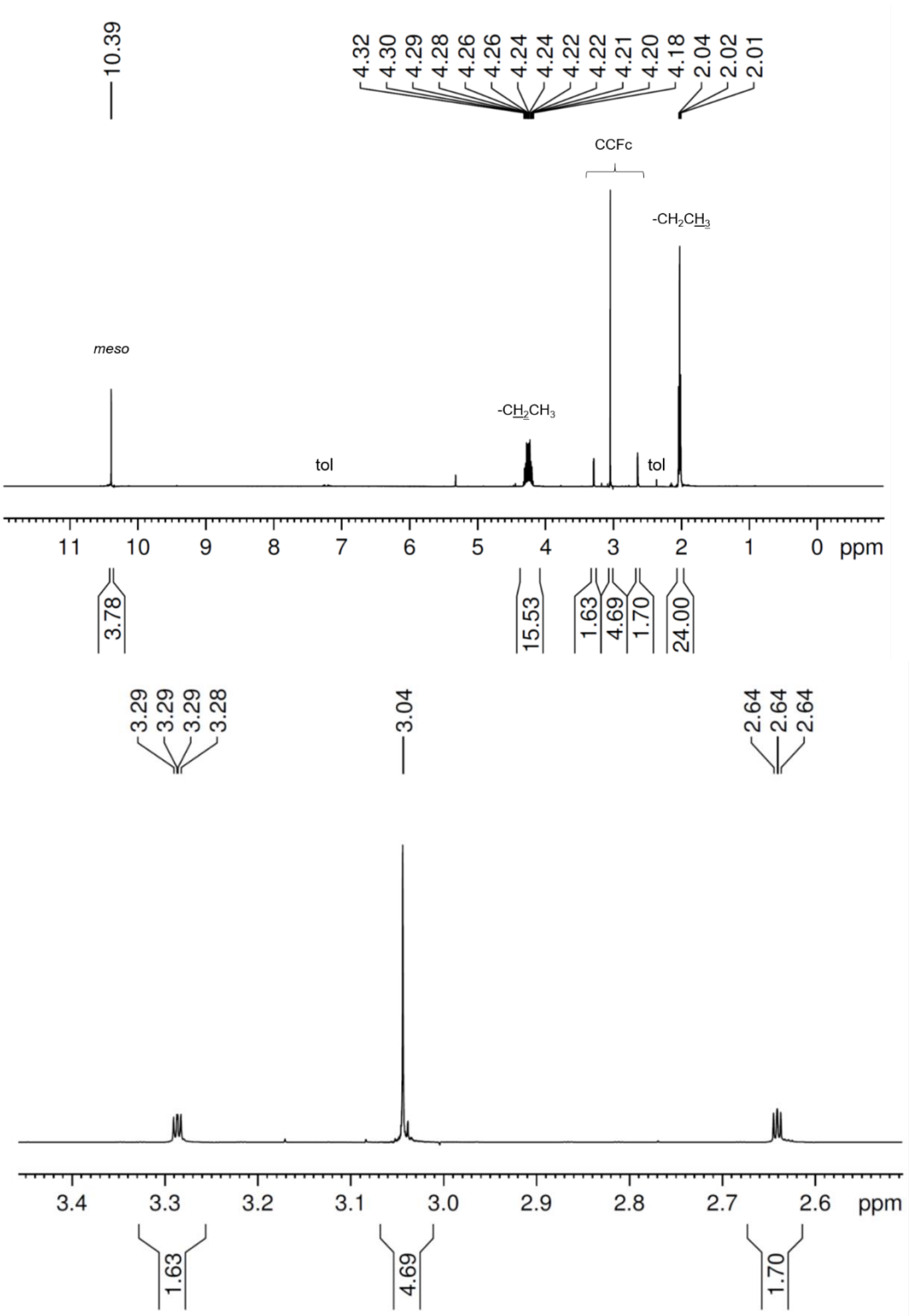


**Figure 6.10.** $^{1}H$ NMR spectrum of Ga(OEP)(CCFc) in $CD_2Cl_2$. The bottom spectrum is an expansion of the top spectrum.

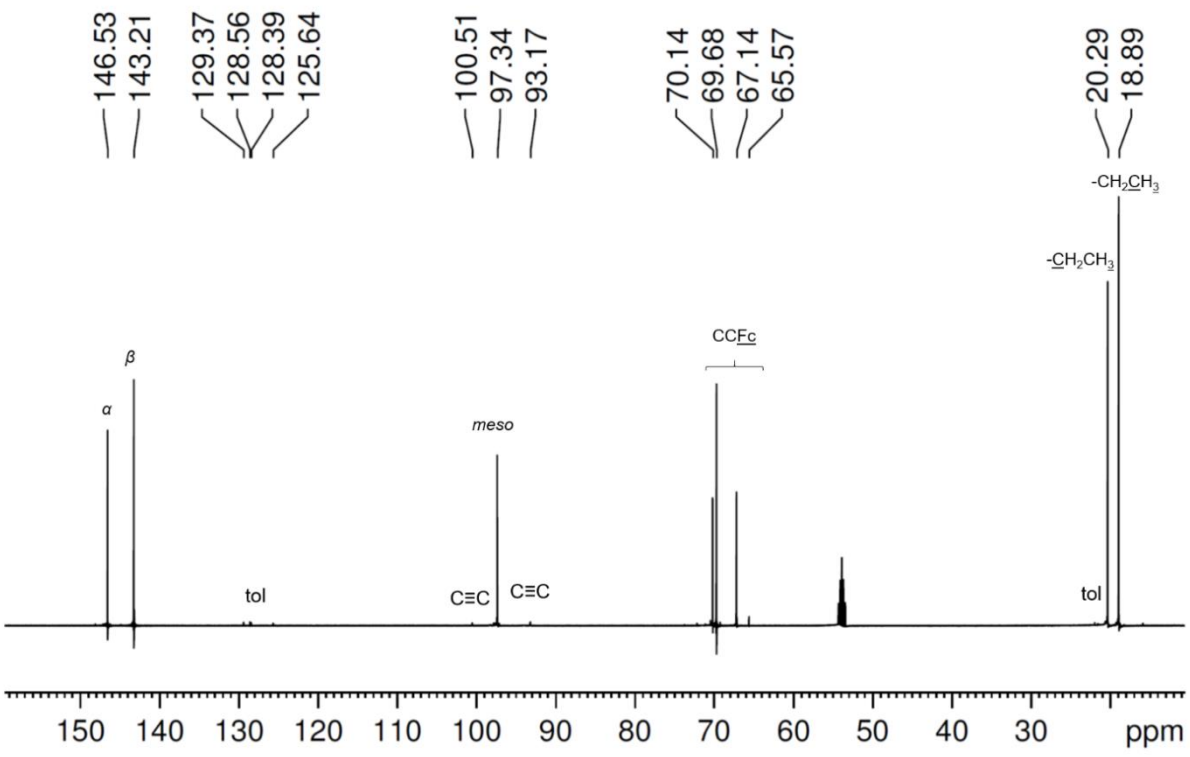


**Figure 6.11.** $^{13}C\{^{1}H\}$ NMR spectrum of Ga(OEP)(CCFc) in $CD_2Cl_2$.

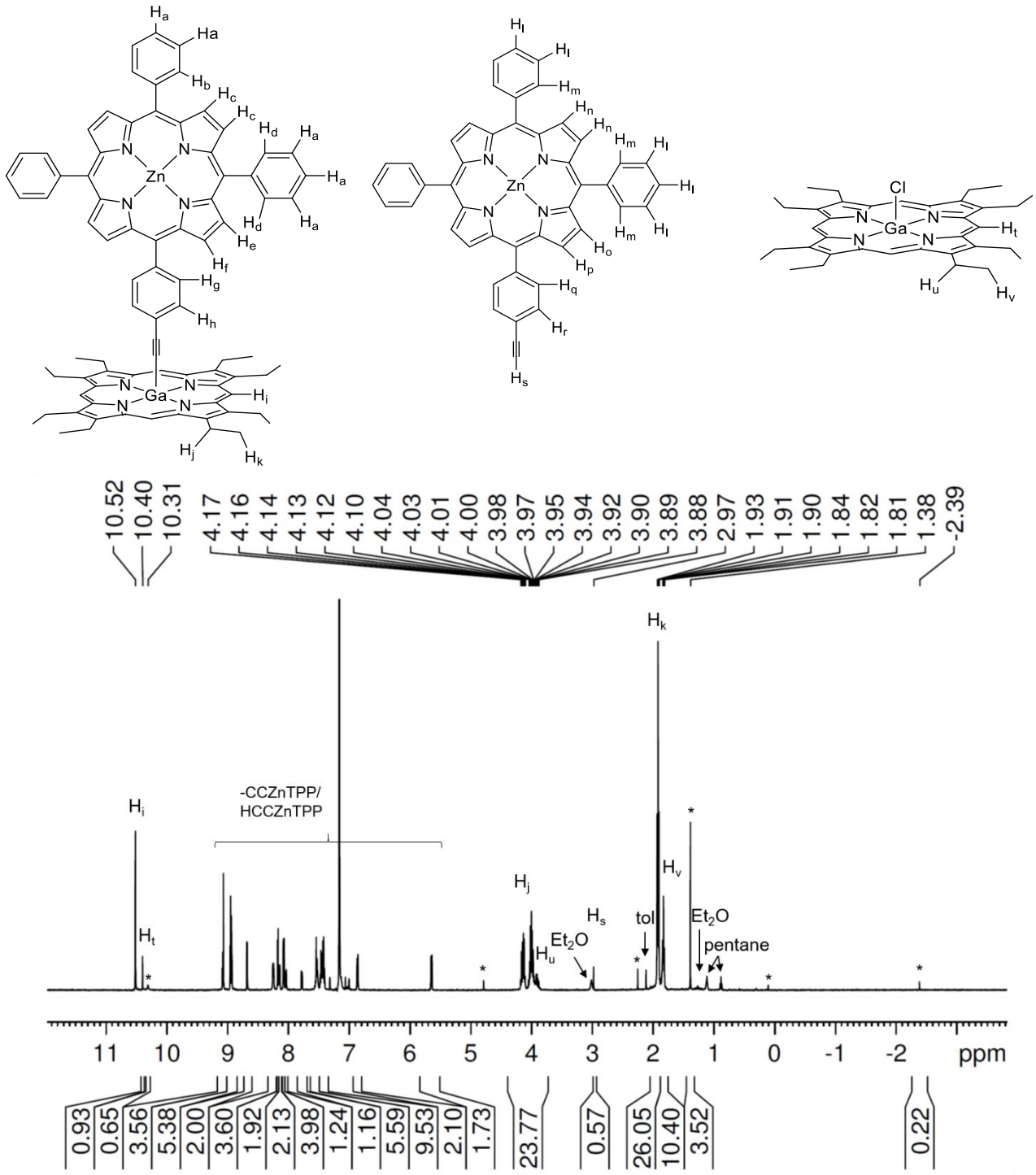


**Figure 6.12.** $^{1}H$ NMR spectrum of Ga(OEP)(CCZnTPP) in $C_6D_6$. The later spectra are expansions of the first spectrum. Resonances marked with an * have not been assigned at this time.

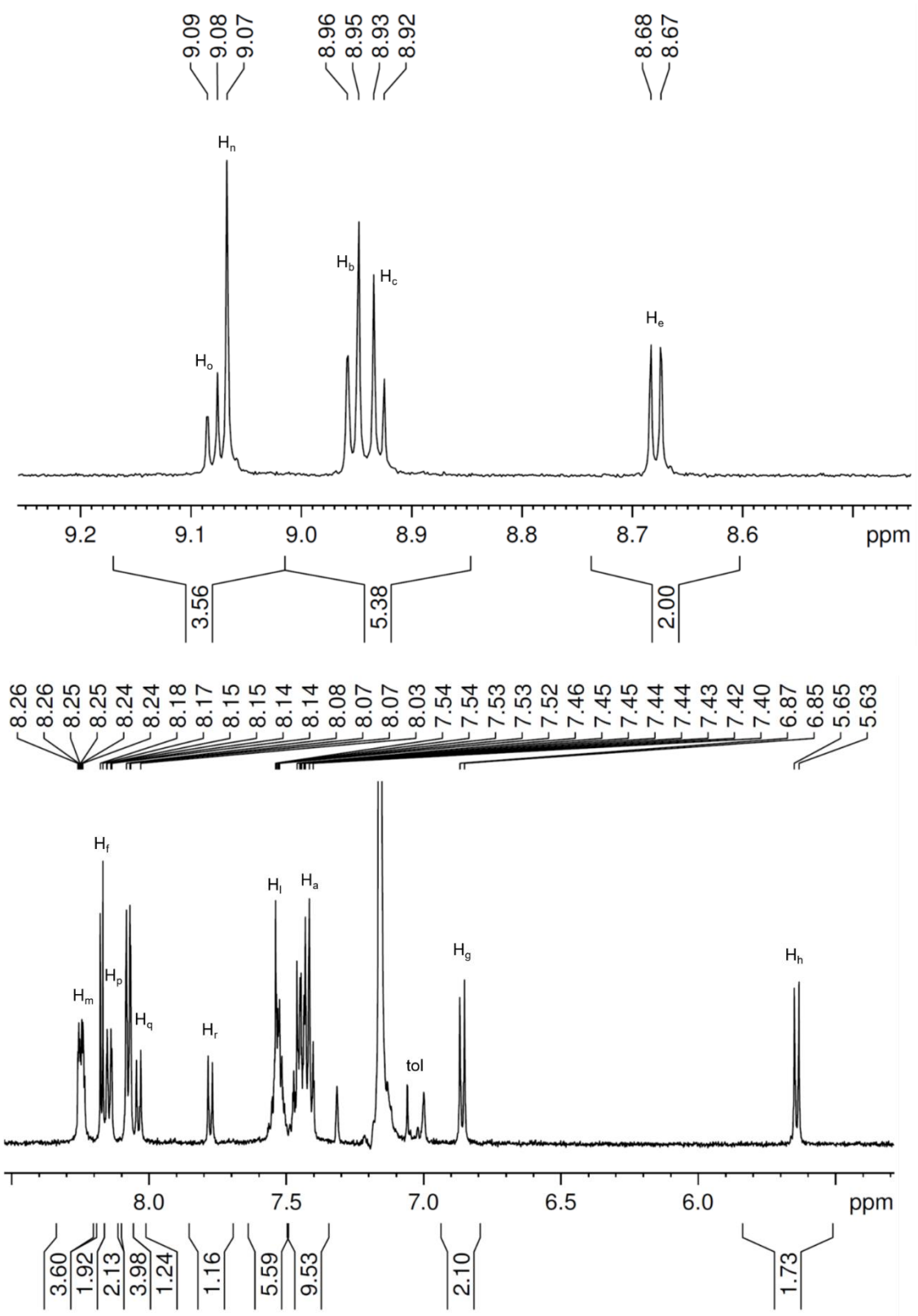


**Figure 6.12 (cont.).** $^{1}$H NMR spectrum of Ga(OEP)(CCZnTPP) in $C_6D_6$. The latter spectra are expansions of the first spectrum. Resonances marked with an * have not been assigned at this time.

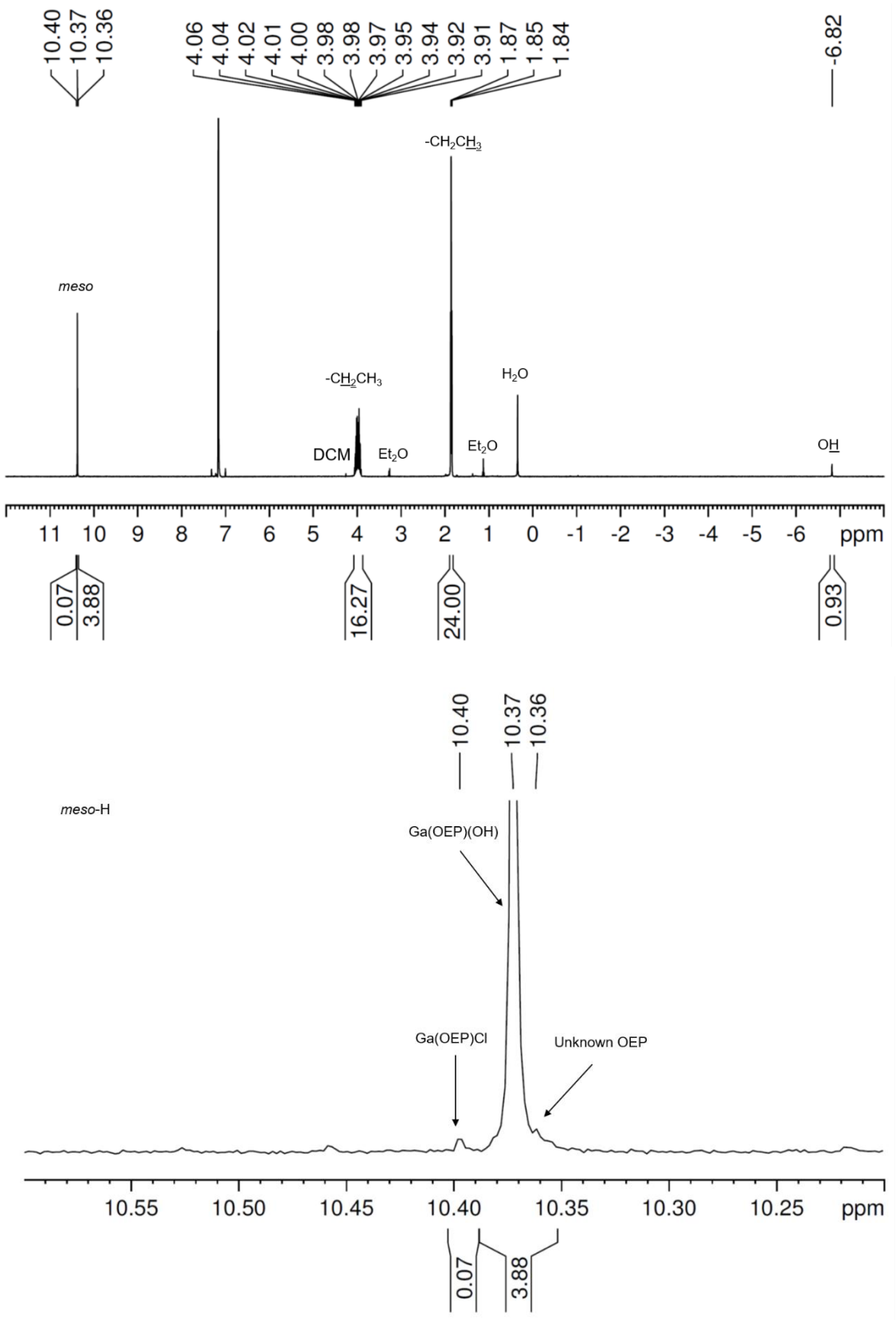


**Figure 6.13.** $^{1}$H NMR spectrum of Ga(OEP)(OH) in $C_6D_6$. The bottom spectrum is an expansion of the first spectrum.

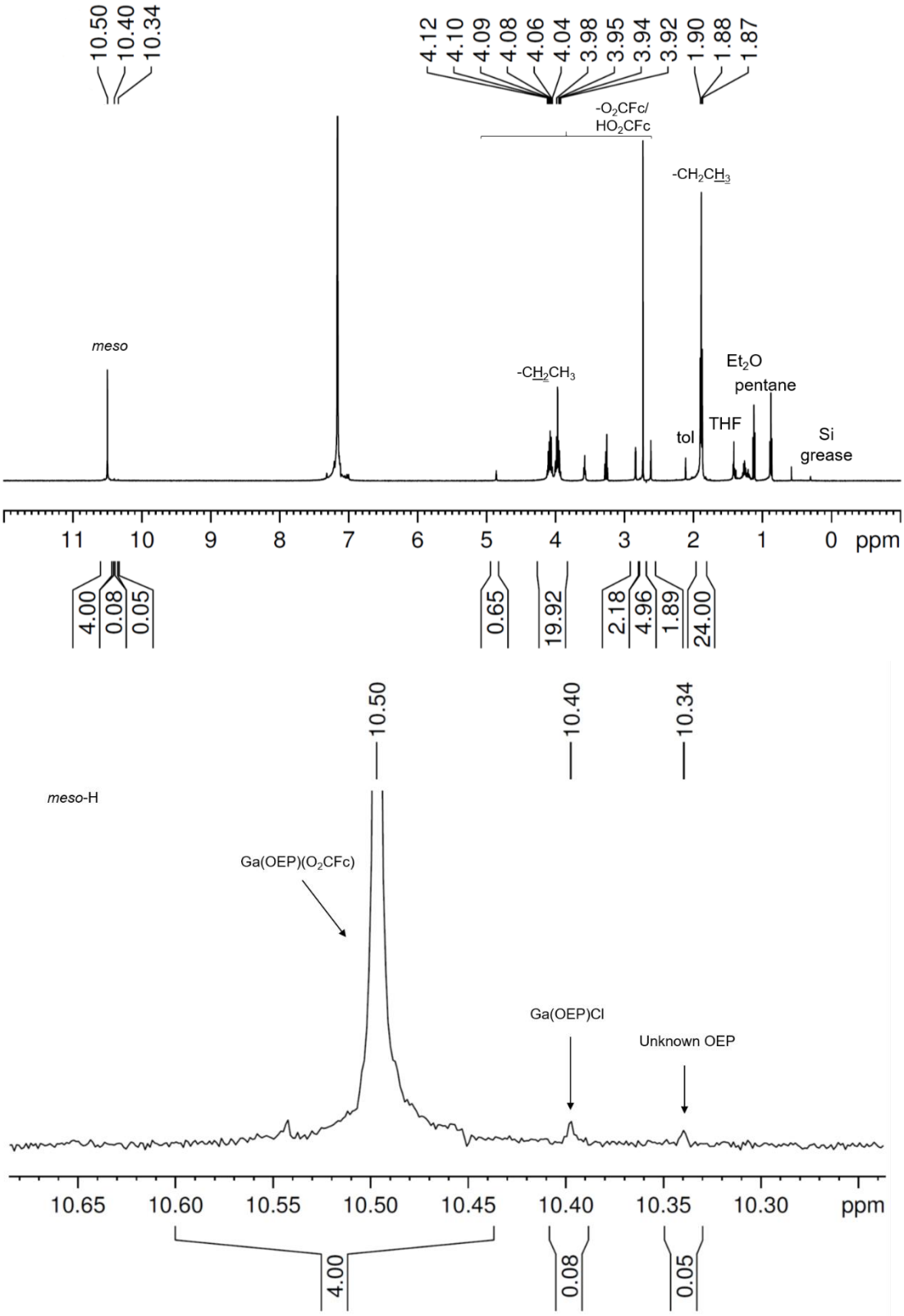


**Figure 6.14.** $^{1}$H NMR spectrum of Ga(OEP)($O_2$CFc) in $C_6D_6$. The latter spectra are expansions of the first spectrum.

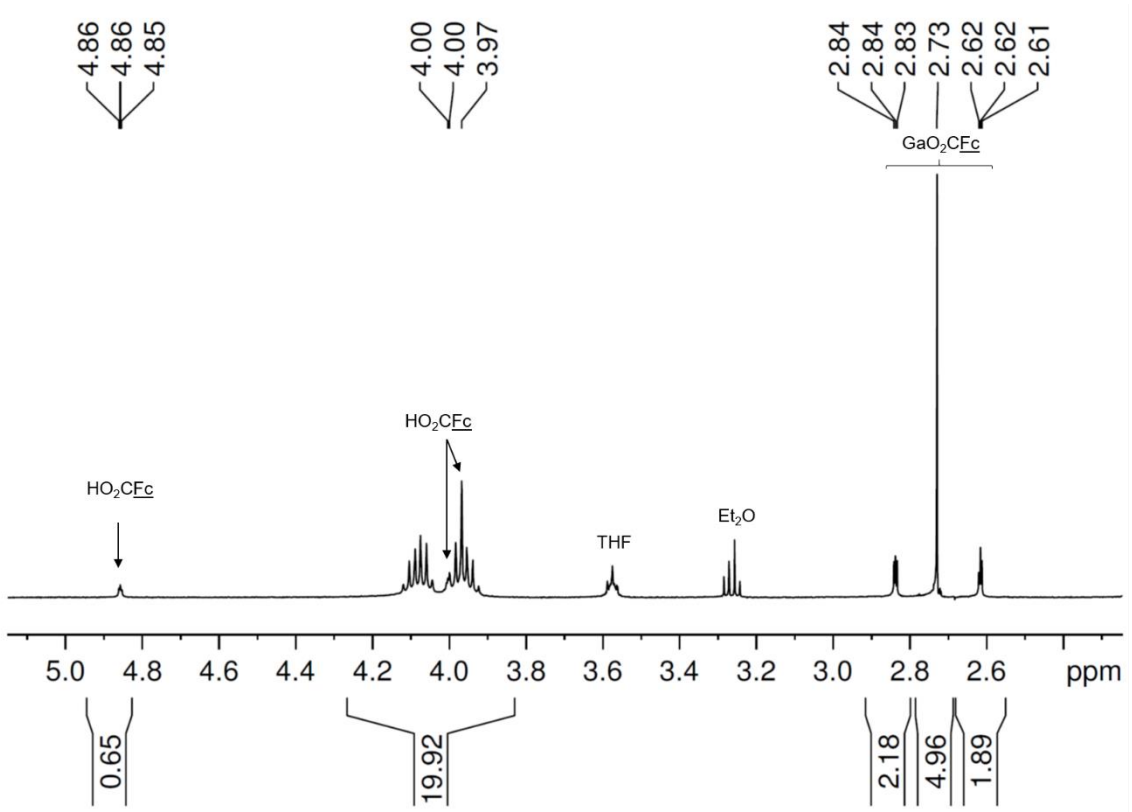


**Figure 6.14 (cont.).** $^1$H NMR spectrum of Ga(OEP)($O_2$CFc) in $C_6D_6$. The latter spectra are expansions of the first spectrum.

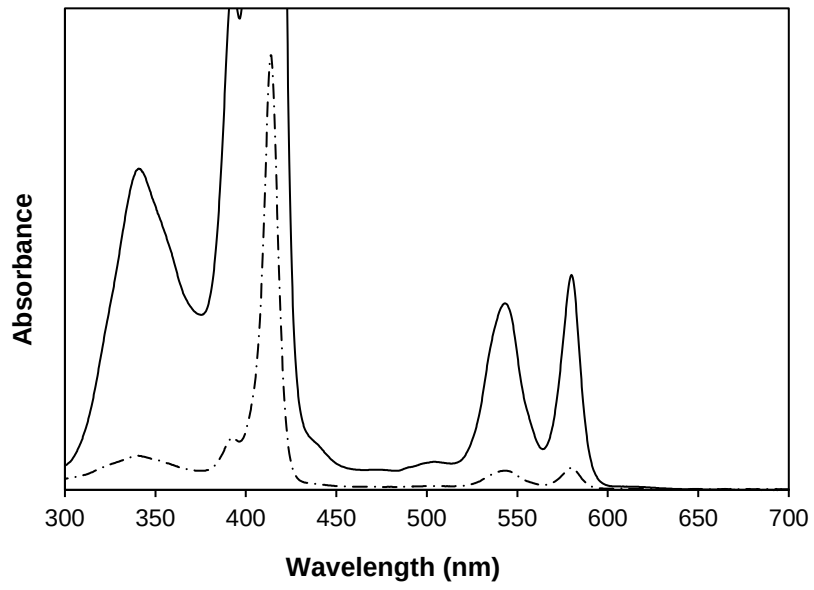


**Figure 6.15.** Electronic-absorption spectrum of Ga(OEP)(CCFc) in toluene at room temperature.

## 6.3 Chapter 4 Supplementary Information

**6.3.1. General Procedures.** The general methods can be found in Section 6.1.1 with the following adaptations. Prior to use, commercial 1-bromopyrene and pyrene were purified by passing them through a silica gel column using hexane as the eluent. Triethylamine was refluxed overnight over calcium hydride, distilled, and sparged with nitrogen prior to use. Hexane and $CD_2Cl_2$ were stored over 3Å molecular sieves under nitrogen. Except where noted, all syntheses were performed under a purified nitrogen atmosphere using standard Schlenk and glovebox techniques.

**6.3.2. Density Functional Theory (DFT) Calculations.** Density functional theory calculations were performed as described in Section 6.1.2. The B3P86 functional[7, 8] was used for all calculations. For gas-phase optimized geometries of Ga(OEP)(CCPyr) complexes, Ga(OEP)(CCH), and ethynylpyrene ligands, the cc-pVTZ basis set[16, 18, 27] was employed for all atoms. For structures optimized in local minima with the ethyl chains rotated toward the axial ligand, the 6-31G* (H, C, N) and LANL2DZ effective core potential basis sets[15, 28] (Ga) were employed. Orbital energies were determined by running single-point calculations with keyword pop=full on optimized structures. Molecular models were built using the Materials Studio software.[29] Molecular orbital images were generated using the Avogadro software[33, 34] (isosurface value = 0.02) (see Figure 6.16 and 6.17).

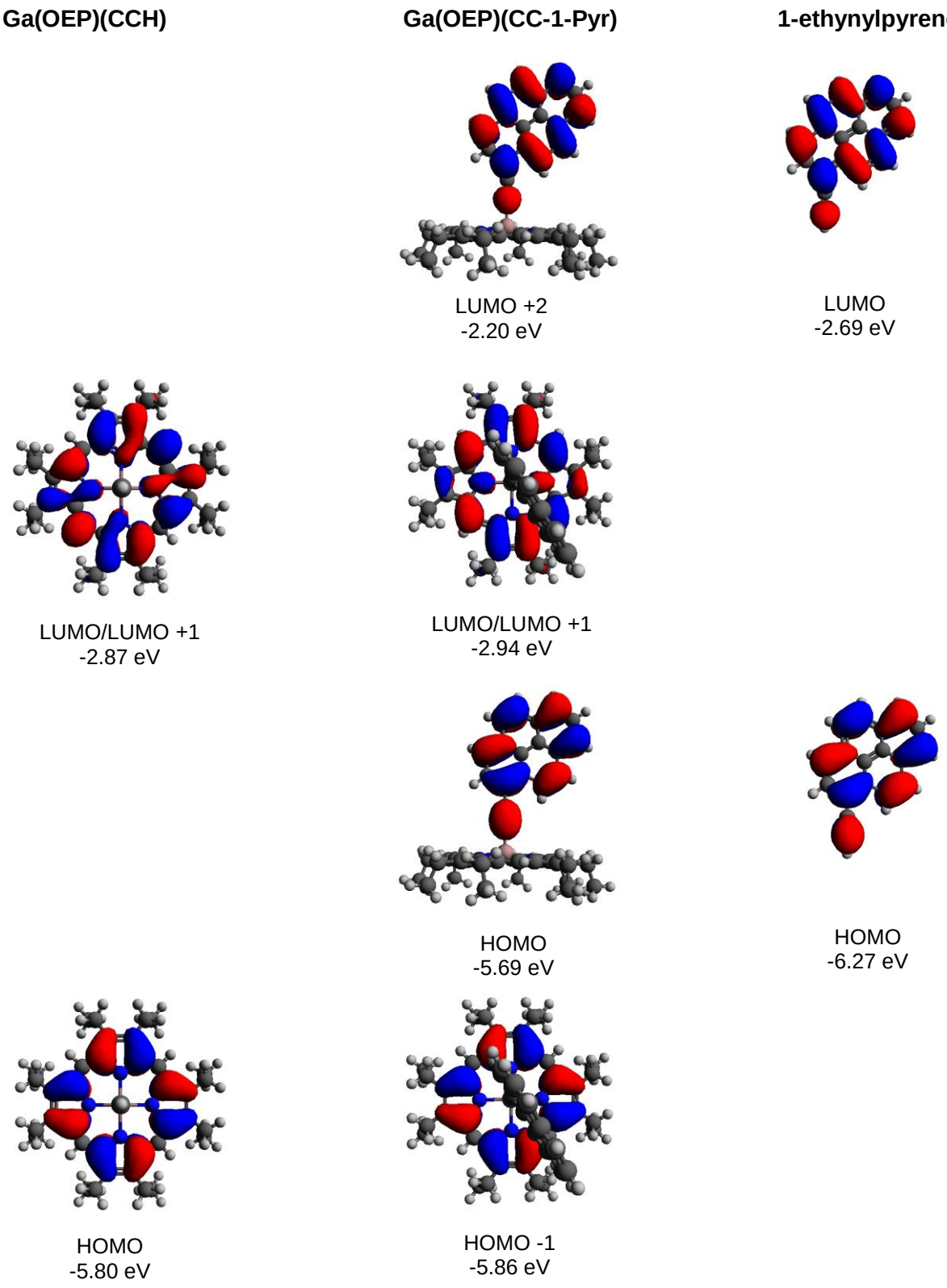


**Figure 6.16.** Calculated frontier orbital energies and isosurfaces of Ga(OEP)(CCH), Ga(OEP)(CC-1-Pyr), and 1-ethynylpyrene (isosurface value = 0.02).

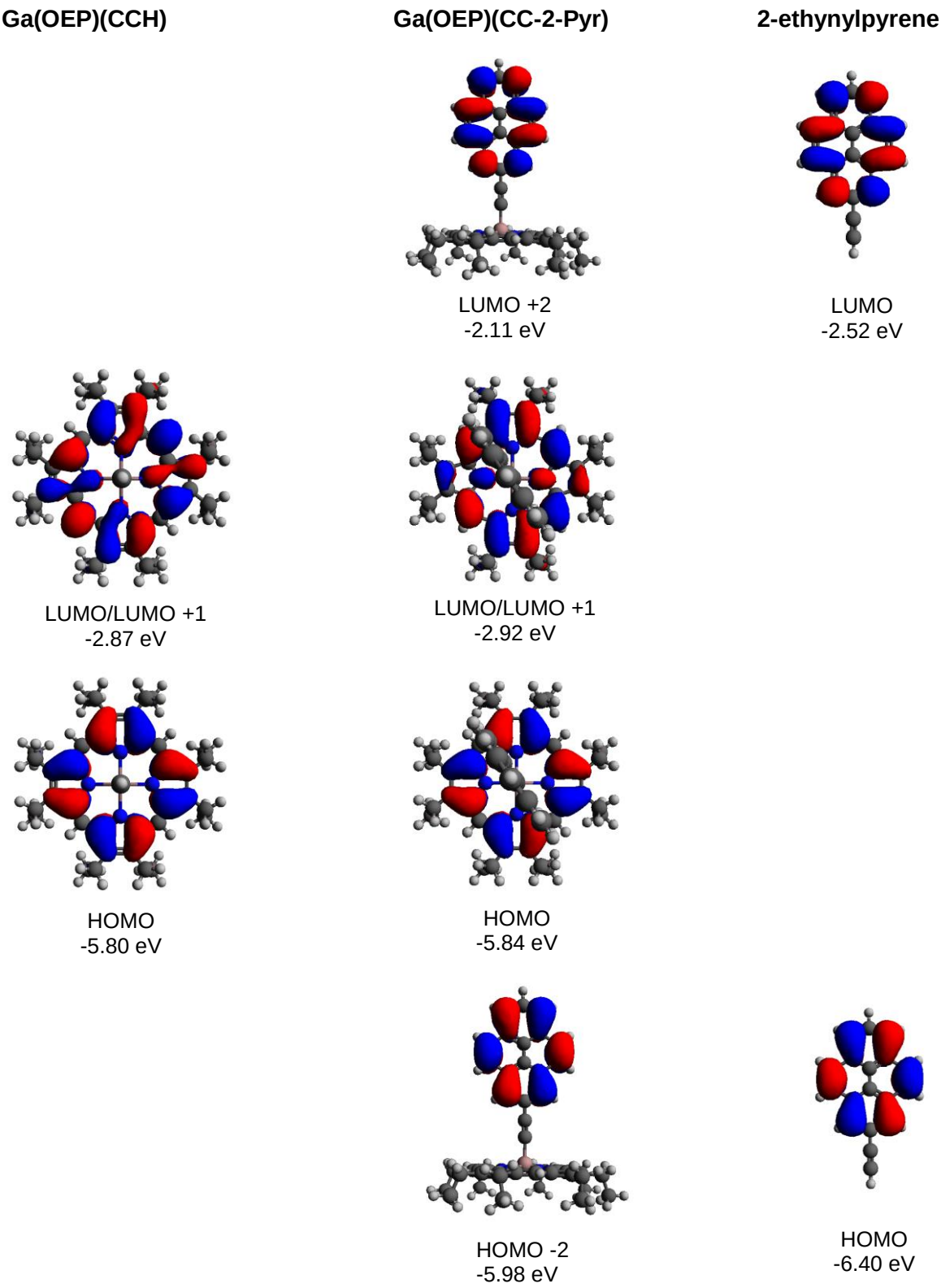


**Figure 6.17.** Calculated frontier orbital energies and isosurfaces of Ga(OEP)(CCH), Ga(OEP)(CC-2-Pyr), and 2-ethynylpyrene (isosurface value = 0.02).

**6.3.3. Scanning Tunneling Microscopy (STM) Sample Preparation.** STM samples were prepared as described in Section 6.1.3 with the following adaptations. One drop of a 1-phenyloctane solution of the porphyrin compound (0.5 mM) was deposited onto the surface. The STM tip was then directly engaged through the drop and the monolayer imaged at the solid–liquid interface. In experiments in which fullerenes were added to preformed porphyrin monolayers, the STM tip was then disengaged, one drop of a solution of the fullerene in 1-phenyloctane (PCBM, 3.0 mM; $C_{60,}$ 0.05–3.0 mM) was added to the drop of porphyrin solution on the surface, the tip was re-engaged, and the resulting sample was imaged. For experiments in which porphyrin compounds and $C_{60}$ were co-deposited on HOPG, the measurement protocol was the same as that above for the porphyrin monolayers but used a 1-phenyloctane solution containing equal volumes of both porphyrin (0.5 mM) and $C_{60}$ (3.0 mM).

**6.3.4. Scanning Tunneling Microscopy (STM) Analysis.** STM data analysis was carried out as described in Section 6.1.4 with the following adaptations. For porphyrin monolayers and for the underlying porphyrin layers in porphyrin/fullerene assemblies, the unit-cell distances were determined from the average distances measured of 100 sets of five consecutive porphyrin molecules; for fullerene overlayers, the average of fifty distances was taken. The unit-cell angles were the average of 40 measurements.

**6.3.5. Synthesis and Characterization.**

**Preparation of 1-(trimethylsilylethynyl)pyrene.** This procedure is a modification of one previously reported.[35] Trimethylsilylacetylene (1.5 mL, 10.613 mmol) was added to a stirred, room temperature solution of 1-bromopyrene (0.336 g, 1.195 mmol), $Pd(PPh_3)_2Cl_2$ (0.052 g, 0.074 mmol), and CuI (0.028 g, 0.147 mmol) in triethylamine (30 mL). Upon mixing at room temperature, the color of the reaction mixture changed from yellow to dark green to dark brown

over several minutes. The reaction mixture was heated at 70 °C for 64 h, cooled to room temperature, opened to air, and reduced to dryness using a rotary evaporator to give a dark brown solid. This solid was purified on a silica gel column with hexanes as the eluent; removal of solvent provided the product as a pale yellow solid (0.191 g, 0.640 mmol, 54% yield). The $^{1}$H NMR data agree with those reported in the literature.[35] $^{1}$H NMR ($CDCl_3$, 500.13 MHz): δ 8.57 (d, 1 H), 8.13 (complex m, 8 H), 0.40 (s, 9 H).

**Preparation of 1-ethynylpyrene.** This procedure is a modification of one previously reported.[36] A solution of 1-(trimethysilylethynyl)pyrene (0.191 g, 0.640 mmol) and ($N^{n}Bu_4$)F•x$H_2O$ (0.300 g, 1.147 mmol) in THF (15 mL) open to air was stirred at room temperature for 2 h, giving a clear, dark brown solution. The solvent was removed using a rotary evaporator, leaving a thick, viscous brown oil. The soluble components were extracted into hexanes and purified on a silica gel column using hexanes as the eluent; removal of solvent provided the product as a white powder (0.041 g, 0.181 mmol, 28% yield) The $^{1}$H NMR data agree with those reported in the literature.[35] $^{1}$H NMR ($CDCl_3$, 500.13 MHz): δ 8.60 (d, 1 H), 8.21 (complex m, 4 H), 8.12 (d, 2H), 8.05 (m, 2 H), 3.63 (s, 1 H).

**Preparation of 1-(LiCC)pyrene.** To a stirred solution of 1-ethynylpyrene (0.041 g, 0.181 mmol) in diethylether (10 mL) at room temperature was added a solution of $^{n}$BuLi (160 μL, 1.6 M in hexanes, 0.256 mmol). After 30 min the solvent was removed in vacuo, and the remaining solid was suspended in pentane, filtered, and washed several times with pentane to give the product as a yellow-brown solid (0.032 g, 0.138 mmol, 76% yield).

**Preparation of Ga(OEP)(CC-1-pyrene).** To a stirred solution of Ga(OEP)Cl (0.050 g, 0.078 mmol) in THF (25 mL) at –78 °C was added a solution of 1-(LiCC)pyrene (0.032 g, 0.138 mmol) in THF (3 mL). The reaction mixture was allowed to warm to room temperature, during

which time the color changed slowly from dark pink to dark purple. After 2 h, the volatile components were removed under vacuum, the remaining solid was extracted into toluene, and the solution was filtered through Celite. Removal of the solvent under vacuum provided a purple powder that was then washed with hexanes (0.049 g, 0.059 mmol, 76% yield). $^{1}$H NMR ($CD_2Cl_2$, 500.13 MHz; see Figure 6.18): δ 10.45 (s, 4 H, *meso* H), 8.03 (dd, 1 H, pyrenyl H), 7.92 (d, 1H, pyrenyl H), 7.85 (t, 1 H, pyrenyl H), 7.69 (d, 1 H, pyrenyl H), 7.58 (d, 1 H, pyrenyl H), 7.50 (d, 1 H, pyrenyl H), 7.18 (d, 1 H, pyrenyl H), 6.13 (d, 1 H, pyrenyl H), 5.26 (d, 1 H, pyrenyl H), 4.27 (complex m, 16 H, C$\underline{H}_2$CH$_3$), 2.01 (t, 24 H, CH$_2$C$\underline{H}_3$). $^{13}$C{$^{1}$H} NMR ($CD_2Cl_2$, 125.76 MHz; see Figure 6.19): δ 143.29 (α), 138.38 (β), 131.24 (pyrene), 130.97 (pyrene), 130.96 (pyrene), 129.67 (pyrene), 127.53 (pyrene), 127.15 (pyrene), 127.10 (pyrene), 126.96 (pyrene), 126.11 (pyrene), 125.10 (pyrene), 125.06 (pyrene), 125.02 (pyrene), 123.97 (pyrene), 123.67 (pyrene), 123.66 (pyrene), 118.17 (pyrene), 97.49 (*meso*), 94.43 (C≡C), 20.34 ($\underline{C}H_2CH_3$), 18.86 ($CH_2\underline{C}H_3$); one C≡C resonance not observed. LDI-TOF MS: *m/z* $[M]^+$ = 826.393, predicted = 826.353. UV-vis (toluene; $\lambda_{max}$, nm (rel. int.); see Figure 6.22): 338(sh) (0.13), 350 (0.16), 363 (0.15), 369 (0.16), 393 (0.16), 413 (1.00), 542 (0.05), 579 (0.06).

**Preparation of 2-(Bpin)pyrene.** This procedure is a modification of one previously reported.[37] To a Schlenk flask containing bis(pinacolato)diboron ($B_2pin_2$, 2.793 g, 11.00 mmol) and pyrene (1.999 g, 9.884 mmol), a yellow suspension (hexane, 6 mL) of $B_2pin_2$ (0.103 g, 0.406 mmol), 4,4'-di-tertbutyl-2,2'-bipyridine (0.049 g, 0.183 mmol), and [Ir(μ-OMe)cod]$_2$ (0.060 g, 0.091 mmol) was added, turning the resulting suspension dark brown. An additional 10 mL of hexane was added, and the flask was sealed. The contents were heated and stirred at 80 °C for 20 h; during this time, all solids slowly dissolved, followed by the formation of a tan precipitate. The reaction mixture was cooled to room temperature and opened to air. The mixture was

filtered through a silica gel plug that was subsequently washed with dichloromethane, resulting in a clear yellow filtrate. The solvent was removed from the filtrate using a rotary evaporator to give the crude product as a pale yellow powder. The crude material was purified by column chromatography (silica gel, hexane/dichloromethane 1:1) and recrystallization from hexane to afford the product as a white crystalline material (0.502 g, 1.534 mmol, 16% yield). The $^1$H NMR data agree with those reported in the literature. $^1$H NMR ($CDCl_3$, 500.13 MHz): δ 8.64 (s, 2 H), 8.17 (d, 2 H), 8.11 (d, 2H), 8.06 (d, 2 H), 8.02 (t, 1 H), 1.47 (s, 12 H).

**Preparation of 2-Bromopyrene.** This procedure is a modification of one previously reported.[37] To a round-bottomed flask open to air containing 2-(bpin)pyrene (0.502 g, 1.534 mmol), a turquoise solution of $CuBr_2$ (1.029 g, 4.609 mmol) in methanol/water (1:1, 35 mL) was added. The suspension (containing white suspended solid) was stirred at 90 °C for 18 h, during which the solution phase turned pale green and noticeably more white precipitate formed. The suspension was cooled to room temperature and $H_2O$ (50 mL) was added, inducing precipitation of more white material. The suspension was filtered through a Büchner funnel and washed with $H_2O$ (5 × 25 mL) to give a clear blue filtrate and the crude product as an olive green solid. The crude material was purified by dissolving in hot hexane and stirring with activated charcoal, followed by filtration to remove the charcoal and subsequent recrystallization of the product from hexane. This afforded the product as white, needle-like crystals (0.204 g, 0.729 mmol, 48% yield). The $^1$H NMR data agree with those reported in the literature.[37] $^1$H NMR ($CDCl_3$, 500.13 MHz): δ 8.29 (s, 2 H), 8.21 (d, 2 H), 8.11 (d, 2H), 8.03 (t, 1 H), 7.99 (d, 2 H).

**Preparation of 2-(trimethysilylethynyl)pyrene.** Several syntheses of this compound have been reported;[37-39] the following is a different route adapted from the synthesis of 2,7-bis(trimethylsilylethynyl)pyrene.[37] Triethylamine (20 mL) was added via cannula to a stirred,

room temperature suspension of 2-bromopyrene (0.204 g, 0.729 mmol), $Pd(dppf)Cl_2$ (0.029 g, 0.040 mmol; dppf = 1,1′-bis(diphenylphosphino)ferrocene), and CuI (0.010 g, 0.053 mmol) in THF (10 mL). The color of the reaction mixture changed from orange to light brown over several minutes. Trimethylsilylacetylene (0.2 mL, 1.444 mmol) was added, and the reaction mixture was heated at 80 °C for 20 h, during which the mixture turned dark brown. The reaction mixture was cooled to room temperature, opened to air, and reduced to dryness in vacuo to give a dark brown residue. This material was purified on a short silica gel column with hexanes/diethyl ether (3:2) as the eluent; removal of solvent provided the crude product as a dark yellow solid. The product was further recrystallized from hexane to afford the pure product as a pale yellow solid (0.088 g, 0.295 mmol, 41% yield). The $^1$H NMR data agree with those reported in the literature.[37]

**Preparation of 2-ethynylpyrene.** This procedure is a modification of a literature procedure.[37] A pale yellow suspension of 2-(trimethysilylethynyl)pyrene (0.088 g, 0.295mmol) and $Na_2CO_3$ (0.124 g, 1.170 mmol) in MeOH/$H_2O$ (30 mL/3 mL) was stirred at room temperature open to air for 20 hr. To this suspension, $H_2O$ (10 mL) was added, immediately precipitating an off-white solid. The suspension was concentrated by rotary evaporation and extracted with diethyl ether (3 × 50 mL). The clear yellow organic layer was dried with $MgSO_4$ and dried via rotary evaporation to give the crude product as a pale yellow solid. This solid was passed through a silica plug with hexanes/$Et_2O$ (4:1) as the eluent, and the filtrate was evaporated to yield the product as a pale yellow solid (0.055 g, 0.243 mmol, 83% yield). Note that the product becomes discolored within a day after deprotection and should be used immediately. The $^1$H NMR data agree with those reported in the literature.[37] $^1$H NMR ($CDCl_3$, 500.13 MHz): δ 8.30 (s, 2 H), 8.20 (d, 2 H), 8.07 (d, 2H), 8.03 (m, 3 H), 3.25 (s, 1 H).

**Preparation of 2-(LiCC)pyrene.** To a stirred, pale yellow solution of 2-ethynylpyrene (0.055 g, 0.243 mmol) in a mixture of pentane (15 mL) and diethylether (3 mL) at room temperature was added a solution of $^{n}$BuLi (200 μL, 1.6 M in hexanes, 0.320 mmol). A white precipitate formed immediately. After 30 min the suspension was filtered and the solid washed several times with pentane to give the product as an off-white solid (0.030 g, 0.129 mmol, 53% yield).

**Preparation of Ga(OEP)(CC-2-pyrene).** To a stirred solution of Ga(OEP)Cl (0.053 g, 0.083 mmol) in THF (25 mL) at –78 °C was added a dark yellow solution of 2-(LiCC)pyrene (0.030 g, 0.129 mmol) in THF (3 mL). The reaction mixture was allowed to warm to room temperature, during which time the color changed slowly from dark pink to dark purple. After 2 h, the volatile components were removed under vacuum, the remaining solid was extracted into toluene, and the solution was filtered through Celite. Removal of the solvent from the filtrate under vacuum provided a purple powder that was then recrystallized at –30 °C from a toluene solution layered with hexane. This yielded the product as a dark purple solid (0.046 g, 0.056 mmol, 67% yield). $^{1}$H NMR ($CD_2Cl_2$, 500.13 MHz, see Figure 6.20): δ 10.42 (s, 4 H, *meso* H), 7.80 (d, 2 H, pyrenyl H), 7.68 (t, 1H, pyrenyl H), 7.57 (d, 2 H, pyrenyl H), 7.21 (d, 2 H, pyrenyl H), 6.22 (s, 2 H, pyrenyl H), 4.26 (complex m, 16 H, C$\underline{H_2}$CH$_3$), 2.02 (t, 24 H, CH$_2$C$\underline{H_3}$). $^{13}$C{$^{1}$H} NMR ($CD_2Cl_2$, 125.76 MHz; see Figure 6.21): δ 146.61 (α), 143.21 (β), 130.91 (pyrene), 130.08 (pyrene), 127.35 (pyrene), 126.82 (pyrene), 126.54 (pyrene), 125.98 (pyrene), 125.02 (pyrene), 124.07 (pyrene), 122.81 (pyrene), 120.74 (pyrene), 97.48 (*meso*), 95.66 (C≡C), 20.32 ($\underline{C}H_2CH_3$), 18.81 ($CH_2\underline{C}H_3$); one C≡C resonance not observed. LDI-TOF MS: *m/z* $[M]^+$ = 826.365, predicted = 826.353. UV-vis (toluene; $\lambda_{max}$, nm (rel. int.); see Figure 6.22): 315 (sh) (5.8), 325 (10.7), 340 (16.8), 392 (11.7), 413 (100), 504 (0.6), 542 (4.2), 579 (5.0).

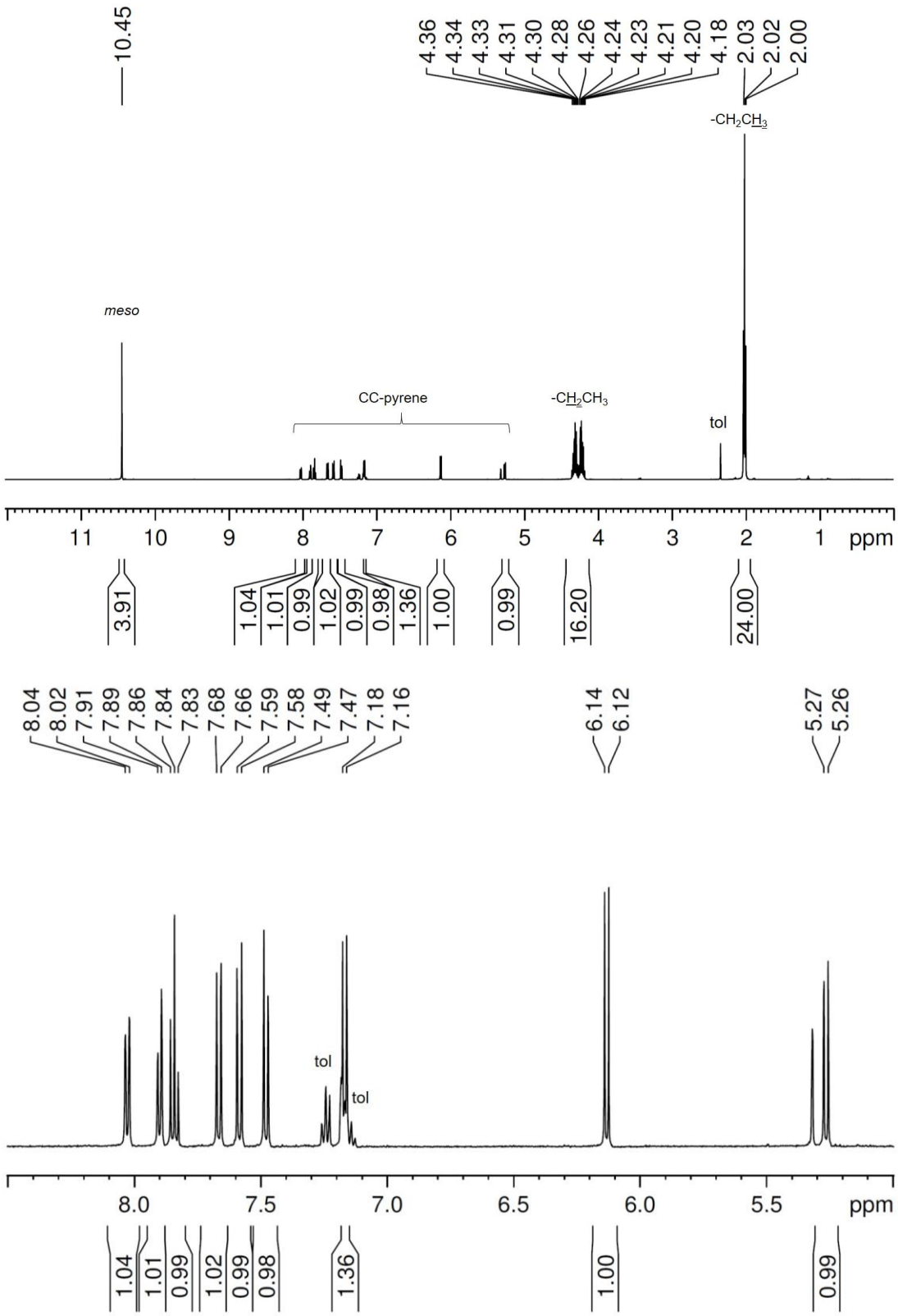


**Figure 6.18.** $^{1}H$ NMR spectrum of Ga(OEP)(CC-1-Pyr) in $CD_2Cl_2$. The bottom spectrum is an expansion of the top spectrum.

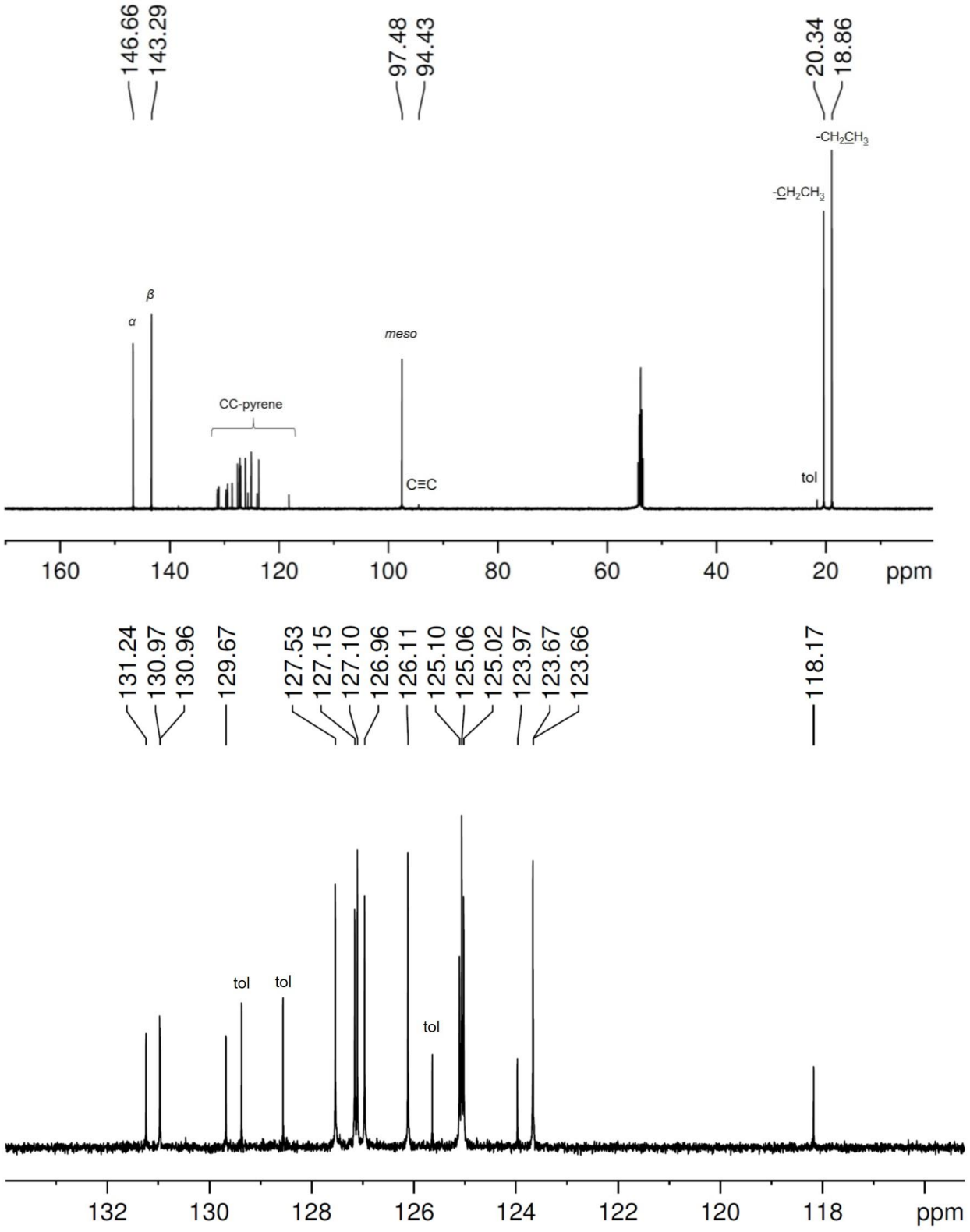


**Figure 6.19.** $^{13}C\{^{1}H\}$ NMR spectrum of Ga(OEP)(CC-1-Pyr) in $CD_2Cl_2$. The bottom spectrum is an expansion of the top spectrum.

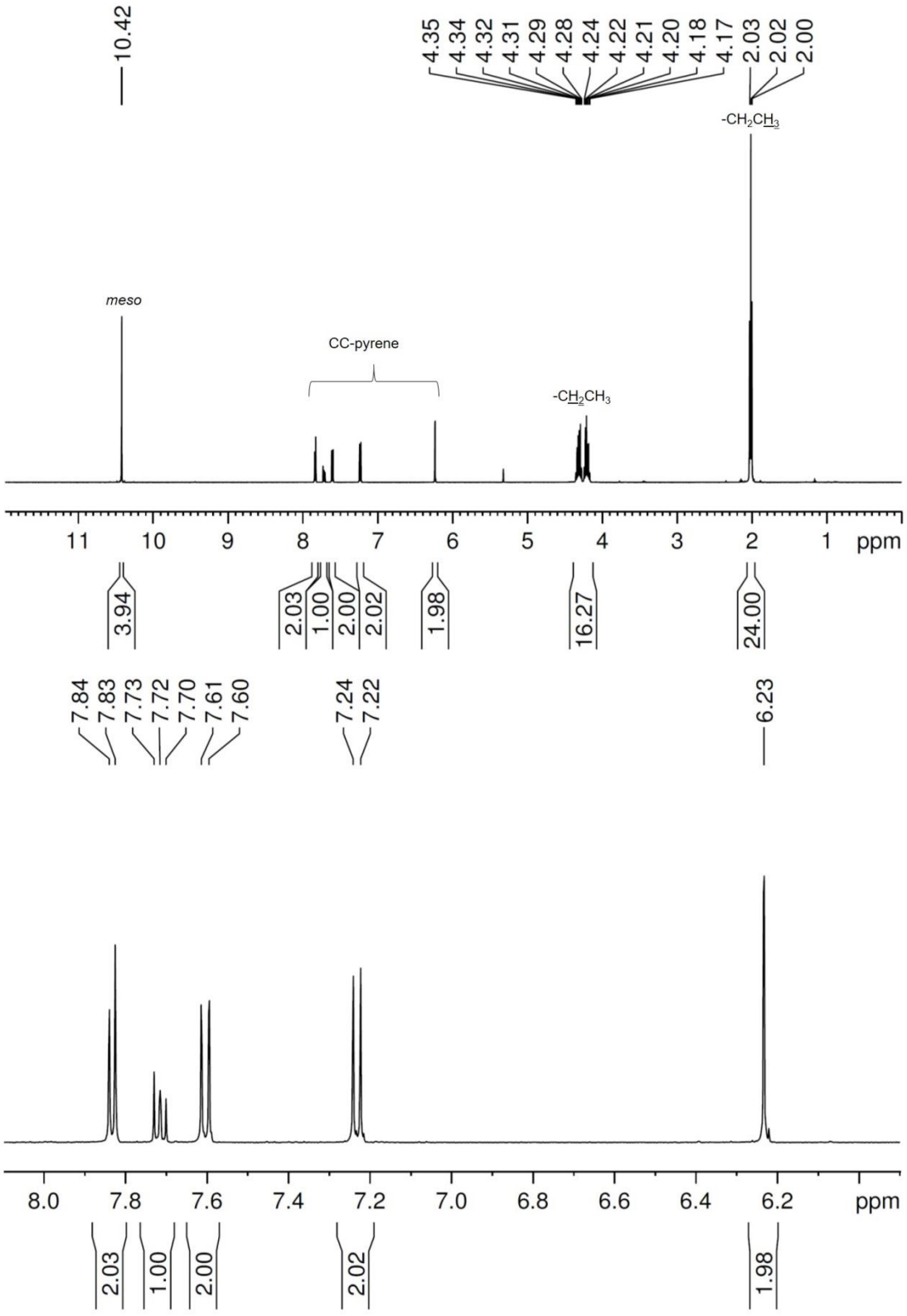


**Figure 6.20.** $^{1}$H NMR spectrum of Ga(OEP)(CC-2-Pyr) in $CD_2Cl_2$. The bottom spectrum is an expansion of the top spectrum.

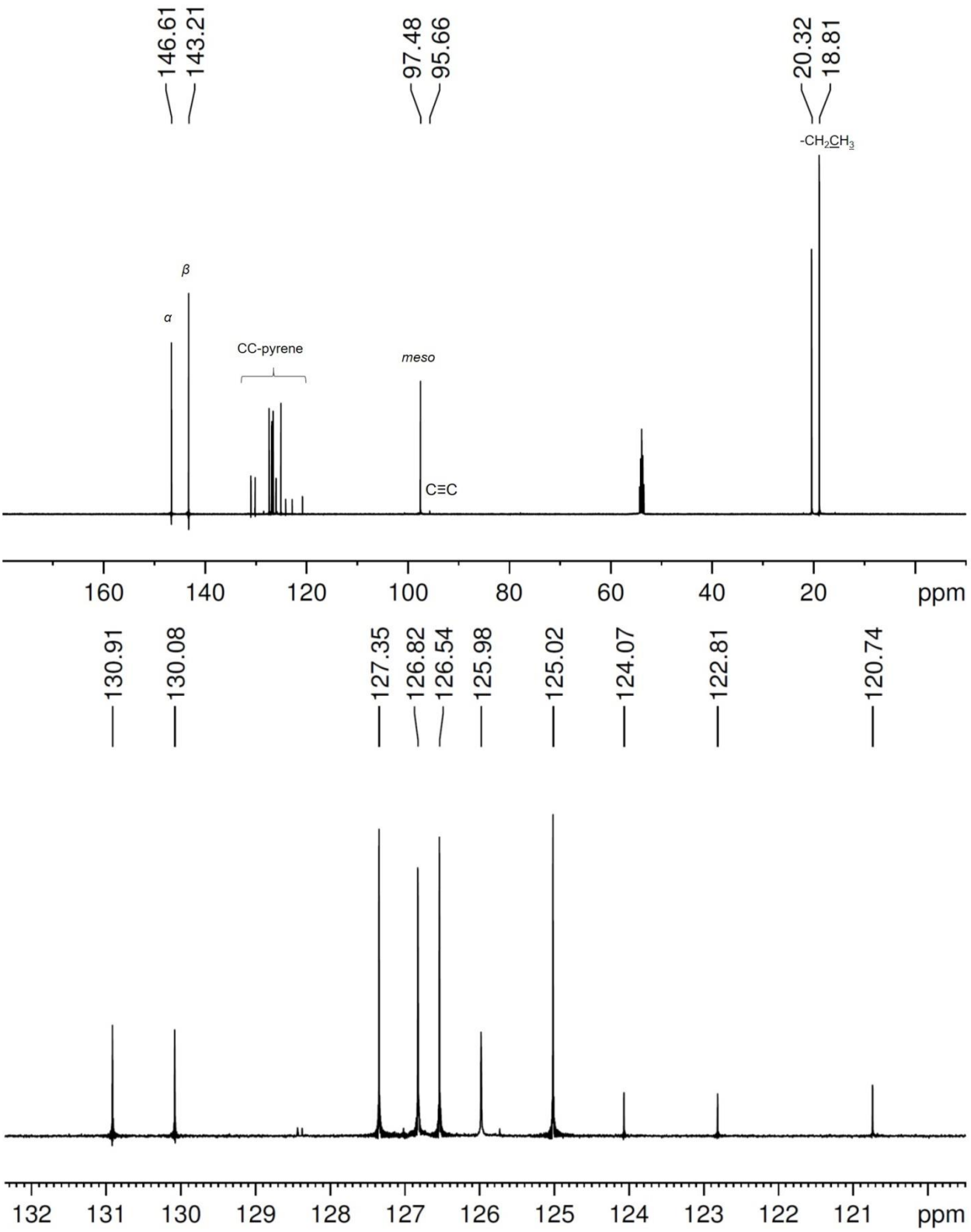


**Figure 6.21.** $^{13}C\{^{1}H\}$ NMR spectrum of Ga(OEP)(CC-2-Pyr) in $CD_2Cl_2$. The bottom spectrum is an expansion of the top spectrum.

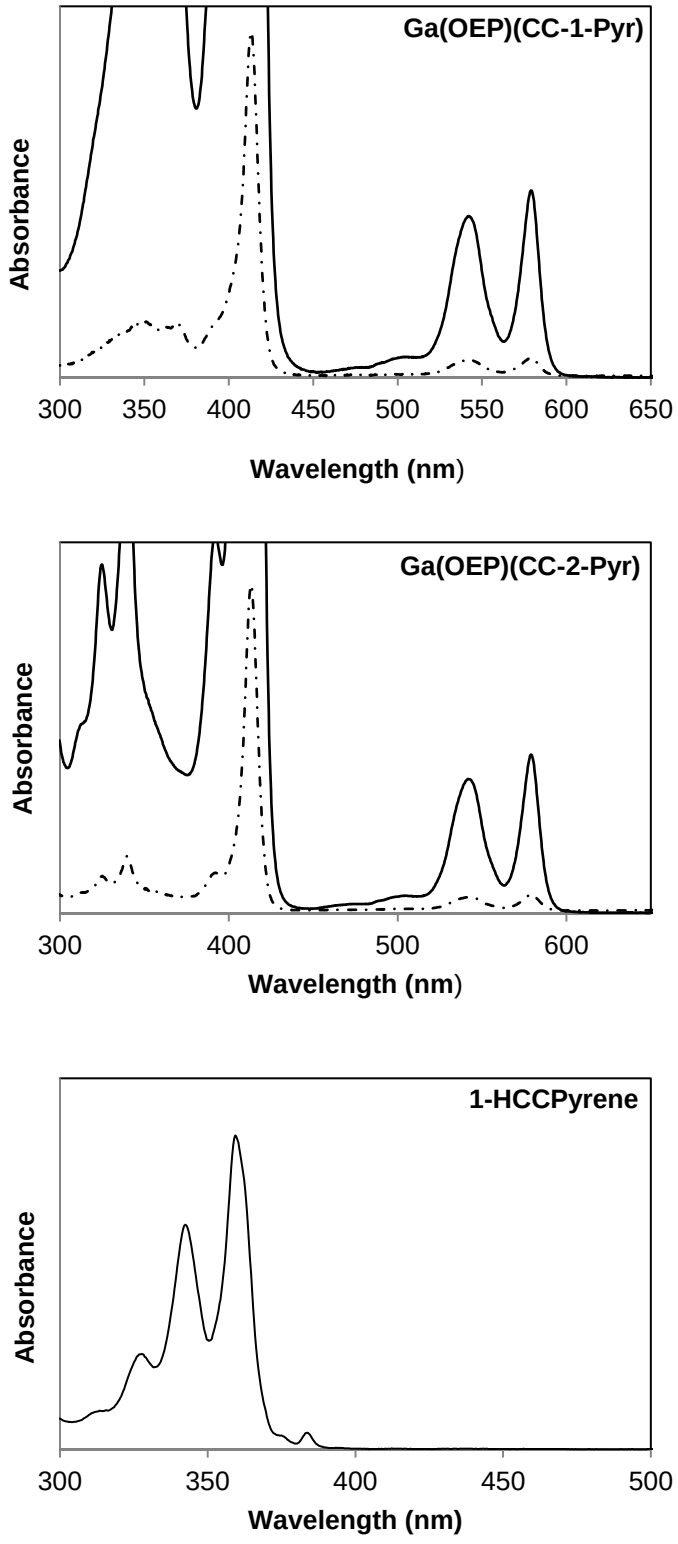


**Figure 6.22.** Electronic absorption spectra of Ga(OEP)(CCPyr) complexes and 1-ethynylpyrene precursor in toluene solutions. Dashed lines are 1 mm path length data and solid lines are 1 cm path length data.

## 6.4. Chapter 5 Supplementary Information

**6.4.1. General Procedures.** The general methods can be found in Section 6.1.1 with the following adaptations. Prior to use, commercial 9-bromoanthracene was purified by column chromatography (silica gel, hexanes) and commercial 1-pyrenecarboxylic acid was purified by column chromatography (silica gel, 5:1 ethyl acetate:acetonitrile followed by THF). Triethylamine was refluxed overnight over calcium hydride, distilled, and sparged with nitrogen prior to use. DME and $CD_2Cl_2$ were stored over 3Å molecular sieves under nitrogen. Except where noted, all syntheses were performed under a purified nitrogen atmosphere using standard Schlenk and glovebox techniques.

**6.4.2. Density Functional Theory (DFT) Calculations.** Density functional theory calculations were performed as described in Section 6.1.2. The B3P86 functional[7, 8] was used for all calculations. For gas-phase optimized geometries, the cc-pVTZ basis set[16, 18, 27] was employed for all atoms. For structures optimized in local minima with the ethyl chains rotated toward the axial ligand, the 6-31G* (H, C, N, O, S) and LANL2DZ effective core potential basis sets[15, 28] (Ga) were employed. Orbital energies were determined by running single-point calculations with keyword pop=full on optimized structures. Molecular models were built using the Materials Studio software.[29] Molecular orbital images were generated using the Avogadro software[33, 40] (isosurface value = 0.02).

**6.4.3. Scanning Tunneling Microscopy (STM) Sample Preparation.** STM samples were prepared as described in Section 6.3.3, with the following adaptations. The porphyrin complexes were studied at a concentration of 0.5 mM with the exception of Ga(OEP)(CCAnthr), whose saturation solubility in 1-phenyloctane is below this, and was therefore studied at 0.25 mM, and Ga(OEP)(CCTh) which was primarily studied at 0.75 mM.

**6.4.4. Scanning Tunneling Microscopy (STM) Analysis.** STM analysis was carried out as described in Section 6.3.4.

**6.4.5. Synthesis and Characterization.**

**Preparation of LiCC-3-thiophene.** This procedure was first reported in our lab by Mollye Levin[41] and was repeated as described below. To a stirred, clear yellow solution of 3-ethynylthiophene (100 μL, 1.015 mmol) in pentane (10 mL) at room temperature was added a solution of $^{n}$BuLi (300 μL, 2.5 M in hexanes, 0.750 mmol), immediately forming a yellow precipitate. After 0.5 hr, the suspension was filtered and washed several times with pentane to give the product as a dark yellow solid (0.028 g, 0.245 mmol, 33% yield).

**Preparation of Ga(OEP)(CC-3-thiophene).** This compound was first prepared by Mollye Levin;[41] the procedure was repeated and characterization data collected as reported below. To a stirred solution of Ga(OEP)Cl (0.050 g, 0.078 mmol) in THF (40 mL) at –78 °C was added a dark yellow solution of LiCC-3-thiophene (0.028 g, 0.245 mmol) in THF (6 mL). The reaction mixture was allowed to warm to room temperature, during which time the color changed slowly from dark pink to dark red-purple. After 2 h the volatile components were removed under vacuum, the remaining solid was extracted into toluene, and the solution was filtered through Celite. Removal of the solvent under vacuum provided the product as a dark pink solid (0.038 g, 0.054 mmol, 69% yield). $^{1}$H NMR ($CD_2Cl_2$, 500.13 MHz; see Figure 6.23): δ 10.35 (s, 4 H, *meso* H), 6.34 (dd, 1 H, aryl H), 5.58 (m, 1 H, aryl H), 5.26 (d, 1 H, aryl H), 4.21 (complex m, 16 H, $C\underline{H}_2CH_3$), 1.97 (t, 24 H, $CH_2C\underline{H}_3$). $^{13}C\{^{1}H\}$ NMR ($CD_2Cl_2$, 125.76 MHz; see Figure 6.24): δ 146.57 (*α*), 143.19 (*β*), 129.21 (thiophene), 126.08 (thiophene), 123.76 (thiophene), 122.33 (thiophene), 97.45 (*meso*), 89.54 (C≡C), 20.31 ($\underline{C}H_2CH_3$), 18.79 ($CH_2\underline{C}H_3$); one C≡C resonance not observed. LDI-TOF MS: *m/z* $[M]^+$ = 708.257, predicted = 708.278; $[M–CCTh]^+$ = 601.305.

UV-vis (toluene; $\lambda_{max}$, nm (rel. int.); see Figure 6.30): 341 (7.3), 392 (11.8), 413 (100), 505 (0.6), 542 (4.2), 579 (4.9).

**Preparation of 9-(Trimethylsilylethynyl)anthracene.** This procedure is a modification of a literature method.[42] To a stirred, room temperature solution of 9-bromoanthracene (0.504 g, 1.960 mmol), $Pd(PPh_3)_2Cl_2$ (0.057 g, 0.081 mmol), and CuI (0.059 g, 0.310 mmol) in triethylamine (15 mL), trimethylsilylacetylene (460 μL, 3.321 mmol) was added. Upon mixing at room temperature, the color of the reaction mixture changed from yellow to dark green to dark brown over several seconds. The reaction mixture was heated at 80 °C for 24 h, cooled to room temperature, opened to air, and reduced in vacuo to give a dark brown residue. This residue was purified on a silica gel column with hexanes as the eluent; removal of solvent provided the product as a pale yellow solid (0.073 g, 0.266 mmol, 14% yield). The $^1$H NMR data agree with those reported in the literature. $^1$H NMR ($CDCl_3$, 500.13 MHz): δ 8.56 (d, 2 H), 8.42 (s, 1 H), 8.00 (d, 2H), 7.59 (m, 2 H), 7.50 (m, 2 H), 0.43 (s, 9 H).

**Preparation of 9-Ethynylanthracene.** This procedure is a modification of a literature procedure.[36] A solution of 1-(trimethylsilylethynyl)pyrene (0.073 g, 0.266 mmol) and $(N^nBu_4)F•xH_2O$ (0.142 g, 0.476 mmol) in THF (15 mL) open to air was stirred at room temperature for 0.5 h, giving a clear, orange solution. Water (25 mL) was added, and the product extracted with dichloromethane (3 × 25 mL). The organic phase was dried with $MgSO_4$, filtered, and dried via rotary evaporation to provide the product as a pale yellow solid (0.065 g, 0.321 mmol, 121% yield). Note that the product becomes discolored within a day after deprotection and should be used immediately. We do not know the nature of the impurities that must be present in the product, based on the isolated yield, but the $^1$H NMR data agree with those

reported in the literature and do not show extraneous resonances. $^{1}$H NMR ($CDCl_3$, 500.13 MHz): δ 8.58 (d, 2 H), 8.48 (s, 1 H), 8.02 (d, 2H), 7.59 (m, 2 H), 7.51 (m, 2 H), 3.99 (s, 1 H).

**Preparation of 9-(LiCC)anthracene.** To a stirred, yellow solution of 9-ethynylanthracene (0.065 g, 0.321 mmol) in pentane (10 mL) at room temperature was added a solution of $^{n}$BuLi (240 μL, 1.6 M in hexanes, 0.384 mmol), immediately forming a yellow precipitate. After 0.5 h, the suspension was filtered and washed several times with pentane to give the product as a yellow-brown solid (0.037 g, 0.178 mmol, 55% yield).

**Preparation of Ga(OEP)(CC-9-anthracene).** To a stirred solution of Ga(OEP)Cl (0.047 g, 0.074 mmol) in THF (30 mL) at –78 °C was added a dark green solution of 9-(LiCC)anthracene (0.037 g, 0.178 mmol) in THF (3 mL). The reaction mixture was allowed to warm to room temperature, during which time the color changed slowly from dark pink to dark purple. After 2 h the volatile components were removed under vacuum, the remaining solid was extracted into toluene, and the solution was filtered through Celite. Removal of the solvent under vacuum provided a dark pink powder that was then recrystallized from toluene layered with pentane at −30 °C. This yielded the product as a dark pink solid (0.018 g, 0.023 mmol, 31% yield). $^{1}$H NMR ($CD_2Cl_2$, 500.13 MHz; see Figure 6.25): δ 10.47 (s, 4 H, *meso* H), 7.69 (s, 1 H, aryl H), 7.45 (d, 2 H, aryl H), 7.06 (m, 2 H, aryl H), 6.87 (m, 2 H, aryl H), 5.58 (d, 2 H, aryl H), 4.30 (complex m, 16 H, C<u>H2</u>$CH_3$), 2.03 (t, 24 H, $CH_2C$<u>H</u>$_3$). $^{13}$C{$^{1}$H} NMR ($CD_2Cl_2$, 125.76 MHz; see Figure 6.26): δ 146.66 (*α*), 143.25 (*β*), 131.16 (anthracene), 130.53 (anthracene), 127.93 (anthracene), 126.27 (anthracene), 125.17 (anthracene), 125.14 (anthracene), 125.10 (anthracene), 117.84 (anthracene), 97.46 (*meso*), 20.32 ($\underline{C}H_2CH_3$), 18.83 ($CH_2\underline{C}H_3$); C≡C resonances not observed. LDI-TOF MS: *m/z* $[M]^+$ = 802.366, predicted = 802.353; $[M–CCAnthr]^+$ = 601.344.

UV-vis (toluene; $\lambda_{max}$, nm (rel. int.); see Figure 6.30): 341 (7.9), 368 (sh) (6.3), 392 (14.8), 413 (100), 503 (0.6), 542 (4.3), 579 (5.2).

**Preparation of 9-(Trimethylsilylethynyl)triptycene.** This procedure is a modification of a literature procedure.[42] In a two-neck Schlenk flask, a clear orange solution of 9-(trimethylsilyl)anthracene (0.947 g, 3.45 mmol) in DME (25 mL) was brought to a gentle reflux. Solutions of isopentyl nitrite (3.7 mL, 27.541 mmol) in DME (2.3 mL) and anthranilic acid (2.851 g, 20.790 mmol) in DME (6 mL) were added over the course of 2.5 h via syringe pump, during which the solution turned dark orange. The reaction mixture was refluxed for 16 h, cooled to room temperature, and the volatile components were removed *in vacuo*, resulting in a viscous brown residue. The flask was opened to air and the product was extracted into several portions of boiling hexanes (10 × 20 mL). The volatile components were removed by rotary evaporation, resulting in an orange solid with a small amount of brown, high-boiling species; this high-boiling material was removed *in vacuo*. This material was purified by silica gel column chromatography with hexanes as the eluent followed by recrystallization from hexanes. This yielded the product as a white crystalline material (0.303 g, 0.864 mmol, 25% yield). The $^1$H NMR data agree with those reported in the literature. $^1$H NMR ($CDCl_3$, 500.13 MHz): δ 7.71 (m, 3 H), 7.37 (m, 3 H), 7.05 (complex m, 6 H), 5.40 (s, 1 H), 0.47 (s, 9 H).

**Preparation of 9-Ethynyltriptycene.** This procedure is a modification of a literature procedure.[42] To a stirred solution of 9-(trimethylsilyl)triptycene (0.303 g, 0.864 mmol) open to air at 0 °C in THF (20 mL) was added ($N^nBu_4$)F•x$H_2O$ (1 mL, 1.0 M in THF, 1.0 mmol). The solution was warmed to room temperature and stirred for an additional 1 h, during which the color of the clear, pale yellow solution was not observed to change. Diethyl ether (30 mL) was added to the solution and the organic mixture was washed with $H_2O$ (3 × 40 mL). The organic

phase was dried over $MgSO_4$, filtered, and reduced to dryness via rotary evaporation to give the crude product as a white solid. This solid was purified by silica gel chromatography with hexanes/dichloromethane (3:1) as the eluent to give the product as a white microcrystalline solid (0.248 g, 0.891 mmol, 103% yield). The $^1$H NMR data agree with those reported in the literature. $^1$H NMR ($CDCl_3$, 500.13 MHz): δ 7.75 (m, 3 H), 7.39 (m, 3 H), 7.05 (complex m, 6 H), 5.42 (s, 1 H), 3.28 (s, 1 H).

**Preparation of LiCCtriptycene.** This procedure is a modification of a literature procedure; the product was reported to precipitate out of THF upon addition of $^n$BuLi and this precipitate was used in the in situ synthesis of 9-(3-hydroxyprop-1-ynyl)triptycene.[42] To a stirred, colorless solution of 9-ethynyltriptycene (0.099 g, 0.356 mmol) in THF (10mL) at −78 °C was added a solution of $^n$BuLi (400 μL, 2.5 M in hexanes, 1.0 mmol), resulting in no visible change to the solution. The solution was warmed to room temperature and stirred for an additional 1 h, during which the solution turned pale yellow. The volatile components were removed *in vacuo*, resulting in a yellow oil. Pentane (20 mL) was added, resulting in a white precipitate. The suspension was filtered and washed several times with pentane to give the product as a white solid (0.079 g, 0.278 mmol, 78% yield).

**Preparation of Ga(OEP)(CC-9-triptycene).** To a stirred solution of Ga(OEP)Cl (0.051 g, 0.080 mmol) in THF (40 mL) at –78 °C was added a colorless solution of LiCC-triptycene (0.037 g, 0.130 mmol) in THF (6 mL). The reaction mixture was allowed to warm to room temperature, during which time the color changed slowly from dark pink to dark purple. After 2 h the volatile components were removed under vacuum, the remaining solid was extracted into toluene, and the solution was filtered through Celite. Removal of the solvent under vacuum provided a dark purple powder that was then recrystallized from toluene at −30 °C. This yielded

the product as a dark pink solid (0.014 g, 0.016 mmol, 20% yield). $^{1}$H NMR ($C_6D_6$, 500.13 MHz; see Figure 6.27): δ 10.47 (s, 4 H, *meso* H), 6.59 (d, 3 H, aryl H), 6.43 (m, 3H, aryl H), 6.32 (m, 3 H, aryl H), 5.13 (d, 3 H, aryl H), 4.44 (s, 1 H, bridgehead H), 4.02 (complex m, 16 H, C$\underline{H}_2$CH$_3$), 1.86 (t, 24 H, CH$_2$C$\underline{H}_3$). $^{13}$C{$^{1}$H} NMR ($CD_2Cl_2$, 125.78 MHz; see Figure 6.28): δ 146.64 (*α*), 143.87 (triptycene), 143.82 (triptycene), 143.24 (*β*), 124.84 (triptycene), 124.56 (triptycene), 122.58 (triptycene), 121.55 (triptycene), 97.42 (*meso*), 52.51 (bridgehead C), 20.30 ($\underline{C}$H$_2$CH$_3$), 18.87 (CH$_2\underline{C}$H$_3$); C≡C resonances and one bridgehead C not observed. LDI-TOF MS: *m/z* $[M]^+$ = 878.281, predicted = 878.384; $[M–CCTrip]^+$ = 601.268. UV-vis (toluene; $\lambda_{max}$, nm (rel. int.; see Figure 6.30): 324 (sh) (7.2), 339 (5.1), 362 (sh) (4.8), 392 (11.9), 413 (100), 503 (0.5), 542 (4.1), 579 (4.8).

**Preparation of Ga(OEP)(O$_2$CPyrene).** In a reaction open to air, Ga(OEP)Cl (0.063 g, 0.099 mmol) was dissolved in dichloromethane (15 mL). To this, an aqueous solution of sodium hydroxide was added (2 M, 15 mL) and the suspension was vigorously stirred for 2.5 h at room temperature. The organic phase was extracted and washed with water (3 × 30 mL). It was further dried with $MgSO_4$, filtered, and dried via rotary evaporation to give a dark pink solid (Ga(OEP)(OH)), 0.049 g, 0.079 mmol, 80% yield) which was taken into the glovebox. The Ga(OEP)(OH) was dissolved in THF (20 mL) and to this, 1-pyrenecarboxylic acid (0.029 g, 0.118 mmol) in THF (5 mL) was added. The solution was stirred for 2 h at room temperature, during which time the dark pink solution was observed to darken slightly. The volatile components were removed *in vacuo*, resulting in a dark pink powder with a small amount of unreacted pyrenecarboxylic acid remaining (40.1 mg, 60% crude yield). Attempts to remove this impurity have been unsuccessful to this point. $^{1}$H NMR ($C_6D_6$, 500.13 MHz, see Figure 6.29): δ 10.51 (s, 4 H, *meso* H), 7.70 (d, 1 H, pyrenyl H), 7.57 (d, 1 H, pyrenyl H), 7.51 (t, 1 H, pyrenyl

H), 7.31 (m, 2 H, pyrenyl H), 7.01 (d, 1 H, pyrenyl H), 6.59 (d, 1 H, pyrenyl H), 5.96 (m, 1 H, pyrenyl H), 4.02 (complex m, 16 H, $C\underline{H}_2CH_3$), 1.87 (t, 24 H, $CH_2C\underline{H}_3$).

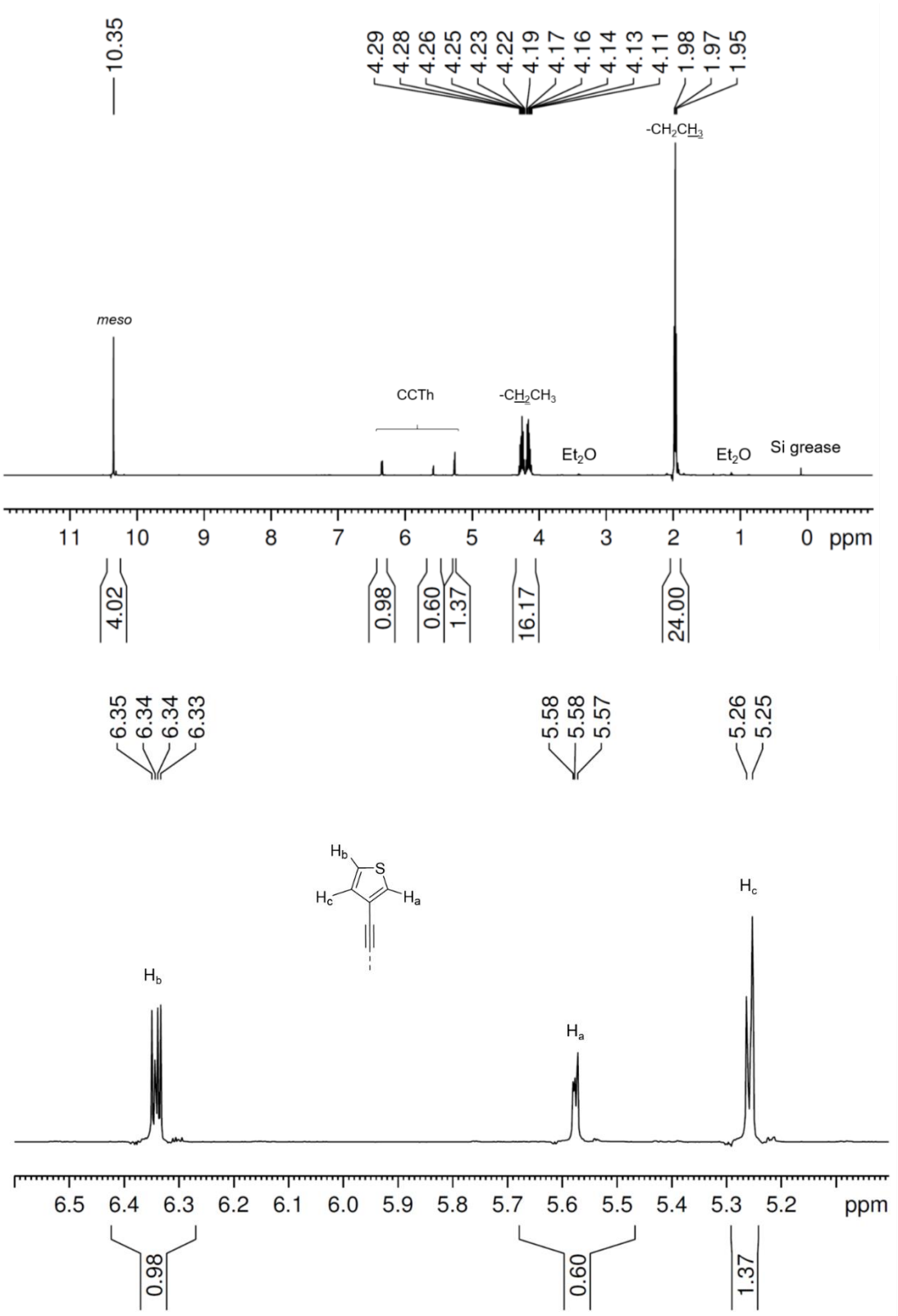


**Figure 6.23.** $^{1}$H NMR spectrum of Ga(OEP)(CCTh) in $CD_2Cl_2$. The bottom spectrum is an expansion of the top spectrum.

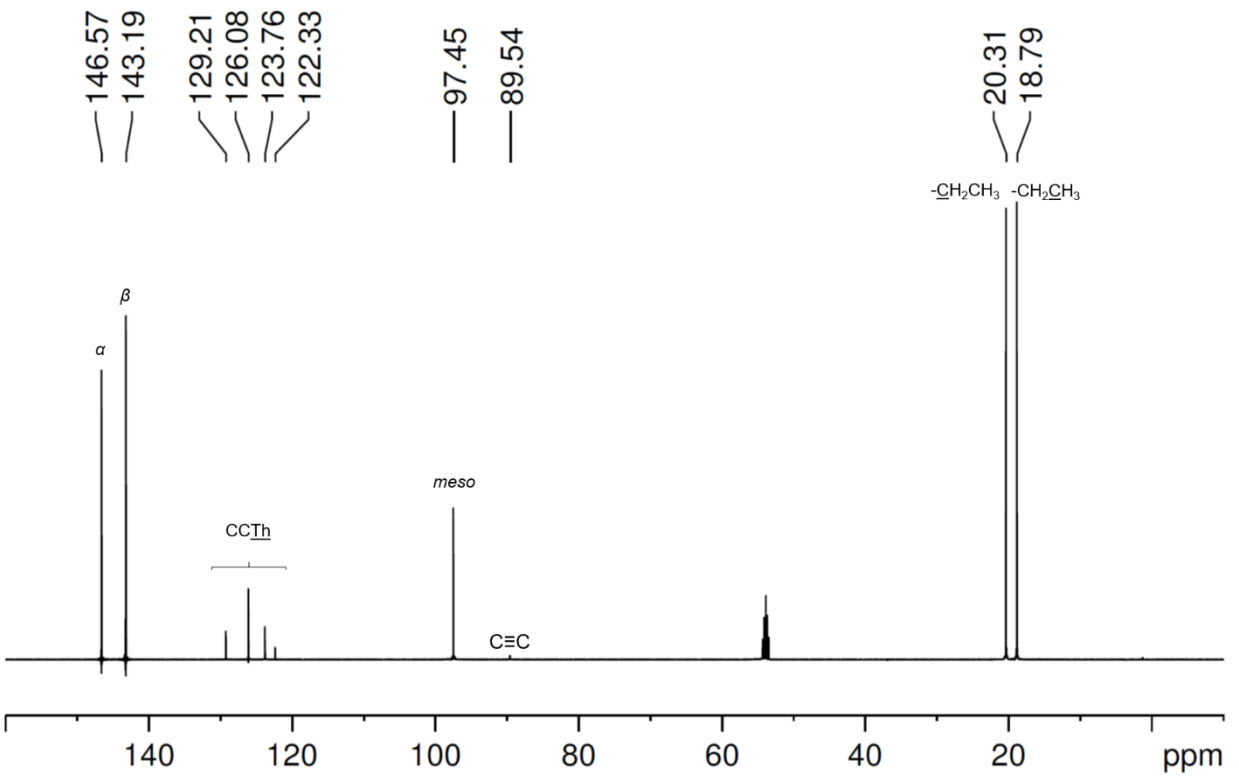


**Figure 6.24.** $^{13}C\{^{1}H\}$ NMR spectrum of Ga(OEP)(CCTh) in $CD_2Cl_2$.

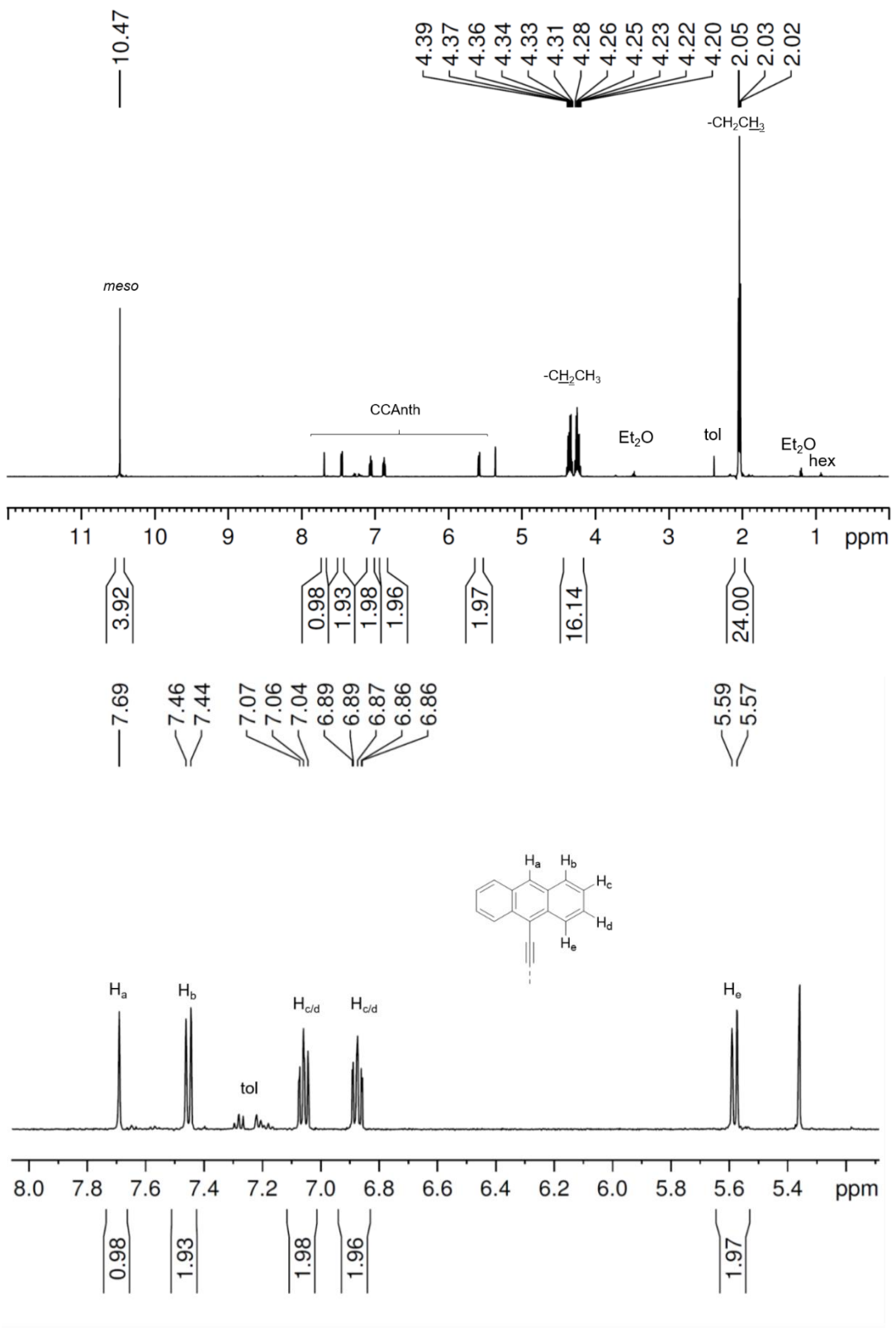


**Figure 6.25.** $^{1}$H NMR spectrum of Ga(OEP)(CCAnthr) in $CD_2Cl_2$. The bottom spectrum is an expansion of the top spectrum.

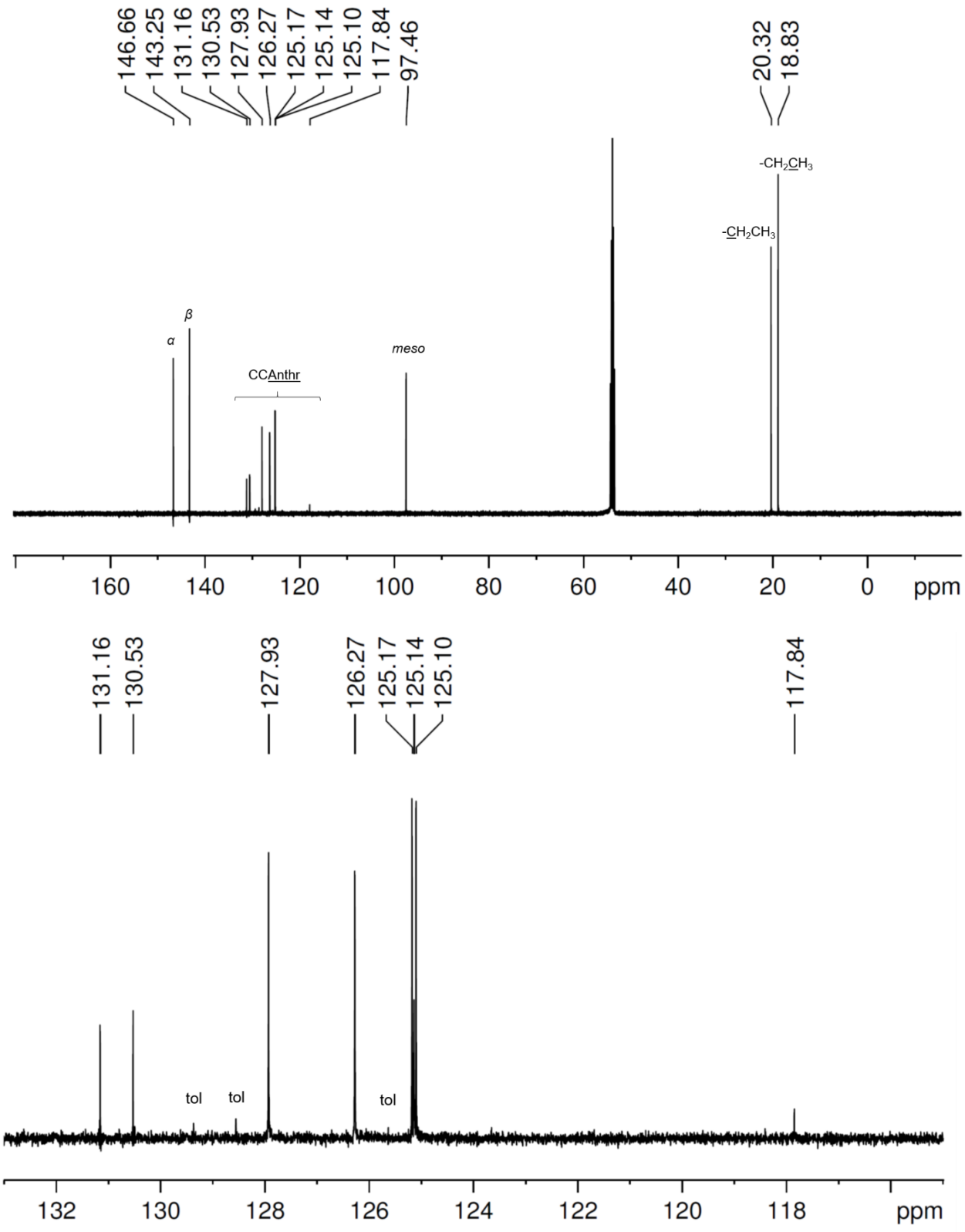


**Figure 6.26.** $^{13}C\{^{1}H\}$ NMR spectrum of Ga(OEP)(CCAnthr) in $CD_2Cl_2$. The bottom spectrum is an expansion of the top spectrum.

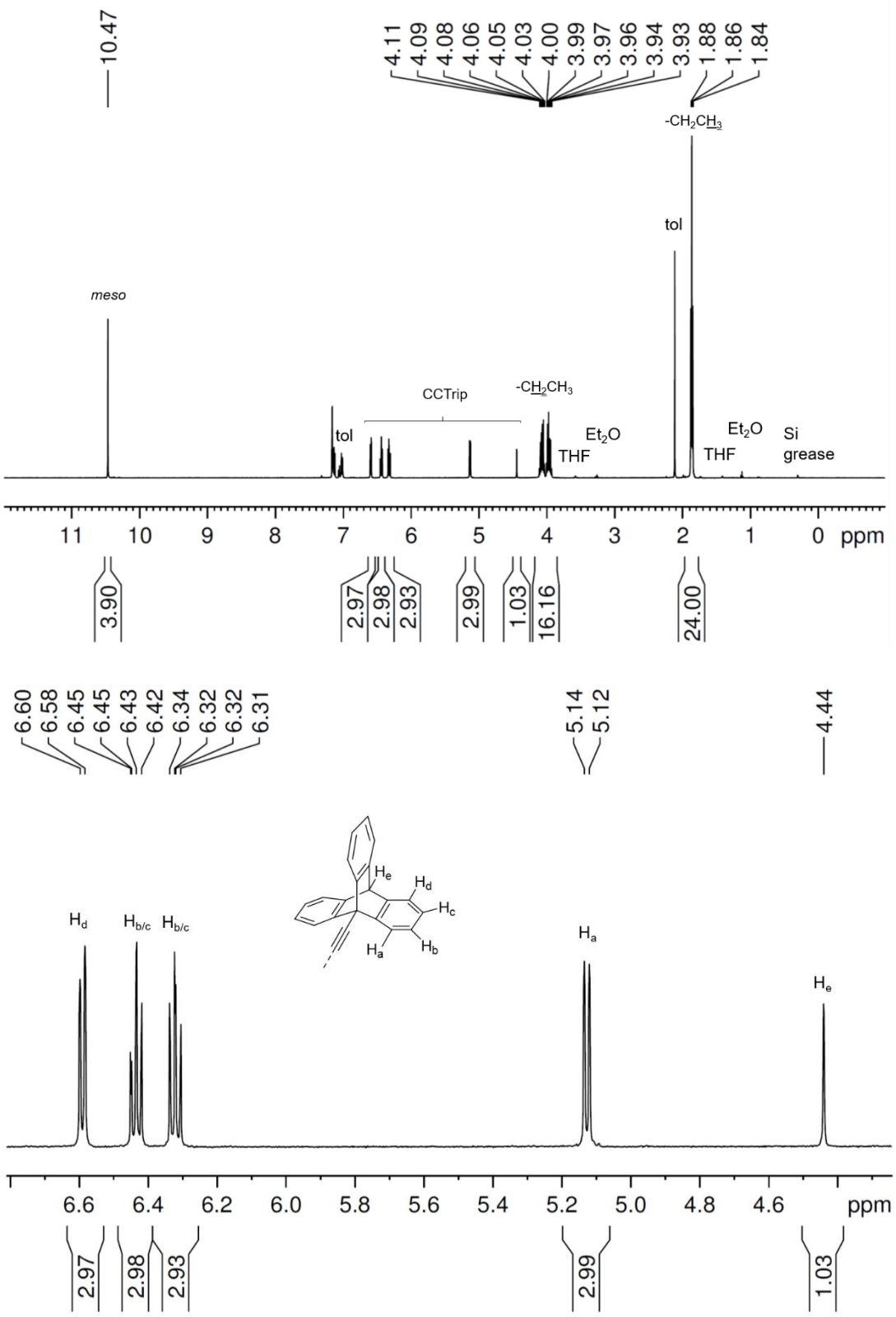


**Figure 6.27.** $^{1}$H NMR spectrum of Ga(OEP)(CCTrip) in $C_6D_6$. The bottom spectrum is an expansion of the top spectrum.

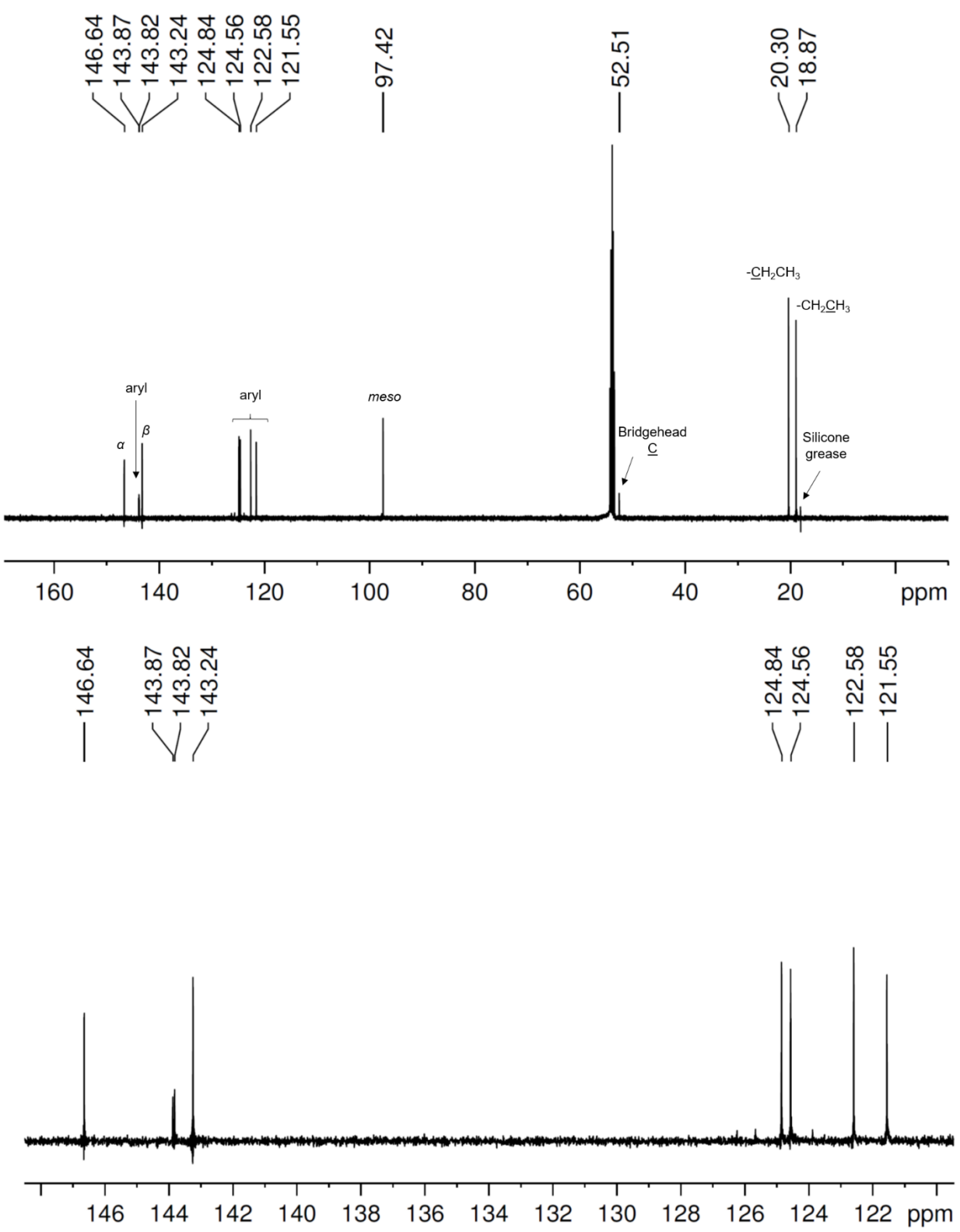


**Figure 6.28.** $^{13}C\{^{1}H\}$ NMR spectrum of Ga(OEP)(CCTrip) in $CD_2Cl_2$. The bottom spectrum is an expansion of the top spectrum.

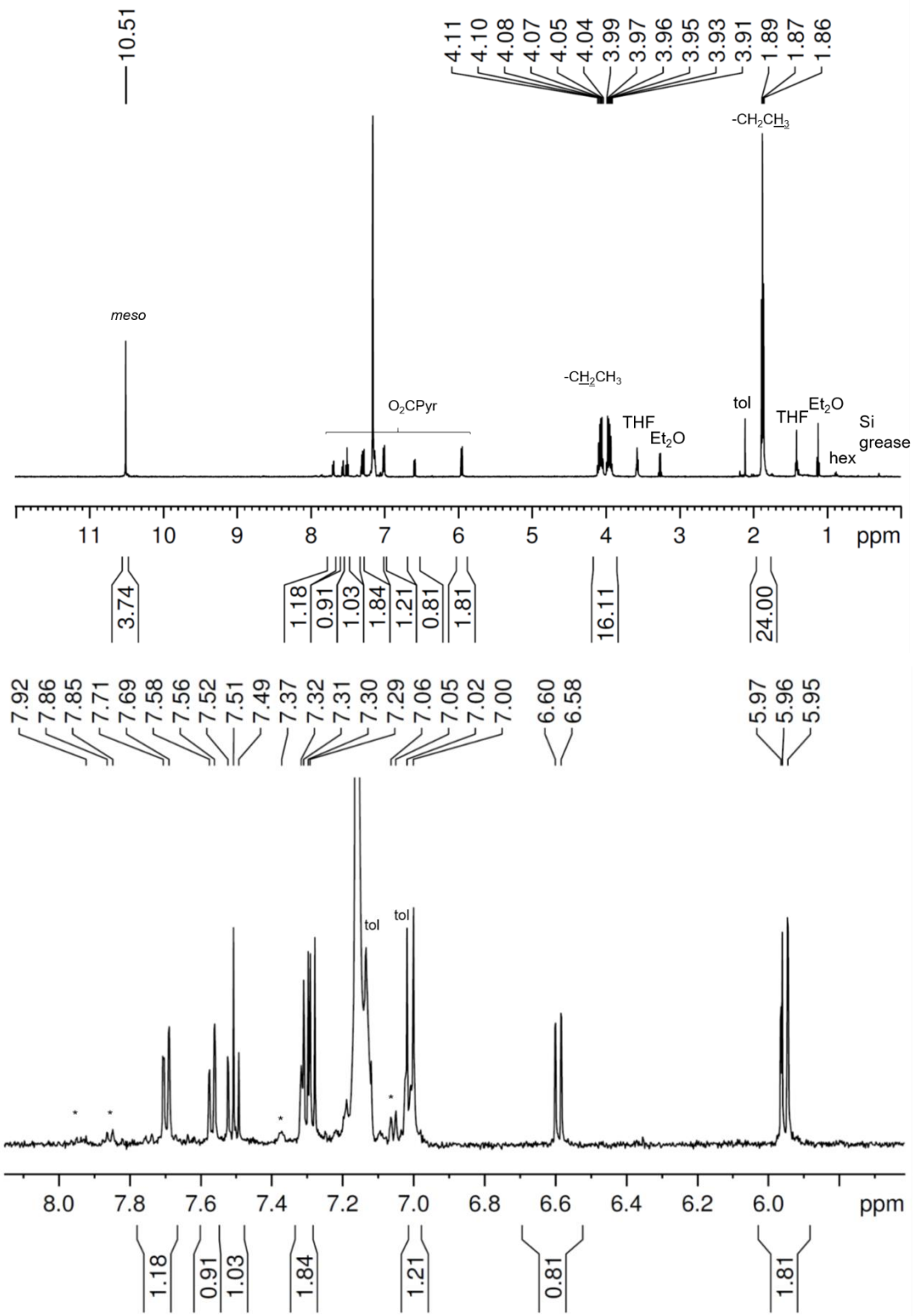


**Figure 6.29.** $^{1}$H NMR spectrum of Ga(OEP)($O_2$CPyr) in $C_6D_6$. The bottom spectrum is an expansion of the top spectrum. Resonances marked with an * are unreacted 1-pyrenecarboxylic acid.

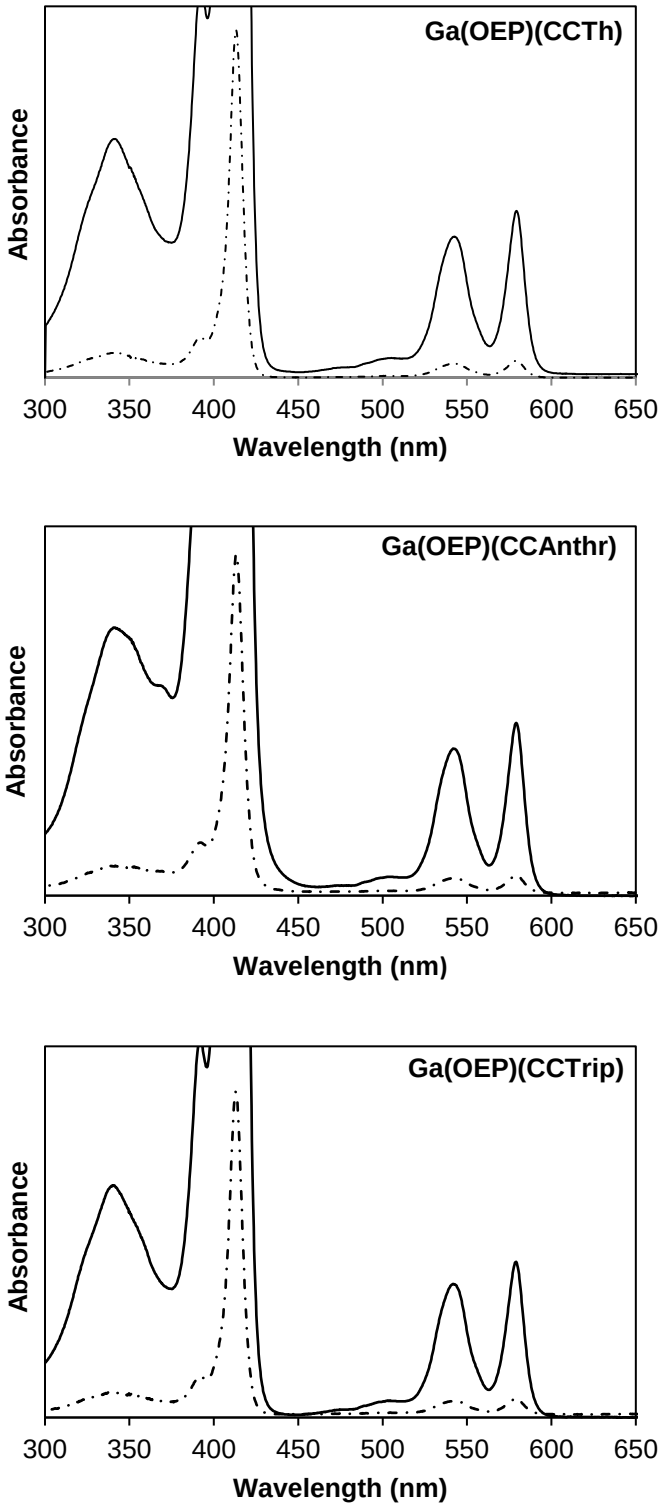


**Figure 6.30.** Electronic-absorption spectra of Ga(OEP)(CCR) complexes in toluene solution at room temperature.

## 6.5. References.


1. Pangborn, A. B.; Giardello, M. A.; Grubbs, R. H.; Rosen, R. K.; Timmers, F. J. Safe and Convenient Procedure for Solvent Purification. *Organometallics* **1996**, *15*, 1518-1520.

2. Coutsolelos, A.; Guilard, R.; Bayeul, D.; Lecomte, C. Gallium(III) Porphyrins - Synthesis and Physicochemical Characteristics of Halogeno Gallium(III) Porphyrins X-Ray Crystal-Structure of Chloro-(5,10,15,20-Tetraphenylporphyrinato) Gallium(III). *Polyhedron* **1986**, *5*, 1157-1164.

3. Brandsma, L., *Preparative Acetylenic Chemistry*. 2nd ed.; Elsevier: New York, 1988; pp 13-15.

4. Fulmer, G. R.; Miller, A. J. M.; Sherden, N. H.; Gottlieb, H. E.; Nudelman, A.; Stoltz, B. M.; Bercaw, J. E.; Goldberg, K. I. NMR Chemical Shifts of Trace Impurities: Common Laboratory Solvents, Organics, and Gases in Deuterated Solvents Relevant to the Organometallic Chemist. *Organometallics* **2010**, *29*, 2176-2179.

5. Kudernac, T.; Lei, S. B.; Elemans, J. A. A. W.; De Feyter, S. Two-Dimensional Supramolecular Self-Assembly: Nanoporous Networks on Surfaces. *Chem. Soc. Rev.* **2009**, *38*, 402-421.

6. Brancato-Buentello, K. E.; Coutsolelos, A. G.; Scheidt, W. R. Chloro(2,3,7,8,12,13,17,18-octaethylporphinato)gallium(III). *Acta Crystallogr., Sect. C: Cryst. Struct. Commun.* **1996**, *52*, 2707-2710.

7. Becke, A. D. Density-Functional Thermochemistry. III. The Role of Exact Exchange. *J. Chem. Phys.* **1993**, *98*, 5648-5652.

8. Perdew, J. P. Density-Functional Approximation for the Correlation-Energy of the Inhomogeneous Electron-Gas. *Phys. Rev. B* **1986**, *33*, 8822-8824.

9. Girichev, G. V.; Giricheva, N. I.; Koifman, O. I.; Minenkov, Y. V.; Pogonin, A. E.; Semeikin, A. S.; Shlykov, S. A. Molecular Structure and Bonding in Octamethylporphyrin Tin(II), $SnN_4C_{28}H_{28}$. *Dalton Trans.* **2012**, *41*, 7550-7558.

10. Barbe, J. M.; Ratti, C.; Richard, P.; Lecomte, C.; Gerardin, R.; Guilard, R. Tin(II) Porphyrins: Synthesis and Spectroscopic Properties of a Series of Divalent Tin Porphyrins. X-Ray Crystal-Structure of (2,3,7,8,12,13,17,18-Octaethylporphinato)Tin(II). *Inorg. Chem.* **1990**, *29*, 4126-4130.

11. Lee, C. T.; Yang, W. T.; Parr, R. G. Development of the Colle-Salvetti Correlation-Energy Formula into a Functional of the Electron-Density. *Phys. Rev. B* **1988**, *37*, 785-789.

12. Vosko, S. H.; Wilk, L.; Nusair, M. Accurate Spin-Dependent Electron Liquid Correlation Energies for Local Spin-Density Calculations - A Critical Analysis. *Can. J. Phys.* **1980**, *58*, 1200-1211.

13. Stephens, P. J.; Devlin, F. J.; Chabalowski, C. F.; Frisch, M. J. Ab Initio Calculation of Vibrational Absorption and Circular-Dichroism Spectra Using Density-Functional Force-Fields. *J. Phys. Chem.* **1994**, *98*, 11623-11627.

14. Becke, A. D. Density-Functional Exchange-Energy Approximation with Correct Asymptotic-Behavior. *Phys. Rev. A* **1988**, *38*, 3098-3100.

15. Wadt, W. R.; Hay, P. J. Ab Initio Effective Core Potentials for Molecular Calculations - Potentials for Main Group Elements Na to Bi. *J. Chem. Phys.* **1985**, *82*, 284-298.

16. Dunning, T. H. Gaussian Basis Sets for Use in Correlated Molecular Calculations. I. The Atoms Boron through Neon and Hydrogen. *J. Chem. Phys.* **1989**, *90*, 1007-1023.

17. Woon, D. E.; Dunning, T. H. Gaussian Basis Sets for Use in Correlated Molecular Calculations. III. The Atoms Aluminum through Argon. *J. Chem. Phys.* **1993**, *98*, 1358-1371.

18. Wilson, A. K.; Woon, D. E.; Peterson, K. A.; Dunning, T. H. Gaussian Basis Sets for Use in Correlated Molecular Calculations. IX. The Atoms Gallium through Krypton. *J. Chem. Phys.* **1999**, *110*, 7667-7676.

19. Peterson, K. A.; Shepler, B. C.; Figgen, D.; Stoll, H. On the Spectroscopic and Thermochemical Properties of ClO, BrO, IO, and Their Anions. *J. Phys. Chem. A* **2006**, *110*, 13877-13883.

20. *SPIP Software*, Version 6.0.9; Image Metrology A/S: Hørsholm, Denmark.

21. Horcas, I.; Fernandez, R.; Gomez-Rodriguez, J. M.; Colchero, J.; Gomez-Herrero, J.; Baro, A. M. WSXM: A Software for Scanning Probe Microscopy and a Tool for Nanotechnology. *Rev. Sci. Instrum.* **2007**, *78*, 013705.

22. Boukhris, A.; Lecomte, C.; Coutsolelos, A.; Guilard, R. Alkylsulfonato(Porphyrinato)Gallium(III): Crystal-Structure Determination of Methylsulfonato(Octaethyl-2,3,7,8,12,13,17,18-Porphyrinato)-Gallium(III). *J. Organomet. Chem.* **1986**, *303*, 151-165.

23. Ohno, O.; Kaizu, Y.; Kobayashi, H. Luminescence of Some Metalloporphins Including the Complexes of the IIIb Metal Group. *J. Chem. Phys.* **1985**, *82*, 1779-1787.

24. Kadish, K. M.; Boisselier-Cocolios, B.; Coutsolelos, A.; Mitaine, P.; Guilard, R. Electrochemistry and Spectroelectrochemistry of Gallium(III) Porphyrins - Redox Properties of 5-Coordinate Ionic and σ-Bonded Complexes. *Inorg. Chem.* **1985**, *24*, 4521-4528.

25. Kadish, K. M.; Maiya, G. B.; Xu, Q. Y. Photoreactivity of σ-Bonded Metalloporphyrins. 1. Formation of Zwitterionic Indium and Gallium Porphyrin Complexes in Tetrahydrofuran. *Inorg. Chem.* **1989**, *28*, 2518-2523.

26. Nomoto, A.; Shiino, G.; Ogawa, A. Palladium-Catalyzed Regioselective Introduction of Chalcogen Moieties into Porphyrin Bearing an Ethynyl Group. *Res. Chem. Intermed.* **2009**, *35*, 965-971.

27. Balabanov, N. B.; Peterson, K. A. Systematically Convergent Basis Sets for Transition Metals. I. All-Electron Correlation Consistent Basis Sets for the 3d Dlements Sc-Zn. *J. Chem. Phys.* **2005**, *123*.

28. Hay, P. J.; Wadt, W. R. Abinitio Effective Core Potentials for Molecular Calculations - Potentials for the Transition-Metal Atoms Sc to Hg. *J. Chem. Phys.* **1985**, *82*, 270-283.

29. *Materials Studio 7.0*, Accelrys, Inc.: San Diego, CA, 2013.

30. Yuan, Z.; Taylor, N. J.; Sun, Y.; Marder, T. B.; Williams, I. D.; Cheng, L. T. Synthesis and 2nd-Order Nonlinear-Optical Properties of Three Coordinate Organoboranes with Diphenylphosphino and Ferrocenyl Groups as Electron-Donors: Crystal and Molecular Structures of (E)-D-CH=CH-B(mes)$_2$ and D-C$\equiv$C-B(mes)$_2$ [D=P($C_6H_5$)$_2$, ($\eta$-$C_5H_5$)Fe($\eta$-$C_5H_4$); mes=2,4,6-($CH_3$)$_3$$C_6H_2$]. *J. Organomet. Chem.* **1993**, *449*, 27-37.

31. Parzuchowski, P. G.; Kampf, J. W.; Rozniecka, E.; Kondratenko, Y.; Malinowska, E.; Meyerhoff, M. E. Gallium(III) and Indium(III) Octaethylporphyrin Dimeric Complexes with a Single μ-Hydroxo Bridge: Synthesis, Structure and Stability in Anion-Containing Organic Media. *Inorg. Chim. Acta* **2003**, *355*, 302-313.

32. Lau, W.-Y. Ph. D. Thesis. The University of Chicago, Chicago, IL, 2016.

33. Hanwell, M. D.; Curtis, D. E.; Lonie, D. C.; Vandermeersch, T.; Zurek, E.; Hutchison, G. R. Avogadro: An Advanced Semantic Chemical Editor, Visualization, and Analysis Platform. *J. Cheminf.* **2012**, *4*.

34. Avogadro: An Open-Source Molecular Builder and Visualization Tool. Version 1.2.0. http://avogadro.cc/.

35. Kanai, M.; Hirano, T.; Azumaya, I.; Okamoto, I.; Kagechika, H.; Tanatani, A. Solvent-Dependent Conformational and Fluorescence Change of an *N*-Phenylbenzohydroxamic Acid Derivative Bearing Two Pyrene Moieties. *Tetrahedron* **2012**, *68*, 2778-2783.

36. Keller, S.; Yi, C. Y.; Li, C.; Liu, S.-X.; Blum, C.; Frei, G.; Sereda, O.; Neels, A.; Wandlowski, T.; Decurtins, S. Synthesis, Structures, Redox and Photophysical Properties of Benzodifuran-Functionalised Pyrene and Anthracene Fluorophores. *Org. Biomol. Chem.* **2011**, *9*, 6410-6416.

37. Crawford, A. G.; Liu, Z. Q.; Mkhalid, I. A. I.; Thibault, M. H.; Schwarz, N.; Alcaraz, G.; Steffen, A.; Collings, J. C.; Batsanov, A. S.; Howard, J. A. K.; Marder, T. B. Synthesis of 2-and 2,7-Functionalized Pyrene Derivatives: An Application of Selective C-H Borylation. *Chem.-Eur. J.* **2012**, *18*, 5022-5035.

38. Foroozesh, M.; Primrose, G.; Guo, Z. Y.; Bell, L. C.; Alworth, W. L.; Guengerich, F. P. Aryl acetylenes as mechanism-based inhibitors of cytochrome P450-dependent monooxygenase enzymes. *Chemical Research in Toxicology* **1997**, *10*, 91-102.

39. Jing, L.; Liang, C.; Shi, X. H.; Ye, S. Q.; Xian, Y. Z. Fluorescent probe for Fe(III) based on pyrene grafted multiwalled carbon nanotubes by click reaction. *Analyst* **2012**, *137*, 1718-1722.

40. Coenen, M. J. J.; Cremers, M.; den Boer, D.; van den Bruele, F. J.; Khoury, T.; Sintic, M.; Crossley, M. J.; van Enckevort, W. J. P.; Hendriksen, B. L. M.; Elemans, J. A. A. W.; Speller, S. Little Exchange at the Liquid/Solid Interface: Defect-Mediated Equilibration of Physisorbed Porphyrin Monolayers. *Chem. Commun.* **2011**, *47*, 9666–9668.

41. Levin, M. S. Senior Thesis. The University of Chicago, Chicago, IL, 2014.

42. Kaleta, J.; Kaletova, E.; Cisarova, I.; Teat, S. J.; Michl, J. Synthesis of Triptycene-Based Molecular Rotors for Langmuir-Blodgett Monolayers. *J. Org. Chem.* **2015**, *80*, 10134-10150.

# APPENDIX

## Scanning Tunneling Microsopy Studies of Metalloporphyrins Under Ambient Conditions on Graphene and Monolayer $MoS_2$

### A.1. Introduction

Throughout this work, we have demonstrated that M(OEP) complexes generally assemble into robust, widespread monolayers on HOPG at the solid-liquid interface, giving an invariant pseudo-hexagonal unit cell despite functionalization with a variety of axial ligands and co-deposition with guest fullerene molecules. Our sole substrate for these investigations to this point has been highly oriented pyrolytic graphite (HOPG) both due to the ease of preparing the substrate with adhesive tape, and porphyrins' well-documented affinity for assembly on graphite due to the favorable π-stacking interactions.[1-3] However, as the substrate plays an integral role in interfacing an assembly to its surrounding environment, and the substrate can have a pronounced effect on a monolayer's self-assembled structure,[4, 5] we are interested in what, if any, effects that alternative substrates will have on the self-assembly of our M(OEP) system.

In this study, we focus on two atomically thin materials in particular: single layer graphene (SLG) and monolayer $MoS_2$. Such atomically thin materials have been investigated for incorporation into devices due to their unique properties that differ markedly from those of the bulk materials. Graphene has a wealth of exceptional properties such as its mechanical strength, high conductivity, and near transparency.[6, 7] However, the lack of a band gap in pristine graphene has led researchers to turn to alternative materials such as monolayer transition metal dichalcogenides for study.[8, 9] Monolayer $MoS_2$ has a band gap that shifts more than 0.6 eV compared to that of the bulk material, and drastically increased quantum yields, making it an intriguing candidate for incorporation into electronic and light-harvesting devices.[8, 10] There are

limited reports of STM studies of monolayer $MoS_2$ in the literature, largely due to limitations in methods of growth or exfoliation of defect-free sheets of suitable size on conductive substrates.[11-17]

The Park lab has developed an improved method of growing monolayer transition metal dichalcogenides (TMDs) on $SiO_2$ by metal–organic chemical vapor deposition.[18] By carefully controlling the concentration and flow rate of the components, control over the grain size can be accomplished, with grain sizes over 10 μm acheived;[18] further, these substrates are able to be transferred to conductive surfaces suitable for STM imaging. In collaboration with them, we hoped to determine if we can functionalize these unique substrates with porphyrin monolayers, and if varying the substrate affects the assembly of our monolayers. In this appendix, we report the preliminary results of the deposition and STM imaging of the well-studied Ni(OEP) on atomically thin substrates SLG/Cu foil and monolayer $MoS_2$/Au/silica at the solid-liquid interface. The five-coordinate Ga(OEP)Cl assembly behavior on monolayer $MoS_2$ was also studied.

**A.2. Scanning Tunneling Microscopy (STM) Sample Preparation**

All substrates used in this study were provided by the lab of Professor Jiwoong Park. Graphene was deposited on polycrystalline copper foil by chemical vapor deposition. The foil was mechanically cut with scissors to give samples of approximately 0.75 cm × 0.75 cm. Monolayer $MoS_2$ was grown on a fused silica substrate by metal–organic chemical vapor deposition methods developed in the Park lab.[18] The $MoS_2$ was delaminated from the fused silica by immersion in water and transferred to a wafer of a thin film gold (~100 nm) on fused silica. These wafers were cut with a diamond-tipped pen to give chips of roughly 0.75 cm × 0.75 cm. The samples were then mounted to 12 mm diameter metal specimen discs with colloidal silver

paste (PELCO, Ted Pella, Inc.), ensuring contact is made between the gold and disc with the paste. Porphyrin solutions in 1-phenyloctane were prepared and deposited on the surface as described in Section 6.1.3; all compounds in this appendix were studied at a concentration of 0.5 mM.

### A.3. Scanning Tunneling Microscopy (STM) Measurements

STM measurements were performed as described in Section 6.1.4, with the following adaptations. Where possible for the samples, images of the underlying substrate (graphene, $MoS_2$) were acquired, and the data for the porphyrin overlayers were corrected post-acquisition for instrument drift in the SPIP software package[3] using the substrate lattice parameters as a reference.[19] For Ni(OEP) on graphene/Cu foil, the average distances of 50 sets of five consecutive porphyrin molecules in each scan direction was used instead of 100.

### A.4. Results and Discussion

**A.4.1. STM Studies of Ni(OEP) on Graphene/Cu Foil.** Initial STM investigations of samples of SLG deposited on polycrystalline copper foil showed that the substrate itself has widespread variability in the topography of the surface (Figure A.1). Though relatively large regions of smooth substrate are observed (Figure A.1a), this was not consistent from region to region and from sample to sample, and some regions appeared rough and unsuitable for observing monolayer formation (Figure A.1d). This variable topography of SLG on copper foil is consistent with previous STM studies performed at the solid-liquid interface.[20] The atomic structure of the graphene can be resolved, and is similar in appearance to that of HOPG (Figure A.2). While subtle differences in the HOPG and SLG can potentially be observed as HOPG is comprised of ABAB stacks of $sp^3$ hybridized carbon, and graphene has only a single sheet, resolving these will be dependent on tip quality and imaging conditions; the overall lattice

structure should be the same.[20, 21] Good resolution of the underlying substrate lattice is critical for the proper calibration of data when accounting for instrument drift.

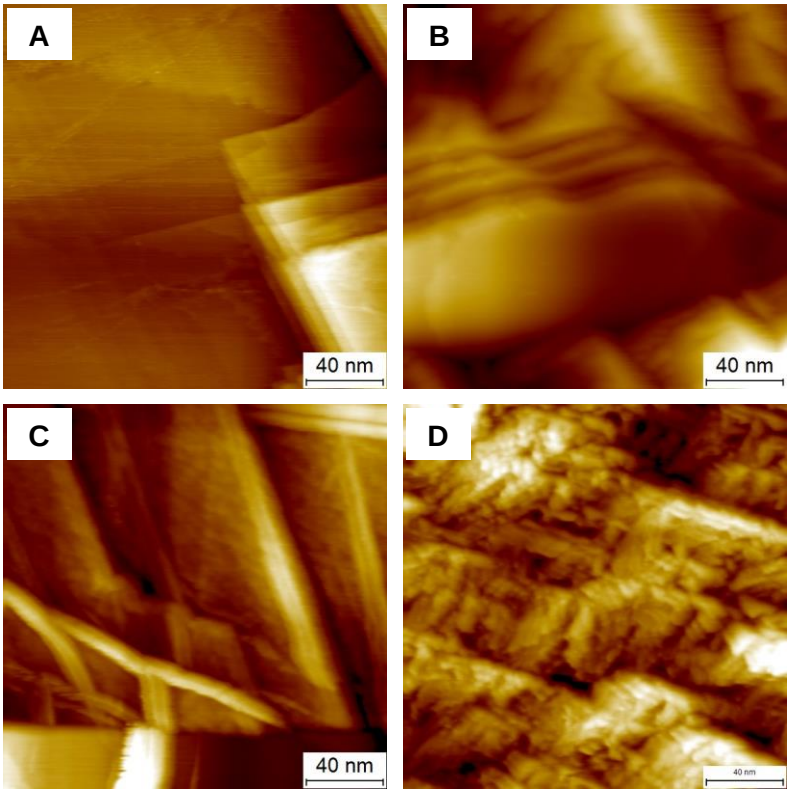


**Figure A.1.** Large-scale STM images of graphene on polycrystalline copper foil showing a high degree of variability in surface topography. The images were acquired at (A): $I$ = 8 pA, $V$ = –500 mV; (B): $I$ = 5 pA, $V$ = –500 mV; (C): $I$ = 10 pA, $V$ = –500 mV; (D): $I$ = 10 pA, $V$ = –500 mV.

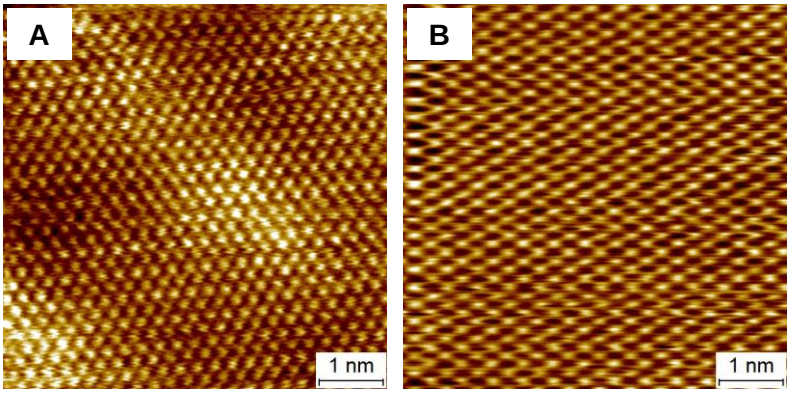


**Figure A.2.** STM images of the atomic structure of (A) graphene on Cu foil and (B) HOPG. The images were acquired at (A): $I$ = 120 pA, $V$ = –30 mV; (B): $I$ = 60 pA, $V$ = +2 mV.

A 0.5 mM solution of Ni(OEP) in 1-phenyloctane was deposited on the graphene substrate and the resulting array imaged at the solid-liquid interface. Due to the uneven macroscale structure of the underlying substrate, only small-scale images have been obtained. However, it is observed that monolayer assembly is occurring, with arrays spanning roughly 20 nm in width (Figure A.3a). As is the case with HOPG, the porphyrin macrocycle can be imaged (Figure A.3b), confirming that the porphyrins are assembling parallel to the surface. Further, we observed that the compound assembles on this substrate with lattice parameters that are indistinguishable from those on HOPG: $a$ = 1.38 (0.05) nm, $b$ = 1.34 (0.06) nm, Γ= 67 (2)°. A similar retention of lattice parameters between graphite and graphene/Cu foil has been observed for monolayers of trimesic acid at the solid-liquid interface.[20] From this, we conclude that any potential substrate-influence on the lattice is not enough to overcome the intermolecular interactions in the OEP unit cell. It is assumed that other OEPs will assemble similarly.

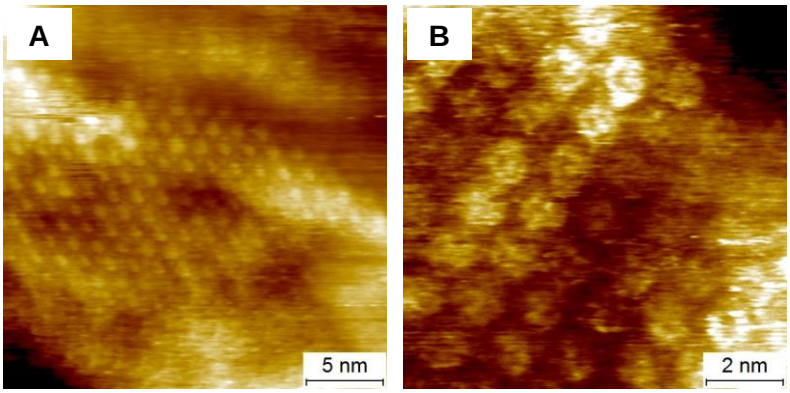


**Figure A.3.** STM images of Ni(OEP) deposited on graphene/Cu foil at the solid-liquid interface (0.5 mM, 1-phenyloctane). The images were acquired at (A): $I$ = 10 pA, $V$ = –500 mV; (B): $I$ = 15 pA, $V$ = –500 mV.

**A.4.2. STM Studies of Monolayer $MoS_2$.** Large-scale images of monolayer $MoS_2$ on an Au/silica support once again reveal a more uneven topoplogy than that observed with HOPG (Figure A.4a and b); this is in agreement with a literature report of monolayer $MoS_2$ imaged

directly on silica.[11] However, the atomic structure of the $MoS_2$ can be resolved in small-scale images (Figures A.4c and d). Interestingly, the atomic structure can be observed at a variety of bias voltages, at approximately −1200 mV to −1500 mV, in accordance with a report of monolayer $MoS_2$ on Au(111) imaged by STM,[12] and also approximately −300 mV to −400 mV. Consistently being able to image the underlying substrate is, again, important to calibrate data and extract lattice parameters from any arrays that might assemble on the substrate.

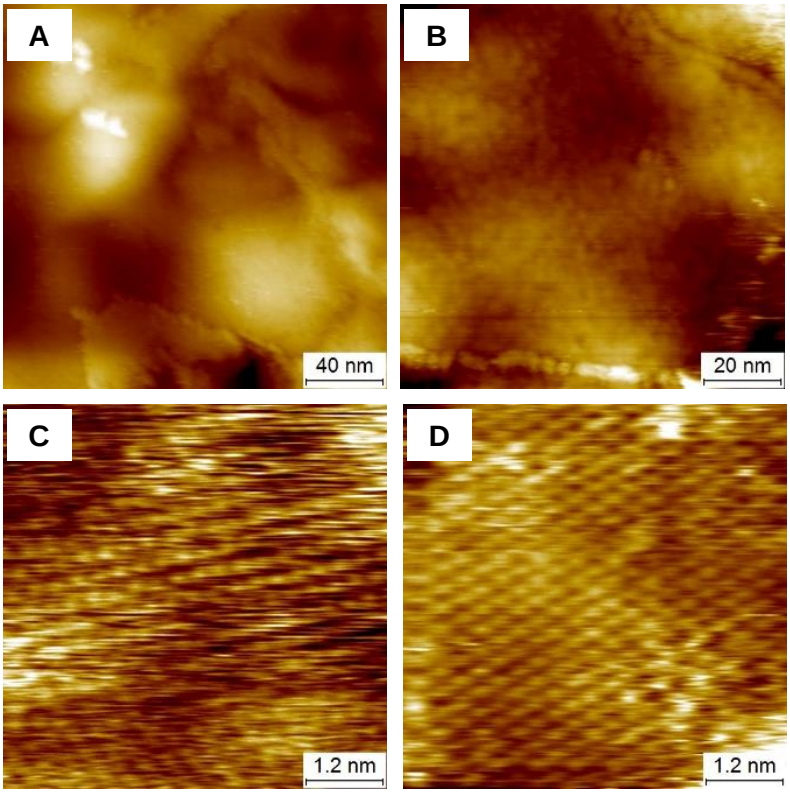


**Figure A.4.** STM images of monolayer $MoS_2$/Au/silica showing a large-scale topography (A and B) and atomic resolution (C and D) The images were acquired at (A): $I$ = 10 pA, $V$ = –500 mV; (B): $I$ = 20 pA, $V$ = –900 mV; (C): $I$ = 65 pA, $V$ = –1500 mV; (D): $I$ = 60 pA, $V$ = –300 mV.

**A.4.3. STM Studies of Ni(OEP) on Monolayer $MoS_2$.** Ni(OEP) deposited from a 0.5 mM 1-phenyloctane solution on $MoS_2$/Au/silica self-assembles rapidly into a monolayer (Figure A.5a and b). Due to macroscale variation in surface topology, the extent of the domains is unclear, but they appear to span approximately 50 nm in width. In a control to ensure that the observed arrays

were indeed assembling on the $MoS_2$ and not on a region of uncovered gold, a 0.5 mM solution of Ni(OEP) was directly deposited on an Au/silica substrate (Figure A.5c). While array formation was not obvious, these results were inconclusive, and further control studies are underway in our lab. Porphyrin assembly on gold is often studied under UHV conditions;[1] a report at the solid-liquid interface of long-chain alkyl meso-substituted metalloporphyrins on Au(111) under a n-tetradecane resulted in numerous polymorphic domains, with the free-base analog providing no assembly.[22] This indicates that the monolayer assembly we observe here is likely favored on the $MoS_2$ substrate.

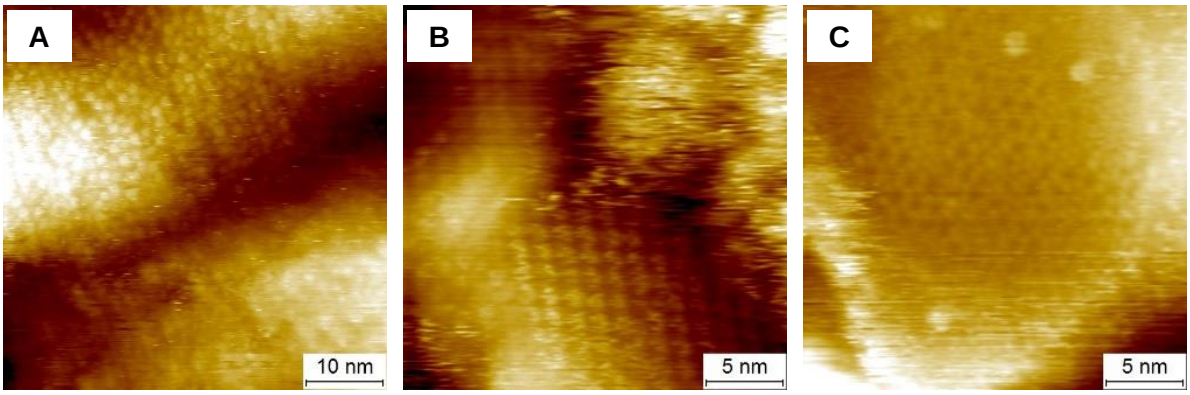


**Figure A.5.** STM images of Ni(OEP) deposited on $MoS_2$/Au/silica (A and B) and attempts to image a sample deposited on a region of Au/silica with no $MoS_2$ (C) and imaged at the solid-liquid interface (0.5 mM, 1-phenyloctane). The images were acquired at (A): $I$ = 12 pA, $V$ = –900 mV; (B): $I$ = 8 pA, $V$ = –500 mV; (C): $I$ = 10 pA, $V$ = –500 mV.

We have also observed high-quality small-scale images of the Ni(OEP) macrocycle when a bias voltage of −1500 mV was applied to the sample (Figure A.6a). This is a notably different bias potential than those previously applied on HOPG, where the macrocycle is typically resolved at −500 mV to −900 mV. This indicates that the electronic structure of the porphyrin relevant to tunneling has noticeably altered by changing the substrate; a similar phenomenon was observed in polydiacetylene nanowires imaged on HOPG and bulk $MoS_2$.[23] Attempts to image the underlying substrate in order to calibrate the data and extract lattice parameters led to an

interesting observation. A confluence of the substrate and monolayer was observed (Figure A.6b), leading to the inability to independently image the underlying substrate. This effect has also been observed in studies of phthalocyanines on bulk $MoS_2$.[24] The similarity of the uncalibrated images to that of Ni(OEP) on HOPG (Figure A.6c) tentatively suggests the lattice parameters are retained on the $MoS_2$/Au substrate. However, future work will use the above result of multiple available bias ranges to image the atomic structure and obtain accurate lattice parameters.

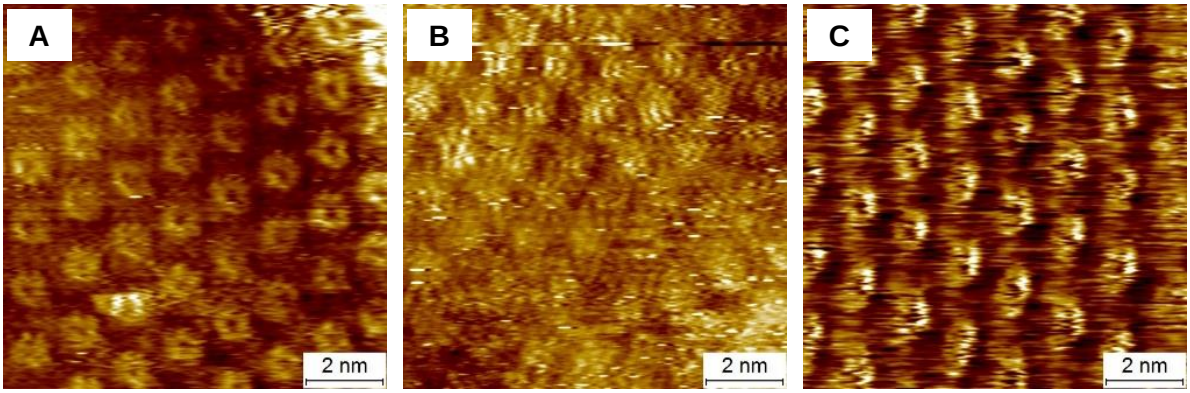


**Figure A.6.** STM images of Ni(OEP) deposited on $MoS_2$/Au/silica (A and B) and HOPG (C) and imaged at the solid-liquid interface (0.5 mM, 1-phenyloctane). The images were acquired at (A): $I$ = 60 pA, $V$ = –1500 mV; (B): $I$ = 50 pA, $V$ = –1500 mV; (C): $I$ = 26 pA, $V$ = –600 mV.

**A.4.4. STM Studies of Ga(OEP)Cl on Monolayer $MoS_2$.** Ga(OEP)Cl deposited from a 0.5 mM 1-phenyloctane solution on $MoS_2$/Au likewise self-assembles rapidly to form a monolayer (Figure A.7). Arrays appear to be on the order of 30 nm in width, but again, the resolution is affected by the overall surface roughness. Unlike HOPG, at all bias potentials studied to this point, only the porphyrin macrocycle has been observed (Figure A.7c); at no bias voltage was the ligand structure resolved. This may be another manifestation of the substrate affecting the overall electronic structure of the porphyrins. During these experiments, it was found that the $MoS_2$ lattice could be imaged at approximately −300 mV to −400 mV (see above); images were subsequently calibrated and lattice parameters extracted. These were found to be in agreement

with unit cell parameters for Ga(OEP)X compounds deposited from 1-phenyloctane on HOPG: *a* = 1.37 (0.03) nm, *b* = 1.36 (0.03) nm, Γ= 66 (2)°.

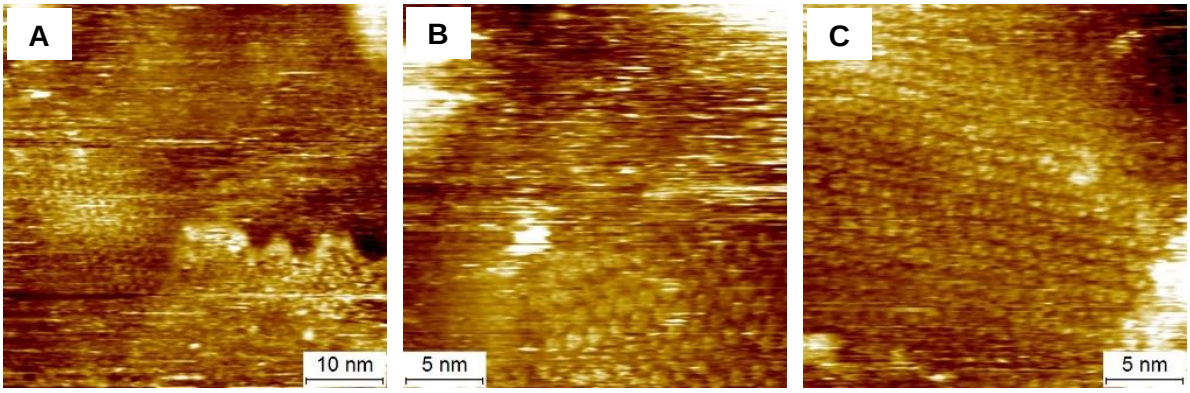


**Figure A.7.** STM images of Ga(OEP)Cl deposited on monolayer $MoS_2$/Au/silica and imaged at the solid-liquid interface (0.5 mM, 1-phenyloctane). The images were acquired at (A): *I* = 10 pA, *V* = –1200 mV; (B): *I* = 20 pA, *V* = –1500 mV; (C): *I* = 12 pA, *V* = –1200 mV.

## A.5. Conclusions

We have shown in a preliminary study that M(OEP) compounds self-assemble on atomically thin substrates under ambient conditions with a retention of the pseudo-hexagonal lattice parameters observed on HOPG. Specifically, Ni(OEP) assembles on both single-layer graphene on copper foil and monolayer $MoS_2$ on a gold/silica support. Further, we can continue our extension of these systems into the third dimension by depositing Ga(OEP)Cl arrays on the $MoS_2$ substrate. These results are preliminary, and further efforts are needed to improve calibration standards, controls, and determination of large-scale assembly behavior. However, this provides a good demonstration of ambient functionalization of novel substrates with unique optical and electronic properties.

## A.6. References

1. Gottfried, J. M. Surface Chemistry of Porphyrins and Phthalocyanines. *Surf. Sci. Rep.* **2015**, *70*, 259-379.

2. Veling, N.; Elemans, J. A. A. W.; Nolte, R. J. M.; Rowan, A. E. Ordered Surface Structures of Self-Assembled Porphyrins. *Handb. Porphyrin Sci.* **2012**, *18*, 1-56.

3. Otsuki, J. STM Studies on Porphyrins. *Coord. Chem. Rev.* **2010**, *254*, 2311-2341.

4. Ludwig, C.; Strohmaier, R.; Petersen, J.; Gompf, B.; Eisenmenger, W. Epitaxy and Scanning-Tunneling-Microscopy Image-Contrast of Copper Phthalocyanine on Graphite and Mos2. *J. Vac. Sci. Technol. B* **1994**, *12*, 1963-1966.

5. Huang, H.; Wong, S. L.; Chen, W.; Wee, A. T. S. LT-STM Studies on Substrate-Dependent Self-Assembly of Small Organic Molecules. *J. Phys. D: Appl. Phys.* **2011**, *44*.

6. Choi, W.; Lahiri, I.; Seelaboyina, R.; Kang, Y. S. Synthesis of Graphene and Its Applications: A Review. *Crit. Rev. Solid State Mater. Sci.* **2010**, *35*, 52-71.

7. Novoselov, K. S.; Geim, A. K.; Morozov, S. V.; Jiang, D.; Zhang, Y.; Dubonos, S. V.; Grigorieva, I. V.; Firsov, A. A. Electric Field Effect in Atomically Thin Carbon Films. *Science* **2004**, *306*, 666-669.

8. Radisavljevic, B.; Radenovic, A.; Brivio, J.; Giacometti, V.; Kis, A. Single-Layer $MoS_2$ Transistors. *Nat. Nanotechnol.* **2011**, *6*, 147-150.

9. Choi, J.; Zhang, H. Y.; Choi, J. H. Modulating Optoelectronic Properties of Two Dimensional Transition Metal Dichalcogenide Semiconductors by Photoinduced Charge Transfer. *ACS Nano* **2016**, *10*, 1671-1680.

10. Mak, K. F.; Lee, C.; Hone, J.; Shan, J.; Heinz, T. F. Atomically Thin $MoS_2$: A New Direct-Gap Semiconductor. *Phys. Rev. Lett.* **2010**, *105*.

11. Zhou, X. D.; Kang, K.; Xie, S.; Dadgar, A.; Monahan, N. R.; Zhu, X. Y.; Park, J.; Pasupathy, A. N. Atomic-Scale Spectroscopy of Gated Monolayer $MoS_2$. *Nano Lett.* **2016**, *16*, 3148-3154.

12. Sørensen, S. G.; Füchtbauer, H. G.; Tuxen, A. K.; Walton, A. S.; Lauritsen, J. V. Structure and Electronic Properties of *In Situ* Synthesized Single-Layer MoS2 on a Gold Surface. *ACS Nano* **2014**, *8*, 6788-6796.

13. Hill, H. M.; Rigosi, A. F.; Rim, K. T.; Flynn, G. W.; Heinz, T. F. Band Alignment in $MoS_2/WS_2$ Transition Metal Dichalcogenide Heterostructures Probed by Scanning Tunneling Microscopy and Spectroscopy. *Nano Lett.* **2016**, *16*, 4831-4837.

14. Liu, X. L.; Balla, I.; Bergeron, H.; Campbell, G. P.; Bedzyk, M. J.; Hersam, M. C. Rotationally Commensurate Growth of $MoS_2$ on Epitaxial Graphene. *ACS Nano* **2016**, *10*, 1067-1075.

15. Liu, X. L.; Balla, I.; Bergeron, H.; Hersam, M. C. Point Defects and Grain Boundaries in Rotationally Commensurate $MoS_2$ on Epitaxial Graphene. *J. Phys. Chem. C* **2016**, *120*, 20798-20805.

16. Shi, J. P.; Liu, M. X.; Wen, J. X.; Ren, X. B.; Zhou, X. B.; Ji, Q. Q.; Ma, D. L.; Zhang, Y.; Jin, C. H.; Chen, H. J.; Deng, S. Z.; Xu, N. S.; Liu, Z. F.; Zhang, Y. F. All Chemical Vapor Deposition Synthesis and Intrinsic Bandgap Observation of $MoS_2$/Graphene Heterostructures. *Adv. Mater.* **2015**, *27*, 7086-7092.

17. Zhang, P.; Fany, Y.; Zhou, Y.; Wan, W.; Xiaolan, Y.; Rui, Z.; Shunquig, W.; Zhu, Z.-Z.; Cai, W.; Kang, J. Epitaxial Growth and Intrinsic Nature of Molybdenum Disulfide on Graphite. *Appl. Phys. Express* **2017**, *10*, 055201.

18. Kang, K.; Xie, S. E.; Huang, L. J.; Han, Y. M.; Huang, P. Y.; Mak, K. F.; Kim, C. J.; Muller, D.; Park, J. High-Mobility Three-Atom-Thick Semiconducting Films with Wafer-Scale Homogeneity. *Nature* **2015**, *520*, 656-660.

19. Ataca, C.; Topsakal, M.; Akturk, E.; Ciraci, S. A Comparative Study of Lattice Dynamics of Three- and Two-Dimensional $MoS_2$. *J. Phys. Chem. C* **2011**, *115*, 16354-16361.

20. MacLeod, J. M.; Lipton-Duffin, J. A.; Cui, D.; De Feyter, S.; Rosei, F. Substrate Effects in the Supramolecular Assembly of 1,3,5-Benzene Tricarboxylic Acid on Graphite and Graphene. *Langmuir* **2015**, *31*, 7016-7024.

21. MacLeod, J. M.; Rosei, F. Molecular Self-Assembly on Graphene. *Small* **2014**, *10*, 1038-1049.

22. Hulsken, B.; van Hameren, R.; Thordarson, P.; Gerritsen, J. W.; Nolte, R. J. M.; Rowan, A. E.; Crossley, M. J.; Elemans, J. A. A. W.; Speller, S. Scanning Tunneling Microscopy and Spectroscopy Studies of Porphyrins at Solid-Liquid Interfaces. *Jpn. J. Appl. Phys., Part 1* **2006**, *45*, 1953-1955.

23. Giridharagopal, R.; Kelly, K. F. Substrate-Dependent Properties of Polydiacetylene Nanowires on Graphite and $MoS_2$. *ACS Nano* **2008**, *2*, 1571-1580.

24. Manivannan, A.; Nagahara, L. A.; Yanagi, H.; Kouzeki, T.; Ashida, M.; Maruyama, Y.; Hashimoto, K.; Fujishima, A. Scanning Tunneling Microscopy Observations of Zincnaphthalocyanine on $MoS_2$. *Thin Solid Films* **1993**, *226*, 6-8.